Dual Fluorescence of 2-(4’-*N,N*-Dimethylaminophenyl) imidazo[4,5-*b*]pyridine: Effect of homogeneous and microheterogeneous environments

by

Nihar Dash

Department of Chemistry
Indian Institute of Technology Guwahati
December 2010

Dual Fluorescence of 2-(4'-*N,N*-Dimethylaminophenyl) imidazo[4,5-*b*]pyridine: Effect of homogeneous and microheterogeneous environments

A Dissertation submitted to the
Indian Institute of Technology Guwahati as
partial fulfillment for degree of
Doctor of Philosophy
in Chemistry

by
Nihar Dash
Roll No: 06612208

Department of Chemistry
Indian Institute of Technology Guwahati
December 2010

Dedicated to

My parents and Grand Mother

My Teachers

For their invaluable advices

Statement

I hereby declare that this thesis entitled "Dual Fluorescence of 2-(4'-N,N-Dimethylaminophenyl)imidazo[4,5-b]pyridine: Effect of homogeneous and microheterogeneous environments" is the outcome of research work carried out by me under the supervision of Dr. G. Krishnamoorthy, at the Department of Chemistry, Indian Institute of Technology Guwahati, India.

In keeping with the general practice of reporting scientific observations, due acknowledgement has been made whenever work described here has been based on the findings of other investigators.

Guwahati Nihar Dash
December 23, 2010

Certificate

Certified that the work described in this thesis entitled “Dual Fluorescence of 2-(4’-N,N-Dimethylaminophenyl)imidazo[4,5-b]pyridine: Effect of homogeneous and microheterogeneous environments” is an authentic record of the results obtained from the research work carried out under my supervision in the Department of Chemistry, Indian Institute of Technology Guwahati, India.

Guwahati
December 23, 2010

G. Krishnamoorthy

Acknowledgements

First and foremost, I would like to thank to my Sir, Dr. G. Krishnamoorthy, who spent a lot of time to read my thesis and gave me a lot of useful suggestions and constructive criticisms, and also for being patient with me through all the times. Throughout my thesis-writing period, he provided encouragement, sound advice, good teaching, good company, and lots of good ideas. I would have been lost without him. I really appreciate the guidance and assistances that he has provided and very grateful him to accept me as his student. I am indebt to this wonderful person for all that he has given me and above all for motivating me towards scientific research. Special thanks to his family for making me feel at home

I gratefully thank the entire Doctoral Committee member for their help in different ways during the course of this work. I also thank my B. Sc. Teachers for their constant support and encouragement. I would like to thank all my friends for their constant encouragement. Many thanks go to the present lab members, Dr. (Mrs.) Monali Dutta Saikia, Dr. A. Thangamani, Francis A.S. Chipem, Anasuya, Mirnmoy, Souma, Aswini who provided a friendly working environment in Lab. I would also like to give special thanks to F A. S. Chipem and Dr. L. Rout, who have given me much useful advices and have comforted me when I faced some setbacks in my research work. Thank you for sharing your opinions with me and I am glad to have a best friend like you. I am very grateful to Dr. Shafique, Dr. Jugal, Dr. Padhi, Dr. Martha, Dr S. C. Sahoo, Himanshu, Ziyauddin Khan, Jyothi, Dipankar, Ashok, Sneha, Sasmita, Sarika, Chaitanya, Kulu, Md. Palashuddin Sk, Vijay Ravi, Tushar, Biswa and Sanjay who have given me tremendous spiritual support throughout the year. I wish to thank everybody with whom I

have shared experiences in life. From the people who first persuaded and got me interested into the study of chemistry, specially those who also played a significant role in my life, to those which with the gift of their company made my days more enjoyable and worth living.

I cannot finish without saying how grateful I am with my family: grandparents, brothers, uncles, aunts, cousins and nephews all have given me a loving environment where to develop. Lastly, and most importantly, I wish to thank my parents (my mother Mrs. Nayana Dash and my father Mr. Alekha Chandra Dash), and my two sisters Gudi, Tiki They have always supported and encouraged me to do my best in all matters of life.

The Department of Chemistry has provided the support and equipment I have needed to produce and complete my thesis. I would like to thank Indian Institute of Technology for the research fellowship and CIF for instrumental facility.

With Regards

Nihar Dash

Synopsis

Intermolecular charge transfer (ICT) is a common excited state phenomenon that occurs in several photochemical and photobiological processes. Organic molecules those consist of an electron donor and acceptor pair linked by a single bond may undergo ICT in the excited state. Such bichromophore compounds have received considerable attention as possible models for the investigation of the primary function of photoelectric devices and chemical energy storage. Though several models are proposed to explain the formation of ICT state, the twisted intramolecular charge transfer (TICT) model proposed by Grabowski et al. is widely accepted. In TICT model, upon excitation, within lifetime of the locally excited state of the molecule, transfer of an electron from the donor to the acceptor is accompanied by rotational relaxation to a twisted conformation of the donor relative to the acceptor to form the TICT state. At perpendicular geometry, the donor and the acceptor are completely decoupled and the electrostatic interaction between them stabilizes the TICT state. The formation of TICT state mostly results in dual fluorescence. The shorter wavelength emission band is called normal or locally excited fluorescence and the longer wavelength emission band is assigned as TICT band. The TICT emission is highly sensitive to environment. This environmental sensitivity of the TICT emission has rendered it useful as a microenvironment probe. Solvent polarity and viscosity usually affects the relative positions and intensities of the TICT fluorescence. Of special relevance to the present work are reports that H-bonding of the solvent plays an important role in formation and stabilization of the TICT state. Such hydrogen bonding may be important in facilitating proton-coupled charge transfer phenomena often observed in biological assemblies and other systems. The present thesis described the effect solvent, pH, metal ions *N*-alkylation and organized assemblies such cyclodextrin, normal and reverse micelle and proteins on the TICT of 2-(4'-*N,N*-dimethylaminophenyl)imidazo[4,5-*b*]pyridine (DMAPIP-b, Chart 1). Besides, investigating the effect of organized assemblies' effort is made to understand the nature and characteristics of these heterogeneous systems.

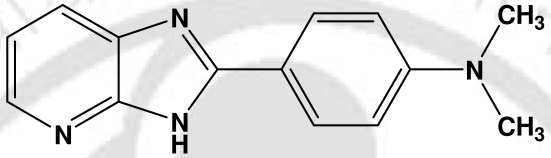

Chart 1: Structure of DMAPIP-b

The thesis is divided into four chapters. Chapter 1 reviews various photophysical processes and the factors affecting those processes, such as solvent, acid-base, temperature etc. In addition a brief introduction to TICT process and organised media such as micelles, cyclodextrins and proteins are also presented. The scope of the present work is briefed in the end of the chapter.

Chapter 2 contains the details of the chemicals and the solvents used in the present work followed by the procedures for the synthesis of the fluorophores. Chapter 2 also elaborates the methods used for the analysis, the calculations and the preparation of the samples. This chapter also describes the methods used for the quantum mechanical calculations and in addition, a brief description of the instruments such as uv-visible asorption spectrophotometer, steady state fluorescence and life resolved fluorescence spectrometers are provided.

Chapter 3 is divided into four sections. The first three sections elaborate the effect of solvent and pH, temperature and metal ions on photophysics characteristics of DMAPIP-b. Single emission from local excited state is observed in aprotic solvents. DMAPIP-b exhibits dual fluorescence only in polar protic solvents . The intensity of the longer wavelength emission of DMAPIP-b increases with increase in H-bond donating capacity and polarity of the solvent. Water is an exception, where it decreases. The fluorescence excitation spectra, recorded for each emission band suggest that both emissions have same ground state precursor. The long wavelength emission is attributed to the formation of a TICT state facilitated by H-bonding of the solvent with the pyridine nitrogen of DMAPIP-b. *ab initio* calculation predicted that the molecule is planar in the ground state. Time resolved measurements suggest that the equilibrium is not established between the locally excited state and the TICT state. In an aqueous acidic medium, DMAPIP-b is protonated and a single emission is observed from the locally excited state.

In the next section the effect of temperature on the excited state characteristics of DMAPIP-b was investigated in six different solvents. In nonpolar cyclohexane, the rate constants of the radiative decay increases and that of the nonradiative decays decreases with rise in temperature. Thus, it appears that there is an increased cross section towards the radiative path in the higher vibrational levels. However, in polar acetonitrile, there is an increase in nonradiative processes related to thermal agitation at high temperature and can be inferred from the enhancement in nonradiative rate and reduction in radiative rate with increase in temperature. Dual emission observed in all the protic solvents and the equilibrium between the locally excited state and the TICT state is not established even near the boiling point of the solvents. The quantum yield and lifetime of both emissions decrease with increase in temperature. The dipole moment is determined from the solvatochromic shift as well as from the thermochromic shift. Both the values are in good agreement with each other. In glycerol, enhancing temperature drastically decreases the fluorescence of both the emission and the intensity ratio of the TICT emission to normal emission also increases with temperature.

The interactions of DMAPIP-b with various metals have been investigated by UV-visible, fluorescence spectroscopy and time-resolved lifetime measurements. Alkai metals Na^+ has no interaction with DMAPIP-b, but Li^+ very weak interaction with the probe molecule. While alkai earth metal ion Ba^{2+} did not form any ground state complex, smaller alkai earth metal ion Ca^{2+} forms ground state complexes at very much concentration. The magnitude of changes in fluorescence characteristics decreases with increase in ionic radii (i.e. $Mg^{2+} < Ca^{2+} < Ba^{2+}$). Transition metal ions Ni^{2+} and Co^{2+} form non fluorescent ground state complexes with DMAPIP-b by binding at the imidazole nitrogen. However Cd^{2+} forms fluorescing complexes with DMAPIP-b by binding at the imidazole nitrogen. On the hand DMAPIP-b has strong affinity for Zn^{2+}, complexation of Zn^{2+} with DMAPIP-b changes initial fluorescence “ON” locally excited state to “ON” TICT state. These changes were revealed by a visible color change from light blue to green in presence of zinc perchlorate. The large bathochromic shift in the absorption spectrum and the formation of TICT indicate that in DMAPIP-b-Zn^{2+}, zinc ion is coordinated through the pyridine nitrogen of the fluorophore. The conclusions are substantiated by time resolved fluorescence measurements. The ability of DMAPIP-b to act as a potential ratiometric sensor for zinc ion is also explored.

In the last section the chapter, the effect of addition of long alkyl chain on the photophysics of DMAPIP-b is discussed. Two different compounds were synthesized namely 2-[4’-(N,N-diemthylaminophenyl)imidazo[4,5-*b*]hexadecylpyridinylium bromide (**1**), where hexadecyl chain is attached at pyridine nitrogen and 1-hexadecyl-2-[4’-(N,N-diemthylaminophenyl)imidazo[4,5-*b*]pyridine (**2**), where the chain is substituted in imidazole nitrogen, >N-H (Chart2).

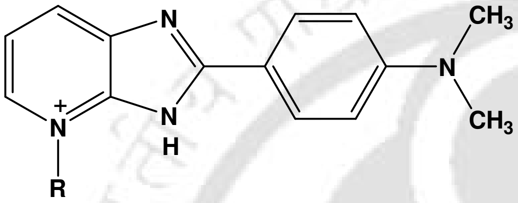

1

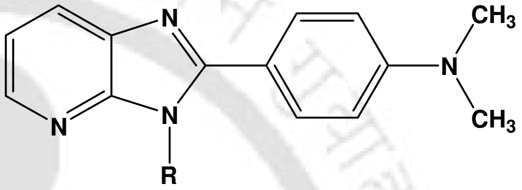

2

Chart 2. Structures of the N-alkylated products

Absorption, steady state and time resolved fluorescence techniques were employed to investigate the spectral properties in different solvents. Density functional theory (DFT) and restricted configuration by singles combined with time dependent DFT (TDDFT) calculations were performed on the ground state and the excited state respectively, to calculate the geometrical and electronic properties of the molecules. Unlike DMAPIP-b where dual emission was observed in protic solvent which originates from both locally excited state and from TICT state, the pyridine nitrogen alkylated product **1**, emits single emission from TICT state and the imizadole nitrogen alkylated molecule (**2**) emits dual emission only in methanol and water and in methanol too the relative contribution of TICT emission is negligible.

Chapter 4 deals with the effects of micro heterogeneous systems such as cyclodextrin, micelle, reverse micelle and protein (bovine serum albumin, BSA) on the spectral features of DMAPIP-b. The effects of β-cyclodextrin (β-CD) inclusion complex formation on the hydrogen bond TICT of DMAPIP-b have been examined by fluorescence excitation, emission and time resolved fluorescence techniques. The study revealed that DMAPIP-b forms 1:1 inclusion complex with β-CD. The host-guest complex is formed by partial inclusion of dimethylaminophenyl ring inside the core of the β-CD nanocavity. However the imidazopyridine ring of the guest molecule resides outside CD cavity and forms H-bond with the water molecules that are present near the rim and in bulk phase. ^{1}H NMR studies are used to confirm the inclusion complex The hydrogen bond of water with pyridine nitrogen ensures the formation of TICT state. But both normal and TICT emissions are enhanced inside the β-CD cavity. Fluorescence lifetime measurements suggest that the equilibrium is not established between the locally excited state and the TICT state. Dual emission is observed in presence of β-CD at pH ~ 3.5, due to emission from monocations formed by the protonation of pyridine nitrogen and imidazole nitrogen. DFT calculations preformed for the monocations reveal that MC1 and MC2 are more stable than MC3, the monocation formed by the protonation of the dimethylamino nitrogen.

The photophysical behaviour of DMAPIP-b has been studied in nonionic triton X-100 (TX-100), cationic, cetyl trimethylammonium bromide (CTAB) and anionic, sodium dodecyl sulfate (SDS) micelles. The molecule emits both normal and TICT fluorescence in SDS and TX-100 but emits only normal fluorescence in CTAB. This difference in behavior of the fluorophore is due to varying extent of hydrogen bonding experience by it in different micelles. Same as in β-CD of the three possible monocations, only two kinds of monocations, MC1 and MC2 are present in all the micelles. MC1 induces micellization of SDS whereas none of the monocation induces micellization of TX-100 or CTAB.

Section three of chapter 4 describes the spectral behavior of DMAPIP-b in nonionic TX100 and cationic CTAB reverse micelle. TX-100/benzene/hexane solution DMAPIP-b exhibits only single emission, upon addition of water dual emission was observed. On the other hand in TX-100/cyclohexane/*n*-hexanol/water reverse micelle even before the addition of water, DMAPIP-b exhibits dual emission. However, in both TX-100 reverse micelles the fluorophore is present at the micellar interface in the water penetrable region. But in CTAB/isooctane/*n*-hexanol/water system DMAPIP-b is present more inside the reverse micelle and the water molecules are not present in that region.

The interaction of DMAPIP-b and its alkylated products (**1** and **2**) with BSA is presented in the last section of this chapter. The interaction of all the probes with BSA causes reduction in the fluorescence emission of BSA. The nonradiative dipole-dipole Förster type energy transfer efficiency is more in the case DMAPIP-b than **1**. The alkylated products have stronger affinity for BSA than DMAPIP-b. The number of binding site is one in all three fluorophores. Both DMAPIP-b and pyridine nitrogen alkylated product **1**, bind at the same site and **2** binds at different site. The non radiative rate is decreased in all the three molecules upon binding with BSA.

List of Abbreviation

A	Acceptor
BSA	Bovine serum albumin
APIP-b	2-(4'-aminophenyl)imidazo[4,5-b]pyridine
CASSCF	Complete active space self-consistent field
CIS	Configuration interaction singles
CD	Cyclodextrins
CMC	Critical micelle concentration
CT	Charge Transfer
CTAB	Cetyl trimethylammonium bromide
D	Donor
DFT	Density functional theory
DMAPIP-b	2-(4'-N,N-dimethylaminophenyl)imidazo[4,5-b]pyridine
DMAPIP–c	2-(4'-N,N-dimethylaminophenyl)imidazo[4,5-c]pyridine
4-DMABN	4-(Dimethylamino)benzonitrile
EA	Electron Affinity

ESA	Equine serum albumin
Exc	Excitation wavelength
FTIR	Fourier transforms infrared spectroscopy
HF	Hartree-Fock
HOMO	Highest Occupied Molecular Orbital
HSA	Human serum albumin
IC	Internal Conversion
ICT	Intramolecular Charge Transfer
IP	imidazopyridine
ISC	Inter System Crossing
LC-Mass	Liquid chromatography-mass spectrometry
LUMO	Lowest Unoccupied Molecular Orbital
MC	Monocation
NMR	Nuclear Magnetic Resonance
PICT	Planar Intramolecular Charge Transfer
PIE	Pseudo-phase ion-exchange

PMT	Photomultiplier Tube
RHF	Radio High Frequency
RICT	Rehybridized Intramolecular Charge Transfer
RSA	Rat serum albumin
SDS	Sodium dodecyl sulfate
TCSPC	Time Correlated Single Photon Counting
TD	Time Dependent
TDDFT	Time Dependent Density Functional Theory
TICT	Twisted Intramolecular Charge Transfer
TLC	Thin Layer Chromatography
Triton X-100	Polyoxyethylene(E9-10)t-octylphenol (also TX-100,surfactant)
UV	Ultra Violet
VIS	Visible
ZINDO	Zerner's Intermediate Neglect of Differential Overlap
μ_e	Dipole moment of ground state
μ_g	Dipole moment excited state.

List of Figures

List of Tables

Contents

Chapter 1

Introduction

1.1. Molecular fluorescence

Certain substances so called fluorophore, on being illuminated by high frequency light, emit light of relatively low frequency known as fluorescence. The emission occurs so long the substance is being illuminated. Fluorescence is the highly sensitive and so frequently used as a tool for the characterization of complex molecular systems in chemistry, physics, material science and biology. Time resolved fluorescence measurements give excited state lifetimes and various photophysical deactivation process occur in the excited state of the fluorescence probes. Lifetimes are used in understanding the dynamics of the macromolecules, micelles, membranes and to obtain the quenching constants in the diffusion and bimolecular quenching reactions. Fluorescence lifetime measurements are also used to determine the distance between a donor and an acceptor which gives the information about the resonance energy transfer process.

1.1.1. Molecular excitation and relaxation processes

At room temperature most of the molecules occupy the lowest vibrational level of the ground electronic state, and on absorption of light they are elevated to the excited states. Photons having energy range in between the ultraviolet to the visible region of the spectrum are needed to activate an electronic transition. Each electronic state is splitted into multiple sublevels representing the vibrational modes of the molecule When light of an appropriate wavelength is absorbed by a molecule (i.e., excitation), the electronic state of the molecule changes from the ground state to one of many vibrational levels in one of the excited electronic states.. An excited state of molecule can be regarded as distinct species, differ from the ground state of the same molecule. The excited molecules are in the states of shorter life time than usual and have considerable energy than that of the ground state precursor. Thus the molecules are more active in their excited state than that of the ground state. Deactivation of an excited state occurs by a photochemical or photophysical process, either intramolecularly or intermolecurlarly [1, 2].

By natural tendency, an excited molecule loses its excitation energy and returns to the ground state by various radiative and non radiative processes. These processes can be illustrated by Perrin's Jablonski diagram (Figure 1.1). These processes are also discussed in standard text books [1, 2]. With few rare exceptions, most of the molecules in the condensed phase undergo rapid vibrational relaxation to the lowest vibrational level of the first excited singlet state, S_1. From this excited state, several processes can cause the molecule to relax to its ground state. The most important pathways are:

(a) Collisional deactivation (external conversion) leading to nonradiative relaxation.

(b) Intersystem crossing (10^{-9} sec): In this process, if the energies of the singlet states overlap with those of the triplet states, vibrational coupling can occur between the two states. Molecules in the singlet excited state can cross over to the triplet excited state.

(c) Phosphorescence: This corresponds to is the relaxation of the molecule from the triplet excited state to the singlet ground state with emission of light. Since it is a forbidden transition, the triplet state has a long lifetime and the rate of phosphorescence is slow (10^{-2} to 100 sec).

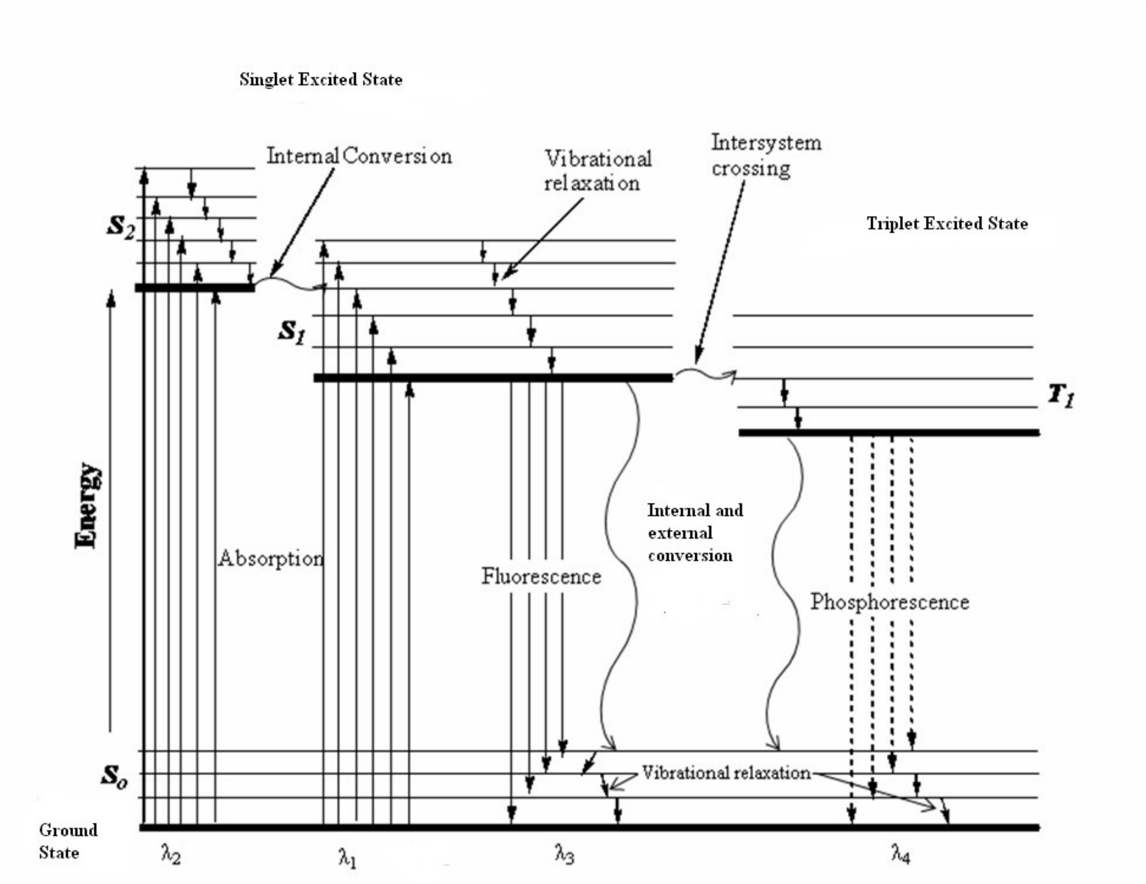

Figure 1.1: Electronic transition energy level diagram (Perrin-Jablonski digram).

(d) Fluorescence: This is the relaxation of the molecule from the singlet excited state to the singlet ground state with emission of light. Fluorescence has short lifetime (~10^{-8} sec) and so that in many molecules it can compete favorably with collisional deactivation and intersystem crossing. The wavelength of the light emitted is dependent on the energy gap between the ground state and the singlet excited state. An overall energy balance for the fluorescence process could be written as:

$$E_{\mathrm{fl}} = E_{\mathrm{abs}} - E_{\mathrm{vib}} - E_{\mathrm{sol.relax}} \qquad (1.1.1)$$

where E_{fl} is the energy of the emitted light. E_{abs} is the energy of the light absorbed by the molecule during excitation, and E_{vib} is the energy lost by the molecule from vibrational relaxation. The $E_{sol.relax}$ term arises from the need for the solvent cage of the molecule to reorient itself in the excited state and then again when the molecule relaxes to the ground state. Equation (1.1.1) clearly states that the energy of the fluorescence is always less than the absorption energy for a given molecule. Thus the light is emitted at longer wavelengths than the excitation.

(e) Internal Conversion: Direct vibrational coupling between the ground and the excited electronic states (vibronic level overlap) and quantum mechanical tunneling (no direct vibronic overlap but small energy gap) are internal conversion processes. This is a rapid process (10^{-12} sec) relative to the average lifetime of the lowest excited singlet state (10^{-8} sec) and therefore competes effectively with fluorescence in most of the molecules.

In addition, processes such photoisomerization, photoionization, photodissociation, proton transfer, charge transfer and acid-base reaction may compete with fluorescence. If the fluorescing molecule forms ground or excited state complexes, the fluorescence intensity may also be reduced or completely quenched

According to Kasha's rule, the fluorescence emission spectrum is independent of excitation wavelength [3] due to rapid relaxation from higher electronic and vibrational levels to lowest vibrational level of S_1 state. When the ground state contains multiple species, in that situation the fluorescence emission and excitation spectrum are dependent on each other Excitation on the extreme red edge of the absorption spectrum frequently results in a red-shifted emission. Also the observed fluorescence excitation spectrum observed for a given emission wavelength differs from that of the absorption spectrum for heterogeneous system. The presence multiple species in the excited state is also responsible for the large spectral width of the emission spectrum compared to the width of the absorption spectrum. In most of the fluorophore, the fluorescence emission and absorption spectrum are generally a mirror image to each other (S_0 to S_1 transition). In case of some molecules the mirror image rule does not holds, because of different geometrical arrangement in the excited state as compared to the ground state or due to formation of complex. A classical example is pyrene [4]. A highly structured emission spectrum was observed only at lower concentration of pyrene.At higher concentration, a long wave length emission band at 470 nm was observed and is due to formation of excimer. In the case of 2-naphthol, the fluorescence emission is not a mirror image of the absorption spectrum. This is because of photoionization in the excited state, 2-naphthol undergoes deprotonation, as its excited state pK_a (= 2.0) is much lower than the ground state pK_a (= 9.2) [5].

Fluorescence intensity is a measure of the probe's ability to decay through radiative mechanism. Fluorescence quantum yield (ϕ_f) is related to the radiative rate and non-radiative rate of the deactivation of the excited state as shown in the equation

$$\phi_f = \frac{k_r}{k_r + k_{nr}} = \frac{k_r}{k_r + k_{IC} + k_{ISC} + k_q[Q]} \tag{1.1.2}$$

where k_r and k_{nr} are the radiative rate of the fluorescence and the nonradiative rate. k_{IC}, k_{ISC} and k_q represent the rate constants for internal conversion, intersystem crossing, and quenching respectively. [Q] denotes the quencher concentration. The nonradiative rate, k_{nr}, is the sum of k_{IC}, k_{ISC} and $k_q[Q]$.

1.1.2. Fluorescence lifetime

Time resolved fluorescence methods give the kinetic information on the various processes involved in the deactivation of the excited state. With the advent of lasers as excitation light sources, it is possible to have the time resolution of the order of femtoseconds for the excited processes under investigation. The typical fluorescence decay is a plot of fluorescence intensity as a function of time. For a simple system having a single fluorophore the fluorescence intensity decay, I(t), is a single exponential and is given by the equation

$$\mathrm{I(t)} = \mathrm{I}_0 e^{-t/\tau} \qquad (1.1.3)$$

where I_0 is the initial intensity and τ is the fluorescence lifetime. The fluorescence lifetime, τ, represents the average time spent by the fluorophore in the excited state before deactivation to the ground state. The fluorescence lifetime is related to the radiative and the nonradiative rates. In the case of the systems having multiple species, decay fits a multi-exponential function and the fluorescence intensity decay equation is shown below

$$\mathrm{I}(t) = \sum_{i=1}^{n} a_i e^{-t/\tau_i} \qquad (1.1.4)$$

Where α_i and τ_i are *i*th pre-exponential factor (amplitude) and the lifetime in the multiexponential decay respectively. Pre-exponential factors are generally positive but can be negative, whenever there is an excited state kinetics. A negative pre-exponential factor indicates the formation of a new emissive species in the excited state reaction. In the case of multi exponential decays it is useful to calculate the average lifetime ($\overline{\tau}$). For biexponential decay $\overline{\tau}$ is given as

$$\bar{\tau} = \frac{a_1\tau_1^2 + a_2\tau_2^2}{a_1\tau_1 + a_2\tau_2} \qquad (1.1.5)$$

Occasionally the average lifetime is given by

$$< \tau > = \frac{\sum_i a_i\tau_i}{\sum_i a_i} \qquad (1.1.6)$$

Where <τ> is proportional to area under the decay curve. It is useful for instance like energy transfer where the transfer efficiency should be calculated using <τ>.

1.1.3. Fluorescence anisotropy

The fluorescence emission, emitted from the samples excited with a polarized light is also polarized. The extent of polarization of the emission is described in terms anisotropy (*r*). Samples whose anisotropies values are non-zero are said to be display polarized emission. This polarization is due the photo selection of the fluorophore according to their orientation relative to the direction of the polarized excitation. This photo selection is proportional to the square of the cosine of the angle between the absorption dipole of the fluorophore and the axis of polarization of the excitation light. The orientational anisotropic distribution of the excited fluorophore population relaxes by rotational diffusion of the fluorophore and excitation energy transfer to the surrounding acceptor molecules. The polarized fluorescence emission becomes depolarized by such processes. The fluorescence anisotropy measurements reveal the average angular displacement of the fluorophore which occurs between absorption and subsequent emission of a photon. This angular displacement depends upon the rate and the extent of rotational diffusion during the life time of the fluorophore in the excited state. The steady state fluorescence anisotropy (r) is defined as in following equation

$$r = \frac{I_{VV} - GI_{VH}}{I_{VV} + 2GI_{VH}} \quad ; \qquad G = \frac{I_{HV}}{I_{HH}} \tag{1.1.7}$$

where I_{VV} and I_{VH} are the emission intensities when the excitation polarizer is vertically oriented and the emission polarizer is oriented vertically and horizontally respectively. G is the correction factor. The terms I_{HV} and I_{HH} are the emission intensity when the excitation polarization is horizontally oriented and the emission polarization is oriented vertically and horizontally, respectively. The time dependent fluorescence anisotropy or fluorescence anisotropy decay, r(t) depends on the size, shape and flexibility of the molecule. It can be calculated from the equation

$$r = \frac{I(t)_{VV} - GI(t)_{VH}}{I(t)_{VV} + 2GI(t)_{VH}} \tag{1.1.8}$$

where $I_{VV}(t)$ and $I_{VH}(t)$ are the fluorescence intensity decays collected with the polarization of the emission polarizer kept parallel and perpendicular to the polarization of the excitation source respectively. For a fluorophore in a simple solvent, the fluorescence depolarization is simply due to rotational motion of the excited fluorophore. Anisotropy decays can be used to estimate the shape of proteins.

1.1.4. Factors affecting fluorescence

Fluorescence spectra are generally more sensitive to the environment than absorption spectra. Both environmental and structural factors affect the molecular fluorescence. A comprehensive account of the influence of the molecular structure and environment on the electronic absorption spectra have been illustrated by Jaffe and

Orchin [6], and Suzuki [7] and a similar effect on the fluorescence spectra have been provided by Sharma and Schulman [8], Lakowicz [9] and Valuer [10] and several others. Some of the important factors are discussed below.

1.1.4.1. Effects of molecular structure on fluorescence

It is well known that, best fluorescence is observed for molecules with π bonds and preferably those having aromatic rings due to the presence of low energy ππ* state. An increase in the extent of the π-electron system (i.e. degree of conjugation), leads to a bathochromic shift of the absorption and the fluorescence spectra, and to an increase in the fluorescence quantum yield.

However, some heterocyclic aromatic rings are non-fluorescent. These include furan, pyrrole, and thiophene. The absence of fluorescence in such molecules is because of the presence of a low lying nπ* state that rapidly converts the excited molecule to the triplet state and prevents fluorescence. Azarenes contain one or more heterocyclic nitrogen atoms (e.g. pyridine, quinoline, and acridine) and so exhibits low-lying nπ* state. However, the fluorescence characteristics of these compounds are strongly solvent dependent. In hydrocarbon they have low fluorescence quantum yields. But in protic solvents, hydrogen bonds formed between the nitrogen atoms and the solvent molecules results in an inversion of the lowest-lying nπ* and ππ* states. This results in much higher fluorescence quantum yield in these solvents.

Since the electron density on the nitrogen atom is reduced upon excitation the ability to form hydrogen bonds is lower in the excited state. The ground state is thus more stabilized by hydrogen bonding than the excited state. This leads to a red-shift of the spectra when going from aprotic solvents to protic solvents. The decrease in fluorescence of the aromatic ring with substitutions of halogens increases with an increase in the atomic weight of the halogen and a subsequent increase in phosphorescence due to the promotion of intersystem crossing. In addition, substitution of a carbonyl or carboxylic acid group also decreases the fluorescence due to enhancement of intersystem crossing. On the other hand electron donating substituent's such as OH, OR, NH_2, NHR and NR_2 induce an increase in molar absorption coefficient and also shift in both absorption and fluorescence spectra. Moreover the spectra are broad and often blurred compared to the parent hydrocarbons.

1.1.4.2. Effect of solvent nature

Solvents characteristics have important effects on luminescent behavior of molecules. Fluorescence spectra may be strongly dependent on solvent. The shifts in the emission bands induced by the change in solvent nature or composition, is called solvatochromic shifts. When a solute is surrounded by solvent molecules, its excited states are more or less stabilized by solute-solvent interaction, depending upon chemical nature of both solute and solvent molecules. This characteristic is most often observed with fluorophore that have large excited-state dipole moments, resulting in fluorescence spectral shifts to longer wavelengths in polar solvents

Three main effects can be recognized:

a. Solvent polarity

A polar solvent lowers the energy of the $\pi\pi^*$ state.

b. Solvent viscosity

A more viscous solvent increases the quantum yield, since the collisional deactivation is lowered at higher viscosities.

c. Heavy atoms effect

Solvents containing heavy atoms decrease the fluorescence quantum efficiency and increase the phosphorescence.

In addition hydrogen bonding is also a key factor.

The electronic spectra of molecules are affected by the solvent through their electrostatic properties. There are mainly four type of interaction of solvent with solute molecules: (a) dipole-dipole (b) dipole-induced dipole (c) induced dipole-induced dipole (d) hydrogen bonding. These interactions mainly depend upon the molecular structures of solvent and solute. Absorption of light by the molecule changes its electronic distribution so that dipole moment of the excited molecule becomes different from that of molecule in ground state. After excitation, the fluorophore reaches the Franck-Condon state from where the molecular geometry relaxes to new conformation and lead to new electronic distribution of the excited molecule. The relaxation process includes reorientation of solvent dipoles about the new dipole of the excited molecule and probable strengthening, weakening, breaking and making of hydrogen bonds as well as rotation of aromatic ring substituents and functional groups into or out of coplanarity. The solvent relaxation depends on the viscosity of the solvent. If the relaxation time is short with respect to the excited-state lifetime, the fluorophore will emit from the relaxed state. If the reorganization time is of the order of the excited state lifetime, the fluorescence spectrum will be shifted but the position of the maximum cannot be related to the solvent polarity.

The intensities of fluorescence spectra are highly sensitive to the polarity and hydrogen-bonding capacity of the solvent. Other than the effect on nπ* state discussed earlier, hydrogen bonding also affects the quantum yields of many molecules, those have low lying ππ* or intramolecular charge transfer states.

1.1.4.3. Temperature effects

Since nonradiative processes related to thermal agitation such as collisions, intramolecular vibrations and rotations in general increase with an increase in temperature. This leads to quenching of the fluorescence intensity and the lifetime at higher temperatures. Usually linear variation of $\ln(1/\phi_f-1)$ with 1/T was found. In addition, the viscosity of the medium are changed by changing the temperature and hence the number of collisions of the molecules of the fluorophore with solvent molecules. Such changes of the medium affect the fluorescence emission intensity. Several other factors also simultaneously vary with varying temperature.

1.1.4.4. pH effects

Relatively small changes in pH will sometimes radically affect the spectral characteristics of the fluorescence. Most of the phenols are fluorescent in neutral or acidic media, but the presence of a base leads to the formation of nonfluorescent phenolate ions [8]. 5-hydoxyindoles, for example, serotonin, show a shift in fluorescence emission maximum from 330 nm at neutral pH to 550 nm in strong acid without any change in the absorption spectrum [9]. Some times the fluorescence spectra will vary with varying the concentration of proton donor or acceptors. The quantum yield of fluorescence and fluorescence decay profile will then vary with pH in a way that reflects the kinetics of the reaction in S_1 state.

.

1.2. Intramolecular charge transfer

Organic molecules composed of directly attached electron donor and electron acceptor moieties may undergo intramolecular charge transfer (ICT) in the excited state. Excitation of such molecules may induce a charge separation, which result from the transfer of an electron from donor to acceptor. This leads to an increase in molecular dipole moment along with structural and electronic rearrangement within the molecule. The molecule often undergoes relaxation towards a highly polar state called ICT state and exhibits dual emission [11-18]. The widely accepted model for the formation of ICT state is the twisted intramolecular charge transfer (TICT) model proposed by Grabowski [10]. In the TICT model, twisting of the electron donor from within the whole molecular

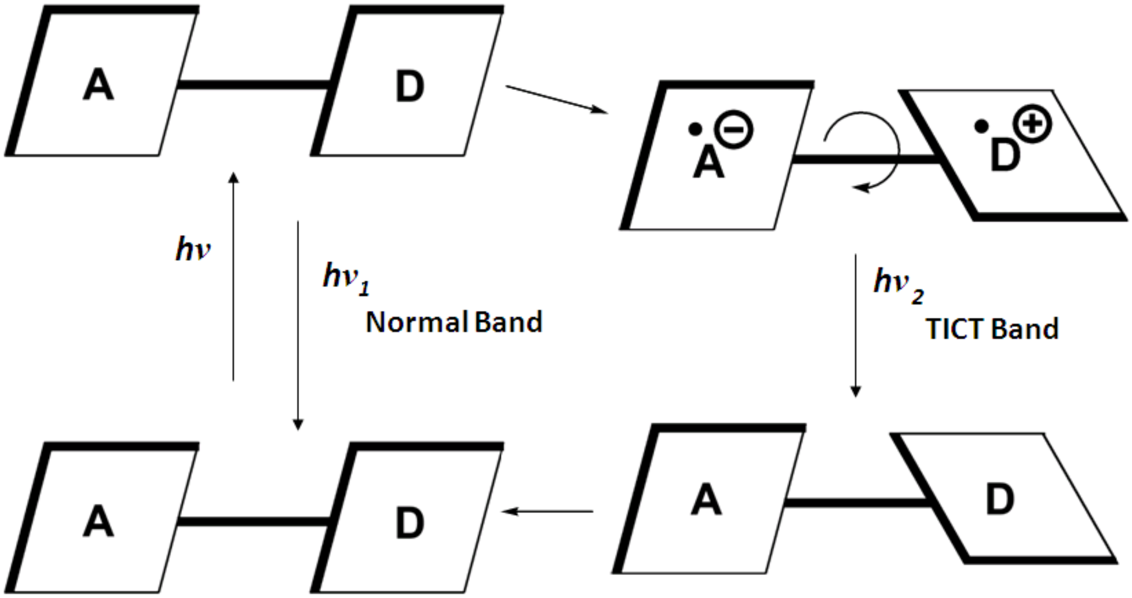

Figure 1.2: Generalized scheme for the TICT model.

plane to a position perpendicular to other moiety of the molecule is accompanying the ICT process from the electron donor to the acceptor during the lifetime of the initially formed locally excited state (Figure 1.2.). However Zachariasse [14, 15] proposed a planar intramolecular charge transfer (PICT) model in which the emitting ICT state has planar structure. A solvent induced vibronic coupling is supposed to take place between the locally excited and CT states leading to formation of a final planar structure. Since direct measurement of the structure of the emitting species is experimentally difficult, the experimental evidence advanced for both TICT and PICT models are largely circumstantial. However, equally convincing indirect evidence has been reported for both models. Dobkowski et al. [19] showed that the ICT process is accompanied by syn-anti isomerization around the C–N bond of desymmetrized analogue 2-(*N*-methyl-*N*-isopropylamino)-5-cyanopyridine in methanol, whereas its ordinary fluorescence in tetrahydrofuran is not accompanied with isomerization. This result indicates the intermediacy of a perpendicular moiety in methanol where dual fluorescence occurs. On the other hand, Yoshihara *et al.* [20] demonstrated that a planar rigidized fluorazene molecule, which cannot attain perpendicular geometry, undergoes fast reversible ICT in the excited state. This implies that large-amplitude motions such as those necessary for the formation of the TICT state are not required for the formation of the ICT state. Recent, theoretical calculation for DMABN and its analogues by Cogan *et al.* [21], predicted two ICT state apart from the locally excited state. They proposed that dual fluorescence may arise from any two of these states, as each has a different geometry at which it attains a minimum. They also suggested that the ICT state is formed by the transfer of an electron from a covalently linked donor group to an antibonding orbital of the π-electron system of benzene. The change in charge distribution of the molecule in the ICT leads to distortion of the benzene ring to a quinoid and an antiquinoid structure. As the dipole moment is larger in the perpendicular geometry than in the planar one, this geometry is preferred in polar solvents. This supports the TICT model, however, they also suggested, in cases where the planar conformation of ICT states is lower in energy than that of the LE state, and then dual fluorescence can be observed also from the planar structures.

Apart from these two models, rehybridization of the acceptor that results in an ICT state was proposed in 4-dimethylaminobenzonitrile (DMABN) and in 4-dimethylamino-benzethyne [22]. Rehybridized ICT (RICT) state was predicted to have higher energy than TICT state in DMABN, but the reverse order was predicted for 4-dimethylaminobenzethyne. Based on that it was suggested TICT and RICT might compete with each other in DMABN and in 4-dimethylaminobenzethyne RICT was strongly preferred over TICT [23]. However the experimental studies on 4-dimethylaminobenzethyne did not support the RICT model [24,25]. In addition, RICT model could not explain the observed ICT emission with other acceptors [26-34].

1.2.1. Energy of the ICT state

The intensity of the ICT emission depends on the relative energies of the first two excited states. The energy gap between the two excited locally excited state and ICT state depend on the strength of donor and acceptor group [13].

$$E_{ICT} - E_{LE} < 0 \qquad (1.1.9)$$

The energy of the locally excited state can be determined by experiment and that of the ICT state can be approximated by following equation

$$E_{ICT} = IP(D) - EA(A) + C + \Delta E_{sol} \qquad (1.1.10)$$

where IP(D) and EA(A) are ionization potential of the donor moiety and the electron affinity of the acceptor moiety respectively. They reflect the donor capability to release an electron and the acceptor ability to bind it. Transfer of an electron from the donor group to the acceptor moiety causes the formation of both cation and anion which attract each other and thus stabilizes, the system by the Coulomb energy, C. Polar solvent molecules around the cation and anion pair adjust each other in order to increase the electric field thereby stabilizes the system by an amount of ΔE_{sol}.

1.2.2. Effect of polarity and viscosity

According to TICT model, the formation of ICT state involves charge separation, as well as twisting motion of the electron donor [11-13]. An increase in polarity leads to an increase of the rate constant for the formation of TICT state, thus favors it. However, a rise in viscosity lowers the rate constant which retards the formation of TICT state. For molecules containing small rotating group, the TICT process is found to be independent of viscosity even up to moderate viscosity [35-37] and only at very high viscosity friction plays a role [38-40]. On the other hand, for molecules with bulky rotating group the viscosity effect lowers the rate constant at increasing viscosity [41]. The viscosity dependence of TICT emission renders the TICT exhibiting molecules as useful probes for microviscosity [42-47]. On the other hand with increase in polarity, the quantum yield and lifetime of the normal emission decreases monotonically with slight red shift in emission maxima. However with a rise in polarity, the TICT emission monotonically shifts to the red, but the quantum yield initially increases and after reaching a maximum decreases with further increase in polarity [12,13,48-51]. An increase in polarity accelerates the formation of the TICT state; it also affects the nonradiative decay rate from TICT singlets to low lying triplets and or ground state. Since the lowest triplet state does not have an appreciable charge transfer character as TICT singlet state and the dipole moment of DMABN in the TICT state more than that in triplet state [12,13]. Thus with a rise in polarity the preferential solvation of the TICT state decreases the energy gap between the TICT state and the triplet state. According to energy gap law of nonradiative transition [52-53], the rate of ISC from TICT singlet state increases as the singlet-triplet energy gap decreases. Due to enhanced ISC rate from TICT singlet, the triplet yields of DMABN and related molecules increases, as the polarity of the medium increases [54]. Evidently, polarity affects the yield of TICT emission in two opposing ways. While acceleration of the TICT process tends to increase the TICT emission, the increase of non-radiative (ISC) rate from the TICT state tend to decrease it. Due to these opposite effects, the TICT emission exhibits rise and fall behavior with a rise in polarity of the medium.

1.2.3. Effect of hydrogen bonding

Apart from polarity and viscosity, specific hydrogen bonding of solvent with the electron donor or the acceptor is shown to influence the TICT process. Cazeau-Dubroca et al. proposed that the hydrogen bonding of solvents with donor group is responsible for the TICT emission in DMABN and its analogues by forming a pretwisted conformer in the ground state that are essential for the formation of TICT state [55-59]. The Cazeou-Dubroca model was extended to other molecules such as ethyl and methyl esters of *N,N*-dimethylaminonaphthyl(acrylic acid) [60,61]. On the other hand few authors suggested that the hydrogen bonding of the solvent with donor rather inhibits the formation of ICT state [62,63]. Fansi et al. proposed rather it is the hydrogen bonding of the solvent with acceptor, that twisted the acceptor with respect to other moiety that favors the formation of TICT state in 2-(4'-aminophenyl)pyrido, thia-, oxa-, and -imida zoles [64]. But Yoon et al. hypothesized that the H-bonding with the solvent causes the acceptor to adopt a more coplanar geometry with the benzene ring, thereby increasing charge flow from the benzene ring to the acceptor which enhanced the formation of TICT state [65, 66]. Dogra et al. also suggested that the hydrogen bonding of the solvent with acceptor makes the acceptor more planar with benzene thus favors the formation of TICT state in 2-(4'-N,N-dimethylaminophenyl)imidazo[4,5-c]pyridine [67, 68]. Herbich et al. proposed that the hydrogen of solvent with para nitrogen induces TICT emission in 4-(*N,N*-dimethylamino)pyrimidine due to increase in electron withdrawing nature [69]. However recently computational study suggested that the isomer, which is hydrogen bonded with water through dimethylamino nitrogen is responsible for the TICT emission in 4-(dimethylamino)methylbenzoate in gas phase and not the one that is hydrogen bonded through oxygen atom of the acceptor [70].

1.3. Organized media

In recent years a great interest has been developed to study the spectral properties of organic molecules in organized media because of their extensive applications and apparent implications in biological and natural processes [71-80]. Since the TICT emission is highly sensitive to environment and having added advantage of dual emission, ICT emitting molecules are extensively used for the studies in the organized media [81-90]. Organized assemblies such as cyclodextrin, micelle and proteins are microhetergeneous in nature. They are discussed in brief in this section.

1.3.1. Cyclodextrin

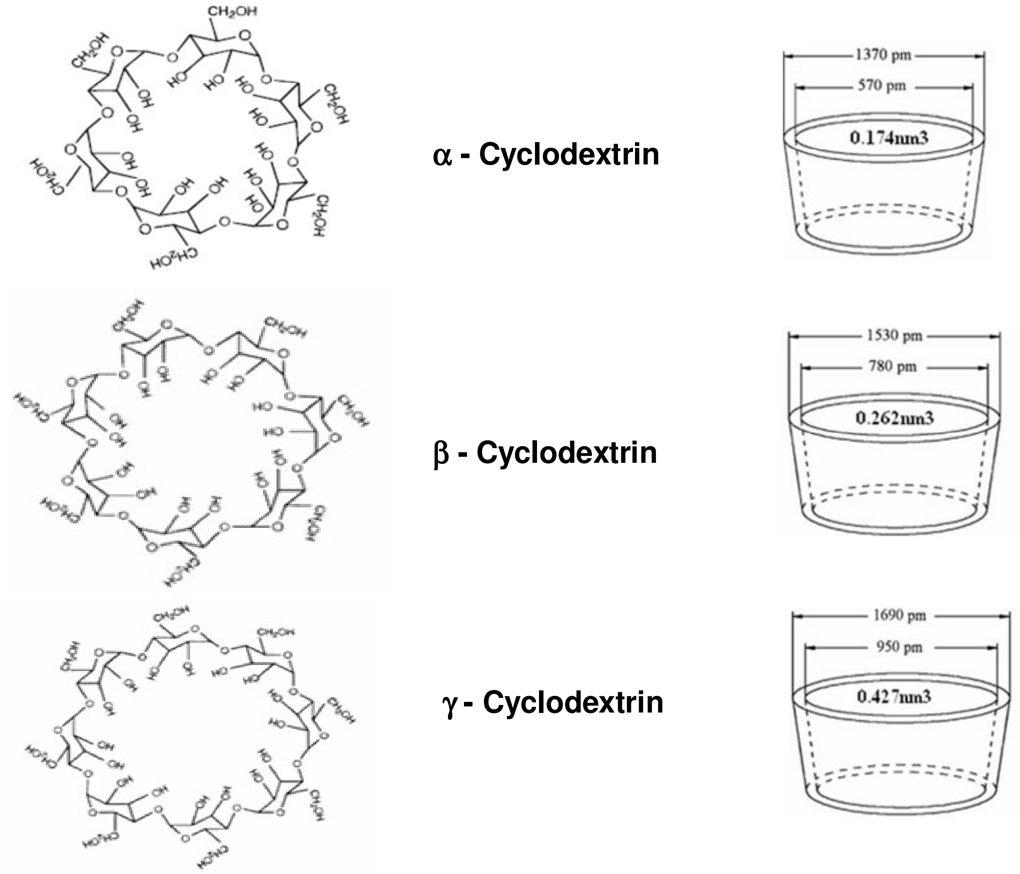

Figure 1.3: Structures of different CDs along with approximate geometric dimensions and cavity volumes.

Cyclodextrin (CD) is a cyclic oligomer of α-D-glucose formed by the action of bacteria such as Bacillus macerans on starch [91-95] and capable of encapsulating a wide range of organic and inorganic molecules [76-106]. Generally three types of cyclodextrins are readily available: α-CD, having six glucose units, β-CD, having seven glucose units, and γ-CD having eight glucoses units (Figure 1.3). The glucose units are connected through glycosidic α-1,4 bonds, as shown in Figure 1.3. As a result of the structural consequence, all the secondary hydroxyl groups are placed on one rim of the ring whereas all the primary hydroxyl groups are situated on the other edge. The ring, in reality is a conical cylinder, which is frequently characterized as doughnut or wreath-shaped truncated cone. The possession of the cavity makes the CDs as attractive medium of study. The exterior of CD is bristling with hydroxy groups and is fairly polar. Whereas the interior of the cavity that is lined with ether oxygens and presents a relatively hydrophobic surface to an incoming guest which enables it to form inclusion complexes with many different such as organic, inorganic, neutral, and ionic molecules. CDs can be considered as empty capsules of a certain molecular size that can include a great variety of molecules in this cavity. Therefore CDs have been studied as “hosts” for “guest” molecules capable of entering (in whole or in part) the cavity and forming noncovalent host-guest inclusion complexes. All the three CDs form inclusion complex in aqueous as well as in nonaqueous solutions with the guest molecules. The inclusion complex formation between host cavity and guest molecule mainly depend on the structure, charge and polarity of the guest, the effect of the reaction medium (solvent) and temperature. The charge and polarity of the guest play also an important role in the CD-substrate host–guest interaction; however, it is less decisive than that of the geometric fitting. The inclusion complex is held together by non-covalent binding forces. The binding of guest molecules within the host CD is not fixed or permanent, but rather it is governed by a dynamic equilibrium thereby affording as ease of assembly and disassembly. The driving forces interacting simultaneously are: (a) hydrophobic interaction, (b) van der waal forces, (c) London dispersive forces, (d) hydrogen bonding, (e) release of high energy water upon guest inclusion and, (f) release of conformational strain in a CD-water adduct. Most frequently the host: guest ratio is 1:1. This is essence of “molecular encapsulation”. However, 2:1, 1:2, 2:2, or even more complicated associations, and higher order equilibria exist, almost always simultaneously. The water solubility of CDs is unusual. β-CD is at least nine times less soluble (1.85 g/100 mL at room temperature) than the others CDs (14.5 g/100 mL and 23.2 g/100 mL for α- and γ-CDs, respectively). The solubility of CDs depends strongly on the temperature. The native CDs apparently undergo self association in aqueous solution [107,108]. The decreased solubility of β-CD in water appears to be due to the marked structure of water arising from water-β-CD interactions, causing a compensation of the favorable enthalpy by the unfavorable entropy of solution [109].

1.3.2. Micelle

Surfactants, amphiphilic molecules that posse both hydrophobic and hydrophilic groups in solutions, with an increase in concentration undergo a spontaneous association of molecules makes aggregates termed "micelles" (Figure 1.4). The concentration at which surfactants start forming micelle is called the "critical micelle concentration (CMC)". With the aid of micelles, surfactants are used as emulsifiers, dispersants, bubbles, antifoams, and detergents. Depending on the nature of the supramolecular assemblies, micelles are classified as (a) normal micelle or (b) inverted micelle.

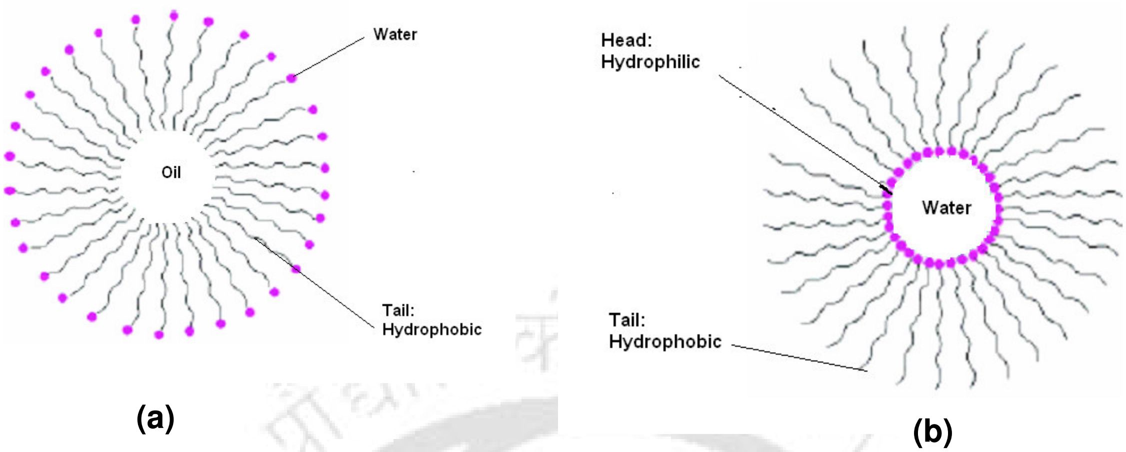

Figure 1.3: Structures of (a) normal micelles and (b) reverse micelles

(a) *Normal or aqueous micelles*

In water, surfactants aggregate in such a way that the interior of the micelle contains the hydrophobic part and the hydrophilic residues are located on the surface and are in contact with water [110,111]. Figure 1.4.a shows that the two dimensional representation of the simplest and the most popular model of a spherical ionic micelle [112]. It is generally assumed that micelles at concentration close to their CMC are roughly spherical. Typically, micelles have average radii of 12 – 30 Å and contain 20 – 100 monomers. Fluorescence and ESR measurements on the rate of rotational reorientation of the probe molecules in micelles indicate that the interior of a micelle can be viewed as being much like a liquid hydrocarbon droplet. Their motion is significantly restricted, indicating a high micro viscosity relative to that in pure organic solvents of low viscosity [113]. The polar head groups are located at the micelle-water interface and are hydrated by a number of water molecules. The polarity at the surface of micellar systems is close to that of ethanol [114]. The surface of micelles formed from ionic surfactants is highly charged. About 80% of these charges are neutralized directly by counterion, forming the Stern layer with a few angstroms of the shear surface. The remainder of the counterions diffuses in Gouy Chaperman layer. The existence of a substantial net charge at the micelle surface provides a large drop in electrical potential across the Stern layer and attracts ions of opposite charges. The amount of water molecules in micelles varies from surfactant to surfactant but it is considered, at present that water molecules penetrate the micellar surface only up to a distance of 3-6 carbon atoms. It has been proposed that micelles are loose porous in which water molecules and hydrophobic regions are constantly in contact with each other. The controversial topic of water penetration into the micelles is still a matter of debate. It is possible to obtain various types of structures by simply increasing the concentration of surfactants in water or by the addition of electrolytes. The increase in number of surfactant molecules leads to the formation of rods or bilayers having cylindrical structure.

A substantial amount of research has been carried out to understand the photophysic and the photochemistry of molecules in micellar solution [115-121]. Incorporation of the molecular probe into the aqueous micelles effectively reveals parameter such as CMC, roughness of the micelle surfaces, polarity, viscosity and degree of water penetration into these surfactant aggregations. Most of the probes have been chosen for their particular affinity for one or two of the principal micellar region: the hydrocarbon core formed from surfactants tails, the interface composed primarily of the amphiphile head groups, or surrounding aqueous solvent phase. Selectively targeting of specific micellar domains has been precisely achieved with the fluorophore such as polycylic aromatic hydrocarbons (e.g. pyrene) [122] with ionic derivatives of aromatic chromophores (e.g. 2-pyrazoline, 4-(2-pyridylazo) resorcinol) [117,121]. However, the probes such as 6-propiorly-2-(dimethylamino)naphalene (prodan) is soluble in an extensive range of media, suggesting the possibility of the simultaneous partitioning of the probe into nearly all the regions of the micelle [123].

(b) Inverted or reverse micelles

In nonpolar solvents, the molecular association of the surfactant monomers occurs in an inverted manner with the polar head groups collected together in an inner core and the hydrocarbon tails spread out into the nonpolar oil phase (Figure 1.4.b). Hence, these aggregates carry the name reverse or inverted micelles. A distinguishing feature of these reverse micelles is their ability to solubilize fairly large amounts of water in polar core.

The structures of reverse micelles depend on the amount of surfactants/co-surfactants/water present in the multi system [124]. The function of co-surfactants is to reduce the repulsion between the polar head groups [125] The degree of hydration in reverse micelles can be controlled by gradual addition of water to the surfactants in organic solvent and hence varying the water/surfactant molar ratio w_0 [126-129]. Two types of water molecules inside the reverse micelles are found viz. motion in bound water and motion in free water. When water molecules are near the interfacial region of reverse micelles, called as bound water, they hydrate the polar head group of molecule. On the other hand, when water molecules remain inside the core of water pool called as core water or free water. By changing the water to surfactant molar ratio (w_0 = $[H_2O]$/ [Surfactant]), the size of water pool in a reverse micelles changes. As the size of the water pool entrapped by the surfactant increases, the microviscosity of the solubilized water decreases and its polarity increases. Addition of water also dramatically increases the average aggregation number of reverse micelles, with little dependence on the hydrocarbon solvent used or the surfactant concentration [111]. With increasing micellar size, its polydispersity increases. Extensive research has been done in order to understand the effect of surfactant-water interaction on the structure and dynamics of encapsulated water molecules [130-141].

Fluorescence technique has also been used to characterize the structure of the reverse micelle [142-152]. Probes employed exhibit a particular affinity for one or more than one of the micellar regions: the water pool, the micellar interface, or the surrounding hydrocarbon solvent phase [111]. For example, 1, 8-anilinonaphthalene sulphonate, pyrenesulphonic acid, rhodamine B, 2,6-toluidinonaphthalenesulphonic acid, auramine and pyranine partition in the aqueous micellar core [153-156]. Indoleactetate ions distribute between the micellar interface and water pools [157]. 1, 2-Dimethylindole remains predominatly in the hydrocarbon phase [158], while pyrene [159] and indole [158] molecules partition into both the hydrocarbon continous phase and the micellar interfacial microphase, where as the microenvironment for prodan [160] include an inner "free" water pool, a bound water region, the micellare phase and the surroundings hydrocarbon solvent phase.

1.3.3. Bovine serum albumin

Proteins are biopolymer molecules that may be distinguished from each other by the difference in amino acid unit sequence which, composes the protein primary structure. This polypeptide chain is transformed into a specific and distinctive three dimensional, folded native state. Protein structure which gives rise to biological function of great, selectivity and variety, depends on hydrophobic, electronic, and steric parameters. Proteins are important for the structure, function, and regulation of cells, tissues, and organs and every protein has a unique function in maintaining life. Serum albumin, the most abundant protein in blood stream, has been one of the most extensively studied proteins for many years. Albumins are accounted for about 60% of total plasma and are identified as major transport proteins [161,162] for many compounds such as fatty acids [163], which are otherwise insoluble in plasma, hormones, bilirubin [164], bile salts [165] and many drugs and protein. They have also capability of binding with metals [166], hormones [157] and a broad spectrum of therapeutic drugs [168,169]. As a multifunctional transport protein albumin is the key carrier of nitric oxide that has been implicated in a number of physiological processes including neurotransmission. As a multifunctional transport protein albumin is the key carrier of nitric oxide that has been implicated in a number of physiological processes including neurotransmission. It plays an important role in regulating the colloid osmotic pressure of blood and provides about 80% of the osmotic pressure and is also responsible for the pH maintenance in blood [170]. Some of these albumins are human serum albumin (HSA), bovine serum albumin (BSA), equine serum albumin (ESA) and rat serum albumin (RSA). BSA is extensively used as a model protein due to its stability, water solubility and versatile binding capacity. In general, albumins are characterized by low tryptophan and high cystine contents. The molecule BSA mainly differs in tryptophan content with respect to human serum albumin (HSA). The 3D structure of BSA is believed to be very similar to HSA, because the two proteins share 76% sequence identity. BSA contains a high content of Asp, Glu, Ala, Leu and Lys residues which is analogous to HSA and RSA. The amino acid compositions of the two proteins (BSA and HAS) are similar. BSA is a relatively large globular protein that is naturally found within the blood and milk of cows. The molecular weight of BSA is 66411 g mol^{-1} and contains 583 amino acids in a single polypeptide chain. The protein BSA contains 17 disulfide bridges and a series of nine loops, assembled in three domains (I, II, III), each containing two subdomains, A and B [171] but the primary binding sites is located in subdomain IIA and IIIA. The presence of one free SH group, which can cause it to form a covalently linked dimmer. There are two tryptophan residues in one BSA molecule: Trp-134 in the eighth helix of D129-R144 in subdomain IA which is more exposed to solvent, and Trp-212 in the second helix of E206-F221 which located in a hydrophobic microenvironment in subdomain IIA [171]. Only the helix of Trp-134 is active to interact with ligand in native BSA. The interior of the protein is almost hydrophobic, while both the charged amino acid residues and apolar patches cover the interface [172-174].

1.4. Scope of the present work

As mentioned earlier (section 1.2.3), the hydrogen bonding of the solvent plays a crucial role in the formation and stabilization of ICT state in number of systems. However researches contradict about the role of hydrogen bonding in ICT process. Nonetheless such a hydrogen bonding may be an important subject in facilitating proton-coupled charge transfer phenomena. The coupling of proton motion to electron transfer is crucial for the most important processes of biological energy conversion: photosynthesis, vision, transmission of the nervous impulses, or respiration. Recently it has been shown that molecules that undergo excited state intramolecular proton transfer, also isomerized via twisted states that have appreciable amount of charge transfer character [175-178]. Though lot of works had been done, the detailed mechanism of proton coupled charge transfer remains unclear in many instances [179-181]. In this respect, the investigation of hydrogen bonding effect on ICT should be extended to other molecules. Thus, we have synthesized and studied the spectral characteristics of 2-(4'-N,N-dimethylaminophenyl)imidazo[4,5-b]pyridine (DMAPIP-b), that capable of emitting hydrogen bond induced TICT emission. Theoretical calculations have been performed to substantiate the experimental results. Fansi et al. reported the formation of only one kind of monocation in their studies on 2-(4'-aminophenyl)-pyrido, -thia, -oxa, and imida zoles [64]. On other hand Dogra et al. showed that 2-(4'-N,N-dimethylaminophenyl)imidazo[4,5-c]pyridine (DMAPIP-c) form to two different monocation of which one of the monocation undergoes proton relay phototautomerism in the excited state to form another monocation [182]. Therefore we have studied the effect of proton to find the influence of the nitrogen position and methylation on the prototropic equilibrium and also to figure the role of protonation site on TICT emission.

The fluorescent molecules capable of luminescence change, responsive to molecular environment, are gaining great interest for their potential applications from typical polarity and viscosity probes [183,184] to more advanced ones including biosensors [185-187], logic gates [188,189], and optical recordings [190]. The emission intensity is also dependent on other factors, such as the sensor/probe concentration, bleaching, optical path length, and illumination intensity. Therefore it is desirable to eliminate the effects of these factors by using a ratiometric sensor. Since DMAPIP-b exhibits dual fluorescence and highly sensitive, to explore its potential application as sensor/probe, we have investigate the effect of different metals and organized assemblies. DMAPIP-b was shown to act as an inhibitor for of Aurora-A, Aurora-B and Aurora-C kinases [191,192]. Thus, it is of biological interest to study the interaction of DMAPIP-b with other proteins. We have studied the interaction of DMAPIP-b and its alkylated derivatives with one of the most common protein, BSA.

Chapter 2

Materials, Methods and Instruments

2.0. Introduction

This chapter contains details of the chemicals and the solvents those are used for the work and the procedures for the synthesis of the fluorophores. The methods used for the analysis, calculations, preparation of the samples are also elaborated in the chapter. The details of the instruments are described in the last section.

2.1. Materials

Fluorophores were synthesized from the commonly available chemicals. Other chemicals and solvents were procured from the chemical companies. Details of are given below.

2.1.1. Solvents

- Acetonitrile (HPLC grade, Spectrochem India)
- Methyl Alcohol (HPLC grade, Rankem India)
- Ethyl Alcohol (ACS grade, Merck)
- Dimethyl formamide (HPLC grade, Rankem India)
- Cyclohexane (HPLC grade, Rankem India)
- Glycerol (AR grade, Rankem India)
- 1, 4-Dioxane (AR grade, Spectrochem India)
- Diethyl ether (HPLC grade, Spectrochem India)
- Toluene (HPLC grade, Rankem India)
- Tetrahydrofuran (HPLC grade, Rankem)

- Chloroform (HPLC grade, Rankem India)
- *n*-Hexane (HPLC grade, Spectrochem India)
- Glycol (AR grade, Rankem India)
- Ethyl acetate (HPLC grade, Rankem India)
- 1-propanol (AR grade, Rankem India)
- 2-propanol (HPLC grade, Rankem India)
- 1-Butanol (HPLC grade, Spectrochem India)
- Isooctane (HPLC grade, Spectrochem India)
- *n*-hexanol (AR grade, Spectrochem India)
- Benzene (HPLC grade, Rankem India)
- H_3PO_4 (AR grade, Rankem India)
- H_2SO_4 (AR grade, Rankem India)
- Water (Milipore water)

All the solvents were tested for spurious fluorescence in the region of measurement before use.

2.1.2. Metal salts

- Lithium perchlorate (95+ %, Sigma Aldrich)
- Sodium perchlorate (≥ 99.0%, Sigma Aldrich)
- Magnesium perchlorate hexahydrate acid (> 99 %, Sigma Aldrich)
- Calcium perchlorate tetra hydrate (99.0%, Sigma Aldrich)
- Barium perchlorate hydrate (≥ 99.0%, Sigma Aldrich)

- Nickel perchlorate hexahydrate (98.0% Sigma Aldrich)
- Zinc perchlorate hexahydrate (98.0%, Sigma Aldrich)
- Cadmium nitrate tetrahydrate (98.0%, Merck)
- Cobalt chloride (98.0%, Merck)
- Mercury chloride (≥ 99.5 % Merck)
- Sodium sulphate anhydrous (≥ 99.5 %, Merck)

2.1.3. Other Chemicals

- 4 -dimethylaminobenzoic acid (98%, Sigma Aldrich)
- 2, 3-diaminopyridine (98%, Sigma Aldrich)
- 1-bromohexadecane acid (≥ 97%, Sigma Aldrich)
- β-cyclodextrin hydrate (β-CD, Sigma Aldrich)
- Triton X-100 (TX-100, 98%, Sigma Aldrich)
- Cetyl trimethylammonium bromide (CTAB, 99% Sigma Aldrich)
- Sodium dodecyl sulfate (SDS, ≥ 98.5%Sigma Aldrich)
- Bovine serum albumin (BSA, 98% Sigma Aldrich)
- Diphosphorous pentoxide (≥ 97%, Merck)
- Sodium hydroxide (≥ 84%, Merck)
- Potassium hydroxide (≥ 84%, Merck)

2.1.4. Synthesis

*2-(4'-N,N-dimethylaminophenyl)imidazo[4,5-b]pyridine. (*DMAPIP-b*)*

DMAPIP-b was synthesized by heating an equimolar mixture of 2,3-diaminopyridine and 4-dimethylaminobenzoic acid in polyphosphoric acid at 230 °C for 4 h as reported for the synthesis similar compounds [193,194]. After 4 h the reaction mixture cooled to 100°, was poured to excess water and neutralized. Reactions were monitored by TLC on silica gel GF_{254} (0.25 mm). The compound was extracted with dichloromethane and further purified by column chromatography followed by recrystallization from methanol and ethanol mixture. Silica gel (60-120 mesh size) was used for the column chromatography. DMAPIP-b was obtained as pale yellow solid. The identities and purity was confirmed by TLC, GC-Mass, FTIR, NMR and X-ray crystallography. NMR peaks were assigned based on the decoupling experiments. NMR details and crystal the data were provided in Appendix I and II respectively (page 193 and 195).

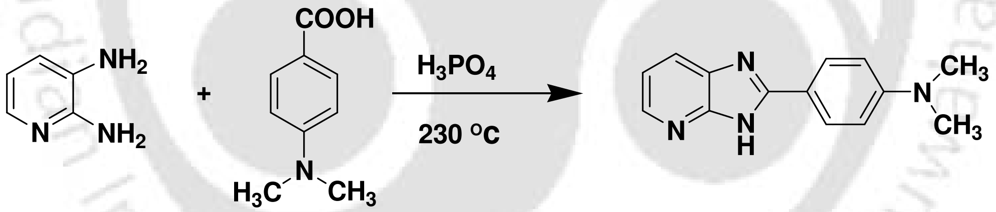

Mass (*m/z)* 239 ([M + H] $^+$, 100)

^{1}**H NMR** (400 MHz, CD3OD), δ: 8.24 (d, 1H, J = 5 Hz), 8.12 (d, 2H, J = 9 Hz), 7.96 (d, 1H J = 8 Hz), 7.14 (dd, 1H, J = 8,5 Hz), 6.74 (d, 2H, J = 9 Hz), 3.05 (s, 6H).

IR (KBr) 3386, 3073, 2902, 1581, 1465 cm^{-1}

*2- [4'-(N,N-diemthylaminophenyl)imidazo[4,5-b]hexadecylpyridinylium bromide (***1***)*:

DMAPIP-b (2 mmol) and 1-bromohexadecane (5 mmol) were completely mixed using ultrasonic bath. The mixture was irradiated intermittently (4 min irradiation with 30 s mixing) in a household microwave oven at 200W for 20 min as reported for the synthesis similar compounds [195]. After irradiation, the mixture was cooled, washed with ether and dried. The compound was purified by column chromatography. Silica gel (60-120 mesh size) was used for column chromatography. The identities and purity was confirmed by TLC, LC-Mass and FTIR spectroscopy.

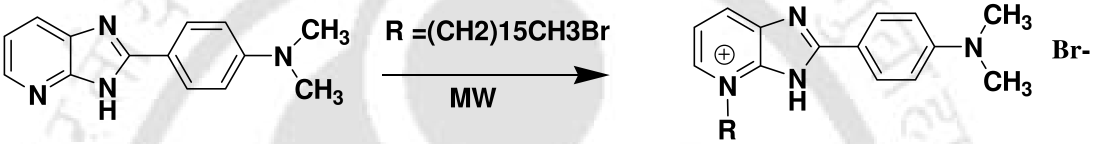

Mass (*m/z)* 463.33 ([M + H]$^+$, 100)

IR (KBr) 3391, 3065, 2922, 1563, 1465 cm^{-1}

1-hexadecyl-2-[4'-(N,N-diemthylaminophenyl)imidazo[4,5-b]pyridine (**2**)

DMAPIP-b (4 mmol) and 1-bromohexadecane (9 mmol) was dissolved in the solvent mixture of 30 ml dimethylformamide and 10 ml tetrahydrofuran. To the above mixture, powered KOH (100 mmol) was added and was heated at 100° C for 24 hour by the procedure reported earlier for alkyl substitution for similar compounds [196]. After 24 hour the compound was extracted with dichloromethane and it was further purified by column chromatography. Silica gel (60-120 mesh size) was used for column chromatography. The identities and purity was confirmed by TLC, FTIR and LC-Mass.

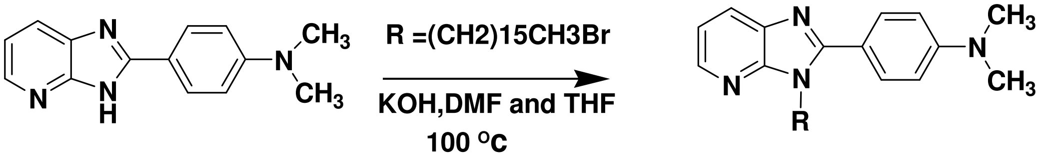

Mass (*m/z)* 463.34 ([M - Br]$^+$, 100)

IR (KBr) 3407, 2922, 2852, 1604, 1464, 1410 cm^{-1}.

2.2. Preparation of Samples

2.2.1. In solvent

A stock solution of the compound of concentration, 1 x 10^{-3} M was prepared in methanol. From the stock solution 50 µl was pipette out to each 10 ml volumetric flask. The solution was kept the in oven for overnight at 50° C in order to remove methanol. After complete removal of methanol 10 ml of different solvent was added to each volumetric flask. For pK_a measurements small amount of H_3PO_4 or NaOH was added to obtain appropriate pH. The final concentration was 5 µM for any absorption or fluorescent measurement unless otherwise mentioned.

2.2.2. Metal solutions

Metal perchlorate solutions were prepared in acetonitrile. Fluorophore was completely dissolved in acetonitrile with sonication and slight warming in a water bath. Metal ion titrations were carried out (by mixing appropriate amount of the metal ion solutions to the fluorophore solution). Spectral measurements were performed at the fluorophore concentration of 5 x 10^{-6} M.

2.2.3. Micelles and cyclodextrin

Surfactant solutions were prepared by dissolving appropriate surfactant (SDS, CTAB or TX-100) in Millipore water. The cyclodextrin solutions were prepared by dissolving desired amount of β-CD in Millipore water. Due to poor solubility of β-CD the solution was heated slightly and kept for some time. The pH of the solutions were adjusted by adding minute quantity of H_2SO_4 or NaOH solution. The fluorescence probe in methanol was completely dried before addition of the surfactant or cyclodextrin solutions. Because of lower solubility of DMAPIP-b in D_2O about 10 % CD_3OD were used for NMR measurements.

2.2.4. Reverse micelles

TX-100/*n*-hexanol/cyclohexane/water reverse micelles were prepared by mixing desired amount of water , n-hexanol-TX-100 (1:4) solution and appropriate amount of cyclohexane. TX-100/benzene/hexane/water reverse micelles were prepared by mixing TX-100 and desired quantity of water in a constant volume ratio of hexane and benzene (7:3). CTAB/isooctane/*n*-hexanol/water reverse micelle was prepared by mixing CTAB in a constant volume ratio of isooctane and *n*-hexanol (9:1). Due to poor solubility of CTAB in isooctane/hexanol mixture, certain known quantity of water was added to make a clear solution. The concentration of CTAB, TX-100 was kept 0.63 M and 0.27 M throughout the experiment respectively. The amount of water present in the system is expressed as the molar ratio between water and the surfactant (w_0). Water was systematically added to the above solution to prepare the reverse micelle to get the desired w_0 value.

2.2.5. Protein samples

10 mM phosphate buffer of pH 7.0 was used to prepare the protein samples. The solutions were mixed thoroughly at room temperature before the spectral measurements. Ligand stock solutions were prepared in 2% methanol because of their lower solubility in water. For FRET experiments, the concentration of BSA was kept constant 10 μM and fluorophores concentrations were varied. For other studies the ligands concentrations were kept constant at 5 μM and BSA concentrations were varied.

2.4. Methods

2.4.1. Quantum yields (ϕ)

The absorption of light results in the formation of excited molecules which can in turn dissipate their energy by decomposition, reaction, or re-emission. The efficiency with which these processes take place is called the quantum efficiency. Quantum yield of fluorescence (ϕ_f) is defined as the ratio of the number of photons emitted to the number of photons absorbed as given by the following equation.

$$\phi_f = \frac{\text{Number of photons emitted}}{\text{Number of photons absorbed}} \tag{2.4.1}$$

Fluorescence quantum yield of a sample (ϕ_s) were determined with respect to that of quinine sulphate in 1N sulphuric acid ($\phi_r = 0.546$) [197] using the equation

$$\frac{\phi_s}{\phi_r} = \frac{I_s A_r n_s^2}{I_s A_s n_r^2} \tag{2.4.2}$$

Where I_s and I_r are the integrated fluorescence area, and A_s and A_r are the absorbance values for the sample and reference respectively. n_s and n_r are the refractive index for the sample and reference solution respectively.

2.4.2. Determination of ionization constant

The pK_a or 'acid dissociation constant' is a measure of the strength of an acid or a base. The pK_a measurements are useful parameters for in understanding the behavior of probe molecules. Different ionic species of a molecule differ in physical, chemical and biological properties and so it is important to find which ionic form of the molecule is present at the site of action. The most familiar Hammettes equation, used for the determination of ionization constant (pK_a) of the dissociation reaction of an acid in aqueous medium is given below.

$$BH^+ + H_2O \rightleftharpoons B + H_3O^+ \qquad (2.4.3)$$

$$H_0 = pK_a + \log\frac{[B]}{[BH^+]} \qquad (2.4.4)$$

Where $[BH^+]$ and [B] are molar concentration of conjugate acid and base respectively. H_0 is called Hammette’s acidity function, which is given by the following reaction

$$H_0 = -\log\frac{a_{H^+} f_B}{f_{BH^+}} \qquad (2.4.5)$$

Where f_B and $f_{BH}{}^+$ are the acidity co-efficient of conjugate base and acid respectively. $a_H{}^+$ is the activity of the proton. For dilute solution H_0 is replaced by pH. A plot of pH versus

$\log\frac{[\mathrm{B}]}{[\mathrm{BH}^+]}$ is a straight line with unit slope and the pH = $\mathrm{pK_a}$ when [B] = [BH^+]. The factor $\frac{[\mathrm{B}]}{[\mathrm{BH}^+]}$ can be determined from following relation.

$$\frac{[B]}{[BH^+]}=\frac{[A_B-A]}{[A-A_{BH^+}]} \tag{2.4.6}$$

Where A_{BH}+ and A_{B} are the absorbance (at the analytical wavelength) of the pure BH^+ and B respectively and A is absorbance (at same wavelength) of any solution in which BH^+ is partially ionized.

$$\frac{[B]}{[BH^+]}=\frac{[B]}{[C]-[B]} \tag{2.4.7}$$

Where [C] = Molar concentration of compound in experimental solution.

$$[B]=\frac{A(\lambda_1)\varepsilon^+_{BH}(\lambda_2)-A(\lambda_2)\varepsilon^+_{BH}(\lambda_1)}{\varepsilon_B(\lambda_1)\varepsilon^+_{BH}(\lambda_2)-\varepsilon_B(\lambda_2)\varepsilon^+_{BH}(\lambda_1)} \tag{2.4.8}$$

ε is molar extinction coefficient. Generally two wavelengths (λ_1 and λ_2) were chosen on both side of isobestic point.

2.4.3. Quantum mechanical calculation

Density functional theory (DFT) is a popular method for ground state electronic calculations. However, calculating molecular parameters for an electronic excited complex molecular system is difficult. Nowadays the configuration interaction singles CIS [198], time dependent DFT (TDDFT) [199, 200] and complete active space self-consistent field (CASSCF) [201,178] methods are very popular computational methods for the excited state electronic structures. Though CASSCF method can better accuracy, it computationally expensive for large systems [202-204]. TDDFT method is good for electronic structure calculations in the excited states for large molecular system due to its moderate efficiency and accuracy [205-208]. But optimization by TDDFT method gives incorrect ordering of energies in few cases [209]. The geometries as well as molecular properties obtained at the CIS level are quite reasonable and correct, at least as a first approximation for a variety of molecules [210, 211]. However it, over estimates the energies in many cases. The TDDFT calculations over CIS optimization has been proven to be an efficient approach in predicting energy parameters for various systems [31, 178, 212-214]. Therefore, we implemented the combined approach of TDDFT over the CIS optimized structures.

Theoretical calculations were performed using Gaussian 03W [215] program to obtain the molecular parameters. The ground state geometries of the complexes were obtained by full optimization of structural parameters using DFT employing 6-31G(d,p) basis set using spin restricted shell wavefunctions [216,217]. The geometry optimizations were carried out using Becke's three-parameter hybrid functional B3, with nonlocal correlation of Lee-Yang-Parr, LYP, abbreviated as B3LYP [218,219]. The minimum energy nature of the stationary points was verified from vibrational frequency analysis. The excitation energies for different species were obtained by single point calculation using the ZINDO [220] or TDDFT [199] method. The geometry optimization was carried out in the first excited state using the ab initio restricted configuration interaction singles method. Further from the relaxed geometry in the first excited state emission transition energy was calculated by TDDFT [199] or ZINDO [220] method. Since ZINDO calculations were found to very good in predicting vertical transition energies [220] we used also ZINDO method to calculate the transition energies.

2.5. Instruments

2.5.1. Absorption Measurements

Absorption spectroscopy is the most widely used spectroscopic tool which provides the wavelength of a transition and the corresponding molar extinction coefficient (ε_λ) of a chromophore under investigation. The modern ultra-violet-visible spectrometers consist of light source, monochromator, detector, amplifier and recording devices. Quartz cells are used for the measurement of the absorption spectra.

In the present work, absorption spectra were recorded on Perkin Elmer Lambda 25, Cary 50 and Cary 100. Lamda 25 and Cary 100 are double beam spectrometer and Cary 50 is a single beam spectrometer. Deutrium and tungsten lamps are used as UV and visible sources respectively in all the three instruments. However, Perkin Elmer use silicon diode detector and Cary instruments use PMT detector.

2.5.2. pH measurements

The pH of different solutions were measured using Jenway (model No 3510) pH meter. The pH meter was calibrated by using three different standard buffer solutions (pH 4, pH 7 and pH 10) within a range of ± 0.01 – 0.02 pH units before a measurement.

2.5.3. Steady state fluorescence measurements

Fluorescence spectra were recorded on Edinburgh Instruments FSP 920, Cary Eclipse and Jobin Yon Spex Fluoromax 4 instruments. Description of FSP 920 instrument is shown in Figure 2.1.

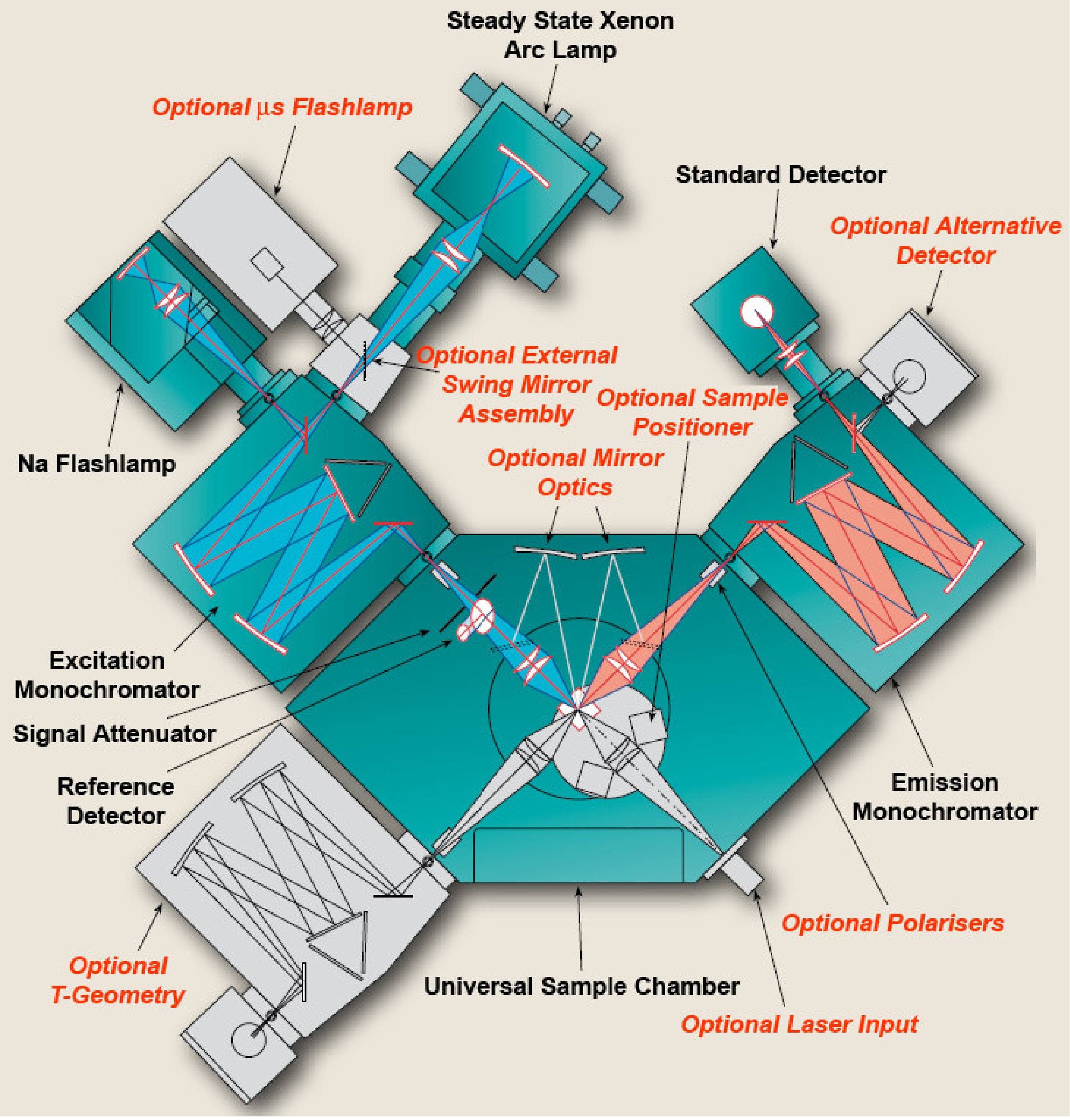

Figure 2.1.Block diagram of Edinburgh FSP 900 steady state fluorescence spectrophotometer.

Optical System

The most common light source for fluorimeters are xenon arc lamps. These lamps provide a relatively uniform intensity over a broad spectral range from the ultraviolet to the near infrared. A monochromator is used to select the excitation wavelength. Fluorescence is collected at right angles with respect to the incident beam and the detected through a monochromator by a photomultiplier. Motorized monochromator is used for automatic scanning of wavelengths. The monochromators are controlled by the electronic devices and the computer. The optical module contains various parts: a sample holder, shutters, polarizers if necessary, and a beam splitter consisting of a quartz plate reflecting a few percent of the exciting light towards a quantum counter or a photodiode.

The emission spectrum reflects the variations of fluorescence intensity as a function of λ_{em} (the wavelength at which the fluorescence is observed) and the excitation wavelength (λ_{exc}), is fixed. The excitation spectrum shows the variations of fluorescence intensity as a function of λ_{exc} with fixed λ_{em}. The spectra are recorded as a function of wavelength and not wavenumber because the monochromators of spectrofluorometers are equipped with gratings, so that for a given width of the input and output slits, the monochromators operate at a constant bandpass expressed in wavelength.

The fluorescence spectra have to be corrected for the distortion by the wavelength dependence of several components of the instrument.

Correction for emission spectra

The emission spectrum is distorted by the wavelength dependence of the emission monochromator efficiency and the photomultiplier response. In general, the correction factors are measured by the manufacturer using a calibrated tungsten lamp or by a standard fluorescent dye whose corrected emission spectrum has been reported. Emission correction factors are provided by the manufacture in the entire three instruments.

Correction for excitation spectra

The excitation spectrum is distorted by the variations of the intensity of the exciting light. These variations are due to the wavelength dependence of the lamp intensity and of the transmission efficiency of the excitation monochromator. Because the quantum counter circumvents the wavelength dependence of the sensitivity of the reference photomultiplier, the ratio of the fluorescence signal from the sample to that from the quantum counter or photodiode, as a function of the excitation wavelength, provides in principle corrected excitation spectra. However, such correction procedures may be insufficient when very accurate measurements are needed (for instance when information is expected from the comparison of the absorption and excitation spectra). In fact, the optical geometry of the reference channel is not identical to that of the main channel, and the wavelength dependence of optical parts (e.g. focal length of lenses) may introduce some distortion into the excitation spectrum. It is then recommended to use correction factors obtained by using a fluorescent compound absorbing in the same wavelength range as that of the sample to be studied, and whose absorption spectrum is identical to its excitation spectrum. The ratio of the measured excitation spectrum of this reference compound – as described above using the quantum counter – to the absorption spectrum provides the correction factors that can be stored in the computer. Spectrofluorometers equipped with a photodiode instead of a quantum counter provide excitation spectra that should be further corrected because, in addition to the reasons explained above, the wavelength response of the photodiode is not strictly flat over the whole wavelength range available. It should be noted that most commercially available instruments are delivered with a file containing the correction factors and the manufacture provided the correction file for all three molecules.

FSP 920 is equipped with double excitation monochromator and the other instruments used for the measurement have single excitation monochromator. FSP 920 and Fluoromax 4 have 450 W and 150 W Xe arc lamps respectively as light source. But Cary Eclipse employs 75 W pulsed Xe lamps as light source.

2.5.4. Fluorescence Lifetime Measurements

The most common technique to measure the fluorescence lifetime is time correlated single photon counting (TCSPC) method (Figure 2.2). The TCSPC method is generally used to measure the relaxation time of molecules from the electronic excited state to its ground state. Since the molecules emit photons at different relaxation times following their excitation by radiation, the decay time of single molecules must have a certain rate rather than occurring at a specific time with excitation. The principle of TCSPC is the detection of single photons and the measurement of their arrival times in respect to a reference signal from the light source. The TCSPC needs a high repetitive light source to accumulate a sufficient number of photons since this is a statistical method and required many numbers of statistical data precision. The time measurement of the start and stop sequence will be represented by an increase of a memory value in a histogram. Thus, this experiment must be repeated many times to gather the sufficient

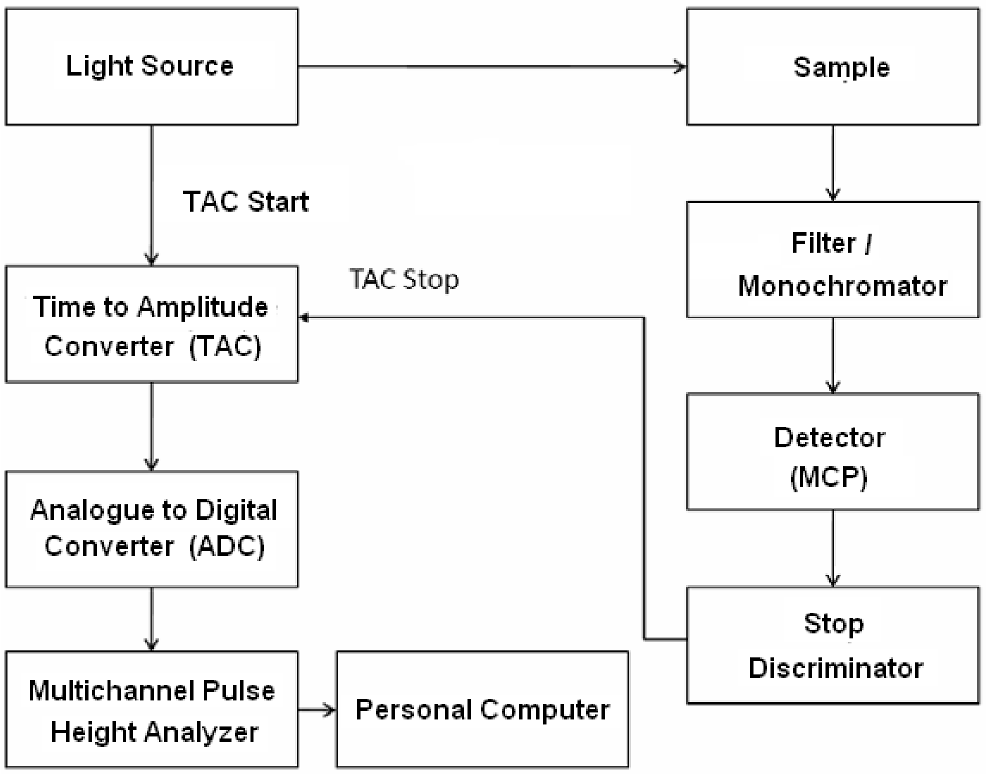

Figure 2.2. Block diagram of the time-correlated single photon counting (TCSPC)

photons in the full range of delays between excitation and emission. The resulting histogram counts versus the time channels on the x-axis will represent the curve of fluorescence decay profiles. Generally, the TCSPC method is composed with the start signal pulse and the stop signal pulse, which splits from a light source beam into two paths. One path travels to a photomultiplier tube (PMT) or micro-channel plate (MCP) photomultiplier, which activates a time-to-amplitude converter (TAC) and is used as a starting signal. Meanwhile, the other path travels through the sample and works as a stop signal. Then, the growth of ramp signal in TAC is stopped by this pulse. The TAC output can be amplified by an amplifier, and this analogue pulse of height corresponding to a measured time of the signal goes through further processing to convert to the digital pulse through the analogue to digital converter (ADC). In most cases, the TCSPC technique has limits for the temporal resolution and lifetime range measurable for the fluorescence lifetimes. Therefore, for the curve fittings, the method involving linearization of the fitting function and least-squares fitting is the most widely used deconvolution technique. The fluorescence temporal profiles were derived by deconvolution procedures with the instrument response using nonlinear least-squares fittings.

In our experiment fluorescence lifetimes were measured with the use of Jobin Yon Spex Fluorocube or Edinburgh Lifespec II instruments. The Fluorocube instrument employs a TBX-04 detector with jitter timing of 250 ps FWHM or better IBH 375 nm LED was used for excitation and emission intensity was recorded using 420 nm Scotch cut-off filter. Lifespec II employs 375 nm laser diode from Edinburgh, that has pulse width of 2 ps was used as to exite the sample. Lifespec II employs Hamamatsu MCP detector that has response time of 50 ps. When fluorescence lifetime was measured in Edinburgh Lifespec II, the fluorescence decay was analyzed by tail fitting method using software provided by Edinburgh. On the other hand when fluorescence lifetime was measured Jobin Yon Spex Fluorocube, the fluorescence decays were analyzed with the reconvolution method using software provided by IBH.

2.5.5 Other instruments

Fourier transform-infra red (FT-IR) spectra were recorded on Nicolet Impact-410 instrument in KBr pellets. FT NMR spectra were recorded in $CDCl_3$ or D_2O with tetramethylsilane as the standard for ^1H (400 MHz) on Varian instrument. Crystal Data were collected with Bruker Smart Apex-II CCD diffractometer using graphite monochromated MoK$_\alpha$ radiation (λ = 0.71073 Å) at 298 K. Cell parameters were retrieved using SMART software and refined with SAINT on all observed reflections. Data reduction was performed with the SAINT software and corrected for Lorentz and polarization effects. Absorption corrections were applied with the program SADABS. The structure was solved by direct methods implemented in SHELX-97 program and refined by full-matrix least-squares methods on F^2. All non-hydrogen atomic positions were located in difference Fourier maps and refined anisotropically. The hydrogen atoms were placed in their geometrically generated positions.

Chapter 3

Effect of homogeneous media on the dual fluorescence of 2-(4'-*N,N*-dimethylaminophenyl)imidazo[4,5-*b*]pyridine

3.0. Introduction

Chapter 3 is divided into four sections. The effect of solvent and pH, temperature and metal ions on the photophysics of DMAPIP-b (Chart 3.0) is discussed in the first three sections of the chapter. The effect of adding long alkyl chain on the photophysics of DMAPIP-b is presented in the last section of this chapter.

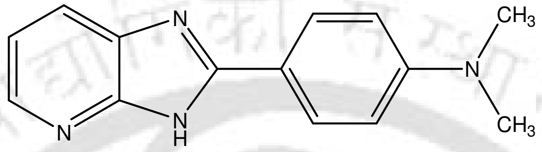

Chart 3.0. Structure of DMAPIP-b

3.1. Effect of solvents and pH

As discussed earlier (Section 1.5) the role of hydrogen bonding on the TICT processes was not early understood. Therefore, we first investigated DMAPIP-b in homogeneous solvent and pH to understand its spectral characteristics especially the role of H-bonding on its TICT emission.

3.1.1 Absorption spectra

Absorption spectra of DMAPIP-b were recorded in different solvents and the observed long-wavelength band maxima along with log$\in_{\max}$ are compiled in Table 3.1.1. Unlike aromatic amines, the absorption spectrum shifts to the red with increasing polarity and H-bonding capacity of the solvent (except in water). The spectra are also red-shifted relative to those of the related unsubstituted amino derivative, 2-(4'-aminophenyl)imidazo[4,5-b]pyridine (APIP-b) [64]. These spectral characteristics and

Table 3.1.1: Absorption band maxima (λ_{max}^{ab}, nm), log $\in_{max}$, fluorescence band maxima (λ_{max}^{fl}), and lifetimes (τ, ns) of DMAPIP-b in different solvents.

Solvent	λ_{max}^{ab} (log $\in_{max}$)	λ_{max}^{fl}	τ (ns)	
			λ_{coll} > 385 nm	λ_{coll} > 420 nm
Cyclohexane	336, 352 (sh)	359, 379, 398	1.99	
Dioxane	340 (4.52)	383	2.30	
Ether	336 (4.49)	374 (sh), 385	1.31	
Ethylacetate	338 (4.49)	390	1.28	
Acetonitrile	345 (4.50)	407	1.50	
Dimethyl formamide	346 (4.50)	428	1.49	
2-Propanol	346 (4.49)	408	0.71 (24.22)	0.85 (21.05)
			2.27 (75.78)	2.07 (78.95)
1-Butanol	348 (4.47)	407	0.98 (42.48)	1.14 (28.94)
		475	2.45 (57.52)	2.67 (71.06)
1-Propanol	349 (4.48)	410	0.90 (24.22)	1.20 (21.05)
		486	2.27 (75.78)	2.53 (78.95)
Ethanol	350 (4.48)	413	0.71 (24.22)	0.85 (21.05)
		494	1.95 (75.78)	2.07 (78.95)
Methanol	350 (4.50)	414	0.29 (67.70)	0.31 (56.50)
		506	1.12 (32.30)	1.16 (43.50)
Glycol	358 (4.50)	428	0.48 (78.17)	0.47 (67.12)
		526	1.11 (21.83)	1.05 (32.88)
Glycerol	360	446		
Water (pH 9.0)	345	451		0.16 (98.75)
				2.13 (01.25)
Water (pH 4.0)	386	451		

the large extinction coefficients of DMAPIP-b are similar to those of DMAPIP-c [67] and 2-(4’-N,N-dimethylaminophenyl)benz- oxa-, thioa- and imidazole [221-222]. The absorption band maxima of DMAPIP-b (Table 3.1.1) are also red-shifted relative to DMAPIP-c [67]. Based on these results it may be concluded that the long wavelength absorption band is due to a π→π* transition. The larger red shifts in the long wavelength band maxima of DMAPIP-b relative to DMAPIP-c suggest a more pronounced charge transfer interaction in DMAPIP-b than in DMAPIP-c.

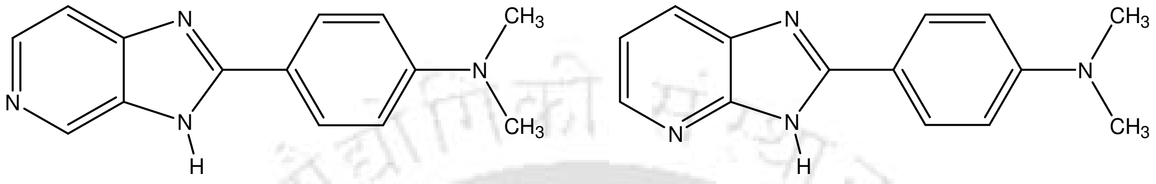

DMAPIP-c **DMAPIP-b**

Chart 3.1.1. Structures of DMAPIP-c and DMAPIP-b.

Table 3.1.2: Theoretical parameters obtained from the optimized geometry of neutral DMAPIP-c, DMAPIP-b and monocations of DMAPIP-b along with experimental excitation energy.

	Neutral DMAPIP-c	**Neutral DMAPIP-b**	**Pyridine N-atom protonated DMAPIP-b**	**Imidazole N-atom protonated DMAPIP-b**
Energy (a. u.)	-751.878	-751.886	-752.278	-752.300
Phenyl ring/NMe_2 dihedral angle	0.0°	0.0°	0.0°	0.0°
Phenyl/PI dihedral angle	0.0°	0.0°	0.0°	0.0°
charge on pyridine nitrogen	-0.690	-0.716	-	-
charge on dimethylamino nitrogen	-0.955	-0.844	-	-
μ_g (D)	7.2	4.5	10.7	2.6
Theoretical excitation energy (eV)	3.82	3.67	3.00	3.05
Experimental excitation energy (eV)	3.80	3.69	-	3.21

The ground state geometries of DMAPIP-c, DMAPIP-b and of protonated DMAPIP-b molecules (Chart 3.1.1) were optimized by RHF/3-21G method using Guassain 03 software [215]. The excitation energies for different species were obtained by single point calculation using the RZINDO/STO-3G method. The theoretical data along with experimental excitation energies are compiled in Table 3.1.2. The theoretical and experimental excitation energies are in reasonable agreement with each other. The *ab initio* calculations suggest that the donor (dimethylamino group), the phenyl ring and the acceptor (IP moiety), are coplanar in the ground state. The calculations predict also that the electron density on the dimethylamino nitrogen is less in DMAPIP-b than in DMAPIP-c and that on the pyridine nitrogen is more in DMAPIP-b than in DMAPIP-c. This indicates the electron densities on the nitrogen atoms are strongly perturbed by the position of the pyridine nitrogen.

3.1.2 Fluorescence Spectra

Fluorescence band maxima in all solvents used in this work are compiled in Table 3.1.1 and selected spectra in representative solvents are shown in Figure 3.1.1. As previously reported for DMAPIP-c [67], the fluorescence spectrum of DMAPIP-b is structured in cyclohexane and vibronic structure is lost as the polarity and H-bonding capacity of the solvent increases. The Stokes shift observed in cyclohexane is quite small. Thus the geometries of DMAPIP-b in the ground state and the first excited state are not very different. The same conclusion had been reached for DMAPIP-c. However the fluorescence spectra of DMAPIP-b are more red-shifted than those of DMAPIP-c, indicating a better charge transfer interaction. This is supported by the large change in

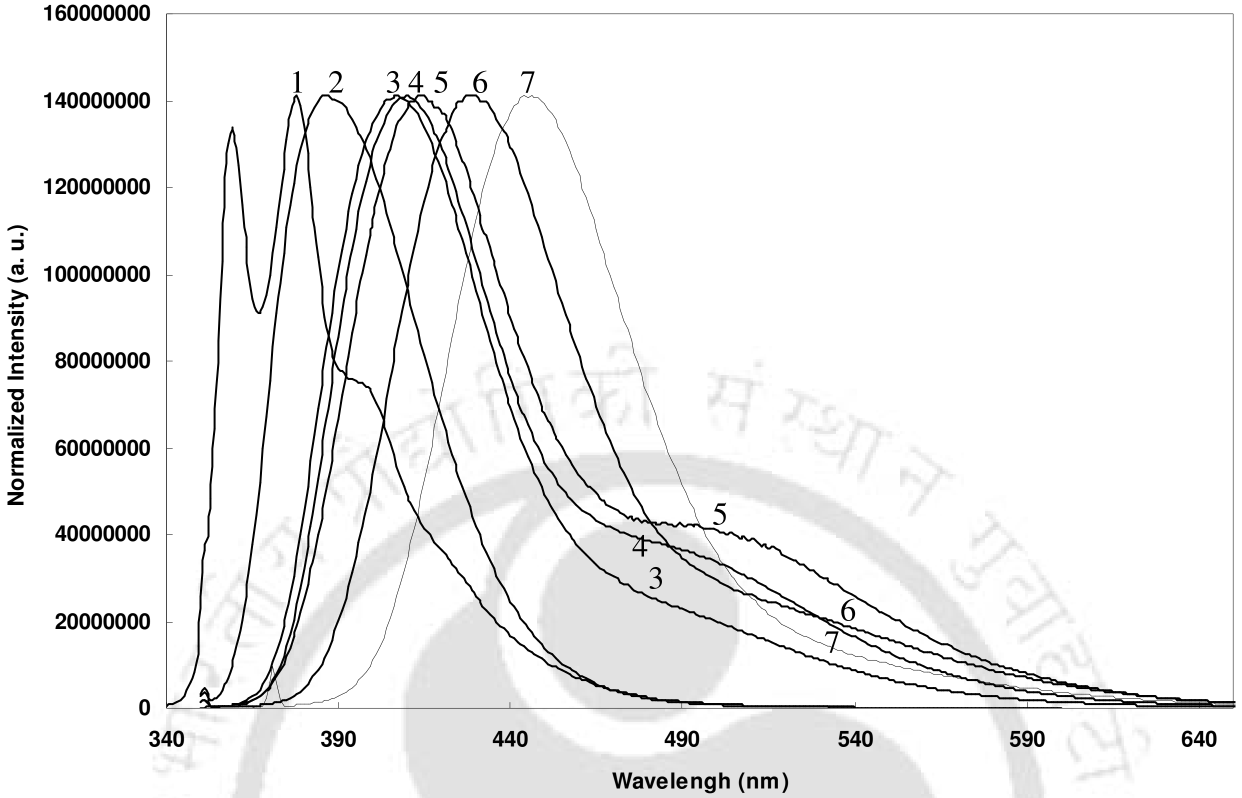

Figure 3.1.1: Fluorescence spectra of DMAPIP-b in cyclohexane (1), ethylacetate (2), 2-propanol (3), 1-propanol (4), methanol (5), ethylene glycol (6) and glycerol (7).

dipole moment (μ_e - μ_g) calculated by Lippert-Mataga plot [223] for DMAPIP-b (7.1 D) than that calculated for DMAPIP-c (5.3 D) [67]. The Lippert-Mataga plot [223] was constructed for DMAPIP-b (Figure 3.1.2) using the relation

$$\bar{\nu}_{SS} = [2(\mu_e - \mu_g)/hca^3]\ \Delta f + \text{constant} \qquad (3.1.1)$$

where $\bar{\nu}_{SS}$ is the Stokes shift, μ_g and μ_e are dipole moments in ground state and excited state respectively, a is Onsager cavity radius, Δf is the orientation polarizability defined as

$$\Delta f = [(\varepsilon - 1) / (2\varepsilon + 1)] - [(n^2 - 1) / (2n^2 + 1)] \qquad (3.1.2)$$

where ε and n are solvent dielectric constant and refractive index respectively. As the Lippert-Mataga equation only takes into account dipole-dipole interactions and neglects polarizability effects, deviations are observed in some solvents. Using 5.2 Å for the Onsager radius of DMAPIP-b and the ground state dipole moment (μ_g), obtained by geometry optimization using the RHF/3-21G method, the Lippert-Mataga plot gives 7.4 D for the excited state dipole moment.

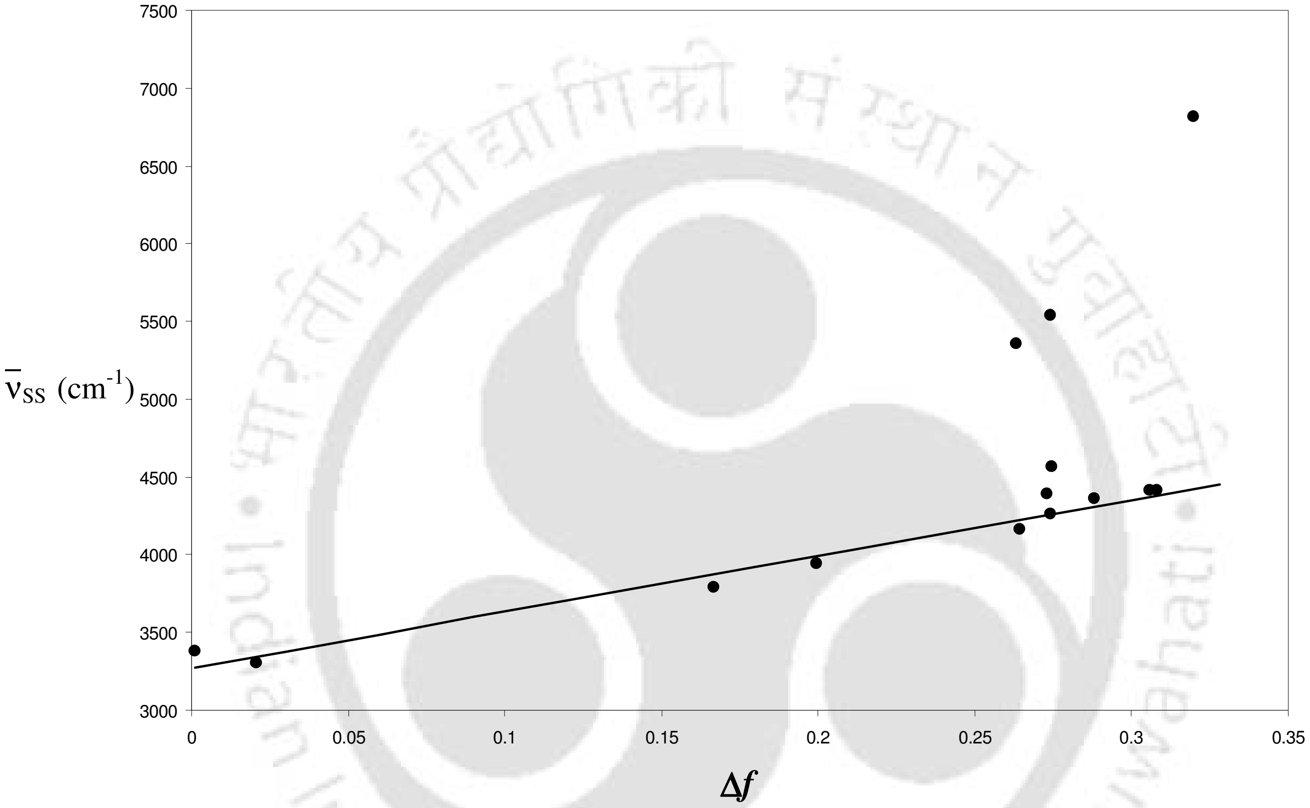

Figure 3.1.2: Lippert-Mataga plot for DMAPIP-b.

Dual emission is observed only in protic solvents and the ratio of shorter wavelength to longer wavelength emission increases with increasing H-donating capacity of the solvent (Figure 3.1.1), except in water. In water no shoulder for the longer wavelength emission is detected. Relative to DMAPIP-c [67] the longer wavelength emission in DMAPIP-b (Table 3.1.1) is shifted to red. The fluorescence intensity is also enhanced enormously. For example, in 1-butanol, 1-propanol, 2-propanol and ethanol, in addition to the shorter wavelength emission band, the longer wavelength band is easily observable in the fluorescence spectra of DMAPIP-b. In contrast the longer wavelength emission band of DMAPIP-c is completely buried underneath the shorter wavelength emission band in these solvents [67]. This shows that the longer wavelength emission is strongly influenced by the position of the pyridine nitrogen. To determine the influence of viscosity, we studied the fluorescence spectra of DMAPIP-b in glycol and glycerol. In glycol the intensity ratio of longer wavelength emission band to shorter wavelength emission band decreases, and in glycerol the longer wavelength emission is completely buried underneath the shorter wavelength emission (Figure 3.1.1).

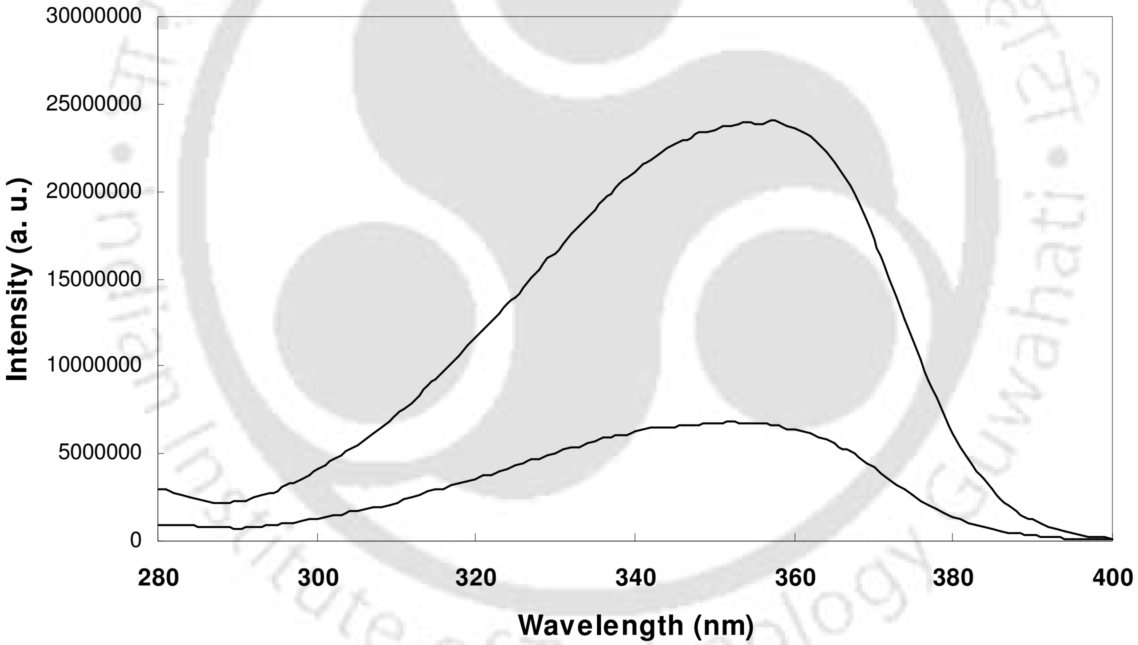

Figure 3.1.3: Fluorescence excitation spectra of DMAPIP-b in methanol at λ_{em} 420 nm and 500 nm.

The fluorescence excitation spectra, recorded for each emission band (Figure 3.1.3) suggest that both states have the same ground state precursor. The DMAPIP-b excited state fluorescence decay is single exponential in aprotic solvents and biexponential in protic solvents (Table 3.1.1). In protic solvents the relative quantum yield of the long-lived species increases when emissions are monitored above 420 nm (λ_{em} > 420 nm) compared to monitoring above 380 nm (λ_{em} > 380 nm). It follows that the shorter wavelength emission corresponds to a short-lived species and the longer wavelength emission corresponds to a long-lived species. The relative amplitude of the long-lived species is negligible in water consistent with observation of a single emission band in that solvent. The lifetime of the shorter wavelength emission is attenuated in protic solvents compare to aprotic solvents.

Dual fluorescence is observed in donor and acceptor substituted benzene derivatives due to formation of an ICT state [224, 225]. ICT state emitting species is assumed either to have a twisted geometry [12, 20, 226], where the donor and the benzene ring are perpendicular to each other, or to have a planar geometry [14, 227, 21], where the torsional angle between the donor and benzene ring is close to 0°. In most molecules the shorter wavelength emission originates from the locally excited state and the longer wavelength is due to the formation of either TICT or PICT states. Recently Haas et al. based on theoretical calculations predicted that, depending on the molecular structure, dual emission may arise from any two of these states [22]. The shorter wavelength and longer wavelength fluorescence in DMAPIP-b can be assigned to the emission from locally excited and TICT states respectively, based on the following observations. (i) The calculated ground state optimized geometry of DMAPIP-b suggests that the molecule is planar. (ii) The Stokes shift observed in cyclohexane is small, suggesting similar geometries of DMAPIP-b in the S_0 and S_1 states (iii) the relative intensity of the longer wavelength emission decreases with increasing protic solvent viscosity, suggesting the presence of a viscosity depended barrier in the formation of the ICT state. Such behavior is also observed in other TICT emitting molecules [12, 76, 45, 228-229].

As indicated earlier, in addition to polarity and viscosity effects, H-bonding may play a role in promoting formation of TICT states. However, we did observed no excitation wavelength dependence in the intensity ratio of TICT emission to normal emission of DMAPIP-b. The excitation spectra recorded at both emission maxima are also identical (Figure 3.1.3). Therefore, involvement of a pre-twisted conformer, formed by H-bonding of the solvent with the donor moiety proposed by Cazeau-Dubroca et al. for dialkylamino benzonitriles [55] can be ruled out in the present case. Since in DMAPIP-b, the benzene ring and the acceptor (PI moiety) are already coplanar (Table 3.1.2), in S_0, planrization of benzene and acceptor through hydrogen bonding of the solvent with acceptor and being responsible for origin of TICT emission (the model adopted for DMAPIP-c [67]) can also be excluded. Nonetheless, we speculate that H-bonding between the protic solvents and the non-bonded electron pair at the pyridine nitrogen plays an important role in the formation of the TICT in DMAPIP-b. This is supported by the following facts (i) H-bonding induced TICT emission is observed only in DMAPIP-b and in DMAPIP-c [67] and not in (*N,N*-dimethylaminophenyl)benzimidazole [221], where the pyridine nitrogen is absent. (ii) When the imidazole nitrogen is protonated no TICT emission is observed in DMAPIP-b (Section 3.1.3) and also in DMAPIP-c [225]. On the other hand, TICT emission is observed in DMAPIP-c only when the pyridine nitrogen is protonated [225]. (iii) H-bonding induced TICT emission is also reported in 4-dialkylaminopyrimidines and the formation of the TICT is attributed to ground state H-bonding at one of the pyrimidine nitrogen atoms [62, 63]. Furthermore it was shown that in 4-dialkylaminopyrimidines the decay of the TICT emission is mono-exponential whereas that of the normal fluorescence is multi- or non-exponential. However, our system differs because in DMAPIP-b both emissions exhibit mono-exponential decay. Instrumental limitations prevented us from measuring the rate of TICT state formation from the locally excited state and the reverse. But the different lifetimes observed for the two emissions show that equilibrium between these states is not established. This may due to stabilization of the TICT state by H-bonding at the pyridine nitrogen which should increase the activation barrier for the reverse process. The same behavior was observed for *p*-diethylaminobenzoic acid and DMAPIP-c, where similar H-bonding between the solvent and the acceptor moiety has been proposed [65, 67]. The absence of TICT emission in water can be explained as follows. The highly polar TICT state can be stabilized by strong dipole-dipole interaction and/or by high H-bonding capacity of solvent. In water it seems that the stabilization of the TICT state is large and thus increasing the rate of non-radiative transitions to the ground and/or low-lying triplet state [67, 230].

3.1.3 Effect of pH

DMAPIP-b absorption band maxima shift to the red on decreasing the pH of aqueous solutions from 9 to 4, with an isosbestic point at ~ 365 nm (Figure 3.1.4). This indicates that an equilibrium is established between the neutral (N) and the monocation (MC) of DMAPIP-b and using the Henderson equation, the pK_a of the equilibrium was determined as 5.4. In contrast, decreasing the pH diminishes the intensity but causes no shift in the fluorescence spectrum of DMAPIP-b (Figure 3.1.5, Table 3.1.1). This establishes that the initially excited state does not emit, leading instead to a common emitting state.

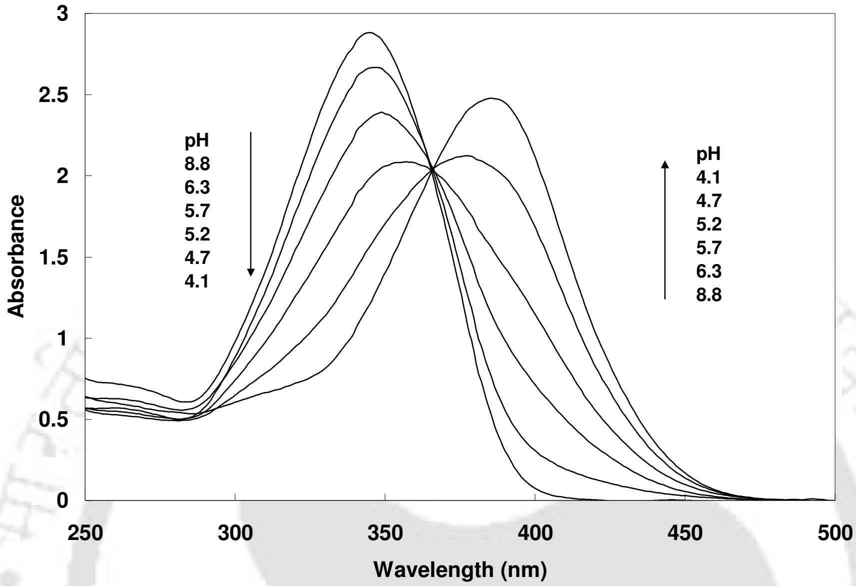

Figure 3.1.4: Effect of pH on absorption spectrum of DMAPIP-b.

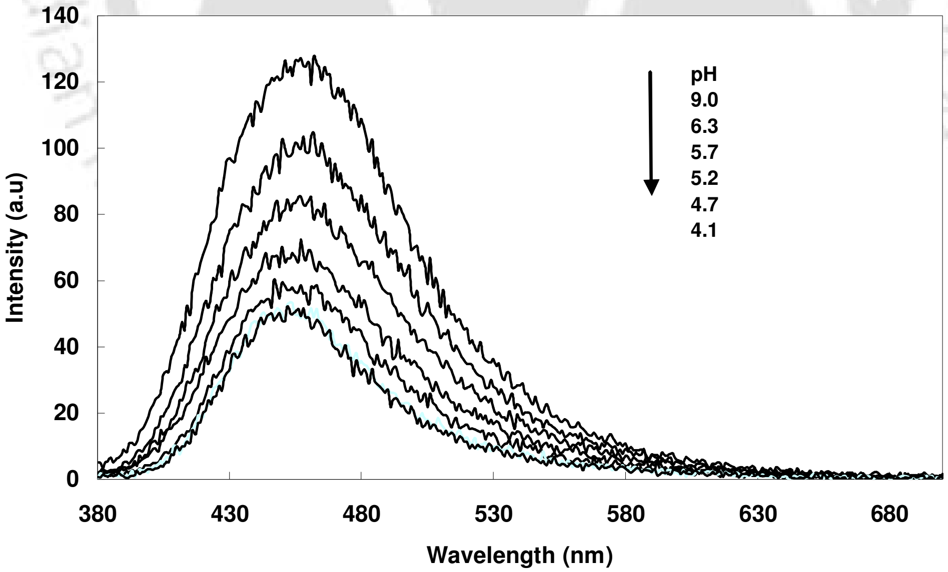

Figure 3.1.5: Fluorescence spectra of DMAPIP at different pH in water.

As in DMAPIP-c, DMAPIP-b also has three basic centers: the dimethylamino nitrogen, the imidazole nitrogen and the pyridine nitrogen. In DMAPIP-c protonations occur at the dimethylamino and the pyridine nitrogen atoms yielding two kinds of MCs in the ground state. However, in the first excited state, the $–NMe_2H^+$ group is deprotonated in favor of protonation of the imidazole nitrogen atom via biprotonic phototautomerism. The normal emission of the pyridine nitrogen protonated MC was quenched due to faster competing nonradiative processes and only the TICT emission was observed [182]. It is well established that when the $\pi\pi^*$ state is the lowest lying state, protonation of either ring nitrogen causes a red shift whereas protonation on the dimethylamino nitrogen leads to a blue shift [231]. The red shift observed in absorption spectra indicates that one of the ring nitrogen is protonated. We favor protonation of the imidazole nitrogen based on the following facts. The pK_a value for the N-MC of DMAPIP-b is 5.4, close to 5.6 and 5.2, the pK_a values of 2-(4'-*N,N*-dimethylaminophenyl)benimidazole [221] and 2-phenyl benzimidazole [232], respectively. In both these molecules the imidazole nitrogen is protonated. The small differences between the pK_a values of the three imidazoles can easily be understood because in DMAPIP-b, the presence of the electron donating $–NMe_2$ substituent increases the charge density at the imidazole nitrogen relative to 2-phenylbenzimidazole and the electron withdrawing pyridine ring has the opposite effect relative to 2-(4'-*N,N*-dimethylaminophenyl)benzimidazole. On the other hand the pK_a reported for the pyridinium ion in DMAPIP-c is considerably higher (6.45) [182]. Furthermore, the absorption maxima obtained for the MC are in better agreement with the theoretical excitation energies predicted by the ZINDO method for the imidazolium than for the pyridinium ion (Table 3.1.2). The fluorescence spectrum of DMAPIP-b at pH 4.0

can be assigned to the same MC that is present in the ground state. The fluorescence spectral characteristics of the MC of DMAPIP-b i.e. band positions and small fluorescence intensity relative to corresponding values for the neutral form, are consistent with imidazole protonated DMAPIP-b. The same behavior is also observed for DMAPIP-c, when the imidazole nitrogen atom is protonated in the excited state.

3.1.4. Conclusion

Dual fluorescence is observed in DMAPIP-b only in protic solvents. The intensity of the longer wavelength emission of DMAPIP-b increases with increasing H-bond donating capacity of the solvent but decreases in water. Experimental results suggest that the H-bonding of the solvent with pyridine nitrogen atom increases the charge flow thus facilitating the formation of the TICT state. TICT emission is enhanced in DMAPIP-b relative to DMAPIP-c. Thus the H-bonding induced emission of the DMAPIPs is strongly influenced by the position of the pyridine nitrogen. The TICT and normal emissions have different lifetimes in DMAPIP-b. This indicates that TICT state formation in DMAPIP-b is irreversible. In aqueous medium only the monocation formed by the protonation of the imidazole nitrogen is found.

3.2. Effect of temperature

Once it is established that DMAPIP-b exhibits hydrogen bonding induced TICT emission, we studied the effect of temperature on the spectral characteristics of DMAPIP-b.

3.2.1. Relative population of the isomers

Though only one isomer of DMAPIP-b was considered in section 3.1, theoretically the molecule can exits in two isomeric forms. The structures of both isomers were optimized by DFT 6-31g(d,p). The calculations suggested that isomer I is more stable than isomer II (Chart 3.2.1) and at room temperature the relative population of isomer II is negligible. But isomer II is predicted as more polar than isomer I. Therefore, solvent polarity and temperature are expected to increases the relative population of isomers. The solvation energy was calculated using following expression [233-234,223]

$$\Delta E = \frac{\mu^2}{a^3}\frac{\varepsilon - 1}{2\varepsilon + 1} \tag{3.2.1}$$

where μ and a are the dipole moment and Onsager radius respectively and were calculated from the DFT optimized structure of isomers. The relative population obtained by Boltzmann distribution (not shown) suggested that the population of isomer II in all the solvents even at boiling temperature of the solvents is less than 1%. Therefore the presence of isomer II can be ignored. X-ray crystal structure data also showed that the molecule is present as isomer I (Appendix II). Since DMAPIP-b emits single emission in

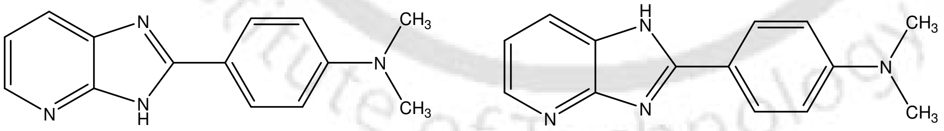

E =-20707.08199 eV
μ_g = 5.07 D
Isomer I

E = -20706.91737 eV
μ_g = 7.04 D
Isomer II

Chart 3.2.1. Structures of different isomers of DMAPIP-b along with their energies in the S_0 state and ground state dipole moment.

aprotic solvents and dual emission in protic solvents, effect of temperature in these two classes of solvents are discussed separately.

3.2.2. Temperature effect in aprotic solvents

The common feature in the absorption and the fluorescence spectra of DMAPIP-b in both nonpolar cyclohexane and polar acetonitrile are hypsochromical shift with increase in temperature (Figure 3.2.1). A clear isosbestic point in the absorption spectra and an isoemissive point in the fluorescence spectra are observed. The isoemissive points are in the red side of the fluorescence maxima in cyclohexane, but it on the blue side of the fluorescence maxima in acetonitrile respectively.

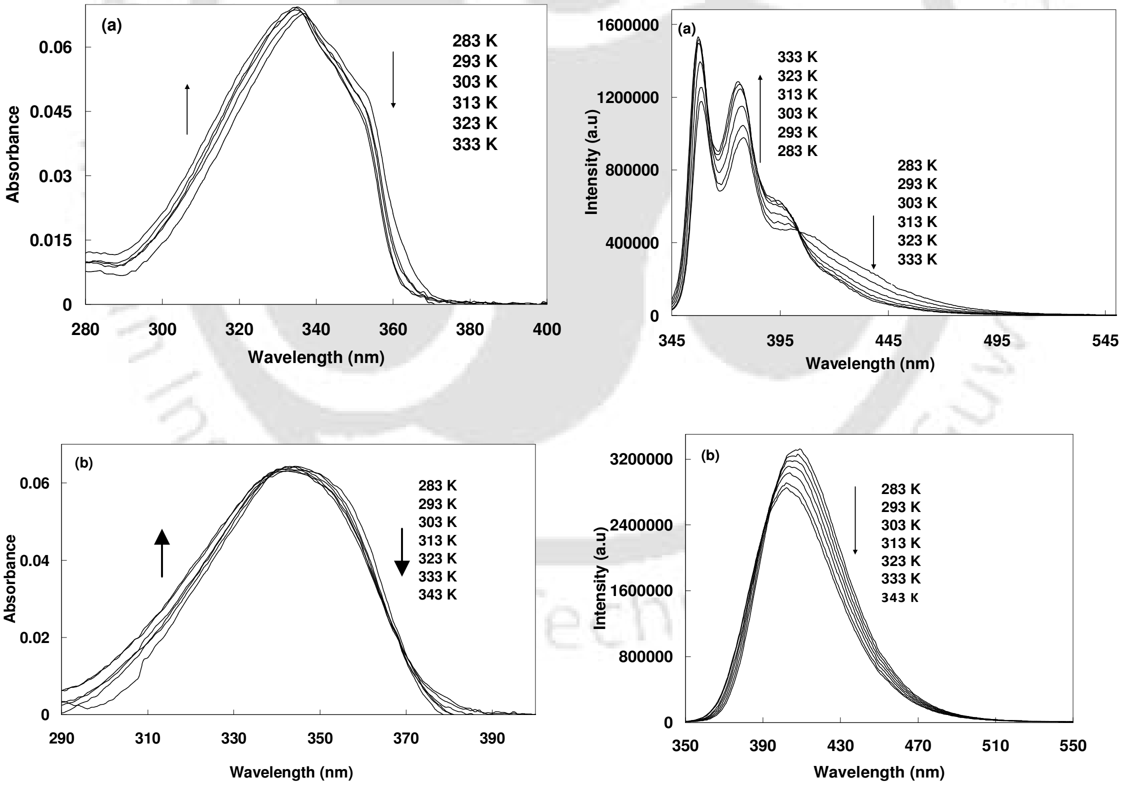

Figure 3.2.1: Absorption (left panel) and fluorescence spectra (right panel) of DMAPIP-b at different temperature in (a) cyclohexane and (b) acetonitrile.

In cyclohexane the variation in temperature, changes the relative population of the vibrational states. This can be ascertained by fact the relative absorption of the 335 nm band increases and that of the 350 nm band decreases with increase in temperature. The fluorescence spectra also suggested the change in relative population of the vibration state. An enhancement of fluorescence quantum yield was observed with rise in temperature, but the lifetime remains nearly constant with temperature change (Table 3.2.1). With rise in temperature the radiative rate increases and the nonradiative rate decrease. It appears that there is an increased cross section towards the radiative path at the higher vibrational levels. On the other hand, in acetonitrile the fluorescence spectrum undergoes a hypochromic shift. The increase of nonradiative processes related to thermal agitation in acetonitrile is evident from the decreases of fluorescence quantum yield and the lifetime with temperature (Table 3.2.1).

Table 3.2.1: Absorption maxima (λ_{max}^{ab}, nm), fluorescence (λ_{max}^{fl}, nm), quantum yield (ϕ), fluorescence lifetime (τ, ns), radiative rate (k_r, s^{-1}) and nonradiative rate (k_{nr}, s^{-1}) of DMAPIP-b in cyclohexane and acetonitrile at different temperature.

T (K)	λ_{max}^{ab}	λ_{max}^{fl}	ϕ	τ	k_r (10^8)	k_{nr} (10^8)
			Cyclohexane			
293	337, 351	359, 379, 398	0.72	1.08	6.72	2.51
303	336, 351	358, 378, 395	0.73	1.09	6.69	2.51
313	336, 350	357, 377, 394	0.74	1.07	6.96	2.36
323	334, 350	356, 376, 393	0.75	1.05	7.19	2.33
			Acetonitrile			
293	346	408	0.76	1.58	4.85	1.48
303	344	406	0.74	1.56	4.88	1.53
313	342	405	0.73	1.54	4.77	1.73
323	341	404	0.72	1.52	4.76	1.82

3.2.2. Temperature effect on dual fluorescence

The effect of temperature on the dual emission was investigated in 1-propanol, ethanol and methanol (Figure 3.2.2). Same as in acetonitrile, the fluorescence spectra in

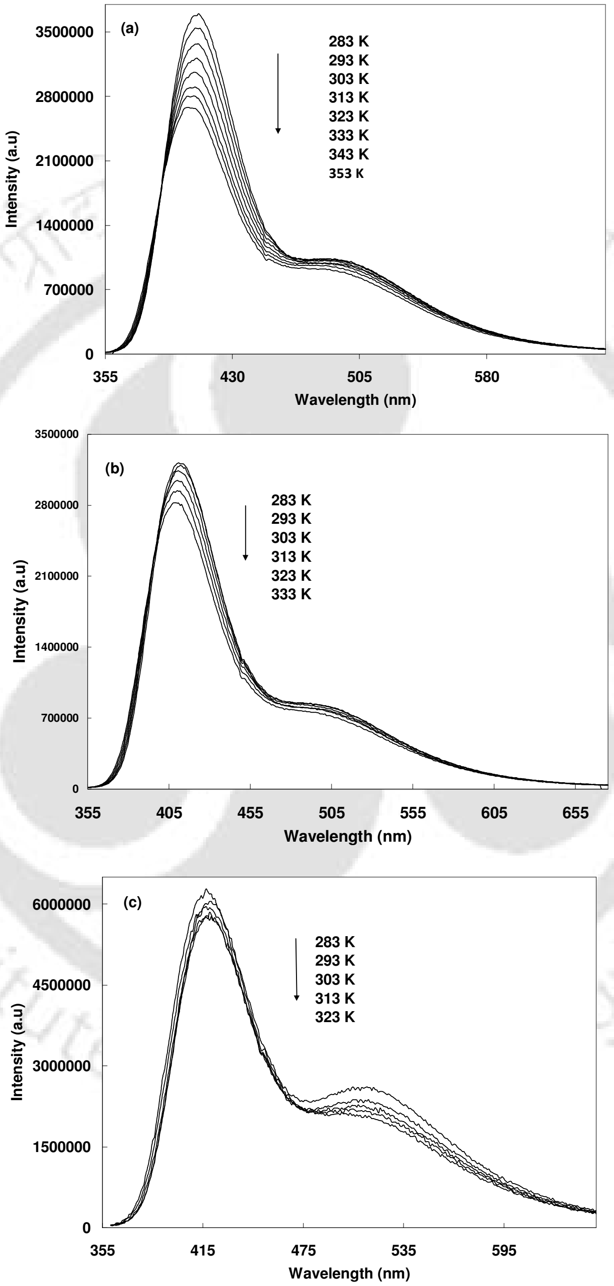

Figure 3.2.2: Fluorescence spectra of DMAPIP-b at different temperature in (a) 1-propanol, (b) ethanol and (c) methanol.

1-propanol and ethanol have clear isoemissive point on the blue side of the band maxima. In propanol an additional quasi isoemissive point is observed at 460 nm in the tail side of the band maxima. However, in all these protic solvents, dual emission is observed in all the temperatures. The quantum yield for the normal band decreases in all the protic solvents (Figure 3.2.3).

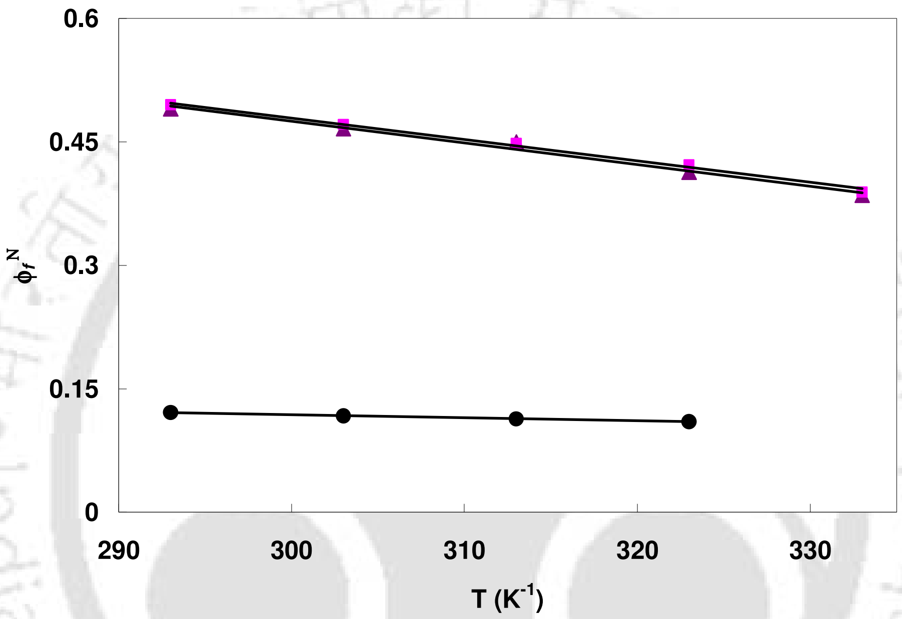

Figure 3.2.3: Temperature dependence of quantum yield (ϕ_f) of normal emission in 1-propanol (▲), ethanol (■) and methanol (●).

The fluorescence decay is biexponential in all the protic solvents at all the temperature. The lifetime is quenched with protic solvents and the attenuation of lifetime increases with hydrogen bonding capacity of the solvent. The lifetime of the locally excited states decreases in 1-propanol and ethanol, but increases in methanol (Figure 3.2.4a). With rise in temperature the radiative rate decreases and the non radiative rate increases for normal emission in all these solvents. The lifetime of TICT emission decreases in all three protic solvents (Figure 3.2.4b).

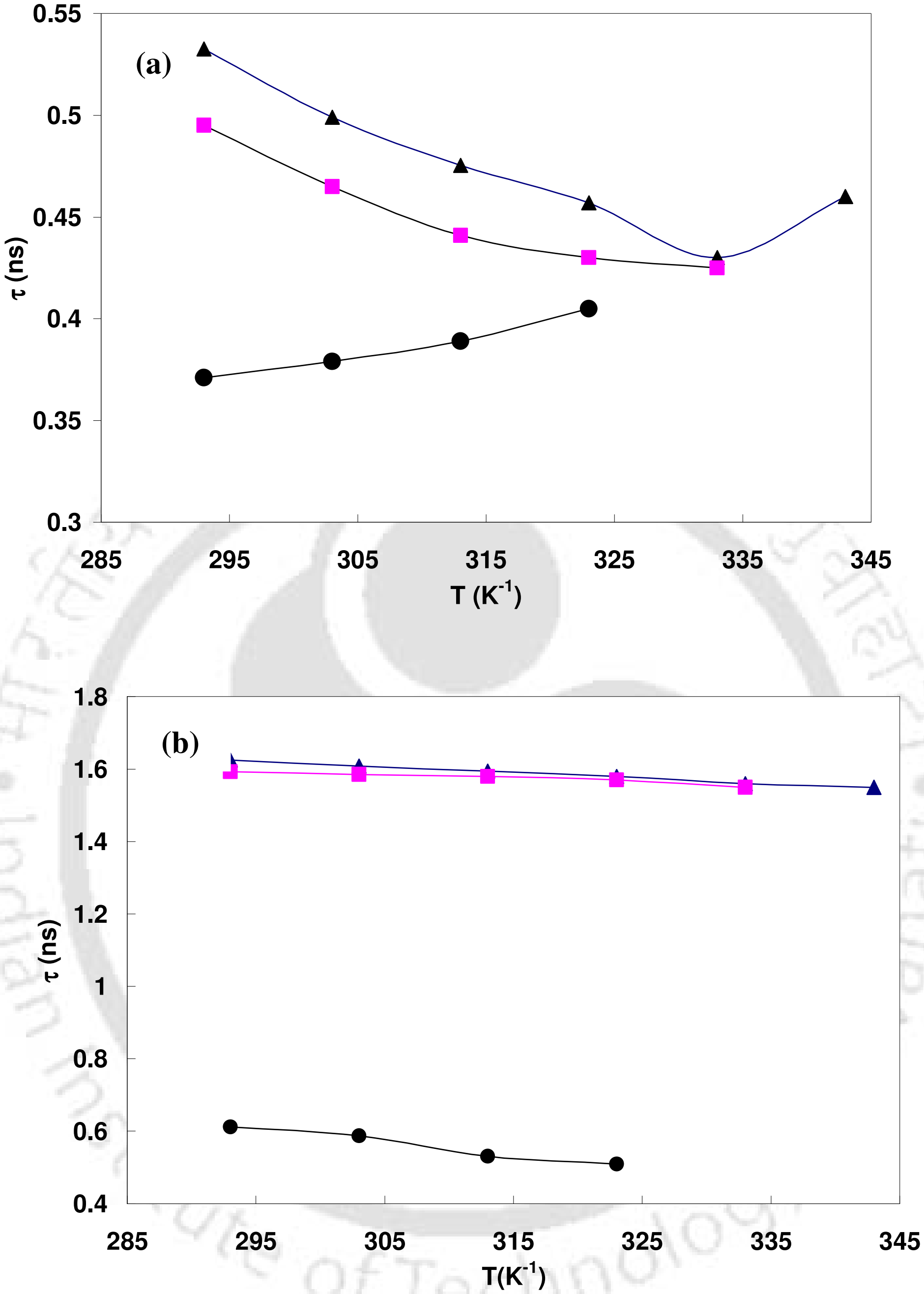

Figure 3.2.4: Temperature dependence of lifetime of normal (a) and TICT (b) emission in 1-propanol (▲), ethanol (■) and methanol (●).

The coupling of the locally excited state and the TICT state, though normally weak, it is strong enough for the charge transfer reaction to take place adiabatically in single potential energy surface process. Since the orbitals involve in the radiative transition from the TICT state to the corresponding Franck-Condon state are located on different part of the molecular system (donor and acceptor) with minimum overlap, the decay is expected to posses a small transition moment, due to its forbidden nature. Upon coupling to suitable vibration, the TICT emission is predicted to barrow the intensity from the allowed higher excited states and is responsible for its appreciable quantum yield. Due to this vibronic coupling, the radiative decay of the TICT emission is temperature dependent and the major part of the TICT emission occurs from the less forbidden higher vibronic levels as hot fluorescence. Therefore, the rate constant for the formation of the TICT state depends on temperature [13]. However, it is shown that both solvent parameters viscosity and polarity, and solute parameters such twist angle of ground state, rotating volumes, molecular shape and electronic nature are found to determine the rate for this forward [13]. The kinetics of TICT emission can be explained by the generalized scheme (Scheme 3.2.1) for the TICT process as shown below [13].

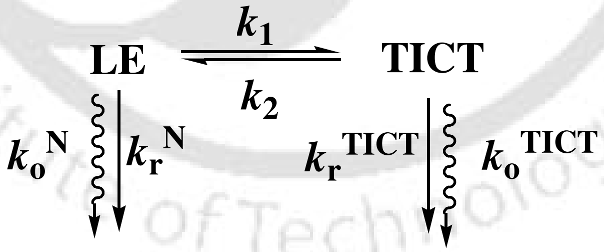

Scheme 3.2.1. Generalized kinetics scheme for TICT processes.

where k_1 and k_2 are the rate constant for the forward and the reverse process respectively. k_r^N and k_r^{TICT} are radiative rate constant for normal and TICT emission respectively and k_0^N and k_0^{TICT} denote corresponding nonradiative rate constant to the ground state. With rise in temperature, the relative intensity of the TICT emission is expected to enhance due to increase in the formation of the TICT state. At the temperature above which the emitting states reach a thermodynamic equilibrium, the characteristics intensity minimum for the normal emission occurs. The equilibrium is shown to shift toward locally excited state, which results in total fluorescence quantum yield.

The generalized scheme for the formation of TICT state is applicable for DMAPPI-b also. However, in DMAPIP-b, the rotating group being a small dimethyl amino group, the viscosity of the solvent except that of glycerol, unlikely to play a role in the rate for the formation of TICT state, but as shown earlier, the hydrogen bond donating ability of the solvent plays a major role in the formation of the TICT state. It was reported that the thermodynamic dynamic equilibrium between the emitting state reaches at room temperature in numerous systems [12]. But, in DMAPIP-b, two different lifetimes observed for normal and TICT states (Figure 3.2.4), suggested that the equilibrium is not established between the two states. As described earlier, the hydrogen bonding and the polarity of the solvent stabilizes the TICT state that results in the enhancement of the barrier for the reverse process (TICT to locally excited state). Therefore, the rate constant for the forward process is higher than that of the reverse process and it may be stated that the formation TICT state is irreversible under these conditions. According to this mechanism, there must be a rising component in the TICT fluorescence, which should be correlated with the decay of the locally excited state. But we could not observe the rising component for the formation of TICT. Though the pulse width of the Laser didode used for excitation is only 1.9 ps, the detector response is 50 ps (Section 2.5.4), therefore it could be inferred that the TICT state of DMAPIP-b is formed from its locally excited state in less than 50 ps. The presence of quasi isoemissive point at 460 nm and the enhancement of the TICT emission (up to 323 K and decreases with further rise in temperature) indicate the equilibrium shifts toward the TICT state with increase in temperature shifts. The decrease in intensity at temperature above 323 K can be attributed to increase in non radiative rate. The temperature dependence of relative quantum yield ϕ_{TICT}/ϕ_N is presented in Figure 3.2.5. In propanol and ethanol the ratio ϕ_{TICT}/ϕ_N increases, but its decreases in methanol. This can be explained as follows: in the absence of back reaction, the increases in temperature shift the equilibrium towards the TICT state that enhances the ϕ_{TICT}/ϕ_N ratio in propanol and ethanol. In methanol, the increase in polarity and hydrogen bonding capacity stabilizes the TICT state more compared to other alcohols. This decreases the energy gap between the TICT state and the low lying state which increases the nonradiative rate.

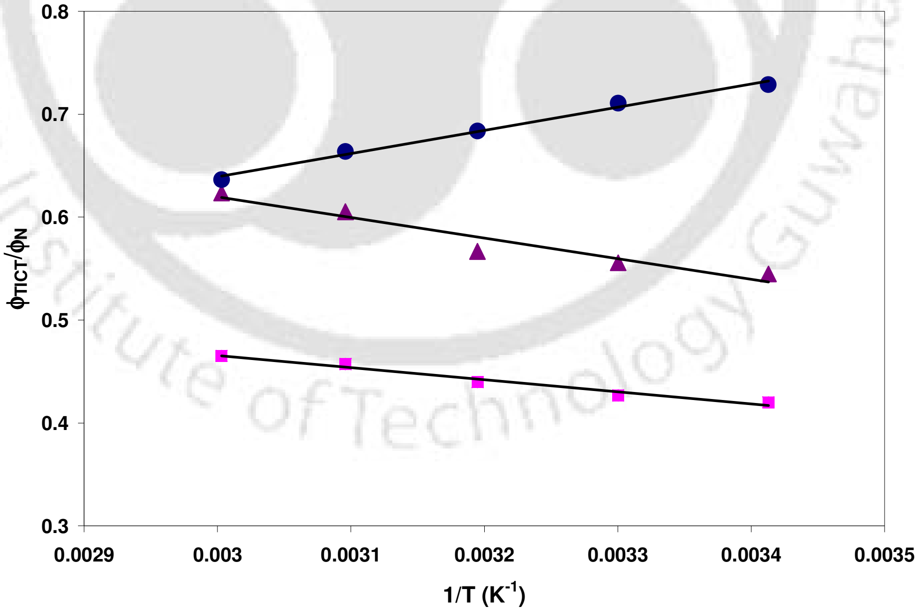

Figure 3.2.5: Temperature dependence of relative quantum yield of 1-propanol (▲), ethanol (■) and methanol (●).

Since the energy gap is more for the locally excited state compared to TICT state, the TICT emission is quenched more than that of the normal emission. This is substantiated by the fact that in most polar water the TICT emission was quenched almost completely and only normal emission is observed (Table 3.1.1 and Figure 3.1.5). In glycerol, unlike in other solvents the fluorescence decreases drastically with temperature and can be attributed to the large variation in its viscosity with temperature (Figure 3.2.6). The TICT emission and the normal emission could not be resolved into components in glycerol, however, the intensity ratio of longer wavelength to that of shorter wavelength increases with rise in temperature (Figure 3.2.6 insert).

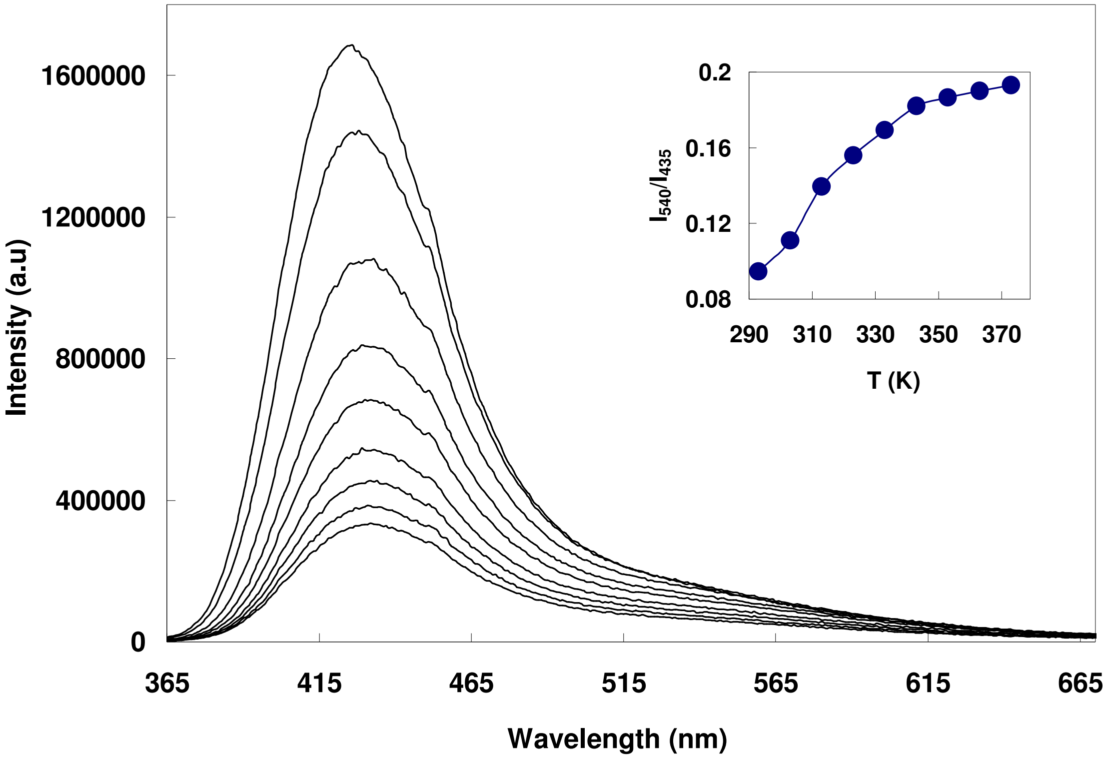

Figure 3.2.6: Fluorescence spectra of DMAPIP-b in glycerol at different temperature (insert show the variation of fluorescence intensity ratio with temperature).

3.2.3. Dipole moment of TICT state

Since DFT calculation predicted the ground state dipole moment as 5.1 D (different from earlier *ab initio* calculations), we recalculated the excited state dipole moment of the locally excited state using Lippert plot as 12.1 D, little higher than the value obtained earlier.

As the absorption spectrum of TICT is not attainable by direct excitation, the dipole moment can not be calculated for the TICT state using Stokes shift from the simple Lippert-Mataga plot (as in the case of locally excited). However, the dipole moment of the TICT state can be calculated using fluorescence data from the following equation [12]

$$\bar{\nu}_{\mathrm{f}} = -\frac{2\mu_e(\mu_e - \mu_g)}{hca^3}\Delta f^{'} - \bar{\nu}_{\mathrm{f}}^{o} \qquad (3.2.1)$$

where $\bar{\nu}_{\mathrm{f}}$ is the fluorescence maximum of the TICT emission, all other parameters have same meaning as earlier (section 3.1.2) and $\Delta f'$ is defined as

$$\Delta f^{'} = \frac{\varepsilon - 1}{2\varepsilon + 1} - \frac{n^2 - 1}{2(2n^2 + 1)} \qquad (3.2.2)$$

A good linear correlation ($r^2 = 0.99$) was obtained between the $\bar{\nu}_{\mathrm{f}}$ of the TICT fluorescence and solvent parameter ($\Delta f'$) and the linear fit is shown in Figure 3.2.7. The dipole moment calculated for the TICT state from this solvatochrmic plot is 24.6 D. This is consistent with Cogan *et al*. prediction of larger dipole moment for the perpendicular geometry than the planar one [22].

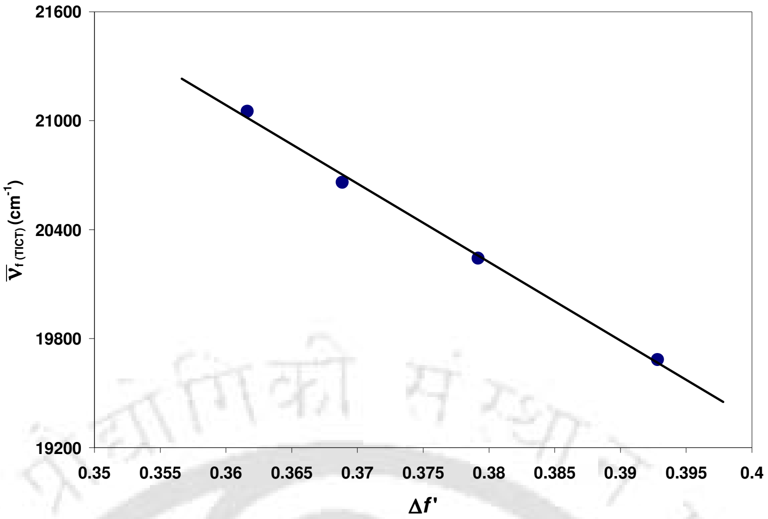

Figure 3.2.7: Solvatochromic plot of TICT band.

The thermochromic shift can also be used to determine large excited state dipole moments such as that of TICT state. The dipole moment of the TICT state was calculated using thermochromic shift, for DMABN by Suppan *et al*. [235] and for bianthryl derivative by Chakraborty *et al*. [236] and were found to be in good agreements with the values calculated from other methods. Adding independently the temperature dependence of the dispersion interactions in the simplest theory of thermochromic shifts, that is based on the temperature dependence of the solvents'static dielectric constant and refractive index, the difference in solvation energies of the ground state and the excited state by the Onsager model of solute-solvent interactions is given by [235]

$$\frac{\Delta E}{\Delta T} = \frac{hc\Delta\tilde{\nu}}{\Delta T} = -\frac{\mu_e(\mu_e-\mu_g)}{r^3}\frac{d[f(D)-f(n^2)]}{dT} - \frac{(\mu_e^2-\mu_g^2)}{2r^3}\frac{df(n^2)}{dT} - C\frac{df(n^2)}{dT} \qquad (3.2.3)$$

where T is the temperature and all other parameters are as defined earlier (section 3.1.2). In the right hand side of the equation the first term is due to orientation, the second term to induction and the third one to dispersion. The dispersion term is important only in nonpolar solvents and for solvatochromic shifts in polar solvents it can be neglected. The dipole moment of the TICT ground state is required to calculate the dipole moment of the TICT excited state. Assuming μ_g(TICT) as μ_g the dipole moment in the TICT excited state can be determined and the assumption will not lead to serious error in calculating the excited state dipole moment as the value of the latter is mush larger [236]. Using orientation and induction parameters of methanol (6.0 x 10^{-5} K^{-1} and 3.1 x 10^{-4} K^{-1} [236] and $\Delta \bar{\nu}_f / \Delta T$ obtained from Figure 3.2.8 (4.64 $cm^{-1}K^{-1}$), the dipole moment of the TICT state is determined as 25.4 D. This is value is in good agreement with the value obtained from the solvatochromic plot.

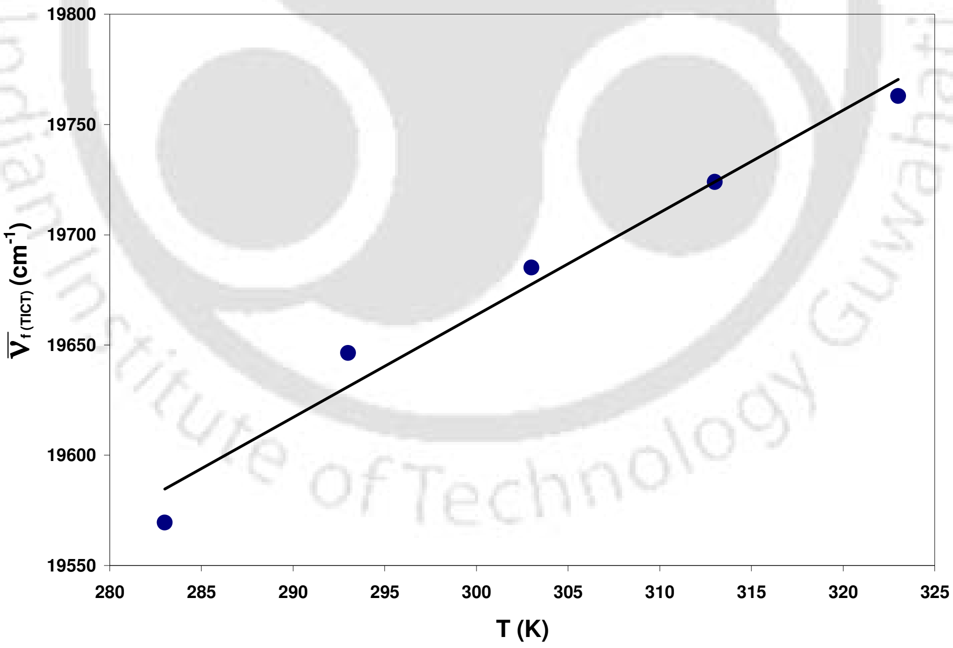

Figure 3.2.8: Temperature dependence of TICT band maxima in methanol.

3.2.4. Conclusion

The radiative and the non radiative transition of both the states of DMAPIP-b are temperature dependent. In cyclohexane there is an increased cross section towards the radiative path in the higher vibrational levels for normal emission. However in other solvents the radiative decay increases with temperature. In alcohols, the formation of TICT state from locally excited state is dominant over the reverse process and the equilibrium is not established between the locally excited state and the TICT state even near the boiling temperature of the solvents. The dipole moment of the TICT state was determined by both solvatochromic and thermochromic shift methods and the values are in good agreement with each others.

3.3. Effect of metal ions

Sensing of metals by fluorescence is an active area of research [237-239] and has potential analytical applications in chemistry, biology, medicine and environment [240-241]. As the hydrogen bonding of solvent with pyridine nitrogen induces the TICT emission of DMAPIP-b, metal ions can also on binding at pyridine nitrogen may induce TICT emission. Since the molecule has two different sites for metal binding depending on the site of binding, TICT emission may be induced. To find out whether the bichromophore DMAPIP-b cause any visual color change, a series of experiments were carried out in the presence of different metal salts.

3.3.1. Ground state complex formation

The metal binding properties was first investigated using absorption spectral measurements. The absorption maximum of DMAPIP-b remains unchanged, only a small hypochromic shift was observed with addition of Li^+ (Figure 3.3.1) or Na^+ (Figure 3.3.2). On the other hand the absorption spectrum was nearly unaffected with addition of Ba^{2+} (Figure 3.3.3).

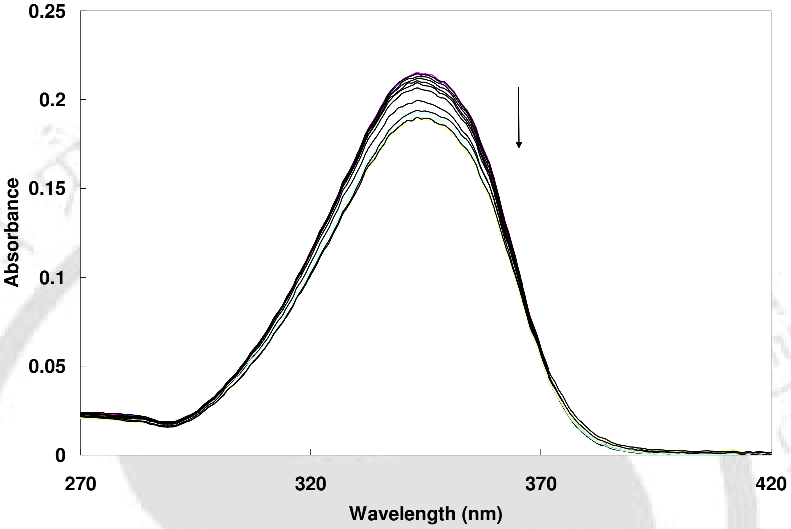

Figure 3.3.1: Absorption spectra of DMAPIP-b (6μM) at different concentration of Li^+ (0-5 mM) in acetonitrile.

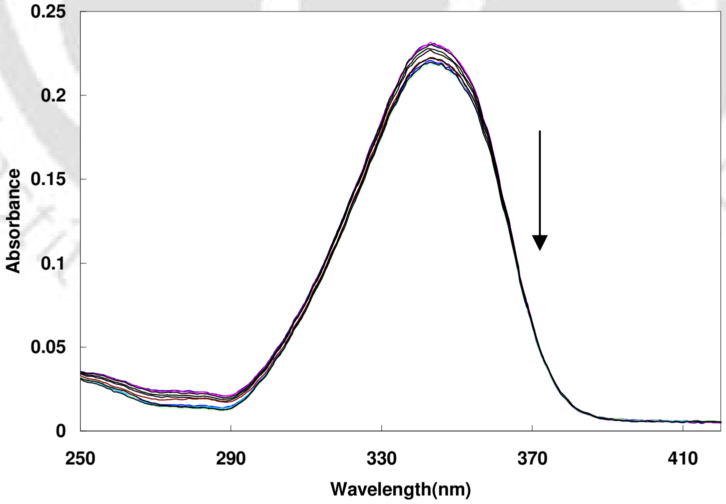

Figure 3.3.2: Absorption spectra of DMAPIP-b (6μM) at different concentration of Na^+ (0-5 mM) in acetonitrile.

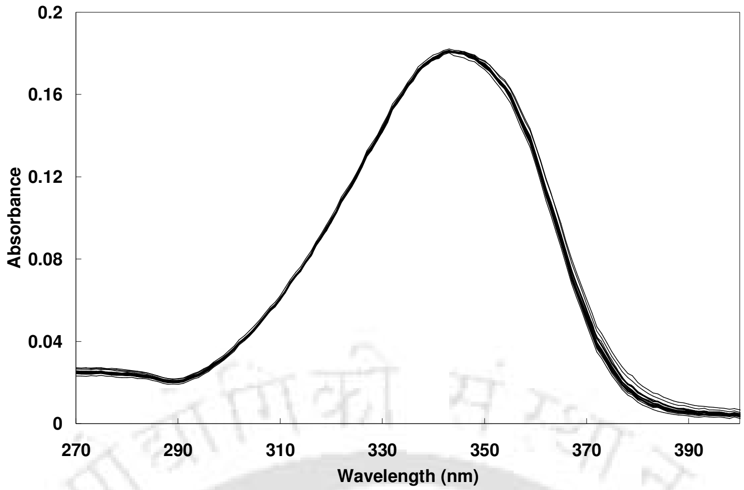

Figure 3.3.3: Absorption spectra of DMAPIP-b (6μM) at different concentration of Ba^{+2} (0-5 mM) in acetonitrile.

Upon addition of other metals the absorption spectrum is red shifted. With the red shift, a new band (on the red side) started to appear for initial addition of Mg^{2+}, but with further addition, though the spectral maximum continues to shift bathochromically, the spectrum narrows toward shorter wavelength (Figure 3.3.4). Same behavior is found for addition of Ca^{2+} (Figure 3.3.5). Narrowing of spectra suggested the shifting of the

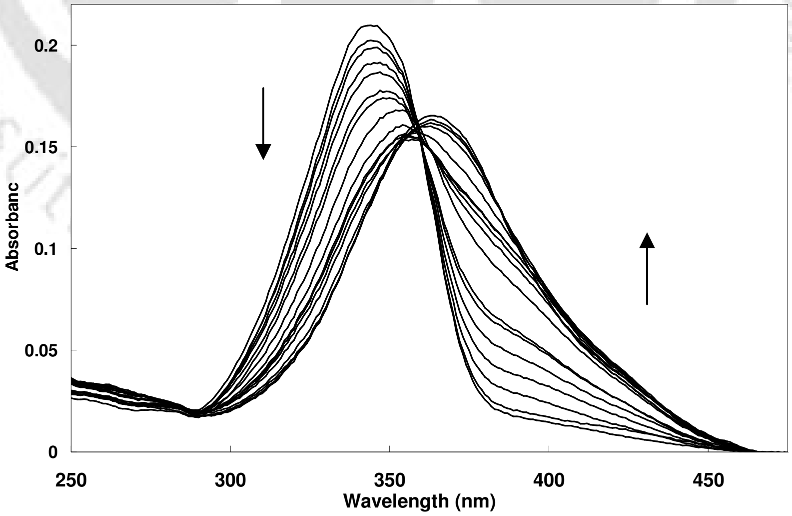

Figure 3.3.4: Absorption spectra of DMAPIP-b (6μM) at different concentration of Mg^{+2} (0-5 mM) in acetonitrile.

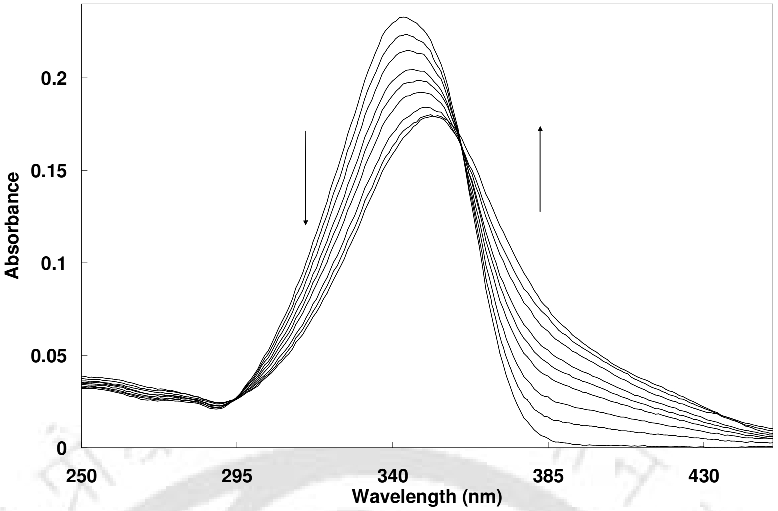

Figure 3.3.5: Absorption spectra of DMAPIP-b (6µM) at different concentration of Ca^{+2} (0-5 mM) in acetonitrile.

equilibrium towards a new complex, before the complete conversion of DMAPIP-b to initially formed complex. The absorption spectral maximum is shifted to 352 nm and 363 nm respectively for Ca^{2+} and Mg^{2+} at 5 mM metal concentration.

The effect of transition metals likes Ni^{2+}, Zn^{2+} and Cd^{2+} (up to 5 mM) on the absorption spectrum of DMAPIP-b are presented in Figure 3.3.6, 3.3.7 and 3.3.8

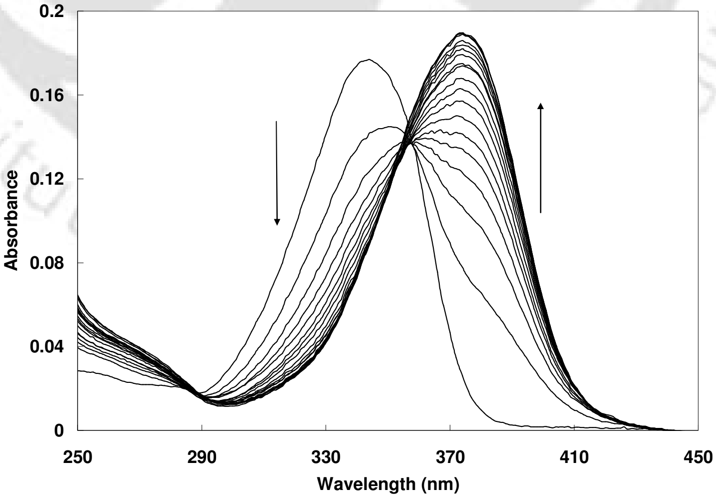

Figure 3.3.6: Absorption spectra of DMAPIP-b (6µM) at different concentration of Ni^{+2} (0-5 mM) in acetonitrile.

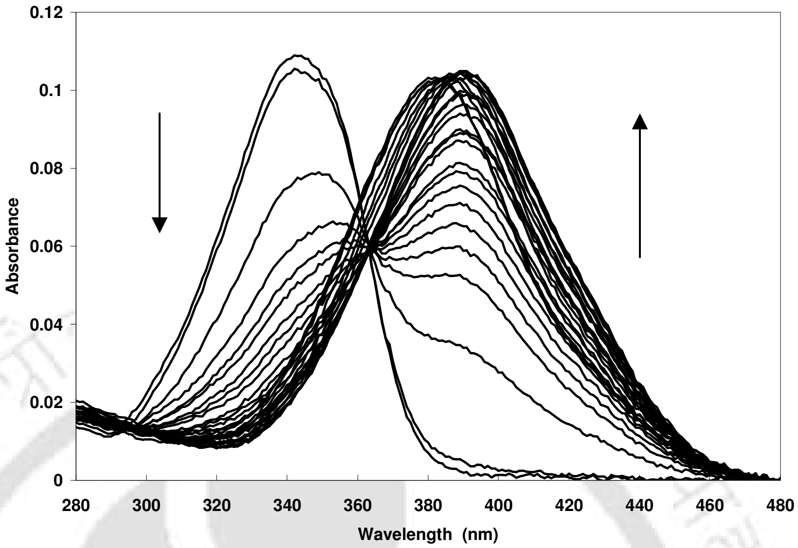

Figure 3.3.7: Absorption spectra of DMAPIP-b (6µM) at different concentration of Zn^{+2} (0-5 mM) in acetonitrile.

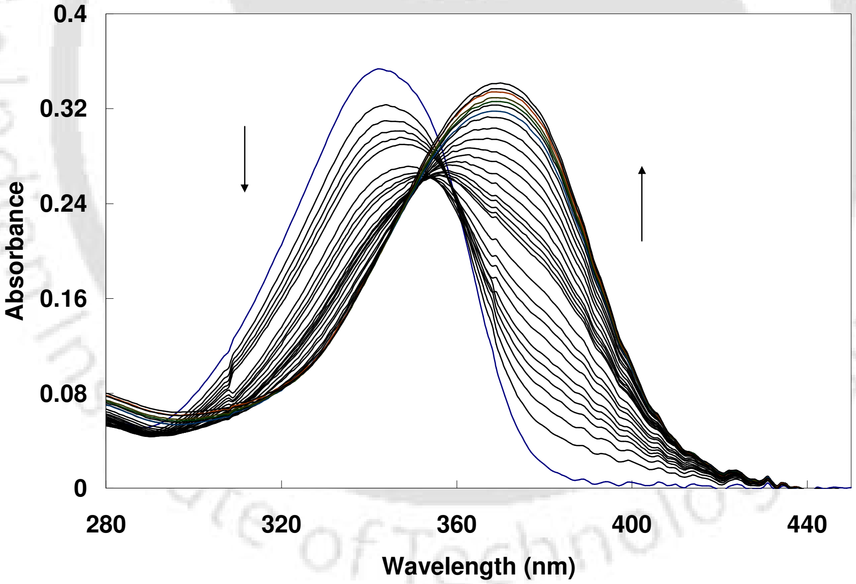

Figure 3.3.8: Absorption spectra of DMAPIP-b (6µM) at different concentration of Cd^{+2} (0-5 mM) in acetonitrile.

respectively. Effect of Zn^{2+} is to some extent complicated. For initial addition of Zn^{2+}, a new band appeared at 390 nm. While 390 nm band gains absorbance with Zn^{2+}

concentration and 345 nm band of DMAPIP-b diminishes with Zn^{2+} concentration. At 0.37 mM concentration of Zn^{2+} only 390 nm band was observed, for further increases in Zn^{2+} amount the spectrum is slowly blue shifted. The red shift in the absorption spectra of DMAPIP-b upon addition of Ni^{2+} (374 nm) and Cd^{2+} (370 nm) are less compared to Zn^{2+} (390 nm). Unlike Zn^{2+}, no blue shift is observed in DMAPIP-b absorption spectrum even up to 5 mM concentration of Ni^{2+} or Cd^{2+}.

The invariant nature of the absorption spectrum indicates that DMAPIP-b is not forming complexes with Li^{+}, Na^{+} and Ba^{2+}. The spectral changes suggest that DMAPIP-b formed complexes with transition metal ions Zn^{2+}, Ni^{2+}, Cd^{2+} and alkaline earth metals like Ca^{2+} and Mg^{2+}. However complexation with alkaline earth metals are inefficient and could not be completed even at very high concentration. It is also known that the complexation of probe with transition-metal cations usually causes electronic spectral shifts that are much greater than the shifts produced by the complexation with non-transition metal ions [10].

The metal can bind at one (or more) of three basic centers: the pyridine nitrogen, imidazole nitrogen and dimethylamino group. As mentioned in section 3.1.3, the absorption spectrum is red shifted on protonation at ring nitrogen due to increase in conjugation. The bathochromic shift is more pronounced on protonation at pyridine ring than at imidazole nitrogen due to greater conjugation. However as result of reduction in conjugation the spectrum is blue shifted upon protonation at dimethylamino group. Same behavior is expected upon complexation with metal ion. Based on these arguments, the largely red shifted band of in Zn^{2+} can be assigned to complexation at pyridine nitrogen of DMAPIP-b with Zn^{2+} (Chart 3.3.1). It may also be noted though acetonitrile is less

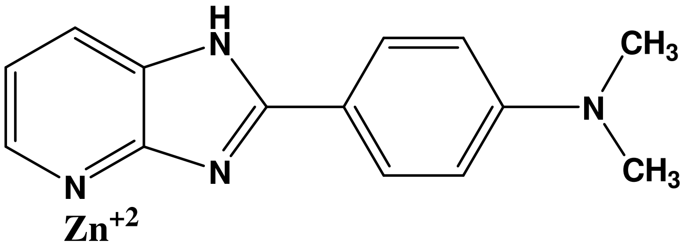

Chart 3.3.1. Structure of Zn^{2+}-DMAPIP-b complex.

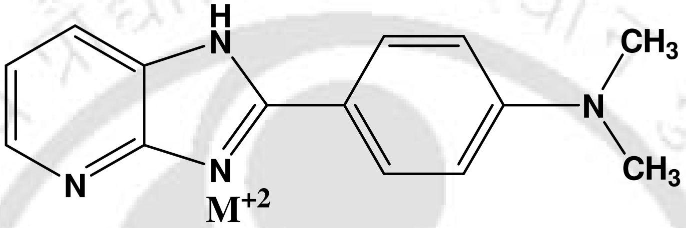

M = Ni^{2+}, Cd^{2+}

Chart 3.3.2. Structure of Ni^{2+}-DMAPIP-b/Cd^{2+}-DMAPIP-b complex.

polar than water, the band is red shifted more than that 386 nm band observed upon protonation in water. Blue shift observed at higher concentration (> 0.37 mM) indicates the addition of second Zn^{2+} at dimethylamino nitrogen of DMAPIP-b-Zn^{2+} complex. The absorption spectra of DMAPIP-b-Ni^{2+} and DMAPIP-b-Cd^{2+} complexes are red shifted compared to DMAPIP-b, but blue shifted relative to DMAPIP-b-Zn^{2+} complex. This is consistent with addition of Ni^{2+} and Cd^{2+} at imidazole nitrogen of DMAPIP-b to form metal complexes (Chart 3.3.2).

3.3.2. Fluorescence characteristics

The fluorescence band maximum of DMAPIP-b is unaffected by the addition of alkai metals (not shown). Like the absorption spectra a small decrease in fluorescence intensity was observed with increase in concentration of smaller ion Li^+, but the intensity is unaffected by presence of Na^+. The fluorescence spectrum of DMAPIP-b undergoes a small red shift with decrease in intensity upon increases in concentration of alkali earth metals (only the effect of Ba^{2+} is shown in Figure 3.3.9). The magnitude of changes in fluorescence characteristics decreases with increase in ionic radii (i.e. $Mg^{2+} < Ca^{2+} < Ba^{2+}$). The 10 nm shift observed with Ba^{2+} in the fluorescence spectrum is much smaller compared to transition metals.

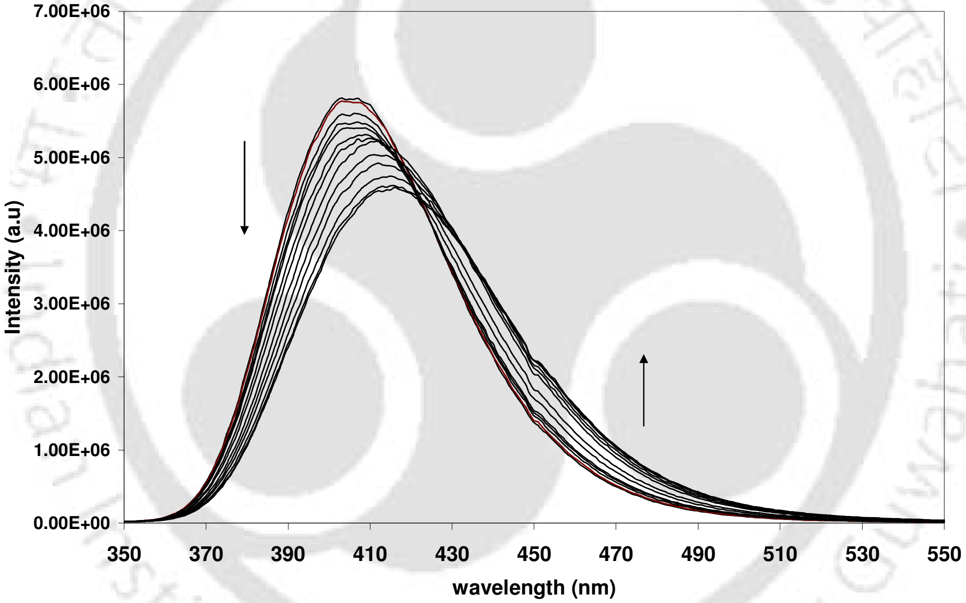

Figure 3.3.9: Emission spectra of DMAPIP-b (6 μM) at different concentrations of Ba^{+2} (0-7 mM) in acetonitrile (λ_{exc} = 355 nm).

The effects of transition metals on the emission characteristics of DMAPIP-b are much more than that of alkali and alkaline earth metals. Fluorimetric titration were performed transition with metal ions Co^{2+}, Ni^{2+}, Zn^{2+} and Cd^{2+} are shown in Figure 3.3.10, 3.3.11, 3.3.12 and 3.3.13 respectively. The fluorescence spectrum of DMAPIP-b

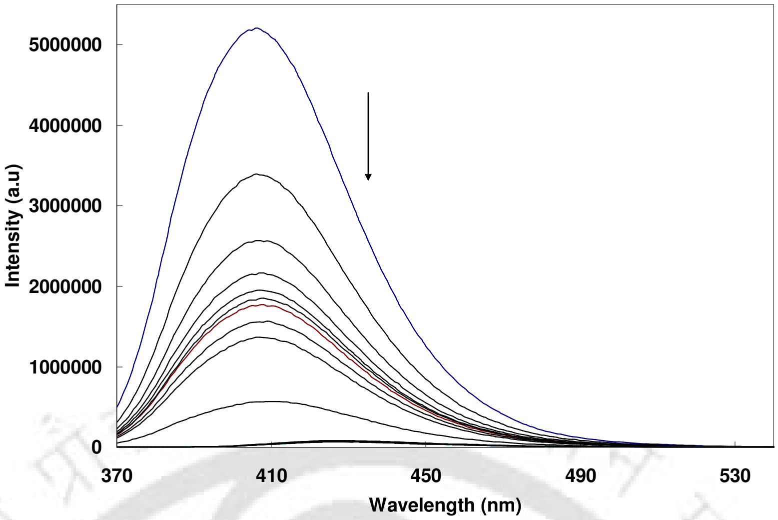

Figure 3.3.10: Emission spectra of DMAPIP-b (6 μM) at different concentrations of Co^{+2} (0-5 mM) in acetonitrile (λ_{exc} = 355 nm).

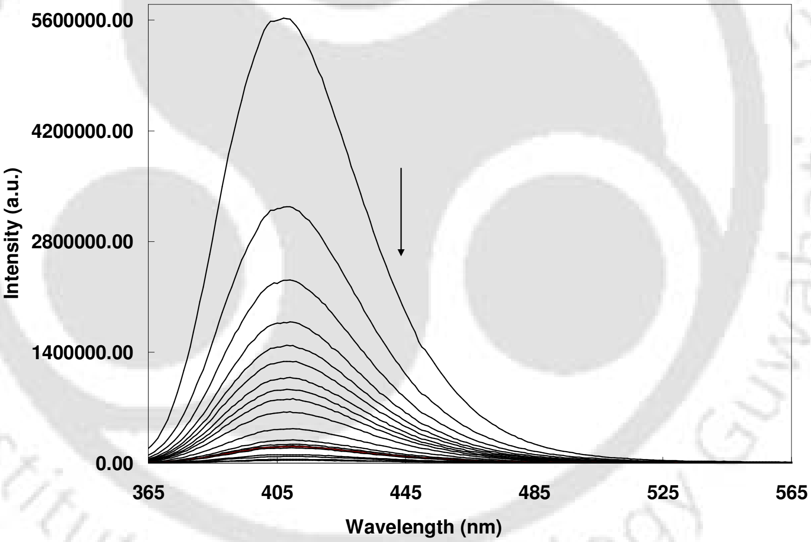

Figure 3.3.11: Emission spectra of DMAPIP-b (6 μM) at different concentrations of Ni^{+2} (0-5 mM) in acetonitrile (λ_{exc} = 355 nm).

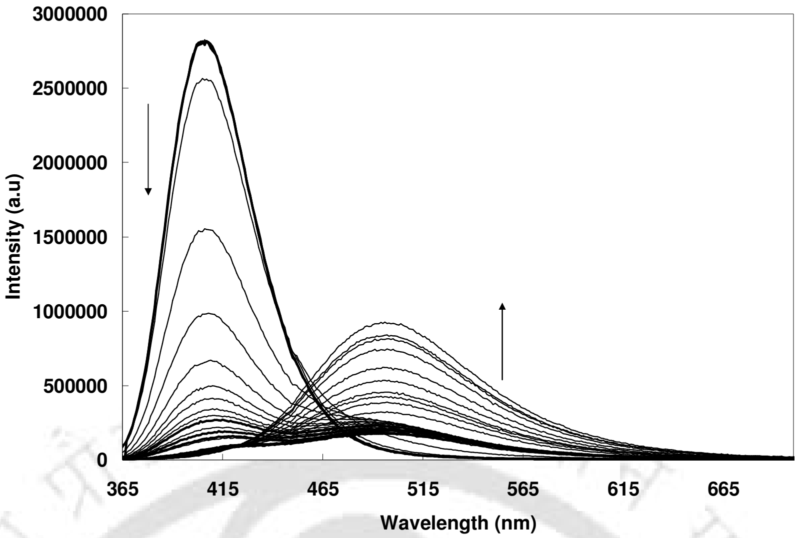

Figure 3.3.12: Emission spectra of DMAPIP-b (6 μM) at different concentrations of Zn^{+2}(0-5 mM) in acetonitrile (λ_{exc} = 360 nm).

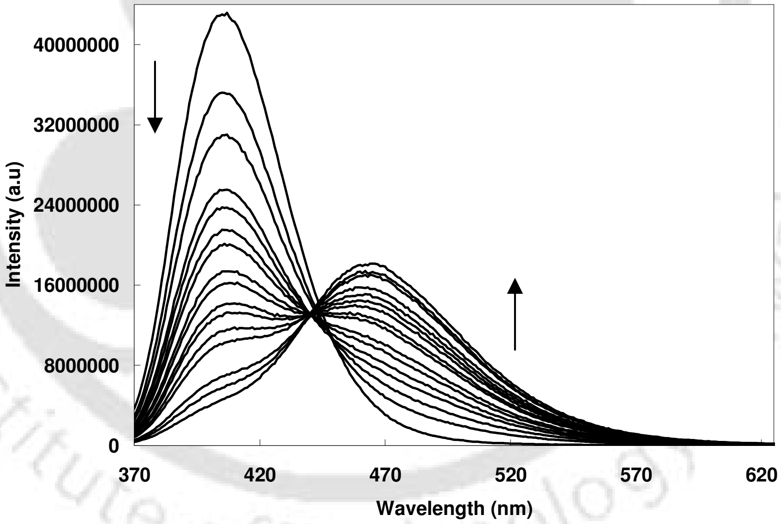

Figure 3.3.13. Emission spectra of DMAPIP-b (6 μM) at different concentrations of Cd^{+2} (0-5mM) in acetonitrile (λ_{exc} = 355 nm).

is quenched by the addition of Ni^{2+} or Co^{2+}. The paramagnetic nature of metal ions Co^{2+} and Ni^{2+} is responsible for the non fluorescent nature of metal ion DMAPIP-b complexes (Chart 3.3.2). Though diamagnetic Cd^{2+} ion also binds at the same site, the effect on the fluorescence spectrum is quite different from that of Co^{2+} and Ni^{2+}. Upon addition of Cd^{2+} a new red shifted band start to appear at 467 nm. It may be assigned to DMAPIP-b-Cd^{2+} complex (Chart 3.3.2).

In presence of Zn^{2+} the single band emission of the fluorophore is replaced by two bands system with a new band at 500 nm. The intensity of the shorter wavelength decreases and that of the longer wavelength increases with metal ion concentration. The Stokes shift of 500 nm band is large and close to TICT emission of DMAPIP-b in protic solvents and thus can be assigned to Zn^{2+} induced TICT emission. The complexation of Zn^{2+} with pyridine nitrogen increases the electron withdrawing ability of the acceptor which induces TICT emission. Same way the protonation at pyridine nitrogen of DMAPIP-b was also found induces TICT emission in cyclodextrin and micelle (Section 4.1.3 and 4.2.4). Herbich et al. reported that 4-(*N*,*N*-dimethylamino)pyrimidine also emits from the TICT state upon coordination with Zn^{2+} [62]. The intensity of the green fluorescence band increases even above 0.37 mM Zn^{2+}. This suggest that upon excitation the second Zn^{2+} ion attached at dimethylamino group dissociate to give DMAPIP-b-Zn^{2+}, which is responsible for TICT emission. It well established that the protonated amino group becomes more acidic upon excitation and dissociates to give proton in the excited state. Dogra et al. had shown that DMAPIP-c forms two types of cation (i) by protonation of pyridine nitrogen and (ii) by protonation of dimethylamino nitrogen in the ground state. While the pyridine nitrogen protonated species remains stable in the excited state, the dimethylamino protonated species dissociated [182].

3.3.3. Fluorescence lifetime

To obtain in-depth mechanistic insight into the photo physical effects allowing the operation of the novel sensor we performed time resolved fluorescence experiments. As can be seen from Table 3.3.1, the fluorescence decays of both DMAPIP-b and its complexes with alkali and alkanaline earth metals (except Mg^{2+}, Zn^{2+} and Cd^{2+}) are monoexponential, and the observed lifetimes were all close to 1.5 ns. This corresponds to uncomplexed DMAPIP-b. In transition metal ions Ni^{2+} and Co^{2+} were the fluorescence is completely quenched the fluorescence decay was measured at different concentration of metal ion and are compiled in Table 3.3.2. It shows that as predicted earlier, the quenching is static in nature. In Cd^{2+}, the second long lifetime is that of DMAPIP-b-Cd^{2+} complex.

Upon addition of Zn^{+2}, the fluorescence decays of DMAPIP-b became biexponential (Table 3.3.1 and 3.3.3). The two component decays are attributed to a mechanism involving the excitation of a single ground state species to a fluorescing

Table 3.3.1: Absorption band maxima ($\lambda_{max}{}^{ab}$, nm), fluorescence band maxima ($\lambda_{max}{}^{fl}$), lifetimes (τ, ns) of DMAPIP-b in different metal cations (100µM) in acetonitrile.

Metal	$\lambda_{max}{}^{ab}$	$\lambda_{max}{}^{fl}$	τ^1
Li^+	346	405	1.54
Na^+	346	405	1.53
Mg^{+2}	353	415	0.96 (10.1) 1.70 (89.9)
Ca^{+2}	345	405	1.55
Ba^{+2}	345	405	1.71
Co^{+2}	348	405	1.54
Ni^{+2}	373	406	1.51
Zn^{+2}	392	498	0.24 (38.2) 1.71 (61.8)
Cd^{+2}	348	411	1.48 (76.1) 2.07 (23.9)

$^1\lambda_{exc}$ = 375, λ_{em} = 410 nm

Table 3.2.2: Fluorescence life time (τ, ns) of DMAPIP-b at different concentration of Ni^{+2} and Co^{+2} in acetronitrile.

$[Ni^{+2}]$ (mM)	τ	$[Co^{+2}]$ (mM)	τ
0	1.53	0	1.53
0.1	1.53	0.1	1.54
0.5	1.51	0.5	1.53
1.0	1.52	1.0	1.49

λ_{exc} = 375, λ_{em} = 410 nm

Table 3.3.3: Fluorescence life time (τ, ns) of DMAPIP-b at different concentration Zn^{+2} in acetronitrile.

$[Zn^{+2}]$ (mM)	τ
0	1.53
0.14	0.24 (61.0) 1.63 (39.0)
0.21	0.24 (56.5) 1.68 (43.5)
0.58	0.24 (53.7) 1.95 (49.3)
2.25	0.25 (50.0) 2.34 (50.0)
3.17	0.25 (49.7) 2.37 (50.3)
4.00	0.26 (45.7) 2.39 (54.3)
5.00	0.26 (39.5) 2.44 (60.5)

λ_{exc} = 375, λ_{em} = 410 nm

locally excited state (shorter wavelength band) followed by a fast reaction to a fluorescent TICT state (longer wavelength band). The fluorescence decay of DMAPIP-b measured in 100 μM Zn^{+2} solutions is biexponential when monitored at 415 nm with fluorescence lifetimes 0.24 (65.2 %) and 1.65 ns (34.8 %). When measured at 500 nm, the decay is monoexponential and only long lifetime component is observed. Thus fast decay component can be attributed to locally excited state and the long lived species correspond to the TICT species. With progressive addition of the transition metal (Zn^{+2}), the relative amplitude of long lifetime component increases and that of short lifetime component decreases as indicated by Table 3.3.3. These changes are accordance with Zn^{2+} induced enhancement of TICT emission of DMAPIP-b by complexation.

3.4.4. Zinc ion sensing

Zinc being the second most abundant transition metal ion in the human body, in recent years, there has been an increasing attention on the design and synthesis of highly selective fluorescent sensors for zinc ion [241-247]. Zinc ion which plays an important role in biological system such as neuronal signal transmission, regulator of enzymes and DNA-binding [248-250], is closely associated with many severe neurological disorders, including Alzheimer's disease [251], cerebral ischemia [252] and epilepsy Frederickson [253]. Consequently, investigation focused on detecting Zn^{2+} has attracted increased focus. Although significant advances have been made in the design of fluorescence probes for Zn^{2+}, most of the sensors are intensity based sensors [254-274]. The ratiometric sensors have advantage in uneven loading, photobleaching and other factor like intensity dependence of path length and illumination intensity. In addition some of the zinc ionc sensors have disadvantages such as insufficient selectivity or sensitivity [275-277]. Other transition metals cations such as Ni^{2+} or Co^{2+} usually interfere with detection of zinc ion. Thus, developing sensitive and selective ratiometric sensor is ultimate goal in fluorometric metal ion analysis.

From a mechanistic point of view, the diamagnetic Zn^{2+} with d^{10} electronic configuration having flexible coordination geometry is advantageous for the specific binding in our system. The binding ability of Zn^{2+} with DMAPIP-b is more than that of other metal ions. Zn^{2+} complexation site is different from that of other transition metal such as Ni^{2+}, Cd^{2+} or Co^{2+} and induces TICT emission in DMAPIP-b. Therefore we explore the selectivity of DMAPIP-b towards Zn^{2+} by comparing the spectral characteristics of different metal ion complexes of DMAPIP-b.

The spectral characteristics at 20 equivalence of different metal ion (100 μM) are compiled in Table 3.3.1. The absorption and the fluorescence spectra were shown in Figure 3.3.14 and 3.3.15 respectively. Complexation of Zn^{2+} with DMAPIP-b changes initial fluorescence "ON" locally excited state to "ON" TICT state. These changes were revealed by a visible color change of fluorescence from light blue to green in presence of

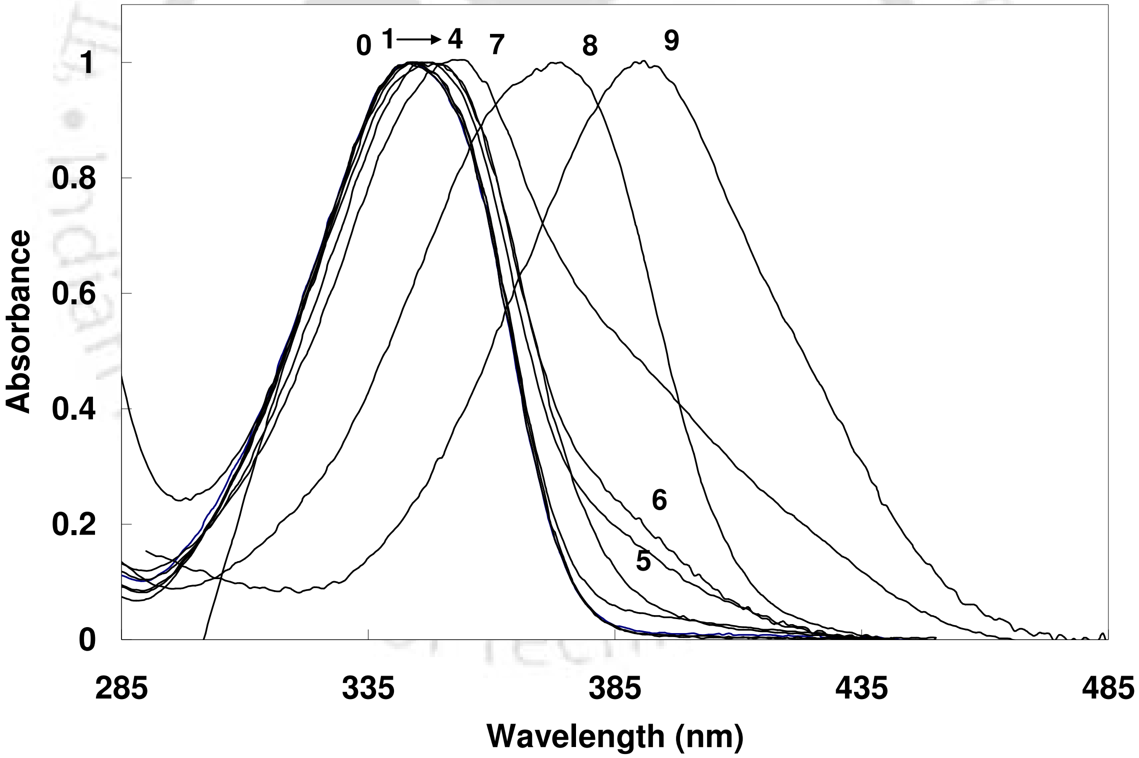

***Figure 3.3.14:* *Normalized absorption spectra of DMAPIP-b in the presence of 20 equivalents of different metal ions*. 0 (no metal ion), 1 (Li^{+}), 2 (Na+), 3 (Ca^{+2}), 4 (Ba^{+2}), 5 (Cd^{+2}), 6 (Co^{+2}), 7 (Mg^{+2}), 8 (Ni^{+2}) and 9 (Zn^{+2}).**

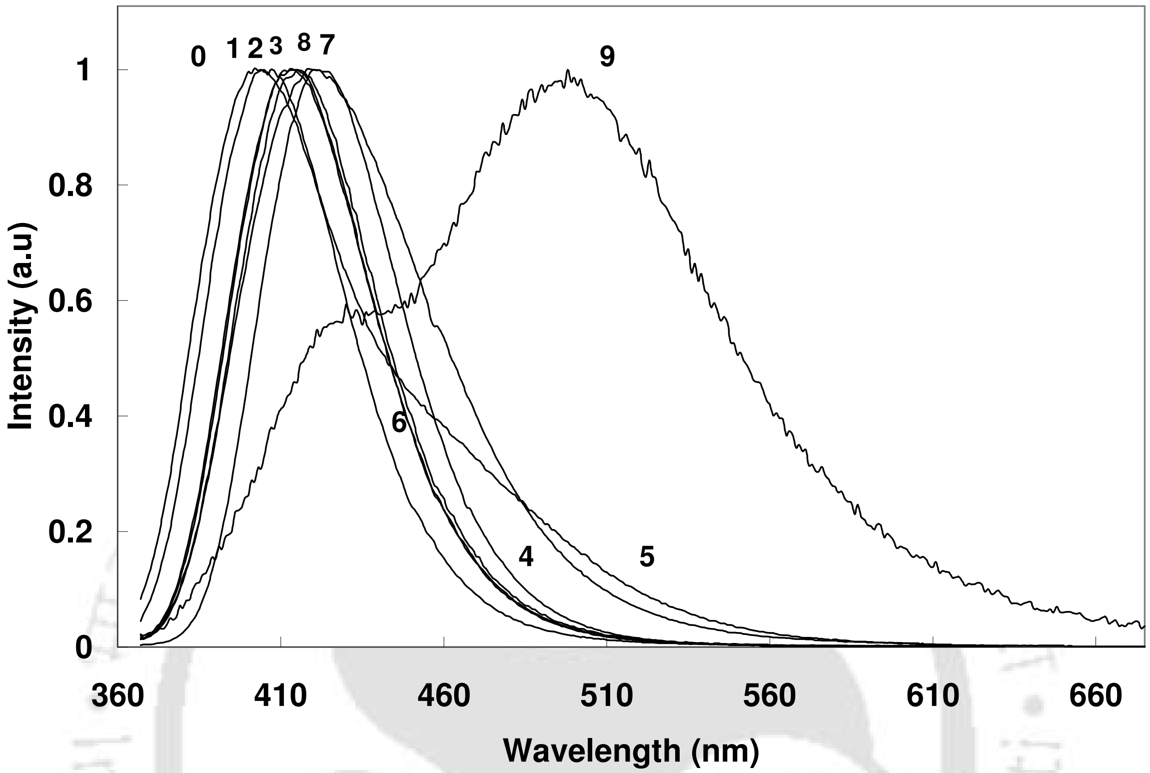

***Figure 3.3.15: Normalized fluorescence spectra of DMAPIP-b in the presence of 20 equivalents of different metal ions*. 0 (no metal ion), 1 (Li^{+}), 2 (Na+), 3 (Ca^{+2}), 4 (Ba^{+2}), 5 (Cd^{+2}), 6 (Co^{+2}), 7 (Mg^{+2}), 8 (Ni^{+2}) and 9 (Zn^{+2}).**

zinc perchlorate (Figure 3.3.16). The color change of fluorescence was specific toward Zn^{+2}, whereas addition of Li^{+}, Na^{+}, Ca^{+2}, Ba^{+2}, Mg^{2+} and Cd^{2+} did not show any change visible color change (Figure 3.3.16). On the other hand, paramagnetic metal ions Co^{2+} and Ni^{2+} changes initial fluorescence “ON” state to “OFF” state. The plot of intensity ratio of different metal ions (Figure 3.3.17) accomplished that DMAPIP-b can act as potential zinc sensor.

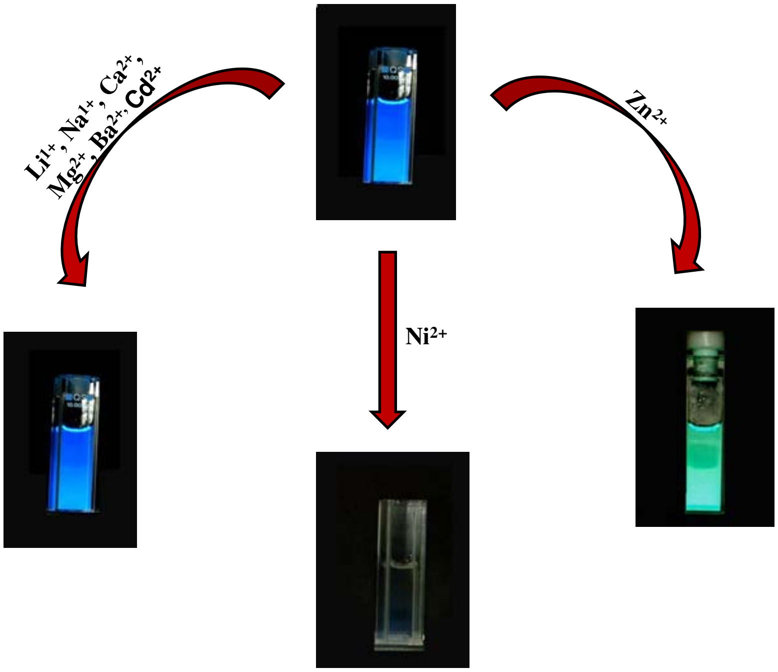

Figure 3.3.16: Fluorescence of DMAPIP-b upon addition of different metal cation.

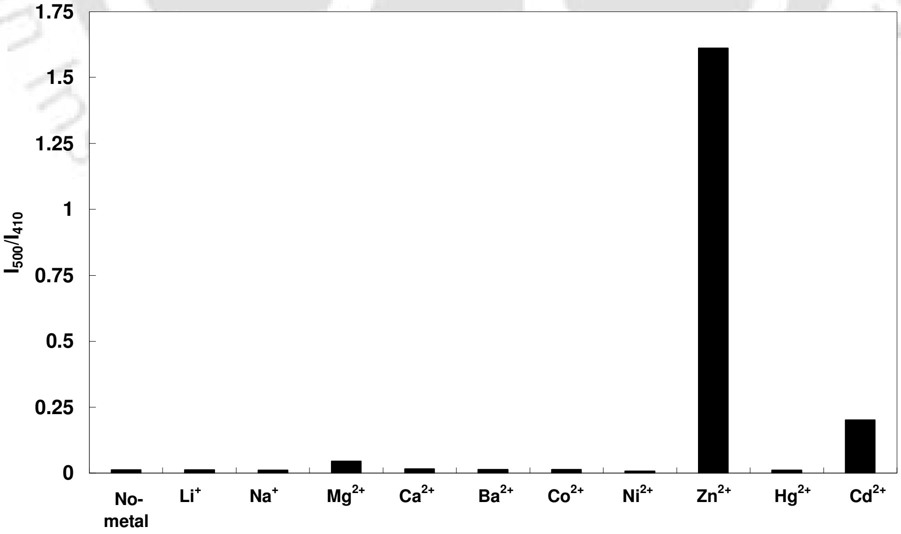

Figure 3.3.17: Fluorescence intensity ratio in presence of different metals (100 μM) λ_{exc} = 360 nm.

3.3.5. Conclusion

Zn^{+2} specifically binds at pyridine nitrogen of DMAPIP-b and produce significant shift in the absorption and the emission spectra. It has strong affinity towards DMAPIP-b, upon complexation with DMAPIP-b, it changes the initial fluorescence “ON” locally excited state of DMAPIP-b to “ON” TICT state. Alkali and alkaline earth metals importantly, biologically significant ions, particularly the coordinatively competing Ca^{2+} and Mg^{2+} induce insignificant photophysical perturbations. However, transition metal ions Ni^{2+} and Co^{2+} form non fluorescent ground state complexes with DMAPIP-b by binding at imidazole nitrogen. But Cd^{2+} forms fluorescing complexes with DMAPIP-b by binding at imidazole nitrogen.

3.4. Effect of long alkyl chain

Research on luminescent organic materials have become attractive field, owing to their wide variety of practical applications in different fields. On that account, a better knowledge of understanding and control of the photophysical properties are not only contribute to the improvement of their technological applications, but also expected to encourage novel and innovative application concepts. Since DMAPIP-b is an interesting molecule and emits dual emission only in protic solvents, we intent to establish the effect of attaching long alkyl chain on the optical properties of the system, in particular on its dual emission.

Periasamy et al. found that the spectral characteristics of aminostyryl pyridinium chromophore are not significantly perturbed by the length of the alkyl chain attached to the pyridinium nitrogen [278]. Thus, we have synthesized two N-alkylated products with same chain length, but attached at different positions. The molecules are namely 2-[4'-(*N*,*N*-dimethylaminophenyl)imidazo[4,5-*b*]hexadecylpyridinylium bromide (**1**), where hexadecyl chain is attached at the pyridine nitrogen and 1-hexadecyl-2-[4'-(*N*,*N*-dimethylaminophenyl)imidazo[4,5-*b*]pyridine (**2**), where the chain is substituted in the imidazole nitrogen, >N-H (chart 3.4.1).

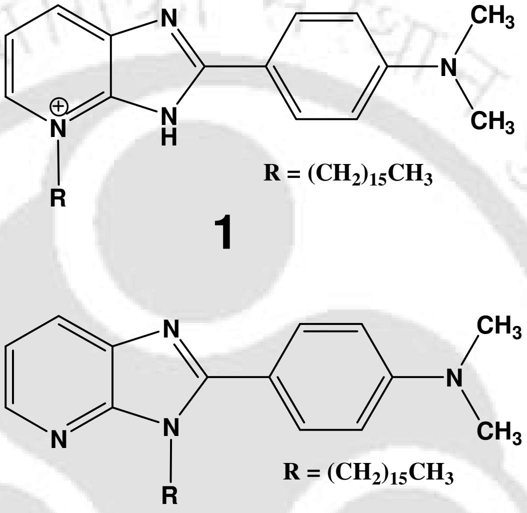

1

2

***Chart 3.4.1: Structures of the alkylated products of DMAPIP-b*.**

3.4.1. Absorption spectra

Absorption spectra of **1** and **2** are recorded in different solvents and the observed long wavelength band maxima are compiled in Table 3.4.1. The absorption spectra of **2** are blue shifted compared to those of DMAPIP-b (Section 3.1.1). On the other hand, the absorption spectra of **1** are strongly red shifted relative to those of parent molecule (Section 3.1.1). However on increasing the polarity and the hydrogen bonding capacity of the medium, the absorption spectra of the alkylated molecules, undergo red shift with loss of vibrational structures, which is same as observed in DMAPIP-b.

Table 3.4.1: Absorption band maxima (λ_{max}^{ab}, nm), fluorescence band maxima (λ_{max}^{fl}, nm), fluorescence quantum yield (ϕ) and lifetimes[1] (τ, ns) of DMAPIP-b in different solvents

Solvent	Molecule 1			Molecule 2		
	λ_{max}^{ab}	λ_{max}^{fl} (ϕ)	τ_f	λ_{max}^{ab}	λ_{max}^{fl} (ϕ)	τ
Cyclohexane	380, 397(sh)	410, 432	1.93	322	361 ,380 (0.58)	
Ether	386	444 (0.89)	2.29	323	375 (0.69)	
Ethyl acetate	378	465 (0.52)	2.49	327	390 (0.70)	1.41
Acetonitrile	383	497 (0.72)	3.15	328	407 (0.73)	1.69
Dimethyl formamide	387	503 (0.74)	3.25	312	422 (0.69)	1.70
Butanol	388	496 (0.66)	3.29	330	412 (0.642)	1.76
2-Propanol	389	496 (0.75)	3.30	327	410 (0.74)	1.78
1-Propanol	389	500 (0.70)	3.24	329	415 (0.72)	1.84
Ethanol	390	505 (0.66)	3.15	330	415 (0.65)	1.84
Glycol	395	525 (0.39)	2.10	335	431 (0.57)	0.76
Methanol	390	515 (0.34)	2.15	331	424 (0.19)	0.64 (97.4) 1.73 (2.6)
Water				347	407 (0.07)	0.24 (59.0) 0.83 (41.0)

[1] λ_{exc} =375 nm, $\lambda_{em} = \lambda_{max}^{fl}$, values in parenthesis are relative amplitude

The optimized geometrical parameters obtained by DFT/B3LYP/6-31G(d,p) are presented in Table 3.4.2. DMAPIP-b is nearly planar in the ground state, the imidazopyridine ring and the dimethylamino groups are out of the phenyl plane only by 0.0° and 2.5° respectively. Attaching alkyl chain at the pyridine nitrogen completely planarize the molecule, the dihedral angles of the imidazopyridine ring and the dimethylamino group with the phenyl ring reduced to 0.04° and 0.07° respectively. Bearing the positive charge on the pyridine ring, the imidazopyridinium ring, acts as better acceptor which increases the conjugation that shifts the spectrum towards red side.

The substitution of the alkyl chain in the imidazole nitrogen makes the molecule nonplanar by twisting the imidazopyridine moiety by 41.4° out of the phenyl plane, the dihedral angles of the dimethylamino group is also increased to 8.9°, thus reduces the conjugation. This is consistent with the blue shift in the spectral maxima of **2**. It is useful to examine the frontier molecular orbitals (FMOs), as it provides a reasonable qualitative indication of the excitation properties. The isosurface plots of FMOs are shown in Figure 3.4.1. The lowest electronic transition of the DMAPIP-b and the alkylated molecules are

Table 3.4.2: Theoretical parameters obtained from the optimized geometry of DMAPIP-b and it's alkylated products (1 and 2) along with experimental excitation and emission energy.

	DMAPIP-b	**Molecule 1**	**Molecule 2**
S_0 State			
Energy (a. u.)	-760.943	-1351.110	-1390.024
Phenyl ring/NMe_2 dihedral angle (°)	2.51	0.07	8.90
Phenyl/PI dihedral angle (°)	0.0	0.04	41.40
Theoretical excitation energy[1] (eV)	3.82	2.97 (2.85)	3.70 (3.94)
Experimental excitation energy (eV)	3.80	3.12	3.85
μ_g (D)	7.2	20.4	4.7
S_1 state			
Phenyl ring/NMe_2 dihedral angle(°)	0.0	0.02	5.50
Phenyl/PI dihedral angle	0.0	0.0	5.0
Theoretical emission energy[1] (eV)	3.56 (3.11)	2.79 (2.66)	3.09 (4.01)
Experimental emission energy (eV)	3.45	2.87	3.44

[1] The values are obtained by TDDFT and those obtained by ZINDO are included within the parenthesis.

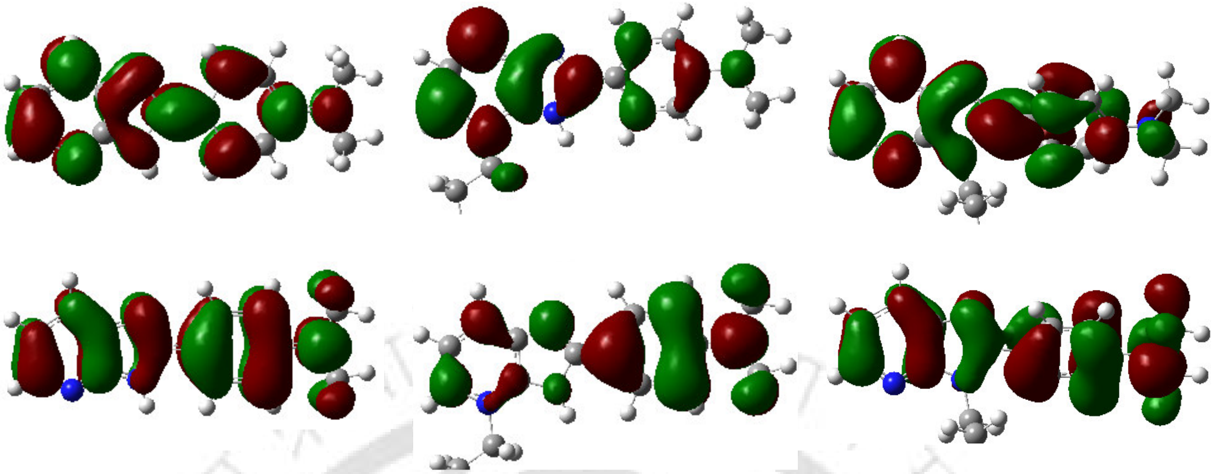

DMAPIP-b **Molecule 1** **Molecule 2**

Figure 3.4.1: The isosurface plots of frontier molecular orbitals, HOMO (bottom) and LUMO (top) of DMAPIP-b, 1 and 2.

described mainly by the promotion of an electron from the highest occupied molecular orbital (HOMO) to the lowest unoccupied molecular orbital (LUMO), which corresponds to a $\pi\pi^*$ excited singlet state. The HOMO and the virtual LUMO distribution patterns show that the LUMO is relatively more concentrated on the imidazopyridine ring than on the dimethylamino group in all three molecules and thus the first electronic transitions should possess some charge transfer nature in all the molecules in general. However in **1** the entire dimethylaminophenyl ring makes only minor contribution and the major contribution is from imidazopyridine ring. This is consistent with higher charge transfer character of **1**. The HOMO of DMAPIP-b and its imidazole alkylated derivative **2**, are more or less declocalized on the dimethylamino, the phenyl and the imidazo pyridine moieties with a nodal plane on the pyridine nitrogen. But the localization on the dimethyl amino group is more in the case of the alkylated derivative (**2**). Upon absorption of photons the molecules are excited to the corresponding Franck-Condon states, which should have the ground state geometries. The vertical excitation energies for the molecules were calculated by performing energy calculation on the DFT optimized structure using ZINDO and TDDFT methods. Small discrepancy is observed between the experimental and the theoretically predicted excitation energies for **1**, that obtained by TDDFT method, but ZINDO value is in reasonable agreement with the experimental value. However in all other cases a good agreement is found between the experimental excitation energies and the theoretical calculated ones from both TDDFT and ZINDO methods (Table 3.4.2).

3.4.2. Fluorescence spectra

The fluorescence spectra of **1** and **2** are shown in Figure 3.4.2 and the data are provided in Table 3.4.1. The fluorescence spectra of both molecules have well resolved vibrational structures in the nonpolar solvents. Upon increasing the polarity of the solvent the spectrum undergoes a bathochromic shift with loss of vibrational structure. The red shift is more pronounced by **1** than that by **2**. The fluorescence decay was measured for both **1** and **2** to obtain the fluorescence lifetimes. The fluorescence decay of **2** in water is shown as a representative plot (Figure 3.4.3) and the fitted data are compiled in Table 3.4.1. The fluorescence lifetime of **1** is also longer than that of **2** and, the emission lifetimes of **1** and **2** are comparable to that of the TICT and the normal emission of DMAPIP-b, respectively. The fluorescence of both **1** and **2** are strongly quenched in methanol. Low fluorescence quantum yield in methanol may be due to the strong intermolecular hydrogen bonding between the fluorophore and the solvent molecules which results in an increase in the nonradiative decay rate. The attenuation of the fluorescence lifetime supports this. The fluorescence of DMAPIP-b was also quenched by the protic solvents (section 3.1.3). Since no hydrogen bonding is possible between the pyridium nitrogen of **1** and the solvent molecules, it is clear that the hydrogen bonding of

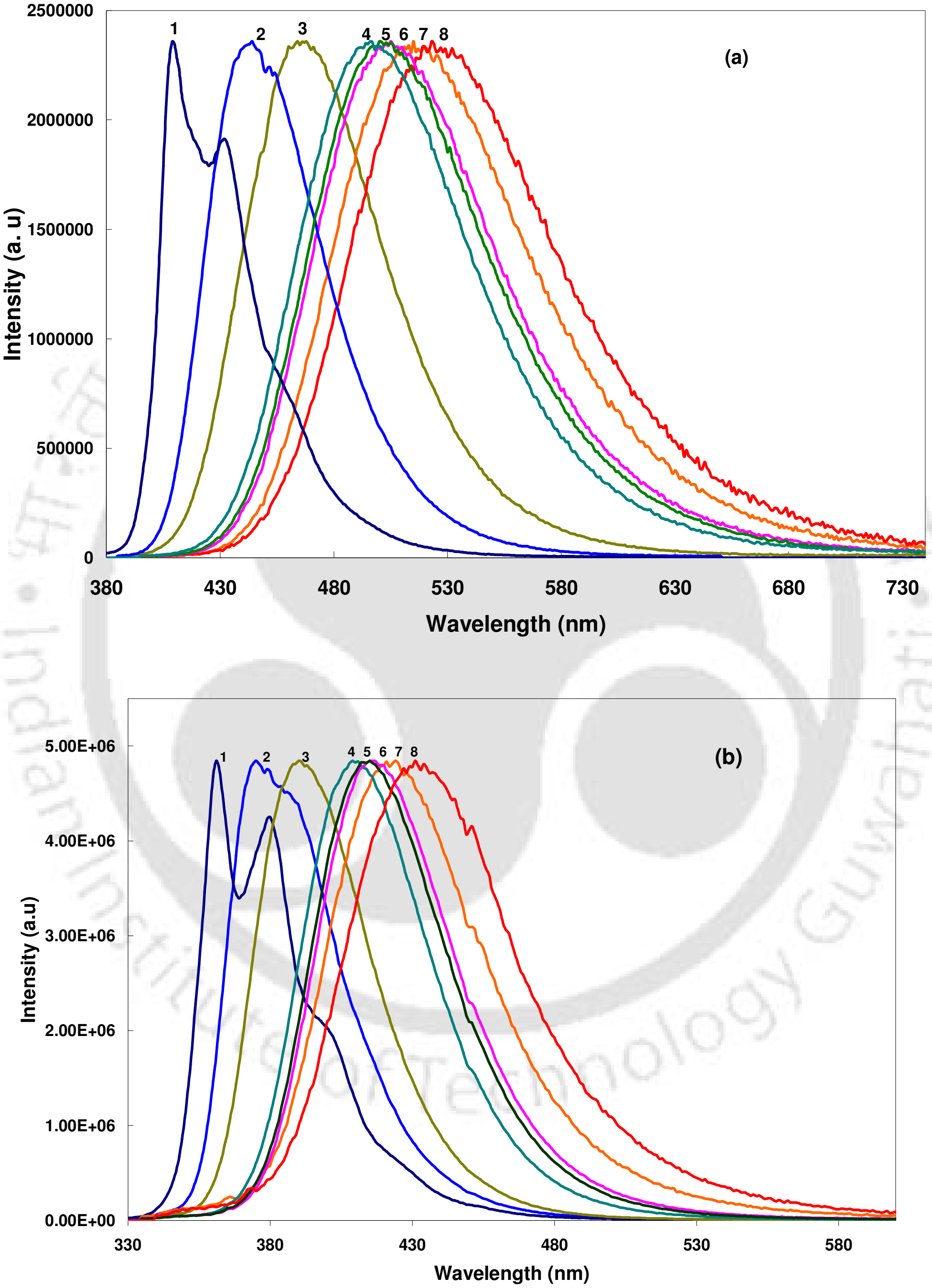

Figure 3.4.2: (a) Fluorescence spectra of 1 in different solvents. (b) Fluorescence spectra of 2 in different solvents. (1) cyclohexane, (2) ether, (3)ethyl acetate, (4) 1-propanol, (5), 2-propanol , (6) ethanol , (7) methanol and (8) glycol.

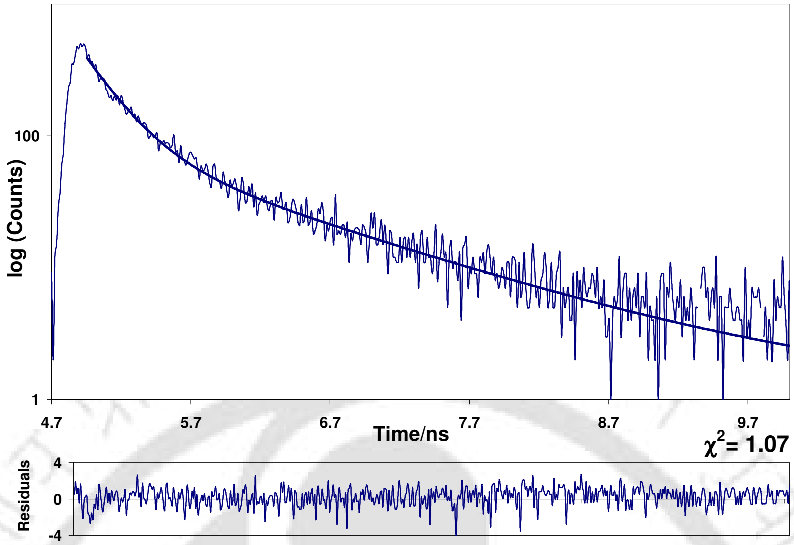

Figure 3.4.3: Fluorescence decay of 2 in water along the fitted curve (the residual plot of double exponential decay fit is also shown).

the solvent with the imidazole nitrogen contribute substantially to the fluorescence quenching in all the three molecules. The fluorescence of DMAPIP-b was also strongly quenched when the imidazole nitrogen of the molecule is protonated (section 3.1.3).

Upon excitation the molecules should relax to their most stable geometry in the first excited state before the emission process could occur, that result in Franck Condon ground state. Since this Franck Condon state possesses the relaxed geometry of the first excited state, the molecules are optimized in the S_1 state with the *ab initio* restricted configuration interaction by singles (RCIS) [198] approach incorporated in Gaussian 03W program. The 6-31G(d,p) basis set are chosen for the excited state calculations also. As expected the planarity increases in the excited state. Only minimal reduction in the angle between the imidazopyridine, the phenyl and the dimethylamino group happens in the excited molecules (DMAPIP-b and **1)** which are already planar in the ground state. In molecule **2**, small reduction in the dihedral angle between the phenyl ring and the dimethylamino group, but a drastic decrease in the angle between the imidazo pyridine ring and the phenyl ring are observed. The fact that in the first excited state DMAPIP-b and **1** do not have significant changes in their geometries, is supported by the small Stokes shifts observed for those compounds (~ 1900 cm^{-1} in cyclohexane). Large geometrical change in the excited structure of **2** is also corroborated by the largely Stokes shifted fluorescence spectrum of **2** (~ 3350 cm^{-1} in cyclohexane). The emission energies from the relaxed excited states are obtained by both TDDFT and ZINDO calculations using the optimized excited state as inputs (Table 3.4.2). A reasonable agreement is found between the theoretically predicted values and the experimental measurements.

Remarkable aspect of the fluorescence behavior of DMAPIP-b is its dual emission in protic solvents. However single emission bands are observed for both **1** and **2** in all the solvents including most of the protic solvents (Table 3.4.1, except in methanol and water for **2**). The fluorescence spectrum of DMAPIP-b in methanol is compared with that of the alkyated molecules in Figure 3.4.4. Comparative spectra clearly suggest that **1** and **2** are emitting from the TICT state and the locally excited state respectively. The TICT fluorescence depends on the strength of the donor and the acceptor [12]. DMAPIP-b exhibits TICT emission in the protic solvents due to hydrogen bonding of the solvent molecule with the pyridine nitrogen. Such a hydrogen bonding increases the electron accepting nature of imidazopyridine ring which favors the formation of the TICT state. Thus, the observation of the TICT emission from **1** is not surprising, addition of the alky chain on the pyridine nitrogen made it positively charged which should increase the electron withdrawing potential of the system. It is further substantiated by the fact that only TICT emission had been observed from the monocations formed by the protonation at pydrine nitrogen of DMAPIP-b (Section 4.1.3 and 4.2.4) as well as in DMAPIP-c [182]. The fluorescence lifetimes of **1** is also longer than that of normal emission of DMAPIP-b and are close to those of the TICT emission of the parent compound. Alkylated aminostyryl pyridinium dyes also reported to have longer TICT emission than normal emission [278].

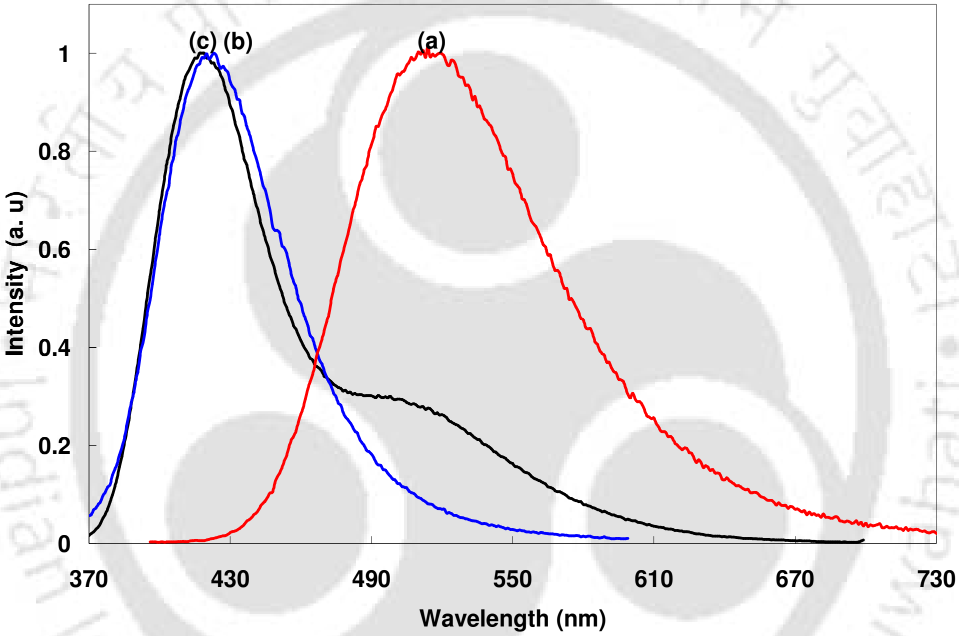

Figure 3.4.4: Normalized fluorescence spectra of (a) 1, (b) 2 and (c) DMAPIP-b in methanol.

Interestingly **2** emits only single emission from the locally excited state in most of the alcoholic solvents (except methanol). This is substantiated by the single exponential decay of **2** in all those solvents. However though no clear two band system is observed in methanol and water, the fluorescence decays are biexponential in these solvents (Table 3.4.1). Such a double exponential decays indicate that the TICT emission is buried underneath the normal emission. In methanol the contribution of the second (TICT) species is negligible (Figure 3.4.4, Table 3.4.1). In water the relative amplitude of the TICT emission increases (Table 3.4.1) and the fluorescence spectrum also has long tail (Figure 3.4.5a).

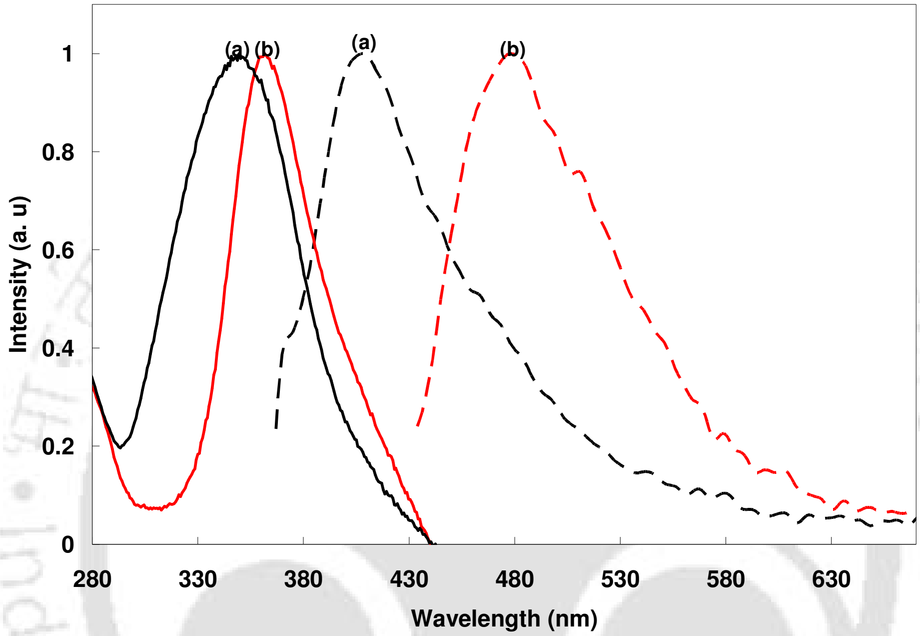

Figure 3.4.5: Absorption (solid lines) and fluorescence (dotted lines) spectra of (a) neutral (pH 7) and (b) monocationic (pH 1.5) forms of 2.

As mentioned earlier (section 1.2.3), Kim et al. proposed that the TICT emission was enhanced in p-diethylamino- and p-dimethylaminobenzoic acids β-CD inclusion complexes due to increase in coplanarity of the acceptor with the benzene ring by hydrogen bonding [65]. According to their model the increase in planarity of the acceptor and the benzene ring increases the charge flow from the benzene ring to the acceptor which is suppose to favor the formation of the TICT state. Unlike in DMAPIP-b and **1**, in **2** the acceptor imidazopyridine ring and the benzene ring are out of the plane by 41.4° in the ground state. This should reduce the charge flow from phenyl ring to imidazole ring. However, we speculate that the absence of TICT emission is due to difficulty in the formation hydrogen bond with pyridine nitrogen by solvent rather than due to twisting of the imidazole ring. Following facts strengthened this hypothesis: (i) though the alkylation push the phenyl ring out of the plane from the imidazopyridine ring in the ground state, in the excited state the angle is reduced to 5°. (ii) Single exponential decay is observed in ethanol and longer alcohols, but the biexponential decay is observed in methanol and the relative contribution of the minor component further increases in much smaller solvent, water. It may also be noted here not only the bulkiness of the solvent decreases, but also the hydrogen bond donating capacity also increases in water compared to methanol. Thus, the combined factor may be responsible for inducing TICT emission in **2**.

To substantiate further we have studied the effect of pH. Upon decreasing the pH, the enhanced electron withdrawing effect of the imidazopyridinium ion that formed by protonation is expected to increase the TICT emission. The absorption spectrum of **2** is red shifted on protonation (Figure 3.4.5). This is consistent with the protonation of the ring nitrogen. The fluorescence spectral band maximum of DMAPIP-b in water is nearly unaffected when imidazole nitrogen is protonated, (Section 3.1.3) but highly red shifted TICT fluorescence was observed on protonation at pyridine nitrogen (Sections 4.1.3 and 4.2.4). On protonation the fluorescence spectrum of **2** is red shifted nearly by 70 nm (Figure 3.4.5). This suggested the monocation formed by protonation at the pyridine nitrogen of **2** and is emitting from the TICT state. The theoretical excitation energies obtained by TDDFT and ZINDO for the monocation are 2.34 eV and 2.95 eV respectively and the corresponding emission energies obtained are 2.50 eV (TDDFT) and 2.73 eV (ZINDO).

3.4.3. Conclusion

N- alkylation strongly perturbed the fluorescence characteristics of DMAPIP-b. Upon addition of long alkyl chain at the pyridine nitrogen in DMAPIP-b, the molecule (**1**) starts to emit from the TICT state even in polar aprotic solvents. On the other hand in case of the imidazole nitrogen substituted molecule (**2**), only normal fluorescence is observed in most of the polar protic solvents also. Methanol and water are the exception where smaller size and larger hydrogen bond donating capacity of solvents facilitate dual emission from **2**. The emission life time of **1** and **2** are close to that of the TICT and the normal emissions of DMAPIP-b.

Chapter 4

Effect of microheterogeneous media on the dual fluorescence of 2-(4’-*N,N*-dimethylaminophenyl)imidazo[4,5-*b*]pyridine

4.0. Introduction

This chapter is also divided into four sections. The effect of four different microheterogeneous systems CD, normal micelles, reverse micelles and protein (BSA) on the dual fluorescence of DMAPIP-b are discussed in four different sections.

4.1. Effect of β-cyclodextrin

The reduced polarity and restricted geometry of the CD nanocavities provide an interesting microenvironment for studying the photophyics and photochemistry of the encapsulated molecules. Thus, increased attention has been paid to study the energetic and dynamics of various photochemical processes in CDs, such as room temperature phosphorescence [279-280], proton transfer [281,103], charge transfer [230, 282-284], and energy transfer [285].

Several groups studied the TICT phenomenon in CD nanocavities [230, 282, 283]. The relative position and intensity of the TICT emission are usually influenced by polarity, hydrogen bonding ability and viscosity of the environment [12, 13, 47, 286, 287]. Thus, the TICT emission has been used as a probe to study the microenvironments [83, 188]. CD forms a hydrophobic and restrictive cavity with hydrophilic external walls in aqueous solution, providing two different microenvironments with an incorporated guest molecules. The enhancement of TICT emission in CD cavity was attributed by Nag et al to decrease in the nonradiative rate due to reduced polarity of the environment [230]. However, Al-Hassan et al. [282] proposed that the formation of the TICT state depends on the restriction on molecular motion rather than the polarity alone. Jiang [289] also reported that the TICT emission of *p*-(*N*,*N*-dimethylamino)benzoic acid depends on the viscosity in the α- and β-CD inclusion complexes. On the other hand, Kim et al. [65] demonstrated that the specific hydrogen bonding plays an important role in TICT emission of *p*-(*N*,*N*-diethylamino)benzoic acid/CD complexes. Recently Matsushita et al. [290] revealed that the polarity effect introduced by the hydrophobic cavity is more important in controlling the TICT fluorescence of 4'-dimethylaminoacetophenone. These controversial and contradicting arguments reveal that overall effect of the CDs encapsulation is complicated and depends on the size of the CD cavity and guest molecules. Thus necessitates more investigation on the effects of CD complex formation on TICT process. The host molecule β-CD provides the most versatile cavity for molecular entrapment among the naturally available CDs.

Thus, in this section, we examined the fluorescence characteristics of DMAPIP-b inside *β*-CD cavity, one of the reasons being that the guest molecule is quite big and can be encapsulated only lengthwise. The TICT fluorescence of DMAPIP-b is induced by hydrogen bond of the solvent with pyrio-nitrogen. Thus in addition to polarity and viscosity, hydrogen bonding may influence the emission characteristics of DMAPIP-b/*β* -CD complex.

4.1.1 Characteristics of Inclusion complex

Absorption data of DMAPIP-b in *β*-CD along with few selected solvents are compiled in Table 4.1.1. The absorption spectra are red shifted with an increase in the absorbance upon increasing the concentration of *β*-CD. The changes in optical density with addition of *β*-CD have been attributed to the incorporation of DMAPIP-b in *β*-CD through the detergent action of host [289].

Table 4.1.1: Absorption band maxima (λ_{max}^{ab}, nm), log $\in_{max}$ $M^{-1}cm^{-1}$, fluorescence band maxima[1] (λ_{max}^{fl}, nm), quantum yield (ϕ) and fluorescence life time[2] (τ, ns) for DMAPIP-b in different media.

Medium	λ_{max}^{ab}	log $\in_{max}$	λ_{max}^{fl} (ϕ)	τ (ns)	χ^2
Cyclohexane	336, 352(sh)	-	359, 379, 398	1.99	1.02
Acetonitrile	345	4.50	407	1.50	0.95
Methanol	350	4.50	414	0.31 (56.5)	1.26
			506	1.16 (43.5)	
Water (pH 9.0)[3]	345	4.39	451 (0.042)	0.16 (98.7)	1.17
				2.13 (01.3)	
β-CD (pH 9.0)[4]	350	4.43	424 (0.19)	0.61 (79.5)	1.21
				2.04 (20.5)	
Water (pH 4.0)[5]	386	-	451 (0.0065)	-	
β-CD (pH 3.5)[5]	388	-	433 (0.028)	0.35	1.25
			535 (0.013)	1.61	

[1] λ_{exc} = λ_{max}^{a}, [2] λ_{exc} =385 nm and λ_{em} > 420 nm, [3] molecule is in its neutral form, [4] 86% complexation, [5] molecule is in its monocationic form. χ^2 values are obtained for fluorescence decay analysis.

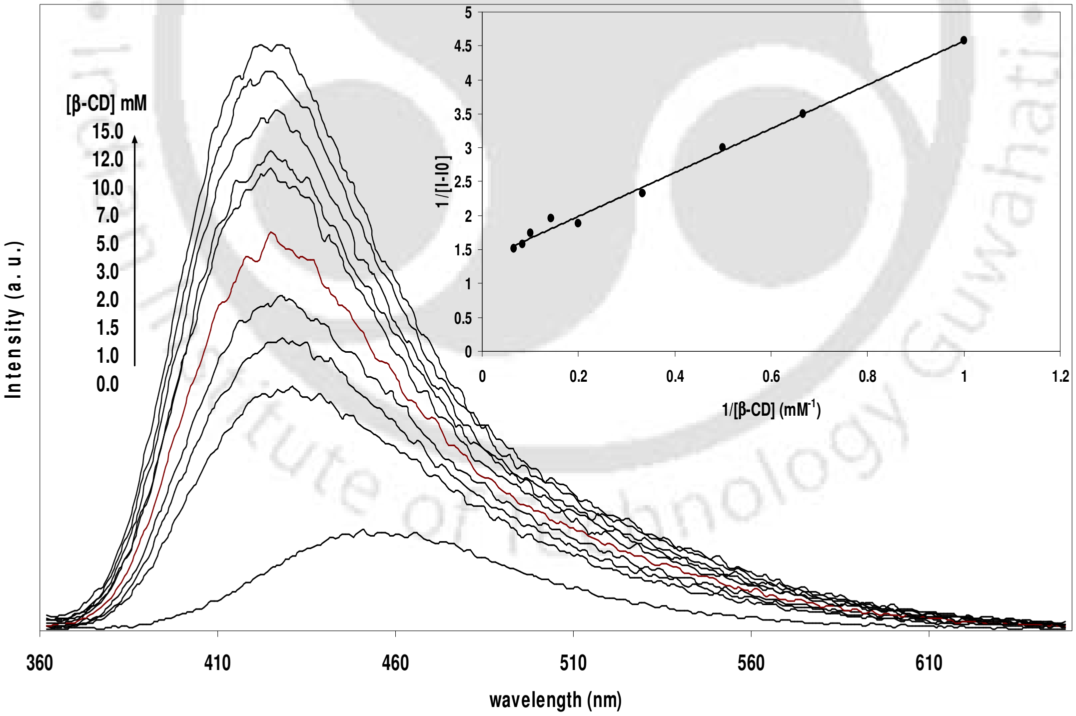

Figure 4.1.1: Fluorescence spectra of DMAPIP-b in aqueous at different β-CD concentration at pH 9, λ_{exc} = 360 nm and the insert shows the double reciprocal plot of 1/(I-I_0) vs 1/[β-CD].

The fluorescence characteristics of neutral DMAPIP-b (at pH ~ 9) in aqueous solution undergo significant changes in the presence of β-CD (Figure 4.1.1). The fluorescence spectra undergo a gradual blue shift with increase in β-CD concentration. The fluorescence intensity is also increased substantially in presence of β-CD. In 15 mM β-CD solution, the fluorescence band maxima is blue-shifted by ~ 30 nm and overall fluorescence yield increases by a factor of 4.5 compared to those observed in the absence of β-CD. The emission maximum ($\bar{\nu}_F$) in β-CD suggests that the molecule experience a methanol/water mixture environment upon encapsulation. The estimated polarity inside the β-CD varies from Kosower's Z value of 88 (similar to ethanol) to dielectric constant of 48 (close dielectric constant of dimethylsulfoxide, 49) [102, 291-293]. The discrepancies are due to the fact that observed polarity inside the cavity depends upon local polarity, number of water molecule trapped inside the cavity, partial encapsulation of the probe, motional freedom etc. But Nigam and Durocher [294] also estimated the polarity of the β-CD to be similar to that of methanol-water mixture using 3H-indole derivatives as probes.

The association constant and the stoichiometric ratios of the complex can be determined by using the Benesi-Hildebrand equation [295, 296]

$$\frac{1}{[I-I_0]}=\frac{1}{[I_1-I_0]}+\frac{1}{[I_1-I_0]K[\beta-CD]} \qquad (4.1.1)$$

Where I_0, I and I_1 are the emission intensities in absence of β-CD, in presence of β-CD and when the molecule is completely solubilized in β-CD respectively. The double reciprocal plot of $1/(I–I_0)$ versus 1/[β-CD] is depicted in Figure 4.1.1 as an insert (the emission intensities at 424 nm are used for Benesi-Hildebrand plot). The linear plot (r^2 =

0.99) confirms the formation of 1:1 inclusion complex between DMAPIP-b and β-CD. The association constant obtained from the plot is 410 ± 20 M^{-1}.

As seen earlier (section 3.1) the intensity ratio of the TICT to normal emission increases with increase in hydrogen bonding capacity of the solvent, but in water the TICT emission is almost completely quenched (life time data indicates mere 1% for decay measurement below 420 nm). This was attributed to greater stabilization of the highly polar TICT state by strong dipole-dipole and hydrogen bond interaction with water, and consequently, rapid nonradiative transition to the ground and/or low lying triplet state. The intensity ratio of the TICT to normal emission also decreases with increase in viscosity of the protic solvent.

The DFT optimized geometry of DMAPIP-b is shown in Figure 2 and important parameter are compiled in Table 4.1.2. The molecule is nearly planar in the ground state

Table 4.1.2: Optimized molecular parameters of DMAPIP-b.

	Ground State	**Excited State**
Energy (a. u.)	-760.943	-755.620
Phenyl/imidazopyridine dihedral angle (^{o})	6.7	0.0
Phenyl/dimethylamino dihedral angle (^{o})	2.5	0.0
μ (D)	5.0	6.7

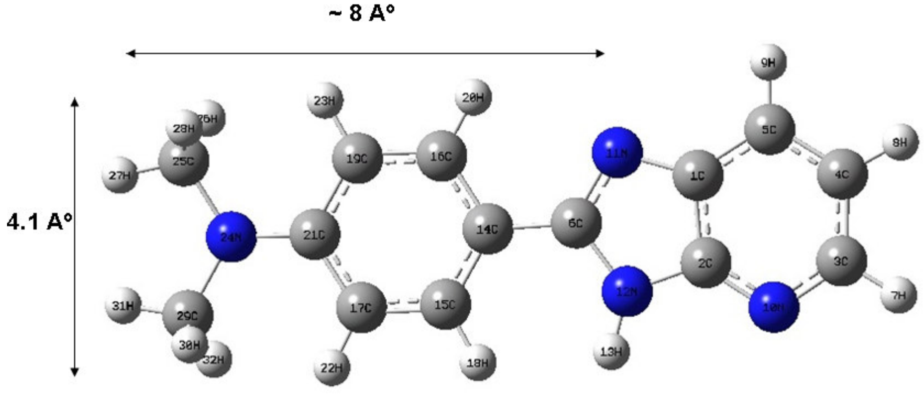

Figure 4.1.2: Optimized geometry of DMAPIP-b at DFT level using 6-31 G(d) basis set.

with the benzene ring having dihedral angle of 0° and 2.5° with the acceptor imdazopyridine ring and the donor dimethylamino group respectively. The geometry optimization was carried out in the first excited state using the ab initio restricted CIS method [198]. The calculations predict that the molecule is complete planar in the first excited state (Table 4.1.2). Small dihedral angle difference between the optimized geometries in the ground and first excited states supports the earlier conclusion that DMAPIP-b be endowed by similar geometry in the S_0 and S_1 states (Table 3.1.2).

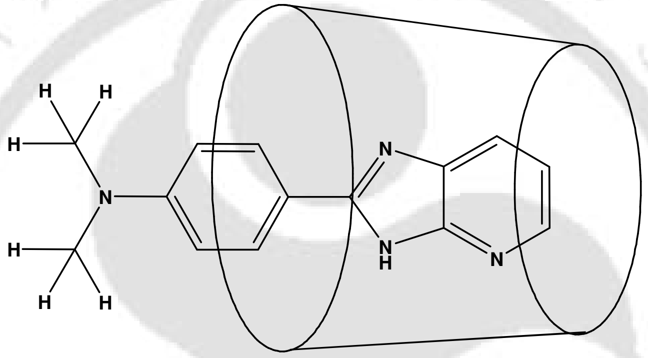

Type (a)

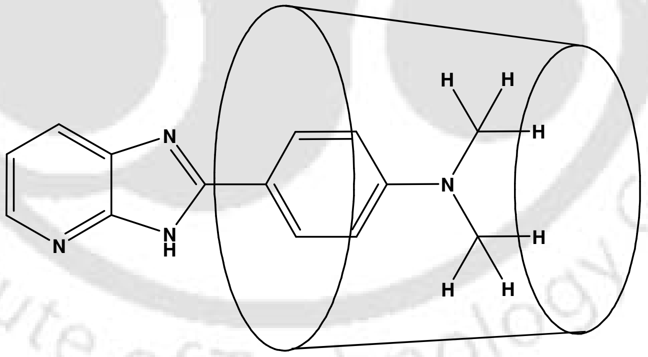

Type (b)

Scheme 4.1.1. Possible structures of inclusion complex

Considering the shape and dimension of DMAPIP-b (Figure 4.1.2) and *β*-CD [100], the guest can enter *β*-CD lengthwise in two ways as shown in Scheme 4.1.1. The protonation of dimethylamino group will lead to a blue shift in the absorption spectra and the protonation of ring nitrogens will result in a red shift in the absorption spectra. Since hydrogen bonding is the first step of protonation, same shift of smaller magnitude is expected by hydrogen bonding. The observed red shift in the absorption spectrum of DMAPIP-b in β-CD solution (Table 4.1.1) suggests that, DMAPIP-b forms type (b) inclusion complex with β-CD, as its formation eliminates the solvation shell around the dimethylamino group of DMAPIP-b. The formation of type (b) complex is further substantiated by the dual fluorescence of the inclusion complex (section 4.1.2). Outside projection of pyridine ring in type (b) complex ensures the hydrogen bonding that is necessary for the formation of TICT state in DMAPIP-b.

To further support the inclusion complex ^{1}H NMR measurements are performed. The chemical shift obtained for β-CD protons were very close to that reported in the literature (Figure 4.1.3a). The β-CD spectrum shifted upfield upon addition of DMAPIP-b (Figure 4.1.3a) and is consistent with the formation of inclusion complex [298]. The NMR spectral data of DMAPIP-b in D_2O and that in β-CD/D_2O are compiled in Table 4.1.3 along with the data in $CDCl_3$. The spectra in D_2O and β-CD/D_2O are shown in Figure 4.1.3b (the spectrum in $CDCl_3$ along with decoupled spectra are provided in the Appendix I). The chemical shift values are in the order $H_f < H_e < H_b < H_c < H_d < H_a$ with splitting of peaks in $CDCl_3$. The peaks are broad without splitting in D_2O. The peaks were assigned in D_2O based on the chemical shift order in $CDCl_3$ and integration values (Table 4.1.3). In D_2O two H_d protons and H_c proton merged to give a broad signal at 7.88, the integration value confirms this. Upon addition of β-CD the peak corresponds to H_e protons (phenyl group protons closer to dimethylamino group), is shifted upfield by 0.10 ppm, the peak of H_f protons (dimethylamino protons) is shifted down field by 0.08

Table 4.1.3: NMR spectral data of DMAPIP-b in different media (for proton label, see Figure 4.1.3)

Proton	$CDCl_3$	D_2O	β-CD/D_2O
H_a	8.24 (d, J = 5 Hz , 1H)	8.22 (brs, 1H)	8.22 (brs,1H)
H_b	7.14 (dd, J = 8, 5 Hz, 1H)	7.25 (brs,1H)	7.24 (brs ,1H)
H_c	7.96 (d, J= 8 Hz , 1H)	7.88 (brs, 3H)	7.88 (brs, 1H)[1]
H_d	8.12 (d, J = 9 Hz, 2H)		7.91 (brs, 2H)
H_e	6.74 (d, J =9 Hz, 2H)	6.87 (brs, 2H)	6.77 (brs,2H)
H_f	3.05 (s, 6H)	2.94 (brs, 6H)	3.02 (brs,6H)

[1] appears as shoulder of δ 7.91 peak

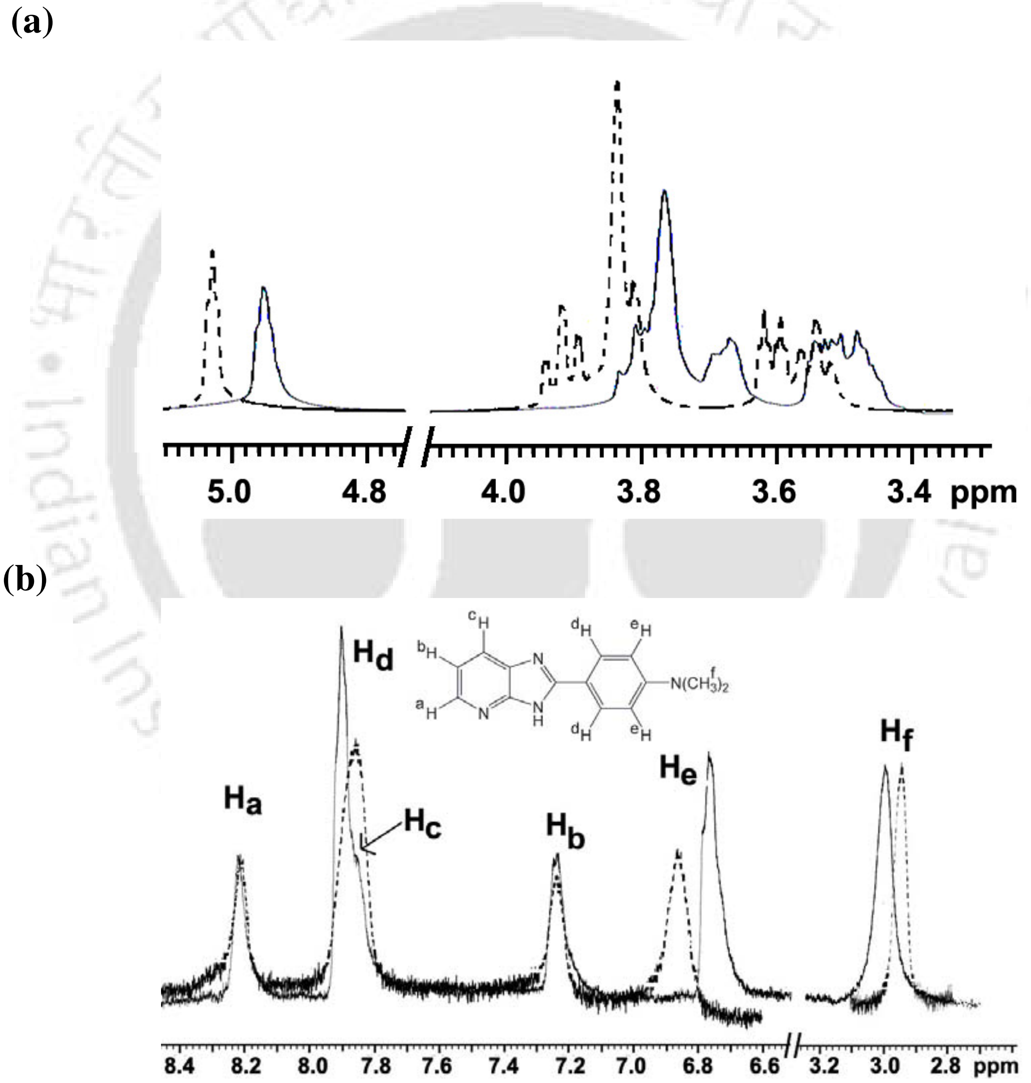

Figure 4.1.3: (a) ^{1}H NMR spectra of β-CD in presence (solid line) and absence (dotted line) of DMAPIP-b in D_2O. (b) ^{1}H NMR spectra of DMAPPI-b in presence (solid line) and absence (dotted line) of β-CD in D_2O (intensity in the aromatic range of the spectra is expanded approximately by a factor of six).

ppm and H_d (phenyl group protons closer to heterocylic ring) peak is shifted down field by 0.03 ppm. But those correspond to heterocylic ring protons are nearly unaffected. The H_c proton i.e. merged with H_d protons in D_2O appears as shoulder in *β*-CD solution due to down field shift of H_d protons. This supports the earlier conclusion that DMAPIP-b/*β*-CD forms type (b) complex. The maximum shift is observed for peak of H_e protons that are present much deep interior of the cavity.

4.1.2. TICT emission

In the fluorescence spectrum though weak shoulder appears at 520 nm, no clear band or shoulder as reported in alcohol is observed for TICT emission of DMAPIP-b in *β*-CD (Figure 4.1.4). Fluorescence decay was measured in 15 mM *β*-CD is presented in

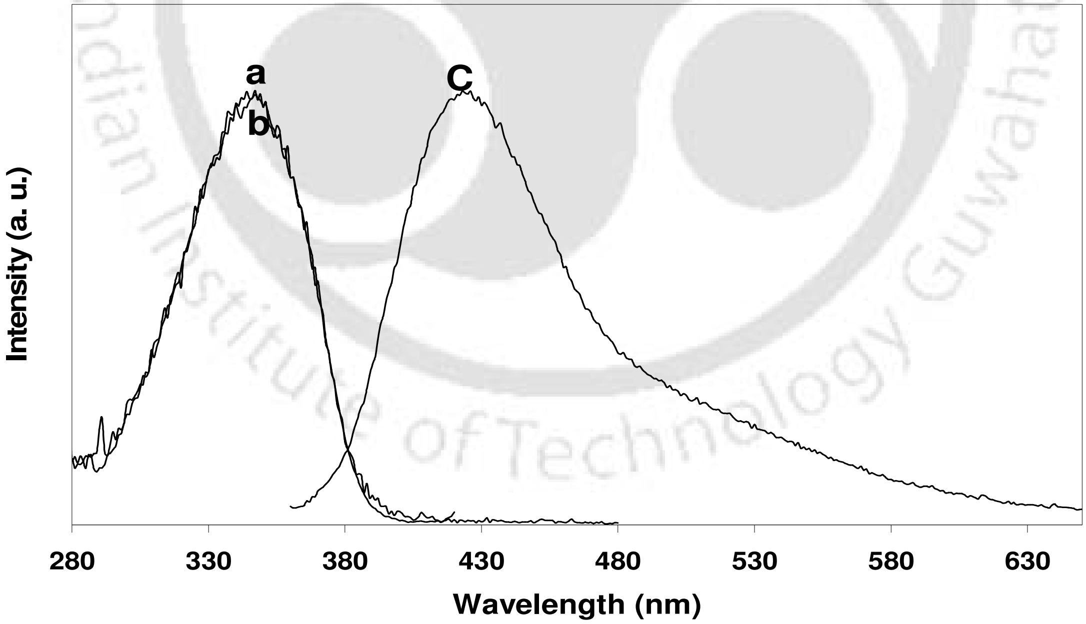

Figure 4.1.4: Normalized fluorescence excitation, (a) λ_{em} = 420 nm, (b) λ_{em} = 520 nm and emission (c) λ_{exc} = 350 nm spectra of DMAPIP-b in 15 mM aqueous β-CD solution.

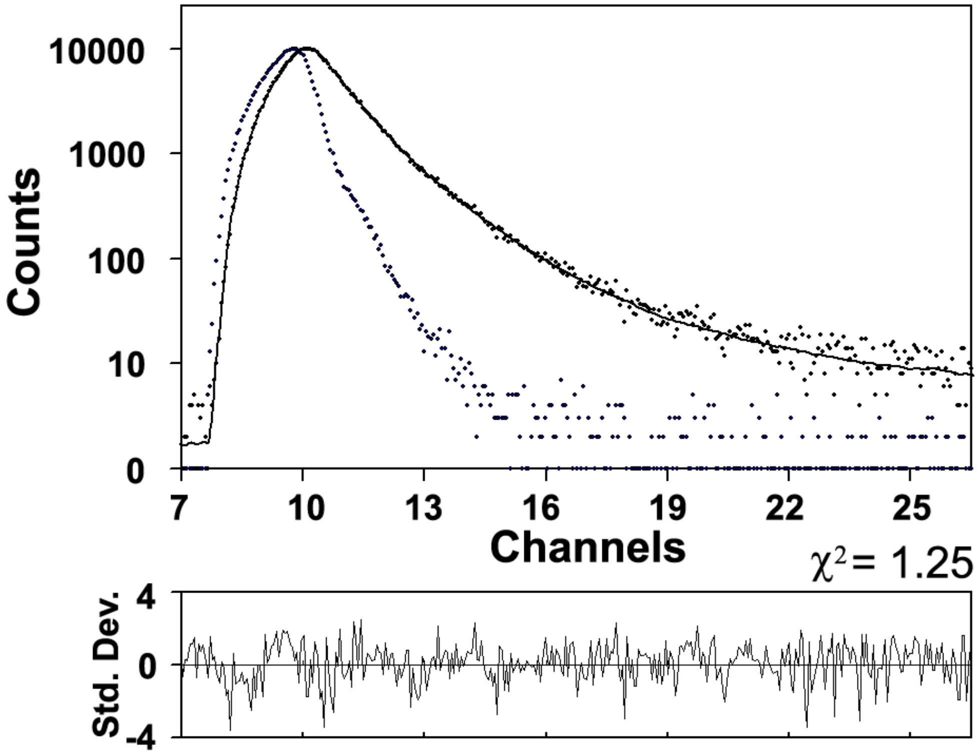

Figure 4.1.5: Fluorescence decay of DMAPIP-b in 15 mM aqueous β-CD at pH 9.0 along with the instrument response function and the solid line shows the fitting (time calibration 0.056 ns/channel).

Figure 4.1.5 and the data are compiled in Table 4.1.1. The biexponential fluorescence decay in *β*-CD clearly indicates the presence of TICT emission. Instrument limitation prevents us from measuring the rate constant for the formation of TICT process and the reverse. But the large difference observed in the lifetimes of both states implies that the formation TICT state is irreversible. This may be due to stabilization of the TICT state by the hydrogen bonding of the water molecules in CD complex which should increase the activation barrier for the reverse process. The behavior is also reported for *p*-(*N*,*N*-diethylamino)benzoic acid [65] and DMAPIP-c [68] inclusion complexes with *β*-CD. The relative increase in TICT emission is small in DMAPIP-b/*β*-CD complex compared to

DMAPIP-c/β-CD [68] complex, where TICT emission appears as clear band with ~ 45 times increase in fluorescence with respect to that in water. Considering the facts two guest molecules differ only in position of pyridine nitrogen and they form same type complex with β-CD, drastic difference TICT fluorescence suggest that the change in position of nitrogen strongly affect the TICT character of the molecule. The TICT state is lower in energy in DMAPIP-b/β-CD inclusion complex than DMAPIP-c/β-CD inclusion complex.

Kundu et al. [299] proposed formation of two types of complexes between 4-dimethylaminobenzaldehyde and β-CD: (i) totally encapsulated molecule, responsible for normal emission and (ii) partially encapsulated molecule, responsible for TICT emission. The excitation spectra recorded for DMAPIP-b in 15 mM β-CD solution at 420 nm and 520 nm are identical (Figure 4.1.4). This implies that both the emissions have same ground state precursor and also substantiates the conclusion only one type of inclusion complex is formed between DMAPIP-b and β-CD. The relative amplitude of the TICT emission increased in β-CD solution (Table 4.1.1). This shows the enhancement of TICT emission of DMAPIP-b inside the β-CD cavity. This indicates that the restriction of the increased viscosity in the CD cavity does not affect the formation of TICT state in DMAPIP-b. On the other hand the reduced polarity of the CD cavity decreases the nonradiative rate as proposed by Nag et al. [230]. Recently based on the computational study it was suggested that the isomer which is hydrogen bonded with water through dimethylamino nitrogen is responsible for the TICT emission in 4-(dimethylamino)methylbenzoate in gas phase not the one that is hydrogen bonded through oxygen atom of the acceptor [70]. However TICT emission from DMAPIP-b/β-

CD complex, where the donor group present in the core and not available for hydrogen bonding substantiates our earlier conclusion that the hydrogen of the solvent with donor group has no role in the formation of TICT in DMAPIP-b. But the dipole-dipole interaction with the donor group through solvation does play a major role in the stabilization of the TICT state.

4.1.3 Effect of pH and acidity constant

Complex formations are known to affect the prototropic equilibrium of the fluorophore molecules [300, 301]. Depending upon the relative affinity of the guest for the host, the pK_a is known to change as a result of complexation. The absorption spectra of DMAPIP-b in 15 mM β-CD solution at different pH are shown in Figure 4.1.6. We

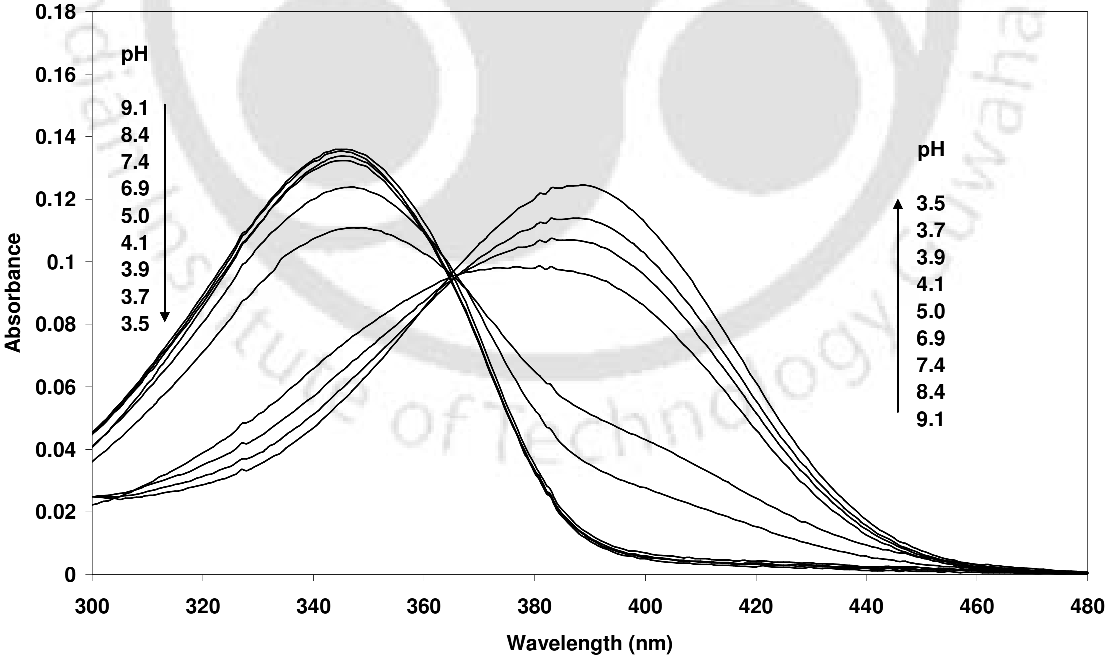

Figure 4.1.6: Absorption spectra of DMAPIP-b in 15 mM aqueous β-CD at different pH.

have calculated the pK_a of the dye from the pH-dependent change in the absorption spectra and found to be 4.8. The value is lower than the value 5.4, that obtained in the absence of β-CD (Section 3.1.3). Thus, no surprise the neutral form of the dye preferentially binds to nonpolar β-CD to form inclusion complex, whereas its monocations interact less with β-CD.

At lower pH, any one of three basic centres (dimethylamino nitrogen or imidazole nitrogen or pyridine nitrogen) of DMAPIP-b get protonated to form monocation (Chart 4.1.1). DFT calculations show that MC2 (E = -761.3307 a. u.) is more stable than MC1 (E = -761.3439 a. u.), which is more stable than MC3 (E = -761.3058 a. u.). On the other hand the order of the dipole moment of the monocation is as follow: MC3 (μ = 17.9 D) > MC1 (μ = 7.8 D) > MC2 μ = (2.6 D).

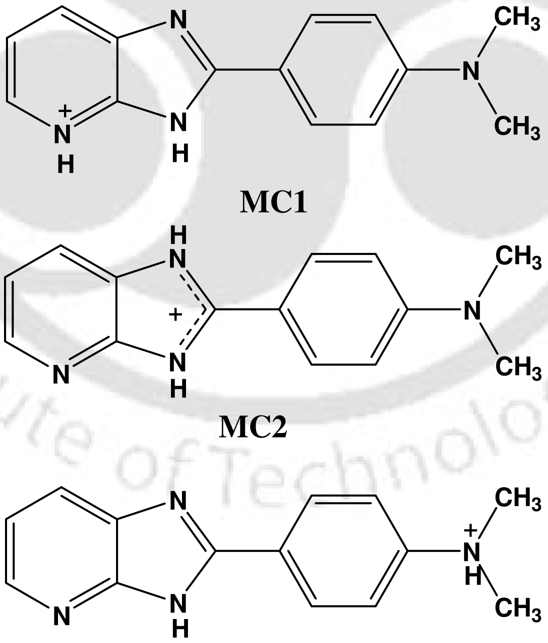

MC1

MC2

MC3

Chart 4.1.1. Structures of possible monocations of DMAPIP-b

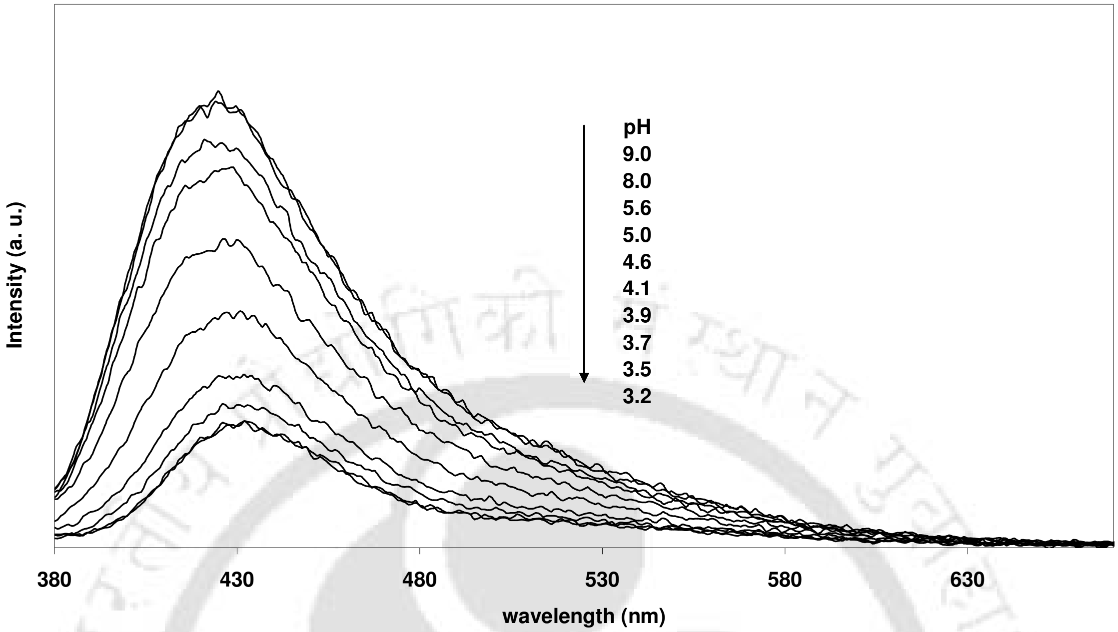

Figure 4.1.7: Fluorescence spectra of DMAPIP-b in 15 mM aqueous β-CD at different pH λ_{exc} = 365 nm.

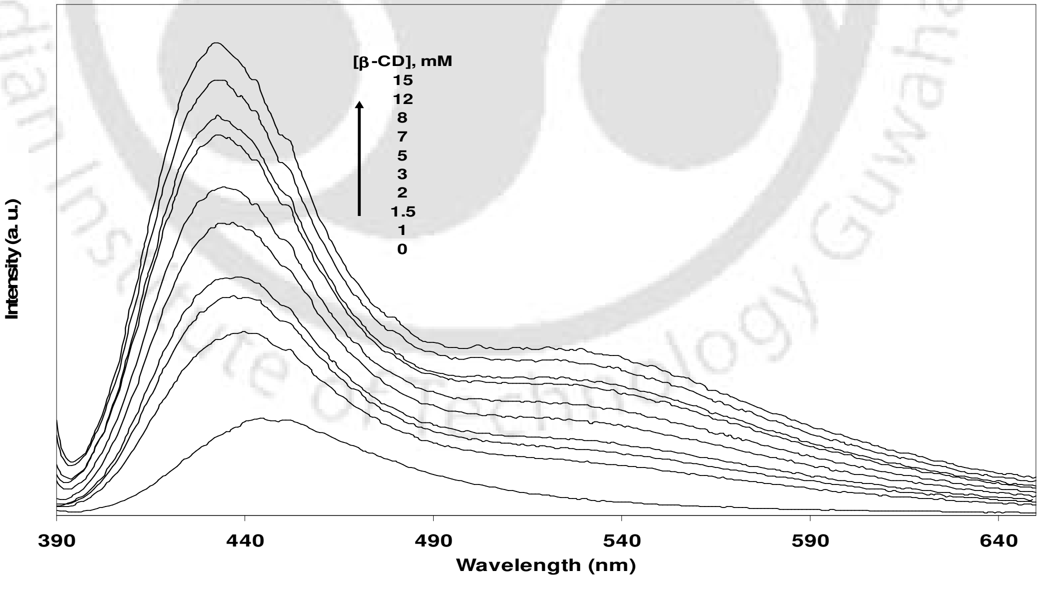

Figure 4.1.8: Fluorescence spectra of DMAPIP-b in aqueous at different β-CD concentration at pH ~ 3.5, λ_{exc} = 385 nm.

The fluorescence spectra of DMAPIP-b recorded in 15 mM β-CD as a function of pH are depicted in Figure 4.1.7. In β-CD solutions the fluorescence intensity of DMAPIP-b decreases with a decrease in pH. Fluorescence spectra recorded at pH 3.5 and 3.2 overlap with each other. This indicates that at pH 3.2-3.5 the molecule is completely in monocationic form. At pH ~ 3.5 only one emission band was observed in water. However upon addition of β-CD another band starts at appear at 535 nm and the intensity of both the bands increase with increase in β-CD concentration (Figure 4.1.8).

Fluorescence excitation spectra recorded at both the band maxima (435 nm and 525 nm) are shown in Figure 4.1.9 and Figure 4.1.10. The fluorescence excitation spectrum recorded at 435 nm shows a single band with maxima at ~ 355 nm in β-CD solution. On the other hand fluorescence excitation spectrum recorded at 525 nm has two band maxima at ~ 400 nm and ~ 355 nm in β-CD solution. These facts clearly establish the presence of two monocations. As both the excitation spectral band maxima are red shifted with respect to the neutral molecule, they can be assigned to the monocations formed by the protonation of ring nitrogens. The protonation of pyridine nitrogen will cause a large red shift in the absorption or excitation spectra of the fluorophore than the protonation of imidazole nitrogen [68, 182, 297]. Accordingly ~ 400 nm band and ~ 355 nm excitation bands and the corresponding emission bands can be assigned to protonation of pyridine nitrogen (MC1) and imidazole nitrogen (MC2) respectively. The shoulder observed at ~ 385 nm in the excitation spectra at λ_{em} = 435 nm is due to the unresolved vibrational structure of MC2 rather than due to the excitation spectra of MC1 or some other species. Such a characteristic vibrational structure was also reported in the excitation spectra

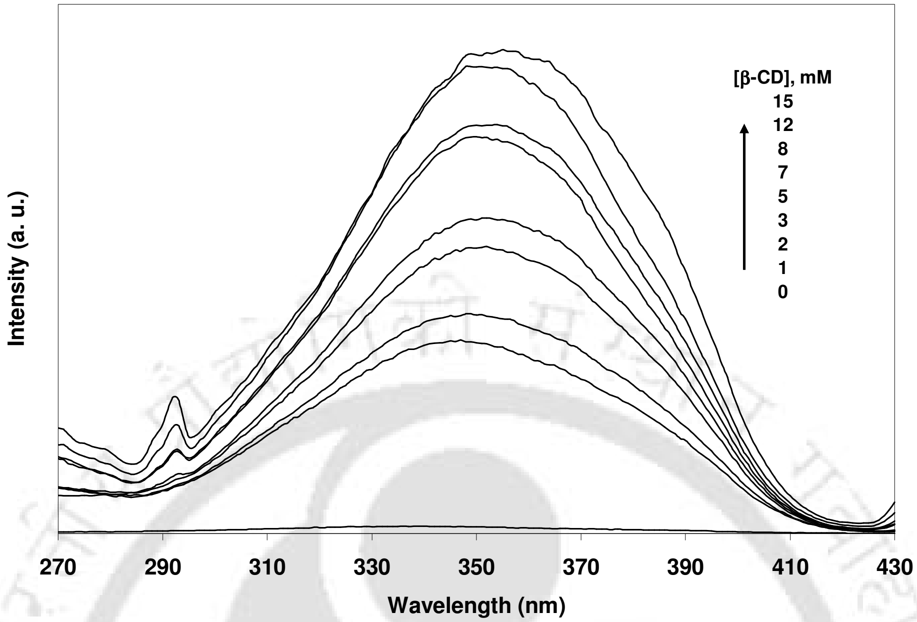

Figure 4.1.9: Fluorescence excitation spectra of DMAPIP-b in aqueous at different β-CD concentration at pH ~ 3.5, λ_{em} = 435 nm.

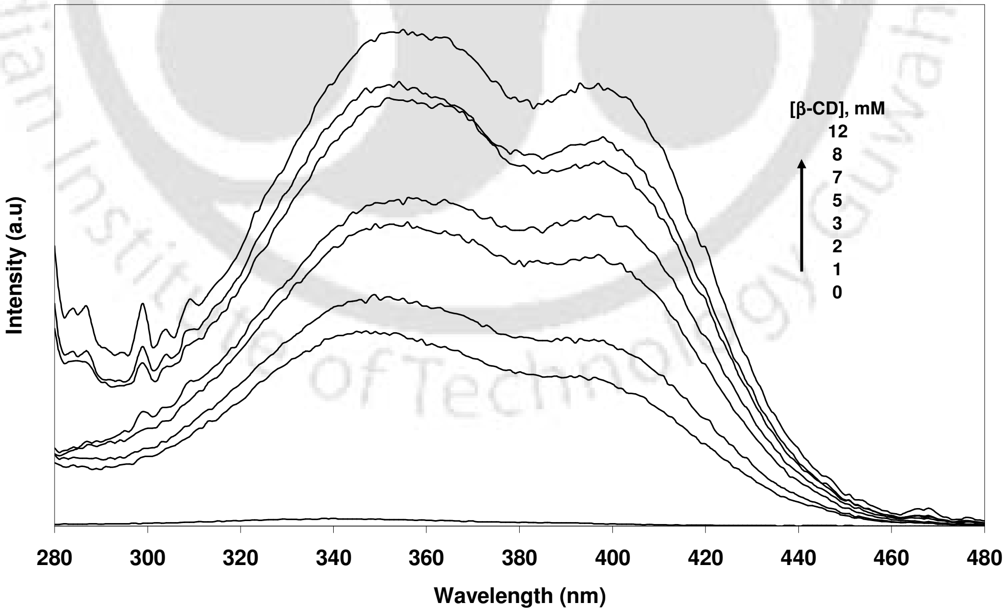

Figure 4.1.10: Fluorescence excitation spectra of DMAPIP-b in aqueous at different β-CD concentration at pH ~ 3.5, λ_{em} = 525 nm.

of monocation formed by the protonation of imidazole nitrogen in 2-(4'-*N*,*N*-dimethylaminophenyl)benzimidazole [182, 297].

Large Stokes shift observed for MC1 (~ 6500 cm^{-1}) compared to that observed for MC2 (~ 5000 cm^{-1}) clearly suggest that MC1 emission band at 525 nm is due to TICT band. This is consistent with the observation of TICT emission in the monocation formed by the protonation of pyridine nitrogen in DMAPIP-c [182]. TICT emission of MC1 further substantiate our earlier conclusion that TICT state formation is induced in DMAPIP-b due to hydrogen bonding of the solvent with pyridine nitrogen. However in aqueous medium only one emission band that corresponds to MC2 was observed (Section 3.1.3). The formation of more polar MC1 in addition to MC2 in a less polar CD cavity is unexpected. But the nonpolar environment inside the β-CD cavity destabilizes the TICT state of MC1 that increases the energy gap between the state and the low lying states. This decreases the nonradiative emission, as observed for TICT emission of neutral DMAPIP-b. Thus a clear emission band is observed in β-CD solution that is strongly quenched in aqueous medium. The association constant obtained using Benesi-Hildebrand plot at emission intensities 435 nm and 525 nm are 300 ± 30 M^{-1} and 270 ± 30 M^{-1}.

For DMAPIP-c in β-CD solution, at lower pH protonation occurs at pyridino and dimethylamino nitrogens in the S_0 state and pyridino and imdazo nitrogens in the S_1 state [68]. Thus formation of MC1 and MC2 in DMAPIP-b indicates the prototropic equilibrium also depends on the position of pyridine nitrogen.

4.1.4. Conclusion

Theoretical calculation predicts DMAPIP-b is almost planar in both ground and excited states. DMAPIP-b forms inclusion complex with β-CD and the host-to-guest ratio of DMAPIP-b/β-CD complex is found to be 1:1. DMAPIP-b enters the β-CD cavity with the dimethylaminophenyl ring, and the imidazopyridine ring remains outside the cavity and has H-bonding with water. The intensity of both normal and TICT emission are enhanced. The reduced polarity inside the hydrophobic β-CD cavity is more important in controlling the emissive nature of DMAPIP-b in the complex rather than the restriction of molecular motion. Biexponential decay is observed for DMAPIP-b/β-CD inclusion complex. Like protic solvent the equilibrium between the locally excited state and the TICT state is not established in the β-CD solution due to H-bonding of water with acceptor. The study of DMAPIP-b in β-CD also reveals that H-bonding of the solvent with donor does not play a role in the formation of TICT state in DMAPIP-b. Of the three possible monocations only two kinds of monocations, MC1 formed by the protonation of pyridine nitrogen and MC2 formed by the protonation of imidazole nitrogen are found in β-CD solution. Unlike water clear emission band is observed also for MC1. The appearance of clear emission band for MC1 in β-CD environment is due to substantial decrease in nonradiative rate inside cavity due to its reduced polarity.

4.2. Effect of normal micelles

The study of micellar solutions is of interest both from the point of view of basic research and applications of surfactants. Micelles also simulate a more complex environmental conditions present in larger bioaggregates such as membranes. Therefore micelles are being extensively studied as rudimentary models for biological lipid membrane systems [75, 302]. Attention has been paid to the micellar activities on the nature and characteristics of different photophysical and photochemical processes [81, 119, 303]. Upon binding, a molecule will experience a different environment inside the microheterogeneous structure of micelle, than that of bulk solvents for e.g., polarity, viscosity and diffusion of water molecules changes on moving towards the core of the micelle. In other words, the micelles can influence the TICT emission of DMAPIP-b in a unique way. Thus we have investigated the effects of TX-100 (nonionic), CTAB (cationic) and SDS (anionic) micelles on the photophysic of DMAPIP-b. The structures of the surfactants are presented in Chart 4.2.1. The studies result in an interesting observation that the TICT emission is induced only in SDS and TX-100, but not in CTAB.

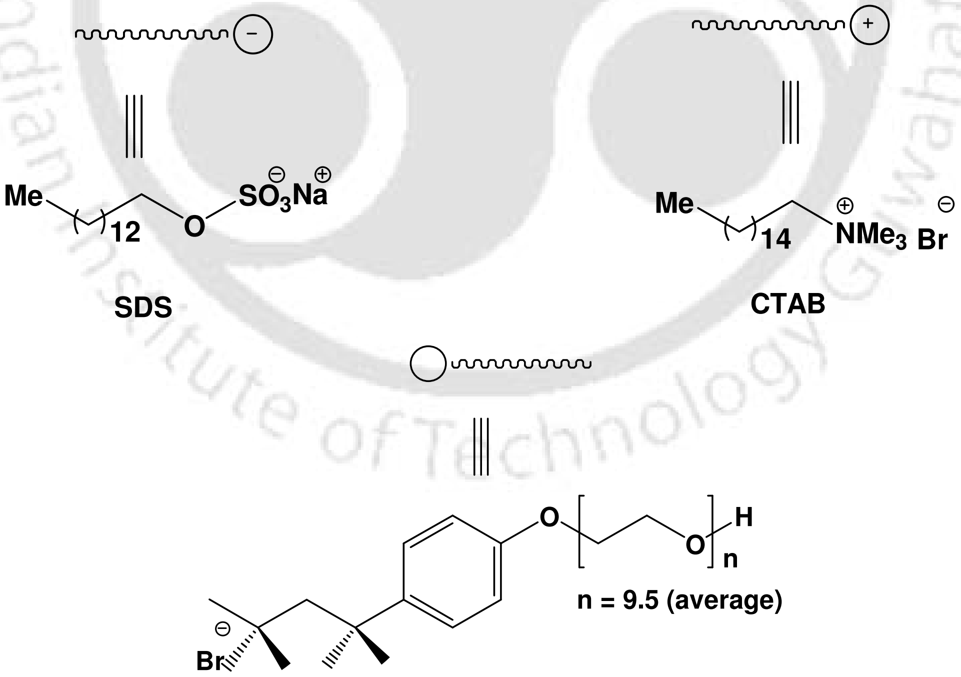

Chart 4.2.1. Structures of surfactants.

4.2.1. Absorption and Steady-state Fluorescence

Spectral data of DMAPIP-b in micelles along with few solvents are compiled in Table 4.2.1. The longer wavelength absorption maximum is red shifted in micelle with small increase in molecular extinction coefficient. The spectral behaviors are consistent with the solublization of the molecule in micelles. Upon addition of surfactant, the fluorescence spectrum of DMAPIP-b is blue shifted with increase in intensity (Figures 4.2.1-4.2.3). But the difference between SDS and other surfactants is, SDS triggers dual emission in DMAPIP-b and two clear emission bands start to appear in SDS solution at concentrations above 4 mM. The intensity of the longer wavelength band increases with further increases in SDS concentration (Figure 4.2.3). No such clear two band spectrum was observed in TX-100 or CTAB even at 40 mM solution. The overall fluorescence increases by a factor of 38 in TX-100, 36 in CTAB and 4.3 in SDS.

Table 4.2.1: Absorption band maxima (λ_{max}^{ab}, nm), log $\in_{max,}$ M^{-1} cm^{-1}, fluorescence band maxima (λ_{max}^{fl}, nm) and fluorescence life time[1] (τ, ns) for neutral DMAPIP-b in different media.

Medium	λ_{max}^{ab}	**log** $\in_{max}$	λ_{max}^{fl}	τ**(ns)**[1]
Acetonitrile	345	4.50	407	1.50
Methanol	350	4.50	414 506	0.31 (56.5) 1.16 (43.5)
Water (pH 9.0)	345	4.39	451	0.16 (98.7) 2.13 (01.3)
SDS (50 mM, pH 10.2)	349	4.50	431 530	0.30 (70.2) 1.25 (29.8)
TX-100 (80 mM, pH 7.3)	352	4.46	416	1.24 (91.3) 3.06 (8.7)
CTAB (80 mM, pH 7.1)	353	4.45	424	1.30

[1] $\lambda_{em} > 420$ nm, figures in parenthesis show relative amplitudes.

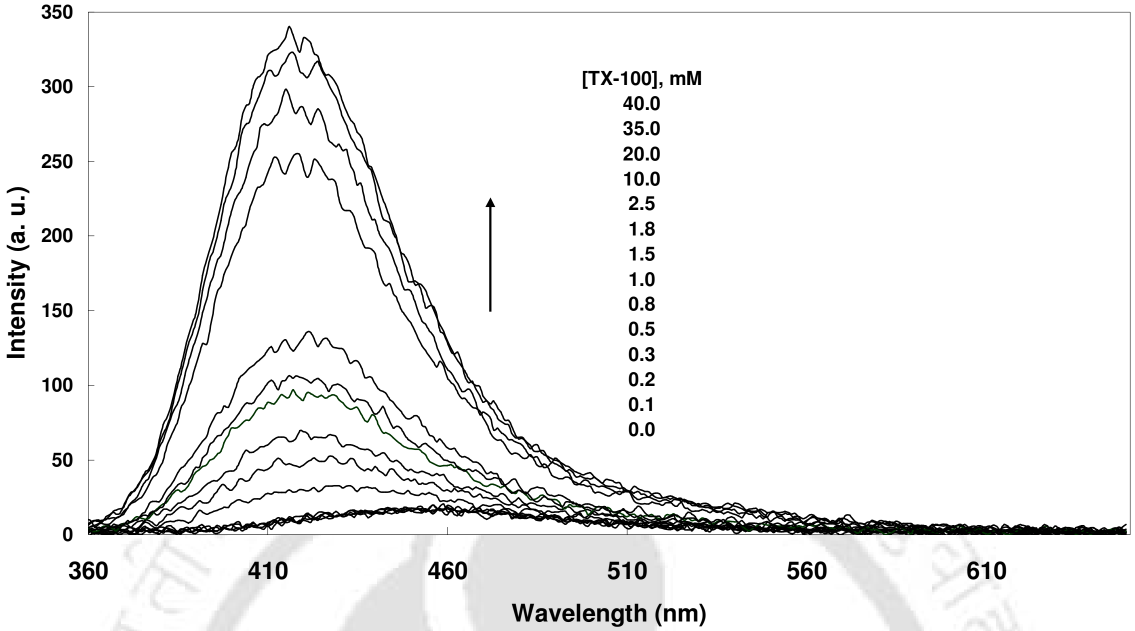

Figure 4.2.1: Fluorescence Spectra of DMAPIP-b as a function of TX-100 concentration, λ_{exc} = 350 nm.

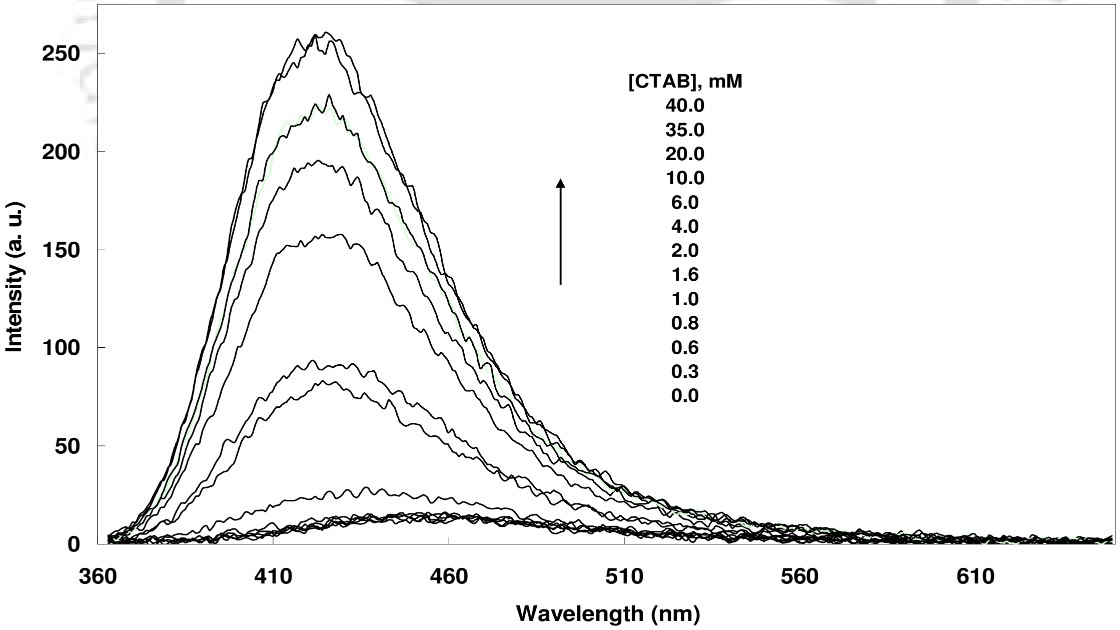

Figure 4.2.2: Fluorescence Spectra of DMAPIP-b as a function of CTAB concentration (λ_{exc} = 350 nm).

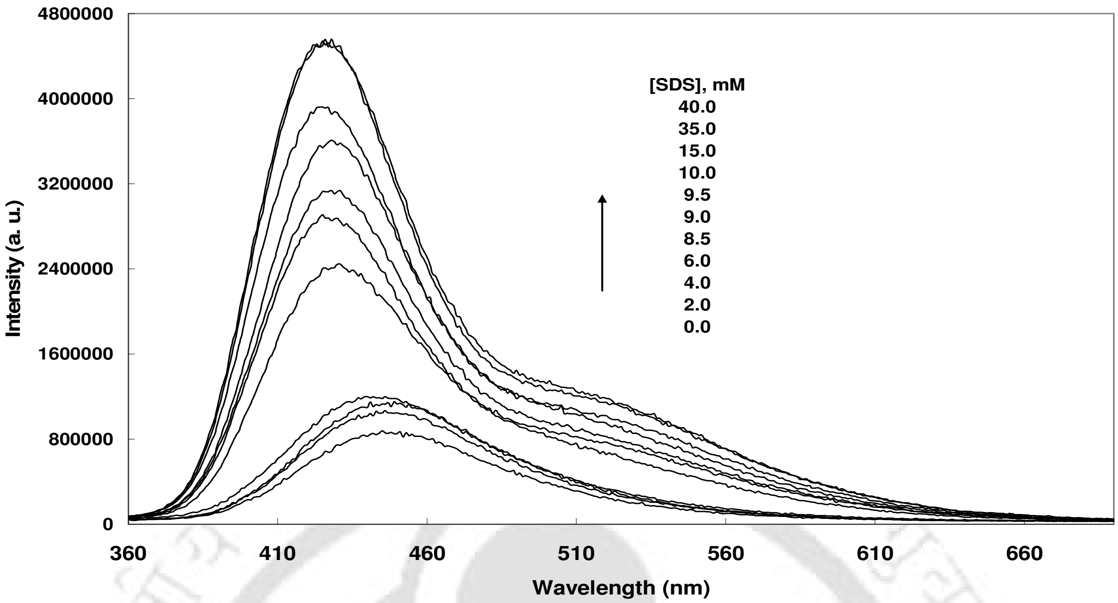

Figure 4.2.3: Fluorescence Spectra of DMAPIP-b as a function of SDS concentration, λ_{exc} = 350 nm.

Based on the spectral characteristics of DMAPIP-b established earlier and considering results in micelle, the shorter wavelength band in SDS and the emission bands in CTAB and TX-100 can be assigned to normal emission and the longer wavelength emission band in SDS can be assigned to TICT emission.

Binding constants of DMAPIP-b with different micelles have been determined following the method proposed by Almgren et al. [304]. According to the method

$$(F_m - F_0)/(F_{in} - F_0) = 1 + (K[M])^{-1} \qquad (4.2.1)$$

where, F_0, F_m and F_{in} are the fluorescence intensities of the probe in absence of surfactant, in micellar solutions of concentration [M], and under conditions of complete micellization respectively. K represents the binding constant between the probe in the excited state and micelle. The micellar concentration

$$[M] = ([S] – CMC)/n \qquad (4.2.2)$$

where [S] is the surfactant concentration and *n* is the aggregation number. The aggregation numbers were taken as 143, 60 and 62 for TX-100, CTAB and SDS, respectively [305]. The binding constants obtained for TX-100, CTAB and SDS are 4.6 ± 0.2 x 10^4, 3.3 ± 0.4 x 10^4, and 5.1 ± 0.8 x 10^5 M^{-1} respectively.

4.2.2. Fluorescence Lifetime

Fluorescence lifetime data obtained in different micelles along few solvents are listed in Table 4.2.1. Single exponential decays were observed in aprotic solvents. However two different lifetimes due to normal and TICT emissions were observed in protic solvents (Table 3.1.1). The lifetime of the locally excited state is attenuated in protic solvents compare to aprotic solvents and the shortest lifetime is observed in water. The short lifetime of the normal emission in protic solvent may due to the strong intermolecular hydrogen bonding between DMAPIP-b and protic solvent molecules, resulting in an increase in the nonradiative decay rate of the locally excited state. Thus, as expected the lifetime of the normal emission increases in all the three micelles compared to water. Biexponential decays are observed in SDS and TX-100. Same as in β-CD environment, no clear band for TICT emission is observed, however biexponential decay clearly established the dual emission. This indicates that not only SDS micelle, TX-100 micelle also triggers the dual emission in DMAPIP-b and the weak TICT emission is buried underneath the strongly enhanced normal emission. Monoexpoential decay of DMAPIP-b in CTAB, clearly suggests the absence of TICT emission in CTAB.

4.2.3. Nature of the binding site

Determination of polarity of the probe binding site inside the micelle has great importance in biological systems, and much attention has been drawn in that direction [117, 306]. In addition determination of micropolarity serves as an indicator of the local environment in which a given fluorophore is placed and enables one to find the probable location of the probe [118]. Single exponential decay for normal band and very high values of *K* establish that DMAPIP-b is present only at one site in the micelles. So we have made an attempt to evaluate the effective polarity at the micellar site of DMAPIP-b location from the correlation diagrams drawn between the fluorescence maxima of the normal band and $E_T(30)$, solvent polarity parameter [307] (not shown). The results clearly show that the micropolarity of DMAPIP-b binding sites in micelles, are close to that of alcohols**.** In other words, the probe molecule resides not in the core region, but in the micellar-water interface with limited exposures to water. The polarity experienced by the fluorophore in SDS is more compared to other micelles. This suggests that the amount of water molecules present in the Stern layer of SDS is more than the palisade region of TX-100 or the Stern layer of CTAB.

Kundu et al. proposed *p-N,N*-dimethylaminobenzonitrile present in SDS and CTAB with the dimethylamino group (donor) at the micellar periphery and the other end (acceptor) deep inside the micellar core [308]. On the other hand Jaffer et al. suggested two different orientation for TICT probe *trans*-2-[4-(dimethylamino)styryl]benzothiazole in SDS and CTAB. It was proposed that the –NMe_2 was oriented toward the micellar phase and the benzothiazole ring was projected toward the bulk aqueous environment in SDS and the orientation was reversed in CTAB [88]. It is well established that –NR_2

group acts as proton acceptor in the ground state [68]. The removal of water solvation shell around the –NMe_2 group would cause a red shift. The red shift in the absorption spectrum of DMAPIP-b in SDS indicates that –NMe_2 group is present in the micellar phase and the imidazopyridine ring is exposed to water. The orientation also ensures the hydrogen bonding of the water with pyridine nitrogen of DMAPIP-b and such a hydrogen bonding is necessary to induce the TICT emission in DMAPIP-b. The reduced polarities experienced by the molecule more destabilize the greater polar TICT state than the locally excited state. As a consequence, the energy of activation for the locally excited to TICT transition is increased, and hence increasing the normal emission [12, 13]. As far as the TICT state is concerned, destabilization inside the micellar environment increases the energy gap between the TICT state and the low lying states. This increase in energy gap reduces the nonradiative rate. This explains the observed TICT emission in SDS. In the reverse orientation, i.e. when imidazopyridine ring resides inside the micelle, the pyridine nitrogen is not available to form hydrogen bonding with water and may explain the absence of TICT emission in CTAB. However the red shift found in the absorption spectra of CTAB compare to water clearly rules out such an orientation for DMAPIP-b in CTAB. Thus, the absence TICT emission in CTAB and small TICT emission in TX-100 may be due to reduced hydrogen bonding experienced by the probe inside the micelle. Bagchi et al. also reported that the hydrogen bond donating capacity in micelles follows the order SDS > TX-100 > CTAB [309]. They also demonstrated that in SDS-TX-100 mixed micelle the hydrogen bonding donating ability decreases with increase in TX-100 concentration [310]. These properties in the micellar phase were attributed to the difference in extend of bound water molecules present in the micellar interface. Several other groups also observed that the environment of SDS is richer in water content as compared to that in TX-100 and CTAB [311, 312].

The large difference observed in the lifetimes of locally excited and TICT states in SDS and TX100 (Table 4.2.1), suggests that the equilibrium is not established between the two emitting states in these micelle also. This can be explained in the same way as that in β-CD. As the -NMe_2 group is projected toward the micellar core and the imidazopyridine ring towards the water rich part of the micelles, the hydrogen bonding of water with acceptors, stabiles the TICT more than that of locally excited state. The shortest lifetime observed for normal emission in SDS (among the micelles) substantiates the conclusion that DMAPIP-b experience a water rich environment inside SDS compared to TX-100 and CTAB.

4.2.4. pH effects

DMAPIP-b has three basic center, but still only one absorption and one fluorescence bands correspond to the imidazole ring nitrogen protonated monocation was observed in aqueous medium (Scetion 3.1.3). But in β-CD, it forms both MC1 (protonation of pyridine nitrogen, Chart 4.1.1) and MC2 (protonation of imidazole nitrogen, Chart 4.1.1). It was reported that micelles strongly influence the formation and relative population of cations [313]. Since our present probe DMAPIP-b have three basic centers and it may form three types of monocations (Chart 4.1.1): MC1 (protonation of pyridine nitrogen), MC2 (protonation of imidazole nitrogen) and MC3 (protonation of dimethylamino nitrogen) as mentioned earlier, we intend to study the effect of micelle on the protropic equilibrium.

The absorption and fluorescence spectra of the dye at different pH were measured in CTAB (80 mM), TX-100 (80 mM), and SDS (50 mM) and the relevant data are along with the pK_a compiled in Table 4.2.2. Absorption spectra are red shifted in all the micelle with decrease in pH. The fluorescence maximum of DMAPIP-b in CTAB is red shifted with decrease in intensity with increase in acid concentration (Figure 4.2.4). The behavior is also observed in TX-100 (not shown). With decrease in pH the fluorescence normal band maximum in SDS is red shifted with increase in intensity and on the other hand the intensity of TICT band decreases (Figure 4.2.5). These red shifts in absorption and fluorescence spectra are consistent with those observed in aqueous medium. But in micelle the fluorescence spectra are more complicated than in water. For example, in SDS at monocationic pH (the pH at which DMAPIP-b is completely present in monocationic form), a fluorescence band is observed at 435 nm with a long tail when λ_{exc} = 360 nm. With increase in λ_{exc} another band appears at longer wavelength side at 550 nm. The intensity ratio of the longer wavelength emission to shorter wavelength emission also increases with increase in λ_{exc} (Figure 4.2.6).

Table 4.2.2: Absorption band maxima (λ_{max}^{ab}, nm), fluorescence excitation band maxima (λ_{max}^{ex}, nm) and emission band maxima (λ_{max}^{fl}, nm) for monocationic DMAPIP-b and pK_a value in different media

Medium	λ_{max}^{ab}	λ_{max}^{ex}	λ_{max}^{fl}	**pK_a**
Water (pH 4.0)	386		451	5.4
CTAB (80 mM, pH 2.6))	379	360, 403	437, 530	3.6
TX-100 (80 mM, pH 2.9)	387	368, 403	428, 523	3.9
SDS (50 mM, pH 5.1)	394	385, 407	434, 550	7.3

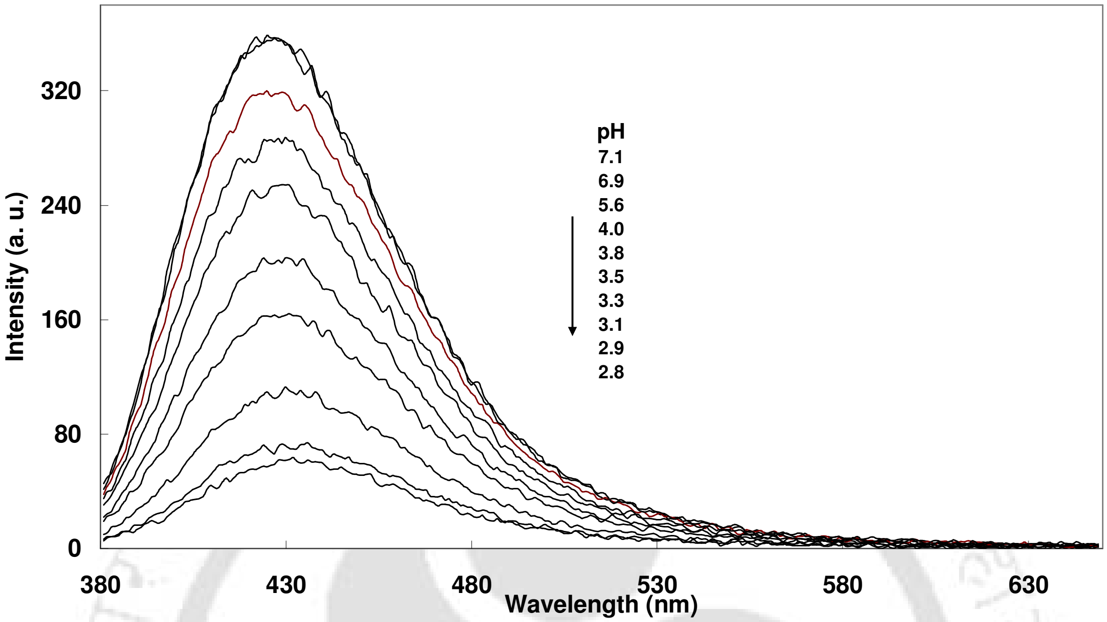

Figure 4.2.4: Fluorescence spectra of DMAPIP-b in 80 mM CTAB as a function of pH, λ_{exc} = 370 nm.

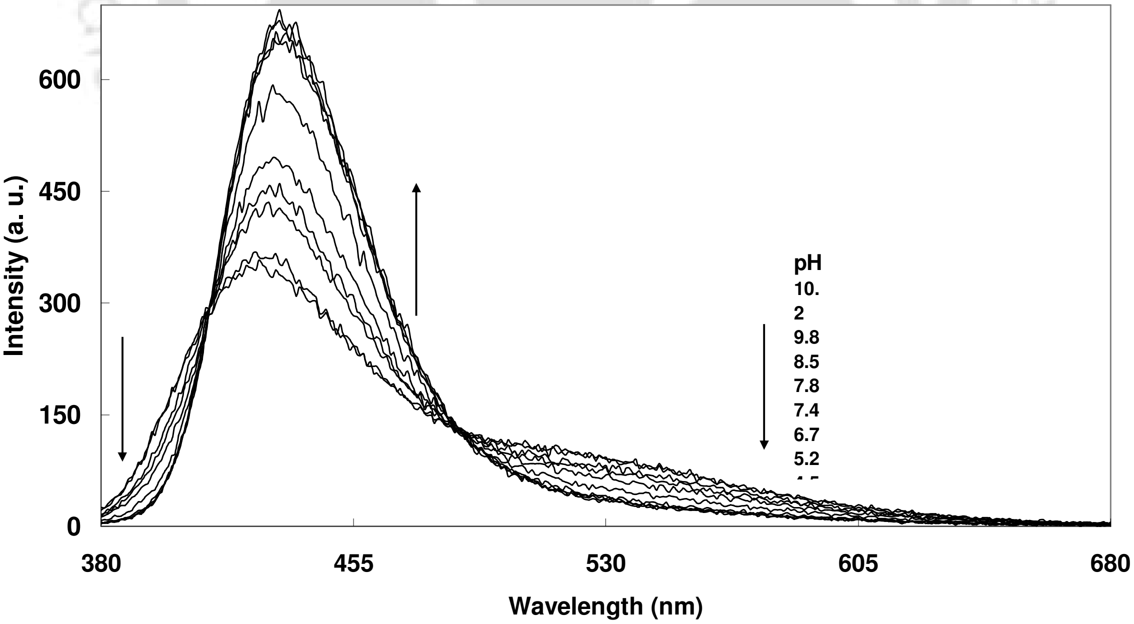

Figure 4.2.5: Fluorescence spectra of DMAPIP-b in 50 mM SDS as a function of pH, λ_{exc} =370 nm.

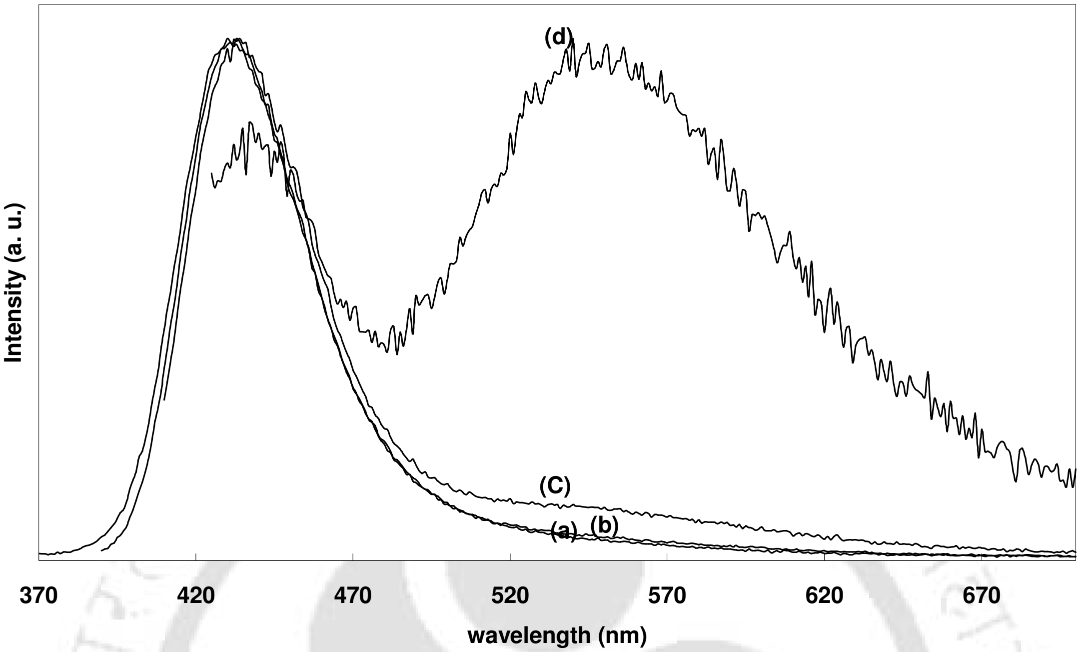

Figure 4.2.6: Normalized fluorescence emission spectra of monocations of DMAPIP-b in SDS at (a) λ_{exc} = 360 nm, (b) λ_{exc} = 380 nm, (c) λ_{exc} = 400 nm, (d) λ_{exc} = 420 nm.

The behavior of the fluorescence excitation spectra (Figure 4.2.7) also matches with emission spectra. Only one band (385 nm) is observed in the excitation spectrum when λ_{em} = 430 nm and the band maxima shift towards red with increase in λ_{em}. At λ_{em} = 610 nm the excitation spectral band appears at 407 nm. These spectral behaviors are consistent with formation of two kinds of monocationic species in SDS. Similar excitation and emission spectral characteristics are also observed in TX-100 and CTAB at monocationic pH, and indicate the presence of two kinds of monocations in these micelles also (Table 4.2.2). The observed red shift in absorption and fluorescence spectra rules out the protonation of dimethylamino nitrogen. However a large red shift is expected in particular with the fluorescence spectrum due to TICT emission, on protonation of pyridine ring nitrogen [182]. Thus, as in β-CD, the longer wavelength excitation and emission spectral bands can be assigned to MC1 and the shorter wavelength excitation and emission ones to MC2.

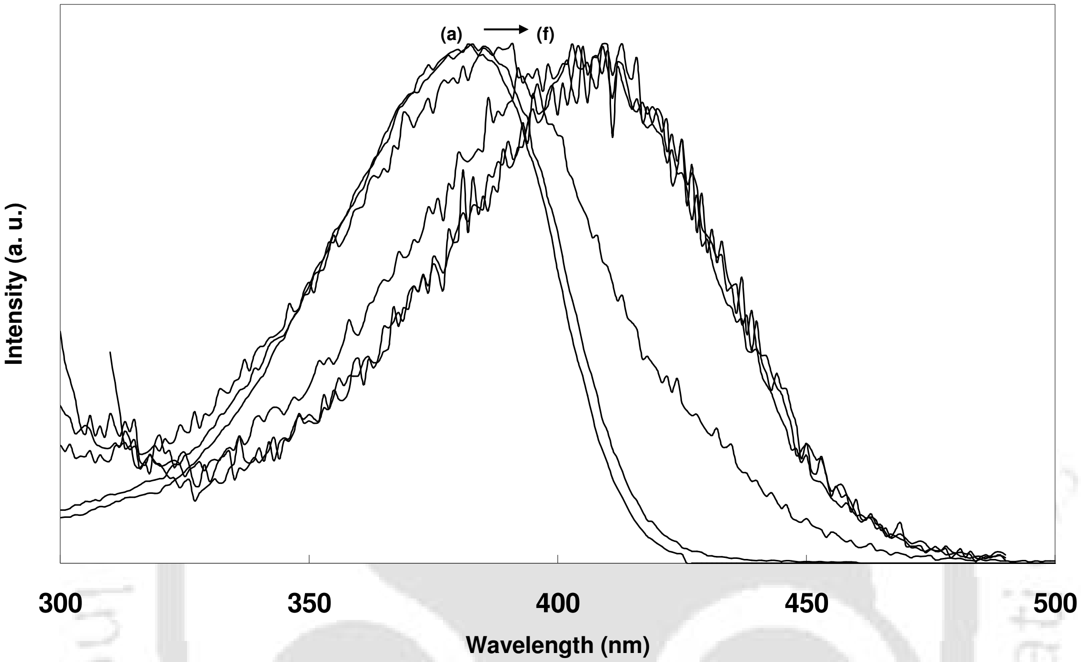

Figure 4.2.7: Normalized fluorescence excitation spectra of monocations of DMAPIP-b in SDS at λ_{em} = 430 nm, (b) λ_{em} = 470 nm, (c) λ_{exc} = 510 nm, (d) λ_{em} = 570 nm (e) λ_{em} = 590 nm, (f) λ_{exc} = 610 nm.

As mentioned earlier, only absorption and fluorescence bands correspond to MC2 was observed in aqueous medium (Section 3.1.3). Same as in β-CD, the observation of MC1, in the less polar micellar media may be due to reduced nonradiative rates. The excitation energies were obtained by vertical excitations of optimized ground states using TDDFT/B3LYP/6-31G calculations. The TDDFT excitation energies values for MC1 and MC2 are 2.50 eV and 3.39 eV respectively. The calculations also predict MC1 is more red shifted than MC2. The theoretical excitation energy obtained for MC2 (3.39 eV) is in very good agreement with experimental value (3.37 eV, TX-100). But the TDDFT excitation energy for MC1 is very small (2.50 eV) compared to experimental value (3.05 eV, TX-100). It is reported in the literature that TDDFT poorly describes some charge transfer situations, in which little or no overlap between the atomic orbitals contributing to the HOMO and those to the LUMO [314, 315]. However ZINDO calculations predicted the excitation energy for MC1 as 2.89 eV which is fair agreement with the experimental value (3.05 eV).

The striking difference between SDS and other micelles is the increase in fluorescence intensity with decrease of pH (Figure 4.2.5). This could be due to large decrease in nonradiative rates for monocationic species than the neutral molecule in anionic micelle. In monocationic forms of the dye, imdazopyridine ring posses more positive charge and it interact with the negative charge of the SDS polar head group. This results in higher binding between cation and SDS. In addition the dipole-dipole interaction attracts the imidazopyridine ring towards the Stern layer and pushes the rest of the cation more deep inside the micelle. This reduces the interaction of monocation with water.

Fluorescence spectra of the monocations were also studied as function of surfactant concentration. The fluorescence intensities of both the monocations increase with increase in surfactant concentration. The fluorescence intensities of both emission and excitation spectra of monocations are plotted against the surfactant concentrations to find the CMC of the surfactant and are compiled for in Table 4.2.3. The increase in the CMC of the nonionic micelles and the decrease in the CMC of the anionic micelle with the addition of protic acids is consistent with earlier works [311, 316, 317]. Interestingly the CMC value obtained for SDS using MC1 fluorescence intensities is lower than the value that obtained using MC2. This shows that MC1 has specific interaction with SDS and induces the formation of micelle at a lower concentration.

Table 4.2.3: Critical micelle concentrations (CMC, mM) determined using emission and excitation intensities of different monocations.

Micelle	MC1		MC2	
	Emission	**Excitation**	**Emission**	**Excitation**
SDS	0.9	1.0	3.3	3.5
TX-100	6.7	6.3	6.9	6.5
CTAB	1.9	1.7	1.6	1.8

The apparent pK_a value is lower in TX-100 and CTAB than in water, but the apparent pK_a value is higher in SDS with respect to water (Table 4.2.2). Similar decrease in the pK_a value was reported for neutral-monocation equilibrium by others [311, 316] in TX-100 and is due to decrease in dielectric constant. A similar kind of explanation does not hold well for the apparent pKa value observed in SDS and CTAB and may be explained on the basis of a pseudo-phase ion-exchange (PIE) model [318, 319]. According to the model, in anionic micelle the protons and the cations tend to concentrate in the Stern layer and suppress the release of protons from the probe, resulting in an increase in apparent pK_a. In contrast, in cationic micelle positively charged species are repelled to the aqueous phase. To ensure that the increase in the apparent pKa value in SDS is only due to the change in dielectric constant and potential (ψ_0) at the surface, we have used the following relation [314]

$$\mathrm{p}K_a^{\mathrm{obs}} = \mathrm{p}K_a^{\mathrm{i}} - (e\psi_0 / 2.303 k_b T) \qquad (4.2.1.)$$

where $\text{p}K_a^{\text{obs}}$ and $\text{p}K_a^{\text{i}}$ are the apparent $\text{p}K_a$ value for the acid–base indicator at the charged surface and for the interface if surface potential is zero, and e, k_b, and T are the charge on the electron, the Boltzmann constant, and the temperature in Kelvin, respectively. Taking the upper limit of surface potential equal to -140 mV for SDS [319] $\text{p}K_a^{\text{i}}$ as 3.9 in TX-100, the $\text{p}K_a^{\text{obs}}$ in SDS will be 6.3, which is much lower than that observed in SDS (7.3). This suggests that the higher value of the apparent $\text{p}K_a$ value in SDS is due to the specific molecular interactions of DMAPIP-b with SDS, besides smaller dielectric constant and electrostatic potential.

4.2.5. Conclusion

DMAPIP-b resides in the micellar-water interface, while the $–\text{NMe}_2$ present inside the micellar phase, the imdazopyridine ring projected towards the micellar periphery. Of three micelles studied, DMAPIP-b emits dual fluorescence only in SDS and TX-100. The reduced polarity and the hydrogen bonding capacity experienced by the fluorophore inside micelles triggers the TICT emission in DMAPIP-b. The TICT emission is strong and emerges as a separate band in SDS, but in TX-100 it is weak and buried underneath the normal emission. The absence of TICT emission in CTAB is due to small hydrogen bond donating ability experienced by the molecule. Unlike water, the fluorescence from MC1 is also observed in micelle in addition to that from MC2. MC1 induces the micelle formation in SDS at lower concentration.

4.3. Effect of reverse micelles

Reverse micelles are one of the attractive models for biological systems, and have been studied to mimic the water in biological systems, such as water in proteins, biomembranes etc. Reverse micelles were used to modulate the photophysics and the photochemistry of fluorophores. As shown in the previous section, the dual fluorescence of DMAPIP-b was modulated in micelles depending on the water content. Reverse micelles are also interesting systems as two kinds of water are present, bound water and free water and their properties differ with each other. In addition they afford the opportunity for examining the molecules with various states of hydration, simulating situations present in water restricted environments prevailing in membrane interfaces. Here we have explored the photophysics of DMAPIP-b in CTAB/isooctane/*n*-hexanol/water, TX-100/cyclohexane/*n*-hexanol/water and TX-100/benzene/hexane/water reverse micelle to find the effect reverse micelle on the hydrogen bond induced TICT emission of the molecule.

4.3.1. Absorption spectra

TX-100 forms a clear solution in benzene/hexane mixture as well as in cyclohexane/*n*-hexanol mixture. No clear solution was obtained by mixing CTAB/isooctane/*n*-hexanol, but after addition of small amount of water the mixture turns to a clear solution. Absorption spectra were recorded in all the three reverse micellar system as a function w_0 (w_0 = [water]/ [surfactant]) and the data are compiled in Table 4.3.1 along with few selected solvents. The absorption spectra undergo a bathochromic shift from 345 nm to 352 nm with a hypochromic effect upon increase in water amount in

Table 4.3.1: Spectral characteristics of DMAPIP-b in reverse micelles along with few selected solvents.

Medium	**λ_{max}^{ab} (nm)**	**λ_{max}^{fl} (nm)**	**τ (ns)^{1}**
Cyclohexane	336, 352 (sh)	359, 379, 398	1.99
n-hexanol	350	403, 485	0.65 (43), 1.55 (57)
Dioxane	340	383	2.30
Acetonitrile	345	407	1.50
Methanol	350	414	0.29 (69), 1.12 (31)
Water	345	451(0.042)	0.16 (99), 2.13 (01)
TX-100/hexane/benzene/water			
w_0			
0	345	400	1.29
0.8	349	410	0.63 (17), 1.42 (83)
1.6	349	412	0.51(15), 1.39 (85)
2.5	350	414	0.46 (13), 1.34 (87)
4.5	351	416	0.48 (16), 1.26 (84)
5.5	351	419	0.55 (22), 1.27 (76)
8	352	420	
9	352	419	
TX-100/*n*-hexanol/cyclohexane/water			
w_0			
0	345	402	0.68 (36), 1.40 (64)
0.8	349	410	0.48 (24), 1.47(76)
1.6	350	413	0.59 (22), 1.46(78)
2.5	350	416	0.52 (24), 1.43(76)
4.5	350	418	0.43 (21), 1.24 (79)
5.5	351	419	0.42 (19), 1.24 (81)
8	352	419	0.36 (19), 1.23(82)
9	352	420	
CTAB/*n*-hexanol/cyclohexane/water			
w_0			
2.5	349	413	0.76 (45), 1.58 (55)
5	349	412	0.69 (43), 1.41 (57)
8.0	349	411	0.67 (42), 1.20((58)
10	349	410	0.65 (38), 1.15 (62)
15	349	409	0.64 (30), 1.15 (70)
20	349	409	
25	349	409	0.63 (27), 1.11 (73)

[1] λ_{exc} = 375 nm.

both TX-100 reverse micelles. These changes in the optical spectra with increase w_0 indicate the interaction of the dye with the environment. On the other hand in CTAB/isooctane/*n*-hexanol/water system, upon increase water amount virtually no variation in the maximum position of the absorption band. These finding suggests that DMAPIP-b is present in different environments in TX-100 and CTAB reverse micelles.

4.3.2. Fluorescence spectra

The emission behavior of DMAPIP-b was also monitored by varying w_0. Figure 4.3.1 and 4.3.2 show the fluorescence spectra in TX-100 reverse micelles and Figure 4.3.3 show that in CTAB micelles. The fluorescence spectra undergo a red shift

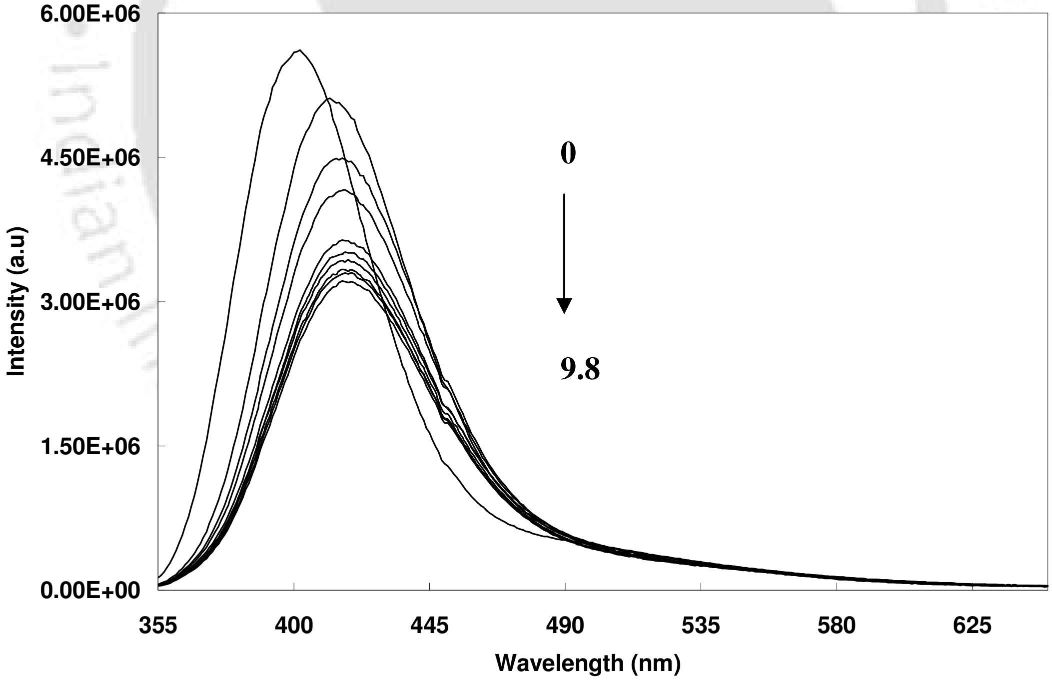

Figure 4.3.1: Fluorescence spectra of DMAPIP-b in 20% solution of TX-100 (0.63 M) in cyclohexane and n-hexanol (n-hexanol: TX-100, 1:4) as a function of added water (w_0), w_0 = 0 (1), 0.8 (2), 1.6 (3), 2.5 (4), 3.3 (5), 4.9 (6), 5.5 (7), 6.5 (8), 9.8 (9). λ_{exc} = 350 nm.

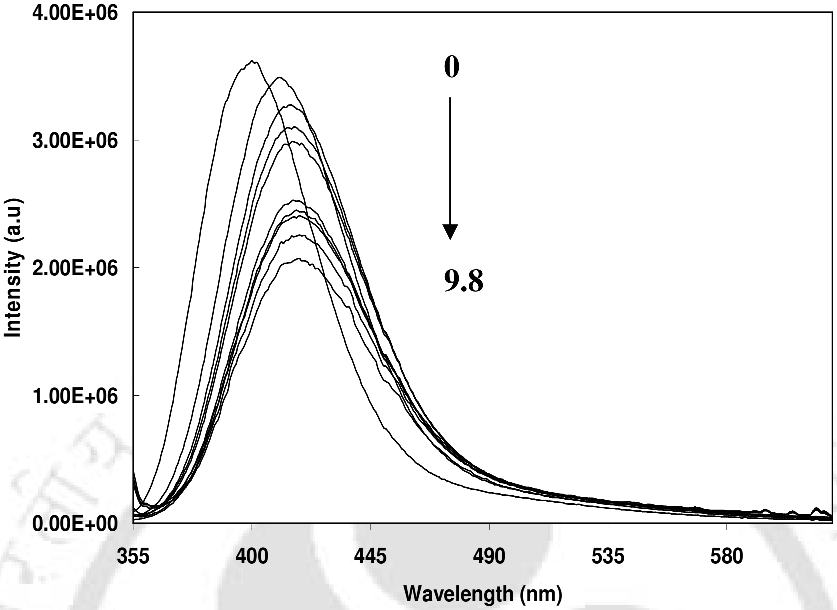

Figure 4.3.2: Fluorescence spectra of DMAPIP-b in TX-100 (0.27 M) in hexane and benzene as a function of added water (w), w_0 = 0 (1), 0.8 (2), 1.6 (3), 2.5 (4), 3.3 (5), 4.9 (6), 5.5 (7), 6.5 (8), 9.8 (9). λ_{exc} = 350 nm.

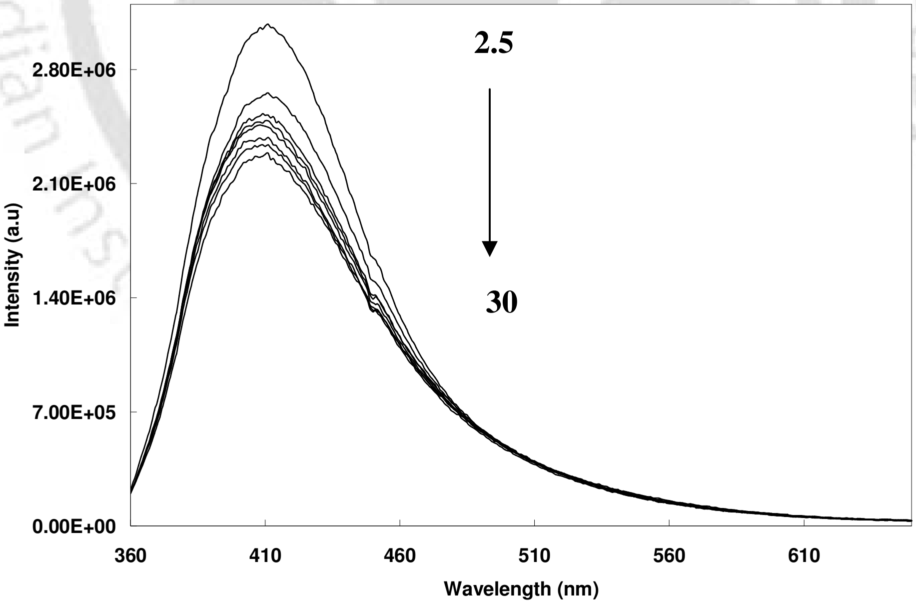

Figure 4.3.3: Fluorescence spectra of DMAPIP-b in CTAB/isooctane/hexanol function of added water (w_0), w_0 = 2.5 (1), 5 (2), 8 (3), 10 (4), 15 (5), 20 (6), 25 (7), 30 (8). λ_{exc} = 350 nm.

with increase in water pool size in case of nonionic reverse micelles in both with and without co-surfactant, hexanol. The bathochromic shift is more for the initial addition of water and is small for further additions. The emission maximum of DMAPIP-b in cationic reverse micelles remains constant, when water content increases from w_0 2.5 to 30, but a small decrease in fluorescence intensity is observed. No clear dual emission was observed in any of the microemulsion. A small increase in fluorescence intensity is noticed at tail portion for initial addition of water in TX-100/benzene/hexane system. But for further increase in water content the intensity changes at the longer wavelengths are negligible. When cosurfactant is present in the reverse micelle, addition of water fails to produce any appreciable change in intensities at the longer wavelengths.

In the absence of water, the surfactants are probably present in solution with little restriction on its rotational mobility [311, 320]. Upon addition of water, the surfactant molecules (and a portion of co-surfactant, if it is present) come together to form reverse micelle and water is solubilized inside the core of the reverse micelles. With further increase in water amount the pool size swells, this leads to increase the polarity of the reverse micellar system.

Fluorescence life time is an excellent method to know the exact location of probe in a multi component environment [9, 146, 321-323]. Monoexponential decay was observed for DMAPIP-b in TX-100/benzene/hexane solution, upon addition of the water the decay become biexponential. However when hexanol was present as co-surfactant in DMAPIP-b exhibits two different lifetimes even in the absence of water. The lifetime of the short lifetime component further shortened in presence of water. In CTAB/isooctane/*n*-hexanol/water reverse micelles also two different lifetimes are observed. The lifetime of the short lifetime component is short in TX-100 reverse micelle compared to that in CTAB reverse micelle. For example in CTAB reverse micelle at $w_0 = 8.0$, the lifetime of the short lived component of DMAPIP-b is 0.69 ns that is reduced to nearly half (0.36 ns) TX-100 reverse micelle at the same water to surfactant ratio (Table 4.3.1).

As discussed earlier sections, the biexponential decay of DMAPIP-b can be attributed to normal and TICT emissions. The shorter and longer life time are of the locally excited state and TICT state respectively. Single exponential decay in TX-100/benzene/hexane solution shows the absence of TICT emission. This is no surprise as DMAPIP-b exhibits dual emission only in protic environment and the hydrogen bonding of the solvent with pyridine nitrogen is absolutely necessary to induce TICT emission in DMAPIP-b. Thus, addition of water not only leads to formation of microemulsion, but also induces the TICT emission in TX-100/benzene/hexane/water system. In contrast the fluorophore exhibits dual emission in TX-100/cyclohexane/*n*-hexanol systems even before the addition of water molecules and is due to the presence of protic *n*-hexanol in the solution.

In many molecules, it was shown that the hydrogen bonding quenches the fluorescence. It was shown that the TICT state of many molecules is de-excited by nonradiative way through internal conversion by hydrogen bonding [67, 324, 325]. In aqueous medium the TICT emission of DMAPIP-b in nearly completely quenched to due the increased stability of the TICT state by polarity and hydrogen bonding capacity of water (Section 3.1.2). Not only the TICT emission, but the normal emission of DMAPIP-b is also quenched by protic solvents. To find the effect of hydrogen bonding on the emission of DMAPIP-b, we have studied the effect of addition of protic solvent on the fluorescence spectra of DMAPIP-b in aprotic solvent. It is well established that the TICT emission is strongly dependent on the polarity of the environment. A polar environment stabilizes the TICT state and could complicate the investigations. In order to minimize the effect of polarity we measure the fluorescence spectra of DMAPIP-b in acetonitrile as a function of methanol percentage. Since the dielectric constants of acetonitrile and methanol differs only by a small magnitude and the perturbation by polarity of the system on the fluorescence spectrum is minimum. The fluorescence spectrum was gradually red shifted with decrease in fluorescence with addition of methanol (Figure 4.3.4). But the fluorescence intensity increases at longer wavelength indicating that the TICT emission start to emerge with addition of protic solvent. The decreases in normal fluorescence and

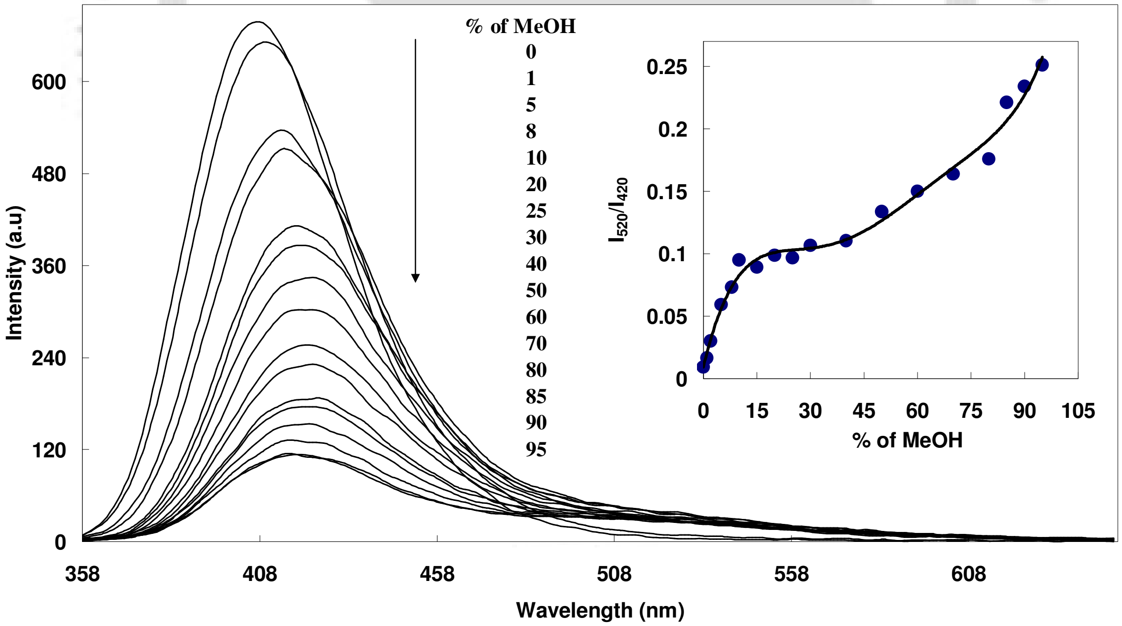

Figure 4.3.4: Effect methanol addition on the fluorescence spectra of DMAPIP-b in acetonitrile (insert shows the variation of intensity ratio of TICT to normal emission with methanol percentage).

the increase in the TICT emission continue up to 10% of methanol (v/v). Further increase in methanol concentration the intensity of both the band decreases, however the increases in the intensity ratio of the TICT emission to normal emission, continues. In other words the normal emission is quenched more than the TICT emission.

The hydrogen bonding of methanol with pyridine nitrogen of DMAPIP-b induces towards the TICT emission and the hydrogen bonding of methanol with imidazole nitrogen increases the internal conversion to the ground state. Both of these lead to the initial decrease in normal emission of DMAPIP-b with addition of methanol. These hypothesis are supported by the facts that (i) only TICT emission was observed from the monocation formed by the protonation of pyridine nitrogen (Section 4.2.4) and (ii) the fluorescence intensity is quenched upon protonation of imidazole nitrogen (Section 3.1.3). Above 10% of methanol, though the increase in hydrogen bonding increases the population of the TICT state, the florescence intensity of the TICT emission also decreases due to greater stabilization of the TICT state which decreases the energy gap between the TICT state and low lying state. According to energy gap law the decrease in energy gap would lead to increases the nonradiative decay. The studies established that the hydrogen bonding of the solvent not only induces the TICT emission, it also plays the dominant role in the stabilization of the TICT state. Depending on the water content the same behavior is expected in reverse micelles also.

4.3.3. Location of the fluorophore

Reverse micelle can host the probe in any of the three regions the organic phase, the micellar phase the water nanopool. The location of fluorophore depends upon number of factors such as the structure of the micelle, water content and micropolarity. The spectral observations indicate that the microenvironment around DMAPIP-b is modified with increase in water content. This finding suggests that the water is accessible to DMAPIP-b. Water is accessible to the fluorophore if it is solublized either in the water pool or the micellar phase near the water pool. It is reported that the fluorescence quantum yield decreases steeply for initial addition of water when the molecule is present in the water pool of the reverse micelle [320]. But no steep decrease only gradual decrease in fluorescence was found in DMAPIP-b in any of the microemulsion (Table 4.3.1). In addition the fluorescence maximum in reverse micelles, are nearly 30-40 nm hypsochromically shifted to that in neat water (Table 3.1.1). All these facts indicate that the fluorophore is present inside the micelle phase in all three microemulsion.

Upon addition of water the absorption spectra of DMAPIP-b are bathochromic shifted in TX-100 reverse micelles. As discussed in section 3.1.3, one could expect a blue shift on hydrogen bonding of water at dimethylamino nitrogen, the observed red shift reflects that the water molecule of the reverse micelle are not hydrating the dimethylamino nitrogen but the ring nitrogens. This indicates that the dimethylamino group is projected towards the organic phase and the imidazopyridine is present near the water pool. Only such an orientation ensures the hydrogen bonding between the pyridine nitrogen of the probe and the water molecule, which is essential to induce the TICT emission of DMAPIP-b. Observation of TICT emission in the microemulsion including the TX-100/benzene/hexane/water also substantiate that the imidazopyridine ring is present in the hydrophilic region.

Chattopadhyay et al. found that the shift in the emission maximum of anthroloxy probes decreases as the distance of the fluorophore increases from the water pool in reverse micelle [326]. They have also showed that the emission maxima of 7-nitrobenz-2oxa-1,3 diazol-4-yl-cholesterol was unshifted only emission intensity decrease with increase in water amount and concluded that the probe is located in a region far for water molecule to seep-in [327]. On the other hand TICT emitting ionic styryl dye 2-(4-(dimethylamino)styryl)-1-methylpyridinium iodide, the fluorescence spectrum is red shifted in anionic sodium 1,4-bis-2-ethylhexylsulfosuccinate reverse micelle and blue shifted in cationic benzyl-n-hexadecyldimethyammonium chloride reverse micelle [90]. The styryl dye was reported to present at the interface of the reverse micelles and was suggested that the probe molecule moves towards core in anionic micelles and remain away from the core in the cationic micelle. The spectral shifts of DMAPIP-b are also minimum in CTAB/isooctane/*n*-hexanol/water reverse micelle, but the fluorescence intensity decreases with increase in water pool size. Since it is found that in cyclodextrin (Section 4.1) and normal micelle (Section 4.2), the dimethylamino group of DMAPIP-b was oriented towards the hydrophobic region and the imidazopyridine ring prefer the hydrophilic region, we speculate the same orientation for the fluorophore in CTAB reverse micelle also. Similar orientation was proposed for *p*-dimethylaminobenzoic acid in CTAB/*n*-heptanol/water reverse micelle [328]. Jiang et al. suggested that dimethylaminobenzoic acid is present in the hydrocarbon chains close to the water pool with it’s the dimethylamino group towards the bulk 1-heptanol in and the carboxylic group interacts with the polar head of the surfactant electrostatically. Jiang et al. found that the intensity of the TICT emission decreases in CTAB reverse micelle relative to heptanol and attributed the decrease in TICT emission due to restriction on conformational relaxation to TICT state by the increased viscosity of the microemulsion. But in DMAPIP-b not only the viscosity but also the reduction in the hydrogen bonding capacity of the environment may also be responsible for the decreased in TICT emission of DMAPIP-b compared to true solution.

Though DMAPIP-b is predicted to be in the same orientation inside the both reverse micelle, the fluorescence maxima of the fluorophore undergo a bathochromic shift only in TX-100 reverse micelle and not in CTAB reverse micelle. These results suggest that the water penetration is more in the interface of TX-100 reverse micelles than CTAB reverse micelle and/or DMAPIP-b is present far away form the water pool in CTAB. Relatively longer decay time of normal emission in CTAB than in TX-100 substantiate this. As mentioned earlier Bachi et al. [309] compared the hydrogen bond donating capacity of the normal micelle and found that the donating capacity is more in TX-100 than CTAB micelle. They have ascertained that the difference in behaviour is due to variation in the amount of water present in the interface. Though the trimethylammonium head group of CTAB is positively charged, the interfering methyl groups restrict the approach of the water molecules from coming closer to the head group and it also prevent penetration of the water molecule inside the hydrocarbon chain. On the other hand in TX-100 the oxyethylene chain is hydrated by bound water molecules. Our studies on normal micelle also suggest that DMAPIP-b experience more hydrated environment in TX-100 than CTAB. Jiang et al. also found that the water molecules in the water pool are not seeping into the hydrocarbon region of the reverse micelle.

4.3.4. Conclusion

DMAPIP-b is present in the water pool-micelle interface in both TX-100 reverse micelles. But in CTAB it is present more toward the micellar phase. Water molecule is not penetrating inside the hydrocarbon region of the CTAB reverse micelle. TICT emission is observed in all the reverse micelles. Addition of water induces the TICT emission in TX-100/benzene/hexane/water. When hexanol was present as a co-surfactant, it induces dual emission, even before addition of water. In all the reverse micelles the pyridine nitrogen is oriented towards the water pool and the dimethylamino group is projected towards the oil phase. The hydrogen bonding of solvent with DMAPIP-b not only induces the TICT emission, but also quenches the fluorescence.

4.4. Effect of Bovine serum albumin (BSA)

Proteins are heteregenous systems. The knowledge about proteins has profited from the use of these different ligands. The molecular interactions are often monitored using optical techniques. These methods are sensitive and relatively easy to use. Fluorescent spectroscopy is a valuable technique to study the binding of ligands to proteins. As mentioned earlier, DMAPIP-b was shown to act as an inhibitor for of Aurora-A, Aurora-B and Aurora-C kinases [191,192]. Since BSA is the most common model protein, we have studied the interaction of DMAPIP-b and its alkyalted product with BSA.

4.4.1. Effect of BSA on the spectral characteristics of ligands

The effect of BSA on the absorption spectra DMAPIP-b and its alkylated products are shown in Figure 4.4.1. Upon increasing the concentration of BSA except a small

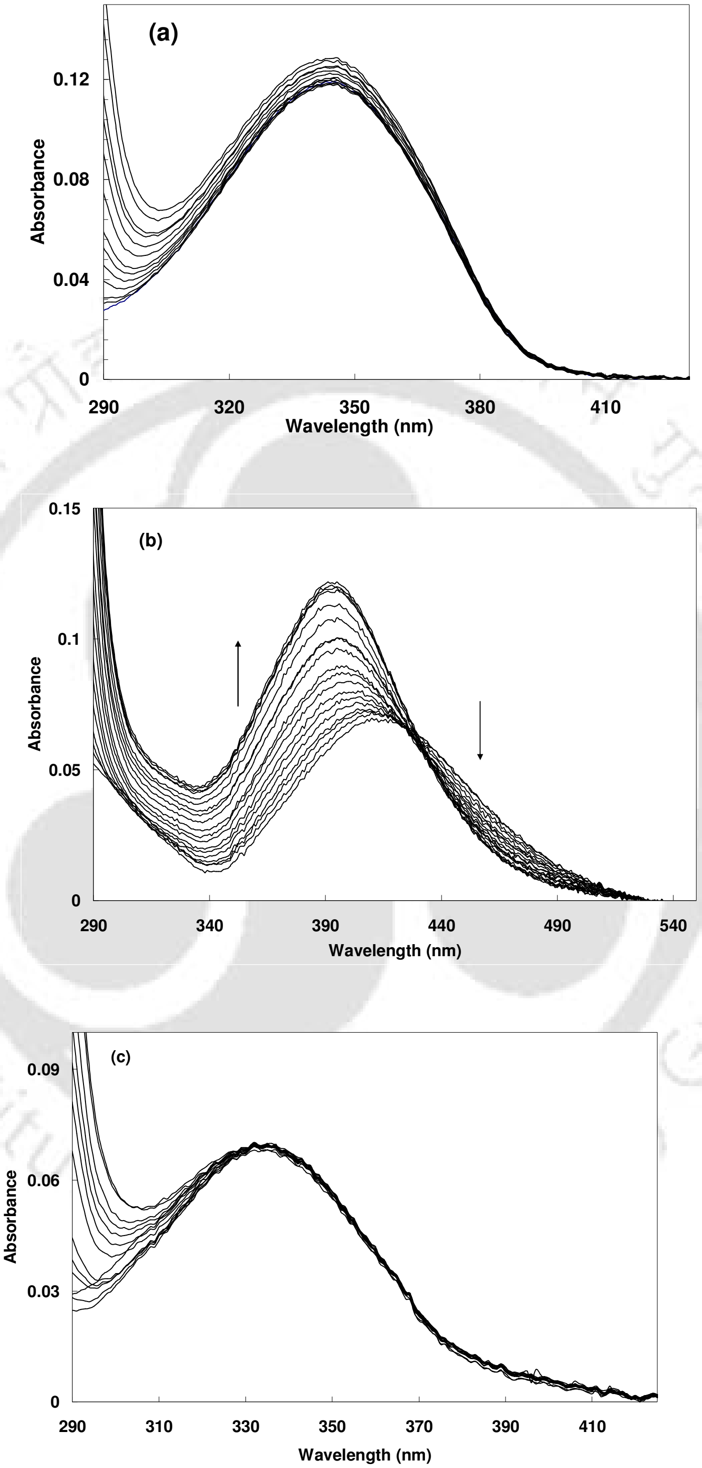

Figure 4.4.1: Absorption spectra of (a) DMAPIP-b (b) 1 and (c) 2 at different concentration of BSA.

increase in absorption no appreciable changes are observed in the absorption spectra of DMAPIP-b and the alkylated product, **2**. However upon binding to BSA the absorption spectrum of **1** is gradually blue shifted to 391 nm from 412 nm in aqueous buffer with a clear isosbestic point at 420 nm. These changes reflect not only the formation of complex 1:1 between **1** and BSA, but also indicate that the binding site of **1** is hydrophobic in nature.

The variation of fluorescence spectra of DMAPIP-b and its alkylated product with BSA concentrations are shown in Figure 4.4.2 and the data are compiled in Table 4.4.1. The fluorescence spectra of DMAPIP-b and **1** are blue shifted with addition of BSA. The spectral shift is also accompanied by an increase in the fluorescence yield. **1** has a broad band at 565 nm in water. Addition of BSA leads to formation of a new band in the blue side at 480 nm. The fluorescence enhancement of DMAPIP-b is small compared to the enormous increase in fluorescence of **1** (Table 4.4.1). Both DMAPIP-b and **1** have low fluorescence quantum yield in water and high quantum yield in nonpolar solvents. Therefore the hypsochromic shift and the fluorescence enhancement can be rationalized to the binding of these molecules to the hydrobhopic site of BSA. On the other hand the fluorescence intensity of **2** increases without a shift in the emission maxima. This can attributed to the entry of **2** into the hydrophilic domain of BSA. The fluorescence spectrum shifts due to change in polarity of the environment, however the change in fluorescence intensity of the flexible molecules depends not the polarity of the medium, but also on the constraint provided by the media [329]. The constrained environment of BSA restricted the internal motions the fluorophore that lead to the rise in the fluorescence quantum yield.

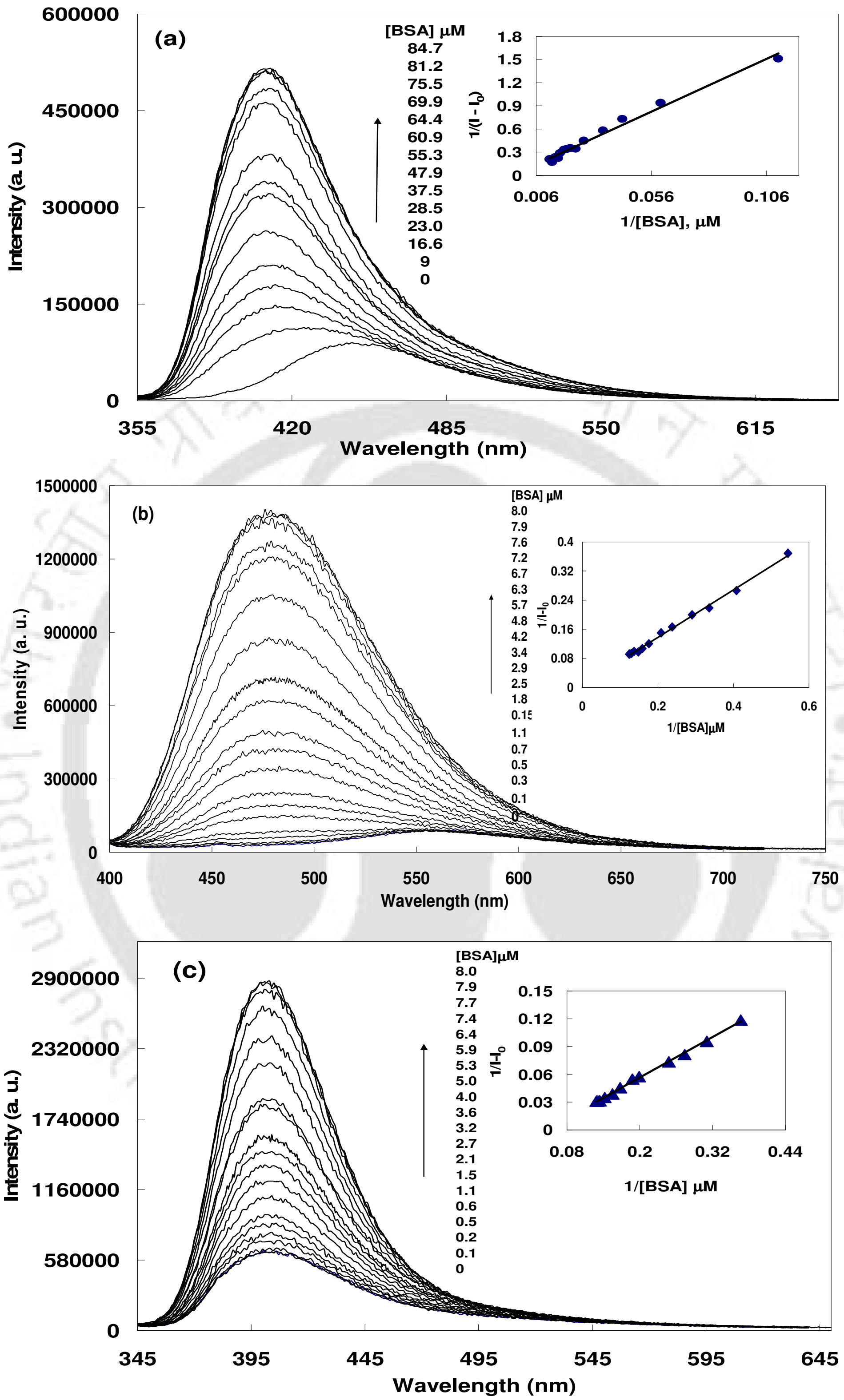

Figure 4.4.2: Fluorescence spectra of (a) DMAPIP-b (λ_{exc} =345 nm) (b) 1 (λ_{exc} = 392 nm) and (c) 2 (λ_{exc} =336 nm) at different concentration of BSA. The inserts show the respective Benesi-Hildebrand plots.

Table 4.4.1: Absorption band maxima (λ_{max}^{ab}, nm), fluorescence band maxima (λ_{max}^{fl}), fluorescence quntum yield (ϕ) and lifetimes (τ, ns) of DMAPIP-b and its alkylated products in the absence and the presence of BSA.

	λ_{max}^{ab}	λ_{max}^{fl} (ϕ)	τ(ns)^{1}
DMAPIP-b			
Water	345	451 (0.04)	0.23 (84.4) 0.95 (15.6)
BSA (85 μM)	345	410 (0.20)	0.88 (31.1) 2.1 (68.9)
Molecule 1			
Water	413	570 (0.06)	0.27 (56.2) 2.47 (43.8)
BSA (8 μM)	390	479 (0.35)	1.51 (20.5) 3.70 (79.5)
Molecule 2			
Water	336	405 (0.07)	0.24 (59.3) 0.83 (40.7)
BSA (8 μM)	336	404 (0.24)	0.67 (35.8) 2.18 (64.2)

$^{1}\lambda_{exc}$ = 375 nm.

4.4.2: Fluorescence anisotropy

As the fluorescence anisotropy (r) is affected by size, shape or segmental flexibility of a molecule, the restriction imposed by the medium can be better understand by anisotropy measurement. Complex biological systems such as proteins form highly organized molecular assembly with considerable degree of anisotropy and the anisotropy measurement can help in finding location of a probe in microheterogenous environments like proteins, DNA, micelles, reverse micelles, and cyclodextrins [330-332]. The anisotropies of all three molecules are plotted as function of BSA concentration (Figure 4.4.3). The increase in anisotropy with BSA concentrations reflects that the probes experiences more constrained environment upon binding. The anisotropy of alkyl derivates are higher than that of parent compound. This indicates that the presence of long alkyl group prevents or restricts the internal motion of alkylated molecules.

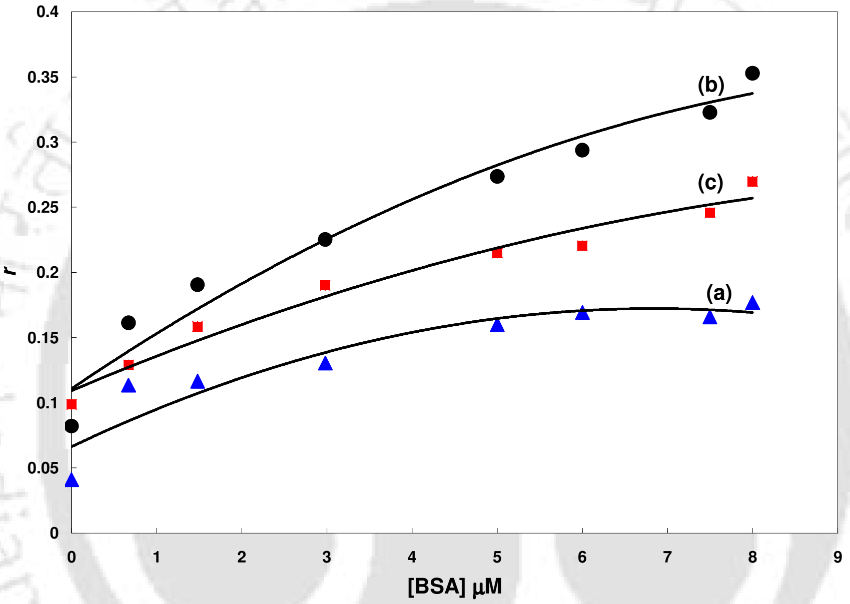

Figure 4.4.3: Fluorescence anisotropy (r) of (a) DMAPIP-b (b) 1 and (c) 2 at different concentration of BSA.

4.4.3. Binding constants

To understand the binding interaction and the type of complex formed between the probe and the protein, the binding constant values were determined from the fluorescence emission data by using Benesi-Hildebrand equation [295, 296]

$$\frac{1}{[I-I_0]}=\frac{1}{[I_1-I_0]}+\frac{1}{[I_1-I_0]K[BSA]} \qquad (4.4.1)$$

where I_0, I and I_1 are the emission intensities in absence of BSA, in presence of BSA and when the molecule is completely solubilized in BSA respectively. The double reciprocal plots of $1/(I–I_0)$ versus 1/ [BSA] are depicted as inserts in Figure 4.4.2. The emission intensities at 410 nm, 480 nm and 405 nm are used for Benesi-Hildebrand plot of DMAPIP-b, **1** and **2** and. The good linear correlations ($r^2 = 0.99$) confirm the formation of 1:1 inclusion complex between the probes and BSA. The binding constants thus obtained from the ratio of the intercepts and the slopes are 4.3×10^3 M^{-1}, 3.5×10^4 M^{-1} and 4.4×10^4 M^{-1} respectively for DMAPIP-b, **1** and **2**. The change in free energy for the probe-protein complexations are -20.72, -25.93, -26.47 kJ mol^{-1} for DMAPIP-b, **1** and **2** respectively. The binding constants indicate a strong binding of the alkyl derivatives with BSA over DMAPIP-b. The high binding constants and the large enhancement of fluorescence quantum yields (Table 4.4.1) upon probes binding to BSA indicates that the alkyalted DMAPIP-b can be applied as a sensitive fluorescent probe even at low concentrations of the probe and BSA.

4.4.4. Time resolved measurements of ligands

Fluorescence lifetime is sensitive to excited state interactions. Difference fluorescence lifetime is expected for probes in protein environment because of different degree of solvent relaxation around the fluorophore. Figure 4.4.4 represents the fluorescence decay curve recorded for **1** at 465 nm in absence and presence of BSA. The fluorescence lifetime data of all the three molecules are tabulated in Table 4.4.1. The fluorescence decays are double exponentials for all the molecules in the absence and presence of BSA. The biexpoential decay suggested that the fluorophores exhibit dual emission in both the environment. The observation of TICT emission inside BSA, suggest that the protein did not resist the formation of the TICT. Considering the fact that DMAPIP-b emits enhanced TICT emission in other organized media, the formation of TICT state in BSA is not surprising. The lifetime of both locally excited state and TICT state increases in BSA. The decreased polarity around the probes in the proteinous environments is reflected by the increase in the fluorescence lifetime of **1** and DMAPIP-b. The increase in the fluorescence life time of **2** with increase in BSA concentration can be explained in terms of change in non-radiative decay pathways of the emitting species, due to their interaction with protein BSA. With increase in BSA concentration, there is a decrease in nonradiative decay of **2** due to the formation of inclusion complex due restriction of the internal motions.

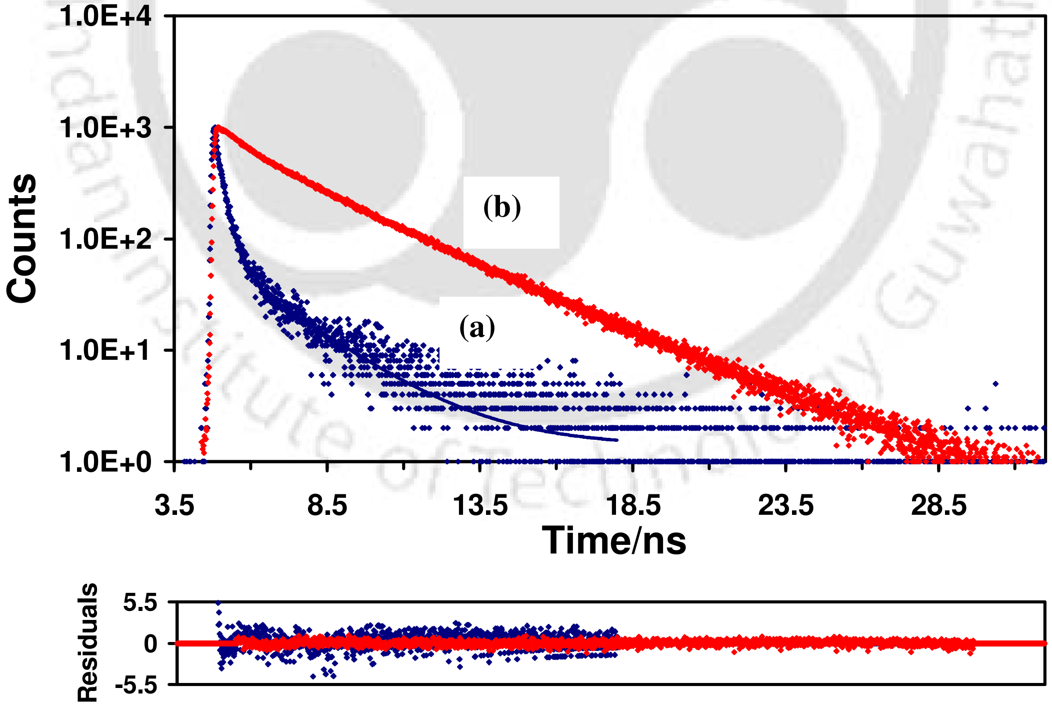

Figure 4.4.4: Fluorescence decay of 1 at 465 nm in (a) absence and (b) presence of BSA.

4.4.4. Quenching of BSA fluorescence by DMAPIP-b and 1

The effects of DMAPIP-b and **1** on the fluorescence spectra of BSA are shown in Figure 4.4.5. BSA exhibits strong fluorescence spectrum with the emission maximum at 345 nm [333]. With addition of the ligands, the fluorescence intensity of the tryptophan decreases and that of ligand increases with an isosemissive point or a quasi isosemissive point. Ligands showed weak emission at the same excitation in the blank experiments. From these changes it can be inferred that the intrinsic fluorescence of BSA is quenching by resonance energy transfer.

The quenching can be static or dynamic in nature, static and dynamic quenching can be distinguished by their different quenching constants dependence on temperature and viscosity, or better by lifetime measurements. The quenching of the fluorescence of tryptophan by BSA can be described by Stern-Volmer equation

$$\frac{I_0}{I} = 1 + \kappa_q \tau_0 [Q] = 1 + \kappa_{SV} [Q] \qquad (4.4.2)$$

where k_q is the biomolecular quenching rate constant, K_{SV} is the Stern-Volmer constant, τ_0 is the lifetime of the protein in absence of quencher, and [Q] is the quencher concentration. A progressing quenching of the fluorescence intensity of BSA is observed with increase in concentrations of the ligands (Figure 4.4.5). The Stern-Volmer plots with both ligands are shown in Figure 4.4.6. At higher concentrations of quencher deviation is observed in the Stern-Volmer plot. In case of DMAPIP-b upward curvature is observed. The upward curvature is expected for static quenching at higher concentrations. Thus the quenching is not dynamic but static in nature. The quenching constant obtained from the linear portion (low concentrations) of the plot is 1.0 x 10^5 M^{-1}.

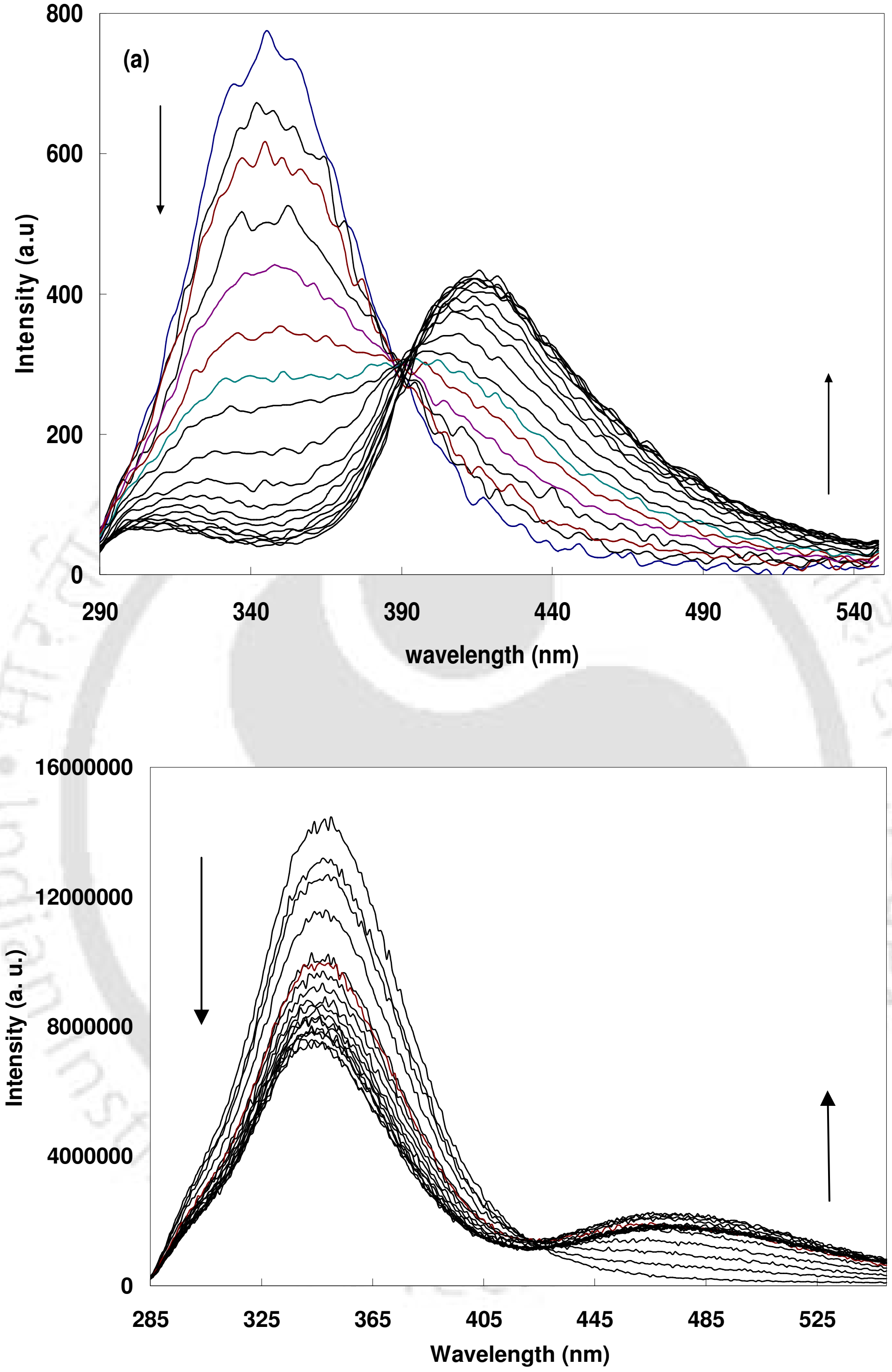

Figure 4.4.5: Fluorescence spectra of BSA (a) at different concentration of DMAPIP-b (b) at different concentration of 1 (λ_{exc} = 280 nm).

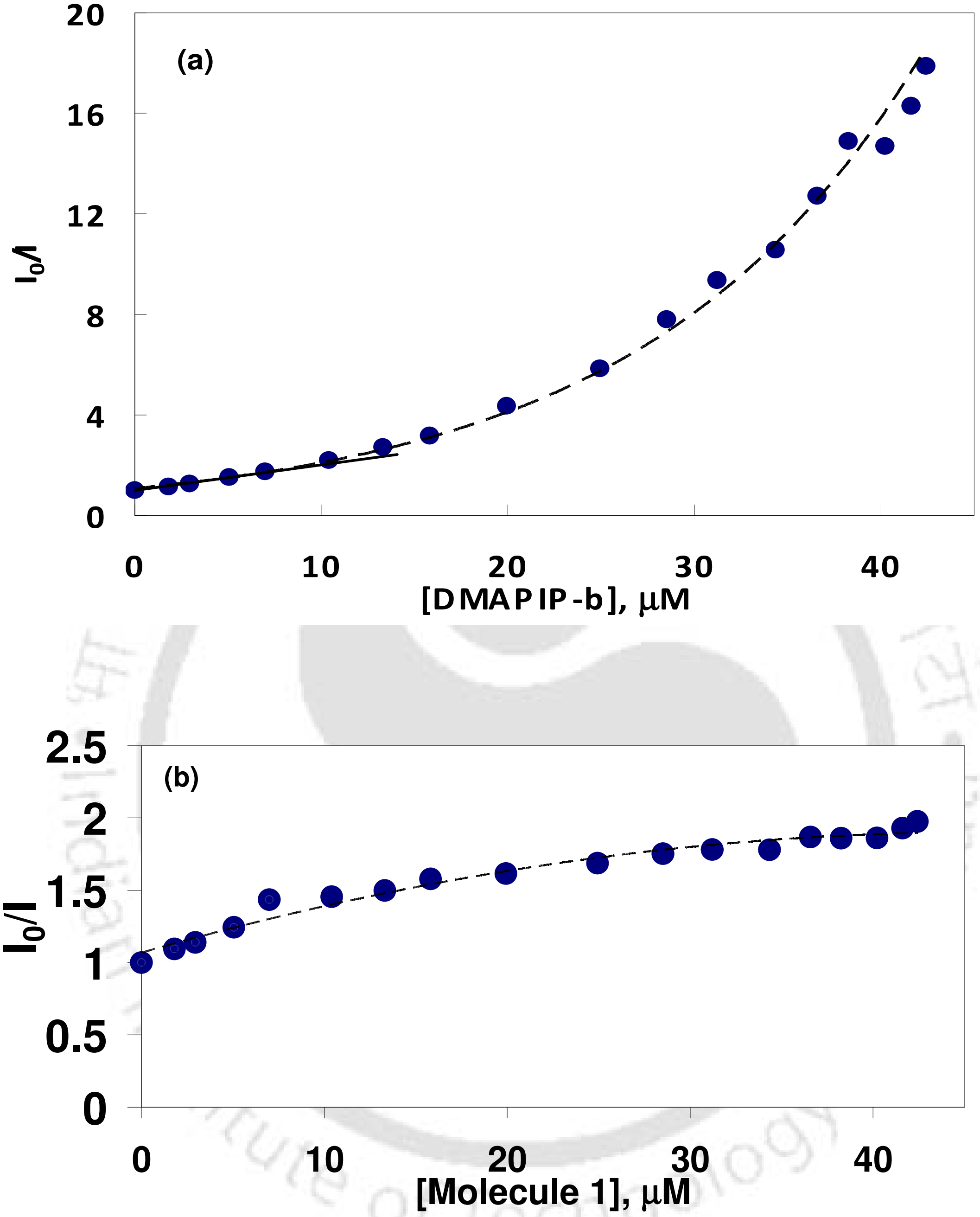

Figure 4.4.6. The Stern Volmer plot quenching of intrinsic fluorescence of BSA by (a) DMAPIP-b (b) 1.

On other hand downward curvature obtained for the quenching by **1**. The downward indicates, of the two tryptophans, one is accessible to ligand and the other is inaccessible or buried or partially accessible to quencher. In presence of quencher only the intensity of the accessible fraction (f_a) is decreased according to the Stern-Volmer equation, but the buried fraction is not quenched. The observed intensity is given by

$$I_0 = \frac{I_{0a}}{1+K_a[Q]} + I_{0i} \qquad (4.4.3)$$

where I_{0a} and I_{0i} are the intensities of the accessible and inaccessible tryptophans and K_a is the Stern-Volmer quenching constant of the accessible fraction. From equation (4.4.3) and the total fluorescence in the absence of quencher ($I_0 = I_{0a} + I_{0i}$), one can obtain following linear equation [9]

$$\frac{I_0}{I_0 - I} = \frac{1}{f_a K_a[Q]} + \frac{1}{f_a} \qquad (4.4.4)$$

A plot of $I_0/(I_0 - I)$ versus 1/[Molecule **1**], is shown in Figure 4.4.7. From the intercept and slope the fraction of the initial fluorescence that is accessible for the quencher and

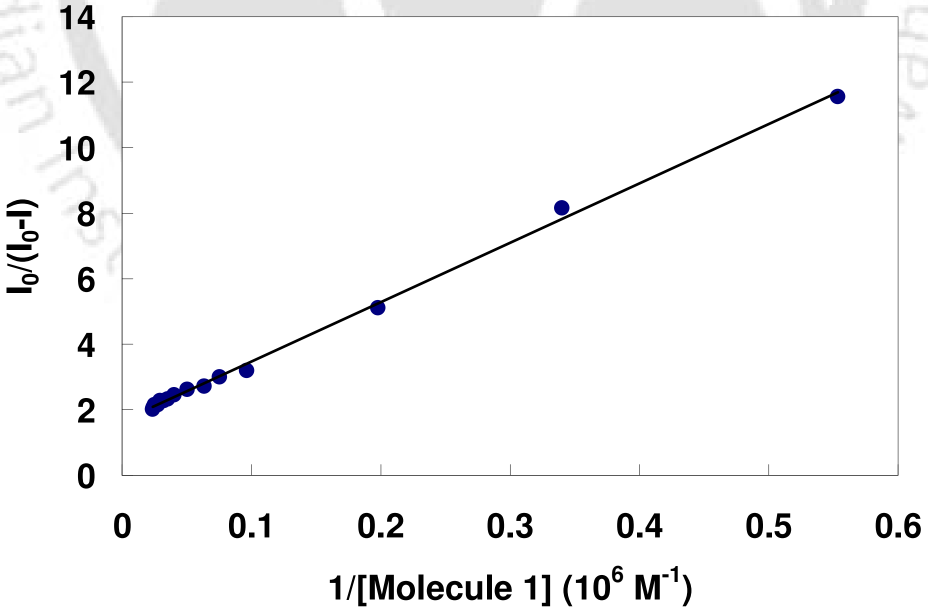

Figure 4.4.7: The plot of $I_0/(I_0-I)$ versus 1/[Molecule 1].

the Stern-Volmer quenching constant of the accessible fraction are calculated. The results show that only 60% of the initial fluorescence is quenched by **1** and the corresponding apparent quenching constant is 9.2 x 10^4 M^{-1}.

4.4.5. Energy transfer

The principle for energy transfer is based on the concept of a fluorophore as an oscillating dipole, which can exchange energy with another dipole with similar resonance frequency. Energy transfer occurs without appearance of photon and may be a result of long range dipole-dipole interaction between the donor and the acceptor. According to Föster theory, the rate of energy transfer depends on the following factors: (a) the extent of overlap between the emission spectrum of the donor with the absorption spectrum of the acceptor (b) proper orientation of transition dipoles of the donor and acceptor (c) quantum yield of the donor (d) the distance between the donor and acceptor and it must be within Föster distance. The efficiency of energy transfer is given by

$$E_T = 1 - \frac{\phi_D}{\phi_D^0} \qquad (4.4.5)$$

where ϕ_D and $\phi_D{}^0$ are the donor quantum yields in the presence and absence of the acceptor respectively. Figure 4.4.8 shows the overlap of the emission spectrum of BSA and the absorption spectra of DMAPIP-b and **1**. Though there is overlap between the absorption spectrum of **1** with fluorescence spectrum of BSA, it is significantly less compared to that of DMAPIP-b, where its absorption spectrum is almost completely overlap with the emission spectra of BSA.

The efficiency is much greater in DMAPIP-b than the corresponding long chain molecule, **1**. No appreciable tryptophan fluorescence is observed at high concentration of

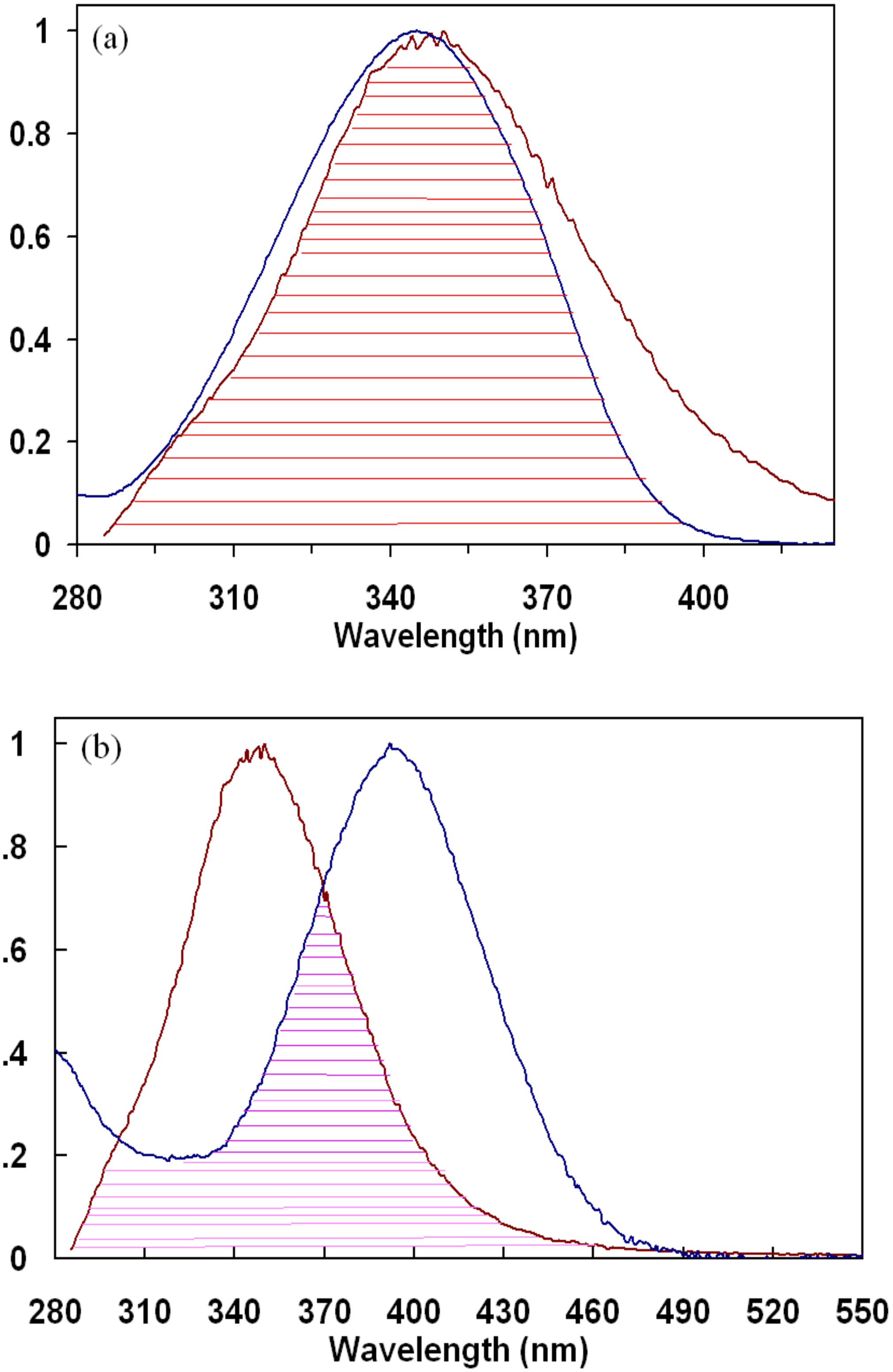

Figure 4.4.8: The overlap of the emission spectrum of BSA with the absorption spectrum of DMAPIP-b (a) and molecule 1 (b).

DMAPIP-b. This indicates energy transfer is nearly 100% from excited tryptophan to DMAPIP-b and it is 53% to **1**. It is not surprising as DMAPIP-b quenches the fluorescence of both tryptophan of BSA and only one tryptophan is available to **1** for quenching.

The distance between the guest and the tryptophan is often determined by resonance energy transfer. According to Föster mechanism, the efficiency of energy transfer (E_T) is related to the distance between donor and acceptor (r) by

$$\mathrm{E_T} = \frac{R_0^6}{R_0^6 + r^6} \tag{4.4.6}$$

where R_0 is the critical distance or Föster radius, i.e. the distance at which the transfer efficiency is 50%, in other words the energy transfer and spontaneous decay of the excited donor are equally probable. Föster radius can be determined from spectroscopic data and is given by

$$R_0 = 0.211[\kappa^2 \eta^{-4} \phi_D J(\lambda)]^{1/6} \tag{4.4.7}$$

where n is the refractive index of the medium, κ is the orientation factor, and ϕ_D^0 is the quantum yield of the donor. The overlap integral, $J(\lambda)$ expresses the degree of spectral overlap between the donor emission spectrum and the acceptor absorption spectrum and is given by

$$J(\lambda) = \frac{\int_0^\infty F_D(\lambda)\varepsilon_A(\lambda)\lambda^4 d\lambda}{\int_0^\infty F_D(\lambda) d\lambda} \tag{4.4.8}$$

where $F_D(\lambda)$ and $\varepsilon_A(\lambda)$ represent the fluorescence intensity of the donor and the molar extinction coefficient of the acceptor, respectively, at the wavelength λ. However, the predictions about the distance of the ligands from the tryptophan using resonance energy transfer in BSA are not that easy, the presence of two tryptophan (Trp-212 and Trp-134) residues complicates it. Therefore we did not attempt to calculate the distance between the tryptophan(s) and the ligands.

4.4.6. Binding constants and binding sites

Assuming that the ligands have same and independent binding sites for the quenching process the number of binding sites (n) and the binding constants (K_A) are calculated from the following expression [334]

$$log\frac{I_0 - I}{I} = n\log K_A - n\log\{\frac{1}{[L]} - \frac{(I_0 - I)[P]}{I_0}\} \qquad (4.4.9)$$

here [L] and [P] are total concentration of ligand and protein respectively. The plot of log [$(I_0$-$I)/I$] against log [(1/[L]) – ((I_0 – I)[P]/I_0)] are shown in Figure 4.4.9. The values thus obtained are compiled in Table 4.4.2. Molecule **1** has only one binding site. However DMAPIP-b has one binding site at lower concentration and two binding sites at higher concentration. The intrinsic fluorescence of BSA is due to tryptophan residues (Trp-134 and 212). Try-134 is in domain I in the eighth helix of D129-R144, which is well exposed, and Try-212 is in domain II, in the second helix of E206-F221, and is buried inside the protein structure. The fluorescence quenching data it can be inferred that **1** is close to one of the tryptophan and DMAPIP-b is close both tryptophans and is consistent with binding sites data. The fluorescence spectral shifts of the ligands in BSA suggest the hydrophobic nature of binding environments. Thus, it may be concluded that **1** binds in the hydrophobic domain II near Try-212 and DMAPIP-b binds in both domain I and II near the tryptophans.

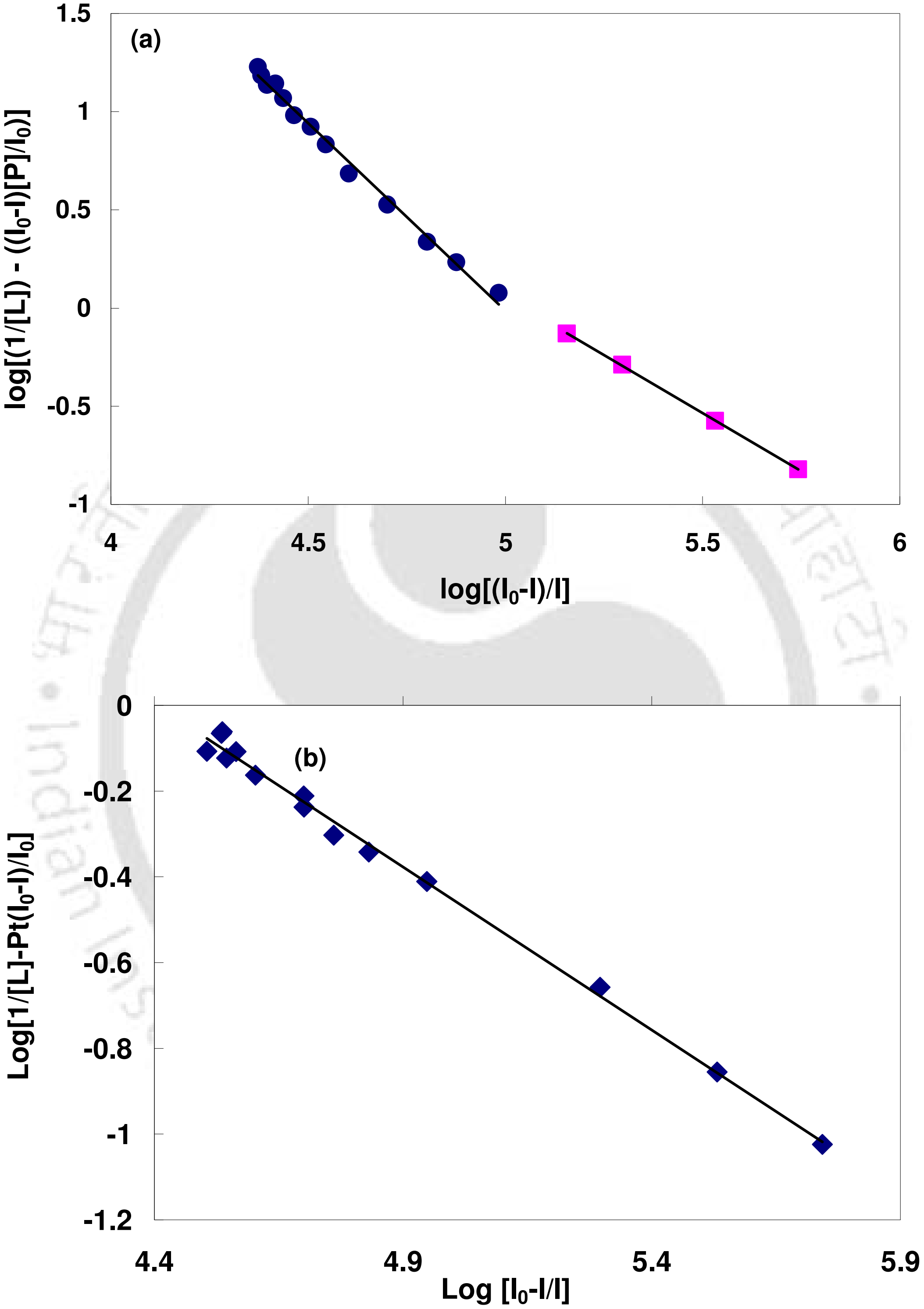

***Figure 4.4.9:** The plot of log[(I_0-I)/I] against log[(1/[L]) – ((I_0 – I)[P]/I_0)] for (a) DAMAPIP-b and (b) 1.*

Table 4.4.2: Binding constant (K_A) and number of binding sites (n) of ligands in BSA.

Molecule	K_A **(M^{-1})**	***n***
DMAPIP-b		
Lower concentrations	10.7×10^4	1.2
Higher concentrations	10.3×10^4	1.9
Molecule 1	2.5×10^4	0.8

4.4.7. Unfolding of BSA by 2

The effect of **2** on the fluorescence spectra of BSA is depicted in Figure 4.4.10. The fluorescence spectrum of BSA is significantly influenced by the addition of **2**. These changes reflect the interaction between **2** and the protein. With increasing concentrations of the ligand, the fluorescence spectrum of BSA is progressive red shifted from 345 in native form to 378 nm in presence of 40 µM. The 33 nm red shift in the fluorescence maximum is accompanied by a large decrease in fluorescence intensity. The fluorescence spectrum is also markedly broadened. The intrinsic protein fluorescence due to tryptophan is the high sensitivity to its local environment. The conformational transitions, subunit association, substrate binding, or denaturation leads to changes in the emission spectra of tryptophan [335-337]. Thus changes in the fluorescence spectra of BSA upon addition of **2** suggest that the interactions of **2** with BSA modified the environment of tryptophan, the emitting species. The bathochromic shift and the reduction in fluorescence intensity specify that the tryptophan environment is changes from hydrophobic to less hydrophobic or hydrophilic. This shows that structure of the hydrophobic subdomain of tryptophan was not compact and addition of ligand leads to conformation change in the segment of polypeptide [338]. The denaturation of proteins usually results in increased exposure of the protein chromophores (tryptophan, tyrosine, and phenylalanine residues) to water. This results in change in their fluorescence characteristics. The most significant transformations occur in the fluorescence behavior of tryptophan, which usually shifted towards longer wavelengths with reduction in fluorescence intensity [336, 339]. Therefore, it can be inferred addition of **2** leads to unfolding of the protein.

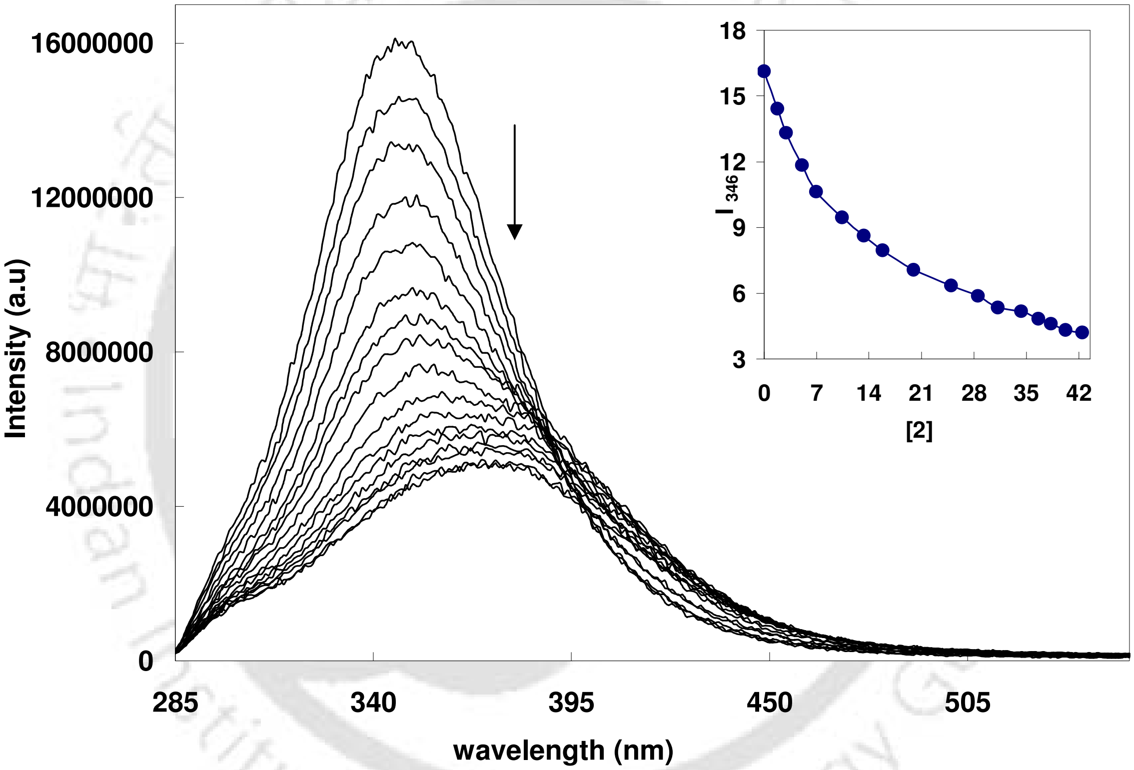

Figure 4.4.10: Fluorescence spectra of BSA at different concentration of 2. The insert shows the variation fluorescence intensity of BSA with 2.

4.4.8. Fluorescence decay of BSA

Fluorescence lifetimes are inherent sensitivity toward excited state interactions, and therefore we have carried out time resolved fluorescence studies on BSA to investigate the mechanism of fluorescence quenching (Table 4.4.3). The intrinsic fluorescence decay of BSA is quite complex, because of the presence of tryptophans which lies in different environments. Thus instead of giving too much emphasis on the magnitude of the individual decay constants of the double exponential decays; rather, the mean (average) fluorescence lifetimes are employed as an important parameter for exploiting the behavior of tryptophans. Only small decrease is observed in the average lifetime of BSA in presence of DMAPIP-b and **1** suggested that the quenching is mainly static in nature. The average lifetime is attenuated more in presence **2**. This suggested that upon unfolding the tryptophans of BSA are exposed to water and the change in the environment is responsible for the decrease in the fluorescence intensity of BSA [337].

Table 4.4.3. Fluorescence characteristics (fluorescence band maximum, λ_{max}^{fl}, nm and fluorescence lifetime, τ, ns) of BSA in absence and presence of ligands.

Ligand	λ_{max}^{fl}	ϕ	τ **(ns)**	**<τ>**
No ligand	345	0.15[1]	3.4 (17.8) 6.7 (82.2)	6.1
DMAPIP-b (40 µM)	345	-	1.9 (2.9) 6.1 (97.1)	6.1
Molecule 1 (40 µM)	345	0.07	1.5 (6.0) 6.1 (94.0)	5.8
Molecule 2 (40 µM)	378	0.06	1.4 (5.4) 6.1 (94.6)	5.5

[1] Ref [340].

4.4.9. Conclusion

The interaction of DMAPIP-b, the aurora kinase inhibitor and its alkylated derivatives with BSA are studied. The studies indicate all the three molecules bind at different binding sites of BSA and the alkylated products have much stronger binding affinity towards protein than DMAPIP-b. DMAPIP-b and its pyridine nitrogen alkylated product, **1** binds at the hydrophobic binding sites, but imidazole alkylated product, **2** binds in a hydrophilic site. The fluorescence of DMAPIP-b and **1** are enhanced due to both reduced polarity and restriction imposed by the hydrophobic binding site inside BSA. However the fluorescence of **2,** increases only due to the reduction in the internal motion of the molecule inside BSA. Both DMAPIP-b and **1** quench the intrinsic fluorescence of BSA by energy transfer. While DAMPIP-b quenches the fluorescence completely, **1** quenches the fluorescence partially. **1** binds in the hydrophobic domain II near Try-212 and DMAPIP-b binds in both domain I and II near the tryptophans. **2** induce conformation change in the structure of BSA that leading quenching BSA fluorescence.

References

1. C. A. Parker, Photoluminescence of solutions, Elsevier, Amsterdam (1968).

2. N. J. Turro, Modern Molecular Photochemistry, University Science Books, Sausalito (1978).

3. M. Kasha, Disc. Faraday Soc. 9 (1950) 14.

4. J. B. Birks, L. G. Christophorou, Spectrochim. Acta. 19 (1963) 401.

5. W. R. Laws, L. Brand, J. Phys. Chem. 83 (1979) 795.

6. H. H. Jaffe, M. Orchin, Theory and application of ultraviolet spectroscopy, John Wiley, New York (1962).

7. H. Suzuki, Electronic absorption spectra and geometry of organic molecules, Academic Press, New York (1967).

8. A. Sharma, S. G. Schulman, Introduction to fluorescence spectroscopy, John Wiley & sons, New York (1999).

9. J. R. Lakowicz, Principles of fluorescence Spectroscopy 3rd ed., Springer, New York (2006).

10. B. Valuer, Molecular fluorescence principles and applications 5th reprint, Wiley-VCH, Weinheim (2009).

11. K. Rotkiewicz, K. H. Grellmann, Z. R. Grabowski, Chem. Phys Lett. 19 (1973) 315.

12. Z. R. Grabowski, K. Rotkiewicz, W. Rettig, Chem. Rev. 103 (2003) 3899.

13. W. Rettig, Angew. Chem. Int. Ed. Engl. 25 (1986) 971.

14. W. Schuddeboom, S. A. Jonker, J. M. Warman, U. Leinhos, W. Kuhnle, K. A. Zachariasse, J. Phys. Chem. 96 (1992) 10809.

15. S. I. Druzhinin, S. A. Kovalenko, T. A. Senyushkina, A. Demeter, K. A. Zachariasse, J. Phys. Chem. A 114 (2010) 1621.

16. R. K. Everett, A. A. Nguyen, C. J. Abelt, J. Phys. Chem. A 114 (2010) 4946.

17. T. S. Singh, S. Mitra, A. K. Chandra, N. Tamai, S. Kar, J. Photochem. Photobiol. A 197 (2008) 295.

18. J. Dobkowski, W. Rettigb, J. Waluk, Phys. Chem. Chem. Phys. 4 (2002) 4334.

19. C. A. Guido, B. Mennucci, D. Jacquemin, C. Adamo, Phys. Chem. Chem. Phys. 12 (2010) 8016.

20. J. Dobkowski, J. Wójcik, W. Koźmiński, R. Kołos, J. Waluk, J. Michl, J. Am. Chem. Soc. 124 (2002) 2406.

21. T. Yoshihara, S. I. Druzhinin, K. A. Zachariasse, J. Am. Chem. Soc. 126 (2004) 8535.

22. S. Cogan, S. Zilberg, Y. Haas, J. Am. Chem. Soc. 128 (2006) 3335.

23. A. L. Sobolewski, W. Domcke, Chem. Phys. Lett. 250 (1996) 428.

24. A. L. Sobolewski, W. Domcke, Chem. Phys. Lett. 259 (1996) 119.

25. K. A. Zachariasse, M. Grobys, E. Tauer, Chem. Phys. Lett. 274 (1997) 372.

26. K. A Zachariasse, T.Yoshihara, S. I. Druzhinin, J. Phys. Chem. A 106 (2002) 6325.

27. A. Ito, S. Ishizaka, N. Kitamura, Phys. Chem. Chem. Phys. 12 (2010) 6641.

28. X. Yang, R. Lu, H. Zhou, P. Xue, F. Wang, P. Chen, Y. Zhao, J. Colloid Interface Sci. 339 (2009) 527.

29. T. Fujiwara , J. -K. Lee, M. Z. Zgierski, C. L. Edward, Chem. Phys. Lett. 481 (2009) 78.

30. M. Shaikh, J. Mohanty, P. K. Singh, A. C. Bhasikuttan, R. N. Rajule, V. S. Satam, S. R. Bendre, V. R. Kanetkar, H. Pal, J. Phys. Chem. A 114 (2010) 4507.

31. F A. S. Chipem, S. Chatterjee, G. Krishnamoorthy, J. Photochem. Photobiol. A 214 (2010) 121.

32. Y. Park, D. C. Apodaca, J. Pullen, R. C. Advincula, J. Phys. Chem. A 114 (2010) 13084.

33. X. H. Qian, Y. Xiao, Y. F. Xu, X. F. Guo, J. H. Qian, W. P. Zhu, Chem. Comm. 46 (2010) 6418.

34. B. K. Paul, A. Samanta, S. Kar, N. Guchhait, J. Lumin. 130 (2010) 1258.

35. J. M. Hicks, M.Vandersall, E. V. Sitzmann, K. B. Eisenthal, Chem. Phys. Lett. 135 (1987) 413.

36. J. M. Hicks, M.Vandersall, Z. Babarogic, K. B. Eisenthal, Chem. Phys. Lett. 116 (1985) 18.

37. K. B. Eisenthal, in W. Kaiser (Ed.) Topics in Applied Physics, Springer-Vergang, New York 60 (1988) 319.

38. S. Tazuke, R. K Guo, T. Ikeda, J. Phys. Chem. 94 (1990)1408.

39. K. A. Al-Hassan, T. Azumi, Chem. Phys. Lett. 121 (1988) 146.

40. K. A. Al-Hassan, Chem. Phys. Lett. 179 (1991) 195.

41. P. Changenet, P. Plaza, M. M. Martin, Y. H. Meyer, J. Phys. Chem. A 101 (1997) 8186.

42. K. A. Al-Hassan, M. A. Meetani, Z. F. M. Said, J. Fluoresc. 8 (1998) 93.

43. W. Rettig, R. Fritz, J. Springer in K. Honda (Ed.) Photochemical Processes in Organized Molecular Systems, Elsevier Science, Amsterdam, North-Holland (1998) 61.

44. J. Paczkowski, D. C. Neckers, Macromolecules 24 (1991) 3013.

45. A. Haidekkar, D. Lichlyter, M. B. Johny, C. A. Grimes, Sens. Lett. 4 (2006) 257.

46. A. Mustafic, H. –M. Huang, E. A. Theodorakis, M. A. Haidekker, J. Fluores. 20 (2010) 1087.

47. A. Rei, G. Hungerford, M. I. C. Ferreira, J. Phys. Chem. B 112 (2008) 8832.

48. M. Li-Hua, C. Z-. Bin, J. Y-. Bao, Chem. Phys. Lett. 372 (2003) 104.

49. K. Dahl, R. Biswas, N. Ito, M. Maroncelli, J. Phys. Chem. B 109 (2005) 1563.

50. R. J. Visser, C. A. G. O. Varma, J. Konijenberg, P. C. M. Weisenborn, J. Mol. Struct. 114 (1984) 105.

51. A. Nag, T. Kundu, K. Bhattacharyya, Chem. Phys. Lett. 160 (1989) 257.

52. R. A. Marcus, N. Sutin, Biochem. Biophys. Acta 811 (1985) 265.

53. W. Siebrand, J. Chem. Phys. 55 (1971) 5843.

54. A. Siemerczuk, Z. R. Grabowski, M. Asher, M. Ottolenghi, Chem. Phys. Lett. 51 (1977) 315.

55. C. Cazeau-Dubroca, S. A. Lyazidi, P. Cambou, A. Peirigua, P. Cazeau, M. Pesquer, J. Phys. Chem. 93 (1989) 2347.

56. C. Cazeau-Dubroca, A. Peirigua, M. Ben Brahim, G. Nouchi, Ph. Cazeau, Chem. Phys. Lett. 157 (1989) 393.

57. C. Cazeau-Dubroca, A. Peirigua, M. Ben Brahim, G. Nouchi, Ph. Cazeau, Proc. Indian Acad. Sci. (Chem. Sci.). 104 (1989) 209.

58. C. Cazeau-Dubroca, G. Nouchi, M. Ben Brahim, M. Pesquer, D. Gorse, Ph. Cazeau, J. Photochem. Photobiol. A 80 (1994) 125.

59. C. Cazeau-Dubroca, A. Peirigua, S. Ait-Lyazidi, G. Nouchi, P. Cazeau, R. Lapouyade, Chem. Phys. Lett. 124 (1986) 110.

60. R. B Singh, S. Mahanta, S. Kar, N. Guchhait, Chem. Phys. 324 (2007) 33.

61. S. Mahanta, R. B Singh, S. Kar, N. Guchhait, J. Photochem. Photobiol. A 194 (2008) 318.

62. J. Herbich, Z. R. Grabowski, H. Wojtowicz, K. Golankiewicz. J. Phys. Chem. 93 (1989) 3439.

63. J. Herbich, J. Karpiuk, Z. R. Grabowski, N. Tamai, K.Yoshihara, J. Lumin. 54 (1992) 165.

64. E. Fasani, A. Albini, P. Savarino, G. Viscardi, E. Barni, J. Heterocycl. Chem. 30 (1993) 1041.

65. Y. H. Kim, D. W. Cho, M. Yoon, D. Kim, J. Phys. Chem. 100 (1996) 15670.

66. Y. Kim, H. W. Cheon, M. Yoon, N. W. Song, D. Kim, Chem. Phys. Lett. 264 (1997) 673.

67. G. Krishnamoorthy, S. K. Dogra, Spectrochim. Acta. A 55 (1999) 2647.

68. G. Krishnamoorthy, S. K. Dogra, J. Phys. Chem. A 104 (2000) 2542.

69. J. Herbich, J. Karpiuk, Z. R. Grabowski, N. Tamai, K. Yoshihara, J. Lumin. 54 (1992) 165.

70. M. Zakharov, O. Krauss, Y. Nosenko, B. B. Brutschy, A. Dreuw, J. Am. Chem. Soc. 131 (2009) 461.

71. A. Mallick, P. Purkayastha, N. Chattopadhyay, J. Photochem. Photobiol. C 8 (2007) 109.

72. K. Kalyanasundaram, Photochemistry in Microheterogeneous Systems, Academic Press Inc, New York (1987).

73. Y. Singh, A. G. Bhattacharya, S. FEBS Lett. 541 (2003) 132.

74. M. S. Ali, N. Gull, J. M. Khan, V. K. Aswal, R. H. Khan, Kabir-ud-Din, J. Colloid Interface Sci. 352 (2010) 436.

75. V. Ramamurthy, Photochemistry in Organized and Constrained Media, VCH, New York (1991).

76. K. Bhattacharyya, M. Chowdhury, Chem. Rev. 93 (1993) 507.

77. L. K. Tiwary, A. Mandal, M. S. Alam, S. Thennarasu, A. B. Mandal, Colloids Surf. B: Biointerfaces 82 (2011) 126.

78. R. B. Singh, S. Mahanta, N. Guchhait, Chem. Phys. Lett. 463 (2008) 183.

79. A. Dan, S. Ghosh, S. P. Moulik, J. Phys. Chem. B 113 (2009) 8505.

80. D. Bose, D. Ghosh, P. Das, A. Girigoswami, D. Sarkar, N. Chattopadhyay, Chem. Phys. Lipids 163 (2010) 94.

81. W. Rettig, R. Lapouyade, in J. R. Lakowicz (Ed.), Topics in Fluorescence Spectroscopy, Probe Design and Chemical Sensing, Plenum Press, New York 4 (1994) 109.

82. Y. Suzuki, K. Yokoyama, Proteomics. 8 (2008) 2785.

83. M. Sowmiya, P. Purkayastha, A. K. Tiwari, S. S. Jaffer, S. K. Saha, J. Photochem. Photobiol. A 205 (2009) 186.

84. R. Gomes, C. A. T. Laia, F. Pina, J. Phys. Chem. B 113 (2009) 11134.

85. S. Syed Jaffer, S. K. Saha, P. Purkayastha, J. Colloid Interface Sci. 337 (2009) 294.

86. T. S. Singh, S. Mitra, J. Photochem. Photobiol. B 96 (2009) 193.

87. Y. Suzuki, K. Yokoyama, J. Am. Chem. Soc. 127 (2005) 17799.

88. S. S. Jaffer, M. Sowmiya, S. K. Saha, P. Purkayastha, J. Colloid Interface Sci. 325 (2008) 236.

89. T. A. Fayed, S. E-. D. H. Etaiw, N. Z. Saleh, J. Lumin. 121 (2006) 431.

90. D. Sahoo, S. Chakravorti, J. Photochem. Photobiol. A 205 (2009) 129.

91. C. L. Jeang, D. G Lin, S. H. Hsieh, J. Agric. Food Chem. 53 (2005) 6301.

92. Q. Qi, M. N Mokhtar, W Zimmermann, J. Inclusion Phenom. Macrocyclic. Chem. 57 (2007) 95.

93. Q. Qi, W. Zimmermann, Appl. Microbiol. Biotechnol. 66 (2005) 475.

94. V. Rimphanitchayakit, T. Tonuzuka, Y. Sakano, Carbohydr. Res. 340 (2005) 2279.

95. J. Szejtli, Chem. Rev. 98 (1998) 1743.

96. D. B. Amabilino, D. F. Stoddart, Chem. Rev. 95 (1995) 2725.

97. J. Szejtli, Cyclodextrin and their Inclusion Complexes, Akademiai Kiado, Budapest (1982).

98. H. Schneider, F. Hacket, V. Rudiger, Chem. Rev. 98 (1998) 1755.

99. M .V. Rekharsky, Y. Inoue, Chem. Rev. 98 (1998) 1875.

100. J. Szejtli, in J. L. Atwood, J. W. Steed (Eds.), Encyclopedia of Supramolecular Chemistry, Marcel Dekker, New York (2004) 398.

101. N. Kandoth, S. D. Choudhury, T. Mukherjee, H. Pal, Photochem. Photobiol. Sci. 8 (2009) 82.

102. K. A. Connors, Chem. Rev. 97 (1997) 1325.

103. M. Sanz, J. A. Organero, A. Douhal, Chem. Phys. 338 (2007) 135.

104. C. Tablet, M. Hillebrand, Spectrochim. Acta. A 70 (2008) 740.

105. A. L. Laza-Knoerr, R. Gref, P. Couvreur, J. Drug Targeting. 18 (2010) 645.

106. L. X. Ding, J. He, K. Fu, J. L. Zhang, Spectrochim. Acta. A 75 (2010) 604.

107. H. Xu, E. A. Ermilov, B. Roder, D. P. K. Ng, Phys. Chem. Chem. Phys. 12 (2010) 7366.

108. K. Higashi, Y. Tozuka, K. Moribe, K. Yamamoto, J. Pharm. Sci. 99 (2010) 4192.

109. S. S. Jaffer, S. K. Saha, G. Eranna, A. K. Sharma, P. Purkayastha, J. Phys. Chem. C 112 (2008) 11199.

110. M. Gratzel, J. K. Thomas, in E .L. Wehry (Ed.), Modern Fluorescence Spectroscopy, Plenum Press, New York (1976).

111. K. L. Mittal, B. Landman (Eds.), Surfactants in Solutions, Plenum Press, New York (1984).

112. M. Shinitzky, A .C. Bianoux, C. Gliter, G.Weber, Biochemistry. 10 (1973) 2106.

113. K. Kano, Y. Ueno, S. Hashimoto, J. Phys. Chem. 89 (1985) 3161.

114. J. A. Butcher, G. W. Lamb, J. Am. Chem. Soc. 106 (1984) 1217.

115. A. Sarkar, S. Pramanik, P. Banerjee, S. C. Bhattacharya, Colloids Surf. A: Physicochemical and Engineering Aspects 317 (2008) 585.

116. M. Ali, M. Jha, S. K. Das, S. K. Saha, J. Phys. Chem. B 113 (2009) 15563.

117. P. Banerjee, S. Pramanik, A. Sarkar, S. C .Bhattacharya, J. Phys. Chem. B 112 (2008) 7211.

118. A. Chakrabarty, P. Das, A. Mallick, N. Chattopadhyay, J. Phys. Chem. B 112 (2008) 3684.

119. F. Lopez, F. Cuomo, A. Ceglie, L. Ambrosone, G. Palazzo, J. Phys. Chem. B 112 (2008) 7338.

120. E. Fuguet, C. Ràfols, E. Bosch, M. Rosés, Langmuir 19 (2003) 55.

121. T. Biver, A. Boggioni, F. Secco, M. Venturini, Langmuir 24 (2008) 36.

122. P. Bandyopadhyay, A. K. Ghosh, S. Bandyopadhyay, Chem. Phys. Lett. 476 (2009) 244.

123. K. K. Karuskstis, S. W. Suljak, P. J. Waller, J. A. whiles, E. H. Z. Thompson, J. Phys. Chem. 100 (1996) 11125.

124. R. G. Laughlin, The Aqueous Phase Behavior of Surfactants, Academic Press, London (1994).

125. J. H. Schulman, D. P. Riley, J. Colloid Sci. 3 (1948) 383.

126. P. L. Luisi, L. J. Magid, C. R. C. Crit. Rev. Biochem. 20 (1986) 409.

127. P. L. Luisi, M. Giomini, M. P. Pileni, B. H. Robinson, Biochim.Biophys. Acta 947 (1988) 209.

128. J. Guharay, P. K. Sengupta, Chem. Phys. Lett. 230 (1994) 75 and references therein.

129. J. Guharay, P.K. Sengupta, Biochem. Biophys. Res. Commun. 219 (1996) 388.

130. K. Bhattacharyya, Acc. Chem. Res. 36 (2003) 95.

131. D. S. Venables, K. Huang, C. A. Schmuttenmaer, J. Phys. Chem. B 105 (2001) 9132 .

132. R. K. Mitra, S. S. Sinha, S. K. Pal, Langmuir 24 (2008) 49.

133. D. S. Venables, K. Huang, C. A. Schmuttenmaer, J. Phys. Chem. B 105 (2001) 9132.

134. N. M. Correa, N. E. Levinger, J. Phys. Chem. B 110 (2006) 13050.

135. K. Bhattacharyya, B. Bagchi, J. Phys. Chem. A 104 (2000) 10603.

136. S. Nave, J. Eastoe, R. K. Heenan, D. Steytlar, I. Grillo, Langmuir 16 (2000) 8741.

137. A. K. Shaw, S. K. Pal, J. Phys. Chem. B 111 (2007) 4189.

138. G. Palazzo, L. Carbone, G. Colafemmina, R. Angelico, A. Ceglieb, M. Giustini. Phys. Chem. Chem. Phys. 6 (2004) 1423.

139. M. A. Sedgwick, D. C. Crans, N. E. Levinger, Langmuir 25 (2009) 5496.

140. L. Yang, K. H. Zhao, Langmuir 23 (2007) 8732.

141. S. Rafiq, R. Yadav, P. Sen, J. Phys. Chem. B 114 (2010) 13988.

142. D. Bose, D. Sarkar, A. Girigoswami, A. Mahata, D. Ghosh, N. Chattopadhyay, J. Chem. Phys. 131 (2009) 114707.

143. G. M. Sando, K. Dahl, J. C. Owrutsky, J. Phys. Chem. B 109 (2005) 4084.

144. G. B. Dutt, J. Phys. Chem. B 108 (2004) 805.

145. R. K. Mitra, S. S. Sinha, P. K. Verma, S. K. Pal, J. Phys. Chem. B 112 (2008) 12946.

146. G. B. Dutt, J. Phys. Chem. B 108 (2004) 7944.

147. R. K. Mitra, S. S. Sinha, S. K. Pal, J. Fluoresc. 18 (2008) 423.

148. J. A. B. Ferreira, S. M. B. Costa, J. Phys. Chem. B 114 (2010) 10417.

149. R. D. Falcone, N. M. Correa, M. A. Biasutti, J. J. Silber, J. Colloid Interface Sci. 296 (2006) 356.

150. E. Gaidamauskas, D. P. Cleaver, P. B. Chatterjee, D. C. Crans, Langmuir 26 (2010) 13153.

151. V. Petrov, C. A. T. Laia, F. Pina, Langmuir 25 (2009) 594.

152. S. Dhar, D. K. Rana, A. Sarkar, T. K. Mandal, S. Ghosh, S. C. Bhattacharya, Colloids Surf. A: Physicochemical and Engineering Aspects. 349 (2009) 117.

153. M. Wong, J. K. Thomas, M.Gratzel, J. Am. Chem. Soc. 98 (1976) 2391.

154. M. Hasegawa, T. Sugimura, Y. Suzaki, Y. Shindo, J. Phys. Chem. 98 (1994) 2124.

155. P .E. Zinsli, J. Phys. Chem. 83 (1979) 3223.

156. H. Konda, I. Miwa, J. Sunamoto, J. Phys. Chem. 86 (1982) 4826.

157. E. A. Lissi, D. Engel, Langmuir 8 (1992) 1070.

158. E. A. Lissi, M. V. Encinas, S. G. Bertolotti, J. J. Cosa, C. M. Previtali, Photochem. Photobiol. 51 (1990) 452

159. C. A. Backer, D. G. Whitten, J. Phys. Chem. 91 (1987) 865.

160. K. K. Karrukstis, A. A. Frazier, D. S. Martula, J. A. Whiles, J. Phys. Chem. 100 (1996) 11133.

161. J. R. Brown, in V. M. Rosenoer, M. Oratz, M. A. Rothschild (Eds.), Albumin structure, Function and Uses, Pergamon Press, Oxford (1977) 27.

162. D.C. Carter, J.X. Ho, Adv. Protein Chem. 45 (1994) 153.

163. E. Bojesen, I. N. Bojesen, J. Phys. Chem. 100 (1996) 17981.

164. M. K. Mathew, P. Balaram, FEBS Lett. 115 (1980) 91.

165. S. Makino, J.A. Reynolds, C. Tanford, J. Biol. Chem. 248 (1973) 4926.

166. W. Bal, J. Christodoulou, P. J. Sadler, A. Tucker, J. Inorg. Biochem. 70 (1998) 33.

167. A. N. Karachentsev, I. A. Melchenko, Eksp. Klin. Farmakol. 60 (1997) 68.

168. P. B. Kandagal, S. Ashoka, J. Seetharamappa, S. M. T. Shaikh, Y. Jadegoud, O. B. Ijare, J. Pharm. Biomed. Anal. 41 (2006) 393.

169. B. Sengupta, P. K. Sengupta, Biochem. Biophys. Res. Commun. 299 (2002) 400.

170. D. C. Carter, J. X. Ho, Adv. Protein Chem. 45 (1994) 153.

171. T. Peters, Adv. Protein Chem. 37 (1985) 161.

172. T. J. Peters, All about Albumin Biochemistry, Genetics and Medical Applications, Academic Press, San Diego (1996).

173. J. F. Foster, in V. M. Rosenoer, M. Oratz, M. A. Rothschild (Eds.), Albumin Structure, Function and Uses, Pergamon Press, Oxford (1977) 53.

174. K. Vijai, J. Forster, Biochemistry 6 (1967) 1152.

175. V. A. Kharlanov, W. Rettig, M. I. Knyazhansky, N. Makarova, J. Photochem. Photobiol. A 103 (1997) 45.

176. S. R. Vázquez, C. R. Rodríguez, M. Mosquera, F. Rodríguez-Prieto, J. Phys. Chem. A 111 (2007) 1814.

177. D. LeGourriérec, V. Kharlanov, R. G. Brown, W. Rettig, J. Photochem. Photobiol. A 130 (2000) 101.

178. F. A. S. Chipem, G. Krishnamoorthy, J. Phys. Chem. A 113 (2009) 12063.

179. A. Muller, H. Ratajczak, W. Junge, E. Diemann (Eds.), Electron and Proton Transfer in Chemistry and Biology, Elsevier, Amsterdam (1992).

180. B. G. Malmstrom, in V. Balzani (Ed.), Electron Transfer in Chemistry, Wiley-VCH, Weinheim, Germany 3 (2001) 39.

181. K. Faxén, G. Gilderson, P. A. Delroth, P. Brzezinski, Nature. 437 (2005) 286.

182. G. Krishnamoorthy, S. K. Dogra, J. Org. Chem. 64 (1999) 6566.

183. W. Zheng, D. Li, J. Y. Qu, J. Biomed. Optics 15 (2010) 037013.

184. V. I. Stsiapura, A. A. Maskevich, V. A. Kuzmitsky, V. N. Uversky, I. M. Kuznetsova, K. K. Turoverov, J. Phys. Chem. B 112 (2008) 15893.

185. H. Shibata, Y. J. Heo, T. Okitsu, Y. Matsunaga, T. Kawanishi, S. Takeuchi, Proc. Natl. Acad. Sci. U S A 107 (2010) 17894.

186. S. L. Wang, J. M. Lin, Chem. Phys. Lett. 444 (2007) 71.

187. J. W. Borst, A. J. W. G Visser, Meas. Sci. Technol. 21 (2010) 102002.

188. K. Szacilowski, Chem. Rev. 108 (2008) 3481.

189. X. J. Zhao, C. Z. Huang, Analyst. 135 (2010) 2853.

190. Y. Otsu, V. Bormuth, J. Wong, B. Mathieu, G. P. Dugue, A. Feltz, S. Dieudonne, J. Neurosci. Med. 173 (2008) 259.

191. Aurora-A, Aurora-B and Aurora-C kinases play a key role in the regulation of mitosis, and are implicated in cancer initiation and progression.

192. V. Bavetsias, C. Sun, N. Bouloc, R. Jóhannes, W. Paul, L. Spiros Linardopoulos, M. Edward, Bioorg. Med. Chem. Lett. 17 (2007) 6567.

193. D. W. Hein, R. J. Alheim, J. J. Leavitt, J. Am. Chem. Soc. 79 (1957) 427.

194. R. W. Middleton, D. G. Wibberely, J. Heterocycl. Chem. 17 (1980) 1757.

195. H. Yu, H. Kawanishi, H. Koshima, J. Photochem. Photobiol. A 178 (2006) 62.

196. Y. –P. Tong, S. –L. Zheng, X. –M. Chen, J. Mol. Struct. 826 (2007) 104.

197. G. A.Crosby, J. N.Demas, J. Phys. Chem.75 (1971) 991.

198. J. B Foresman, M. Head-Gordon, J. A. Pople, M. J. Frisch, J. Phys. Chem. 96 (1992) 135.

199. M. E. Casida, Time-dependent density functional response theory for molecules, in: D. P. Chong (Ed.), Recent Advances in Density Functional Methods Part I, World Scientific, Singapore (1995) 155.

200. E. K. U. Gross, J. F. Dobson, M. Petersilka, Top. Curr. Chem. 118 (1996) 81.

201. M. J. Frisch, I. N. Ragazos, M. A. Robb, H. B. Schlegel, Chem. Phys. Lett.189 (1992) 524.

202. P. -A. Malmqvist, B. O. Roos, Chem. Phys. Lett. 155 (1989) 189.

203. J. Stalring, A. Bernhardsson, R. Lindh, Mol. Phys. 99 (2001) 103.

204. M. J. Paterson, M. A. Robb, L. Blancafort, A. D. DeBellis, J. Phys. Chem. A 109 (2005) 7527.

205. T. Pal, M. Paul, S. Ghosh, J. Mol. Struct. (THEOCHEM) 860 (2008) 8.

206. G. J. Zhao, K. L. Han, J. Phys. Chem. A 113 (2009) 14329.

207. R. Casadesús, M. Moreno, J. M. Lluch, J. Photochem. Photobiol. A 173 (2005) 365.

208. C. Jamorski, J. B. Foreseman, C. Thilgen, H. –P. Lüthi, J. Chem. Phys. 116 (2002) 8761.

209. Z.Yang, S. Yang, J. Zhang, J. Phys. Chem. A 111 (2007) 6354.

210. J. F. Stanton, J. Gauss, N. Ishikawa, M. Head-Gordon, J. Chem. Phys. 103 (1995) 4160.

211. K. B. Wiberg, Y. –G. Wang, A. E de Oliveira, S. A. Perera, P. H. Vaccaro, J. Phys. Chem. A 109 (2005) 466.

212. M. K Shukla, J. Int. Leszczynski, J. Quantum. Chem. 105 (2005) 387.

213. G. Gahungu, J. Zhang, J. Phys. Chem. B 109 (2005) 17762.

214. M. Belletête, N. Blouin, P. –L. T. Boudreault, M. Leclerc, G. Durocher, J. Phys. Chem. A 110 (2006) 13696.

215. M. J. Frisch, G. W. Trucks, H. B. Schlegel, G. E. Scuseria, M. A. Robb, J. R. Cheeseman, J. A. Montgomery, Jr., T. Vreven, K. N. Kudin, J. C. Burant, J. M. Millam, S. S. Iyengar, J. Tomasi, V. Barone, B. Mennucci, M. Cossi, G. Scalmani, N. Rega, G. A. Petersson, H. Nakatsuji, M. Hada, M. Ehara, K. Toyota, R. Fukuda, J. Hasegawa, M. Ishida, T. Nakajima, Y. Honda, O. Kitao,

H. Nakai, M. Klene, X. Li, J. E. Knox, H. P. Hratchian, J. B. Cross, V. Bakken, C. Adamo, J. Jaramillo, R. Gomperts, R. E. Stratmann, O. Yazyev, A. J. Austin, R. Cammi, C. Pomelli, J. W. Ochterski, P. Y. Ayala, K. Morokuma, G. A. Voth, P. Salvador, J. J. Dannenberg, V. G. Zakrzewski, S. Dapprich, A. D. Daniels, M. C. Strain, O. Farkas, D. K. Malick, A. D. Rabuck, K. Raghavachari, J. B. Foresman, J. V. Ortiz, Q. Cui, A. G. Baboul, S. Clifford, J. Cioslowski, B. B. Stefanov, G. Liu, A. Liashenko, P. Piskorz, I. Komaromi, R. L. Martin, D. J. Fox, T. Keith, M. A. Al-Laham, C. Y. Peng, A. Nanayakkara, M. Challacombe, P. M. W. Gill, B. Johnson, W. Chen, M. W. Wong, C. Gonzalez, J. A. Pople, Gaussian 03, Revision E.01, Gaussian, Inc., Wallingford CT, (2004)

216. P. Hohenberg, W. Kohn, Phys. Rev. B 136 (1964) 864.

217. W. Kohn, L. J. Sham, Phys. Rev. A 140 (1965) 1133.

218. A. D Becke, J. Chem. Phys. 98 (1993) 5648.

219. C. T. Lee, W. Yang, R. G. Parr, Phys. Rev. B 37 (1988) 785.

220. J. E. Ridley, M. C. Zerner, Theo. Chim. Acta. 42 (1976) 223.

221. J. Dey, S. K. Dogra, J. Phys. Chem. 98 (1994) 3638.

222. G. Krishnamoorthy, S. K. Dogra, Chem. Phys. 243 (1999) 45.

223. E. Lippert, Z. Electrochem. 61 (1957) 962.

224. S. Murali, W. Rettig, J. Phys. Chem. A 110 (2006) 28.

225. S. I. Druzhinin, V. A. Galievsky, T. Yoshihara, K. A. Zachariasse, J. Phys. Chem. A 110 (2006) 12760.

226. J. S. Yang, K. L. Lian, C.Y. Li, M. Y. Chen, J. Am. Chem. Soc. 129 (2007) 13183.

227. Y.V. Il'ichev, W. Kühnle, K. A. Zachariasse, J. Phys. Chem. A 102 (1998) 5670.

228. T. Morozumi, T. Anada, H. Nakamura, J. Phys. Chem. B 105 (2001) 2923.

229. S. K. Saha, P. Purkayastha, A. B. Das, J. Photochem. Photobiol. A 195 (2008) 368.

230. A. Nag, R. Dutta, N. Chattopadhyay, K. Bhattacharyya, Chem. Phys. Lett. 157 (1989) 83.

231. J. F. Ireland, P. A. H. Wyatt, Adv. Phys. Org. Chem. 12 (1976) 132.

232. A. K. Mishra, S. K. Dogra, Spectrochim. Acta. A 39 (1983) 106.

233. E. Butty, P. Suppan, Polym. Photochem. 5 (1984) 171.

234. E. Lippert, Z. Naturforsch. A 10 (1955) 541.

235. T. Hagan, D.D. Pilloud, P. Suppan, Chem. Phys. Lett. 139 (1987) 499.

236. A. K. Chattopadhyay, S. Basu, S. C. Chakraborty, J. Lumin. 65 (1995) 269.

237. G. Pagona, S. P. Economopoulos, G. K. Tsikalas, H. E. Katerinopoulos, N. Tagmatarchis, Chem. Euro. J. 16 (2010) 11969.

238. S. S. Tan, Y. N. Teo, E. T. Kool, Org. Lett. 12 (2010) 4820.

239. H. Wang, J. Lin, W. Huang, Wei, W. Wei, Sens. Actuators B: Chem. 150 (2010) 798.

240. X. F. Wu, B. W. Xu, H. Tong, L. X. Wang, Macromolecules 43 (2010) 8917.

241. E. L. Que, D. W. Domaille, C. J. Chang, Chem. Rev. 108 (2008) 1517.

242. R. Uauy, M. Olivares, M. Gonzalez, Am. J. Clin. Nutr. 67 (1998) 952.

243. E. M. Nolan, S. J. Lippard, Inorg. Chem. 43 (2004) 8310.

244. C. J. Chang, E. M. Nolan, J. Jaworski, K. I. Okamato, Y. Hayashi, M. Shang, S. J. Lippard, Inorg. Chem. 43 (2004) 6774.

245. R. Parkesh, T. C. Lee, T. Gunnlaugsson, Org. Biomol. Chem. 5 (2007) 310.

246. H. Y. Gong, Q. Y. Zheng, X. H. Zhang, D. X. Wang, M. X. Wang, Org. Lett. 8 (2006) 4895.

247. K. Komatsu, Y. Urano, H. Kojima, T. Nagano, J. Am. Chem. Soc. 129 (2007) 13447.

248. E. Kimura, S. Aoki, E. Kikuta, T. Koike, Proc. Natl. Acad. Sci, USA 100 (2003) 3731.

249. S. C. Burdette, S. J. Lippard, Proc. Natl. Acad. Sci, USA 100 (2003) 3605.

250. J. M. Berg, Y. Shi, Science 271 (1996) 1081.

251. A. I. Bush, W. H. Pettingell, G. Malthaup, M. Paradis, J. P. Vonsattel, J. F. Gusella, K Beyreuther, C. L. Masters, R. E. Tanzi, Science 265 (1994) 1464.

252. J- Y. Koh, S. W. Suh, B. J. Gwag, Y. Y. He, C. Y. Hsu, D. W. Choi, Science 272 (1996) 1013.

253. C. J. Frederickson, M. D. Hernandez, J. F. McGinty, Brain Res. 480 (1989) 317.

254. T. Hirano, K. Kikuchi, Y. Urano, T. Nagano, J. Am. Chem. Soc. 124 (2002) 6555.

255. K. Komatsu, K. Kikuchi, H. Kojima, Y. Urano, T. Nagano, J. Am. Chem. Soc. 127 (2005) 10197.

256. K. R Gee, Z. -L Zhou, W. -J. Qian, R. J. Kennedy, J. Am. Chem. Soc. 124 (2002) 776.

257. S. C. Burdette, G. K.Walkup, B. Spingler, R. Y. Tsien, S. J. Lippard, J. Am. Chem. Soc. 123 (2001) 7831.

258. S. C. Burdette, C. J. Frederickson, W. Bu, S. J. Lippard, J. Am. Chem. Soc. 125 (2003) 1778.

259. C. J. Chang, E. M. Nolan, J. Jaworski, S. C. Burdette, M. Sheng, S. Lippard, J. Chem. Biol. 11 (2004) 203.

260. E. M. Nolan, J. Jaworski, K. -I Okamoto, Y .Hayashi, M. Sheng, S. J. Lippard, J. Am. Chem. Soc. 127 (2005) 16812.

261. E. M. Nolan, J. Jaworski, M. E. Racine, M. Sheng, S. J. Lippard, Inorg. Chem. 45 (2006) 9748.

262. E. M. Nolan, J. W. Ryu, J. Jaworski, R. P. Feazell, M. Sheng, S. J. Lippard, J. Am. Chem. Soc. 128 (2006) 15517.

263. B. Tang, H. Huang, K. H. Xu, L. L Tong, G. W. Yang, X. Liu, L. G. An, Chem. Commun. (2006) 3609.

264. S. Maruyama, K. Kikuchi, T. Hirano, Y. Urano, T. Nagano, J. Am. Chem. Soc. 124 (2002) 10650.

265. K. Kiyose, H. Kojima, Y. Urano, T. Nagano, J. Am. Chem. Soc. 128 (2006) 6548.

266. K. R. Gee, Z. -L. Zhou, D. T.-That, S. L Sensi, J. H. Weiss, Cell. Calcium 31 (2002) 245.

267. K. Komatsu, Y. Urano, H. Kojima, T. Nagano, J. Am. Chem. Soc. 129 (2007) 13447.

268. C. C. Woodroofe, S. J. Lippard, J. Am. Chem. Soc. 125 (2003) 11458.

269. M. Taki, J. L.Wolford, T. V. O'Halloran, J. Am. Chem. Soc.126 (2004) 712.

270. C. J. Chang, J. Jaworski, E. M. Nolan, M. Sheng, S. J. Lippard, Proc. Natl. Acad. Sci. U.S.A 101 (2004) 1129.

271. M. M. Henary, Y. Wu, C. J. Fahrni, Chem. Eur. J. 10 (2004) 3015.

272. N. C. Lim, J. V. Schuster, M. C. Porto, M. A. Tanudra, L. L. Yao, H. C. Freake, C. Bruckner, Inorg. Chem. 44 (2005) 2018.

273. A. Ajayaghosh, P. Carol, S. Sreejith, J. Am. Chem. Soc. 127 (2005) 14962.

274. Y. J. Mei, P. A. Bentley, Bioorg. Med. Chem. Lett. 16 (2006) 3131.

275. T. Koike, T. Watanabe, S. Aoki, E. Kimura, M. Shiro, J. Am. Chem. Soc. 118 (1996) 12696.

276. L. Fabbrizzi, M. Licchelli, P. Pallavicini, A. Taglietti, Inorg. Chem. 35 (1996) 1733.

277. Q. -J. Ma, X. -B. Zhang, Y. Zhao, C. -Y. Li, Z. -X. Han, G. -L. Shen, R.-Q. Yu, Spectrochim. Acta. A 71 (2009) 1683.

278. A. Mishra, G. B. Behera, M. M. G. Krishna, N. Periasamy, J. Luminesc. 92 (2001) 175.

279. X. H. Zhang, Y. Wang, W. J. Jin, Talanta. 73 (2007) 938.

280. A. M. de la Pena, N. M. Diez, D. B. Gil, E. C. Carranza, J. Fluoresc. 19 (2009) 345.

281. A. Banerjee, K. Basu, P. K. Sengupta, J. Photochem. Photobiol. B 89 (2007) 88.

282. K. A. Al-Hassan, U. K. A. Klein, Chem. Phys. Lett. 212 (1993) 581.

283. M. Shaikh, J. Mohanty, A. C. Bhasikuttan, H. Pal, Photochem. Photobiol. Sci. 7 (2008) 979.

284. J. A. Faiz, L. E. P. Kyllonen, P. C. -Carballada, R. M. Williams, L. De. Cola, Z. Pikramenou, Dalton Trans. (2009) 3980.

285. S. Ralkshit, S. Vasudevan, ACS Nano. 2 (2008) 1473.

286. T. S. Singh, N. S. Moyon, S. Mitra, Spectrochim. Acta. A. 73 (2009) 630.

287. A. Pigliucci, E. Vauthey, W. Rettig, Chem. Phys. Lett. 469 (2009)115.

288. C. –Y.Yang, Y. Liu, D. Zheng, J. –C. Zhu, J. Dai, J. Photochem. Photobiol. A Chem.188 (2007) 51.

289. Y. –B. Jiang, J. Photochem. Photobiol. A Chem. 98 (1995) 109.

290. Y. Matsushita, T. Suzuki, T. Ichimura , T. Hikida, Chem. Phys. 286 (2003) 399.

291. V. Ramamurthy, D. F. Eaton, Acc. Chem. Res. 21 (1988) 300.

292. A. Heredia, G. Requena, F. G. Sanchez, J. Chem. Soc. Chem. Commun. (1985) 1814.

293. K. W. Street, W. E. Acree, Appl. Spectrosc. 42 (1988) 1315.

294. S. Nigam, G. Durocher, J. Phys. Chem. 100 (1996) 7135.

295. H. A. Benesi, J. H. Hildebrand, J. Am. Chem. Soc. 71 (1949) 2703.

296. S. Hamai, J. Phys. Chem. 93 (1989) 2074.

297. G. Krishnamoorthy, S. K. Dogra, J. Photochem. Photobiol. A 123 (1999) 109.

298. A. A. Abdel-Schafi, S. S. Al-Shihry, Spectrochim. Acta A 72 (2009) 533.

299. S. Kundu, N. Chattopadhyay, J. Photochem. Photobiol. A Chem. 88 (1995) 105.

300. M. K. Singh, H. Pal, A. S. R. Koti, A. V. Sapre, J. Phys. Chem. A 108 (2004) 1465.

301. M. A. Voinov, I. A. Kirilyuk, A. I. Smirnov, J. Phys. Chem. B 113 (2009) 3453.

302. J. H. Fendler, Membrane Mimetic Chemistry, Wiley-Interscience, New York (1982).

303. A. K. Singh, M. Darshi, Biochim. Biophys. Acta 1563 (2002) 35.

304. M. Almgren, F. Grieser, J. K. Thomas, J. Am. Chem. Soc. 101 (1979) 279.

305. G. Saroja, B Ramachandan, S. Saha, A. Samanta, J. Phys. Chem. B 103 (1999) 2906.

306. A. Mohr, P. Talbiersky, H. G. Korth, R. Sustmann, R. Boese, D. Bläser, H. Rehage, J. Phys. Chem. B 111 (2007) 12985.

307. E. M. Kosower, An Introduction to Physical Organic Chemistry, Wiley, New York (1968).

308. S. Kundu, S. Maity, S. C. Bera, N. Chattopadhyay, J. Mol. Struct. 405 (1997) 231.

309. M. Shannigrahi, S. Bagchi, J. Phys. Chem. B 108 (2004) 17703.

310. N. Deb, M. Shannigrahi, S. Bagchi, J. Phys. Chem. B 112 (2008) 2868.

311. G. Krishnamoorthy, S. K. Dogra, J. Colloid Interface. Sci 213 (1999) 53.

312. M. Gaber, S. A. El-Daly, Y. S. El-Sayed, Colloid Surf. B 66 (2008) 103.

313. G. Krishnamoorthy, S. K. Dogra, Phys. Chem. Chem. Phys. 2 (2000) 2521.

314. A. Dreuw, J. L. Weisman, M. Head-Gordon, J. Chem. Phys. 119 (2003) 2943.

315. A. L Sobolewski, W. Domcke, Chem. Phys. 294 (2003) 73.

316. S. K. Das, S. K. Dogra, J. Chem. Soc. Faraday Trans. I 94 (1998) 139.

317. S. Pandey, R. S. Sarpal, S. K. Dogra, J. Colloid Interface Sci. 172 (1995) 407.

318. C. J. Drummond, F. Grieser, T. W. Healy, J. Chem. Soc. Faraday Trans. 1 85 (1989) 521.

319. L. S. Romsted, D. Zanethe, J. Phys. Chem. 92 (1988) 4690.

320. C. Kumar, D. Balasubramanian, J. Colloid Interface Sci. 74 (1980) 64.

321. S. D. Choudhury, M. Kumbhakar, S. Nath, S. K. Sarkar, T. Mukherjee, H. Pal, J. Phys. Chem. B 111 (2007) 8842.

322. D. A. Kelkar, A. Chattopadhyay, J. Phys. Chem. B 108 (2004) 12151.

323. P. K. Singh, M. Kumbhakar, H. Pal, S. Nath, J. Phys. Chem. B 113 (2009) 1353.

324. P. R. Bangal, S. Panja, S. Chakravorti, J. Photochem. Photobiol. A 139 (2001) 5.

325. W. M. Kwok, M. W. George, D. C. Grills, C. Ma, P. Matousek, A. W. Parker, D. Phillips, W. T. Toner, M. Towrie, Angew. Chem. Int. Ed. Engl. 42 (2003) 1826.

326. A. Chattopadhyay, S. Mukherjee, J. Phys. Chem. B 103 (1999) 8180.

327. D. A. Kelker, A. Chattopadhyay, J. Phys. Chem. B 108 (2004) 12151.

328. Y.-B. Jiang, L. Lin, Appl. Spectrosc. 49 (1995) 1017.

329. B. Bhattacharya, S. Nakka, L. Guruprasad, A. Samanta, J. Phys. Chem. B 113 (2009) 2143.

330. A. Mallick, B. Haldar, N. J. Chattopadhyay, Photochem. Photobiol. B 78 (2005) 215.

331. P. Das, A. Chakrabarty, B. Haldar, A. Mallick, N. Chattopadhyay, J. Phys. Chem. B 111 (2007) 7401.

332. A. Mallick, B. Haldar, S. Maiti, N. Chattopadhyay, J. Colloid Interface Sci. 278 (2004) 215.

333. J. M. Vanderkooi, D. B. Calhoun, S. W. Englander, Science 236 (1987) 568.

334. S. Bi, L. Ding, Y. Tian, S. Song, X. Zhou, X. Liu, H. Zhang, J. Mol. Struct. 703 (2005) 37.

335. M. R. Eftink, Methods Biochem. Anal. 35 (1990) 117.

336. E. A. Burstein, Luminescence of protein chromophores. Model Studies in Advance Science and Technology Results; Biophysics, VINITI, Moscow, 6 (1976).

337. B. Ojha, G. Das, J. Phys. Chem. B 114 (2010) 3979.

338. T. Yuan, A. M. Weljie, H. Vogel, Biochem. 37 (1998) 3187.

339. O. K. Abou-Zied, O. I. K. Al-Shihi, J. Am. Chem. Soc. 130 (2008) 10793.

340. F. L. Cui, J. Fan, J. P. Li, Z. Hu, Bioorg. Med. Chem. 12 (2004) 151.

Appendix I

^1H NMR in $CDCl_3$ and Assignment of Protons

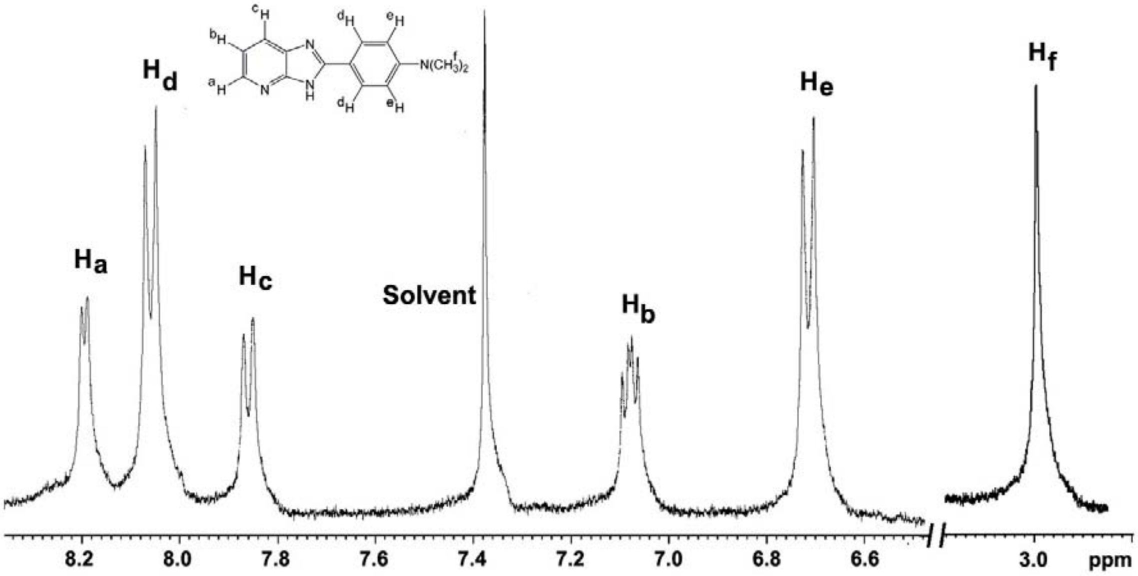

Figure S1: ^1H NMR spectrum of DMAPIP-b in $CDCl_3$ (intensity of aromatic region is expanded approximately by a factor of six).

Assignment of protons in the aromatic region

H_a, **H_c** type protons expected to be a doublet due to splitting of neighboring **H_b** proton, and **H_a** is expected in down field due to the presence of neighboring hereto atom. Accordingly δ 8.24 (d, J = 5 Hz , 1H) and 7.96 (dd, J = 8, 5 Hz, 1H) can be assigned to **H_a** and **H_c** respectively.

H_b is expected to be doublet of doublet, only doublet of doublet at δ 7.14 (dd, J = 8, 5 Hz, 1H) thus corresponds to **H_b**.

H_d, **H_e** type protons expected to be a doublet due to splitting of neighboring proton of other type i.e. **H_d** by **H_e** and **H_d** by **H_e**. **H_d** is expected in downfield (compare to **H_e**) due to the presence of neighboring heterocylic ring. Thus δ 8.12 (d, J = 9 Hz, 2H) and 6.74 (d, J = 9 Hz, 2H) can be assigned to **H_d** and **H_e** types of protons respectively.

The assignments were further substantiated by the decoupled spectra shown below.

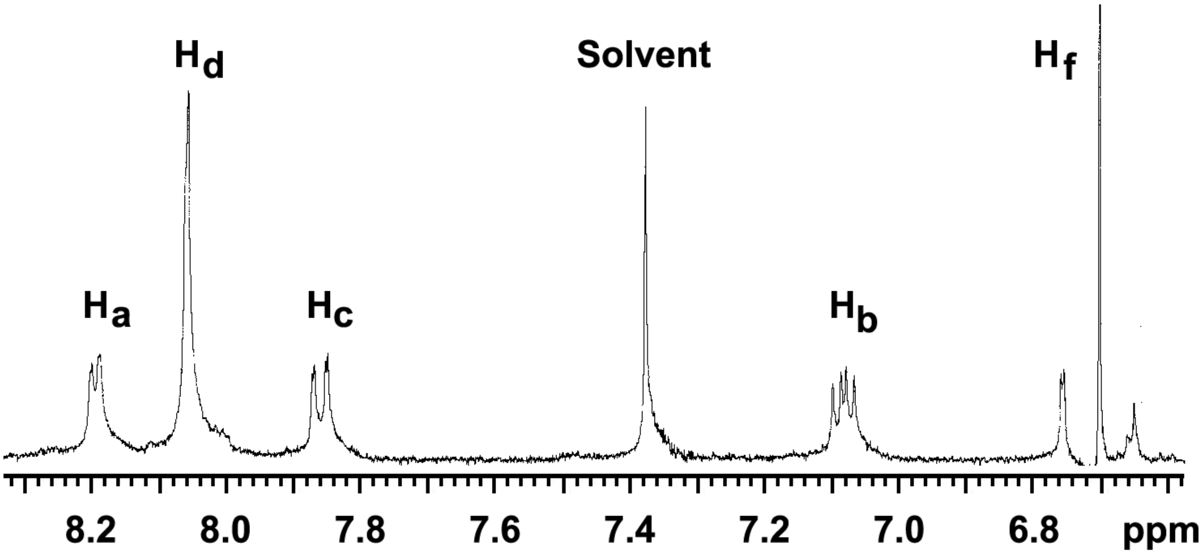

Figure S2: H_f protons decoupled aromatic region of ^1H NMR spectrum of DMAPIP-b in $CDCl_3$.

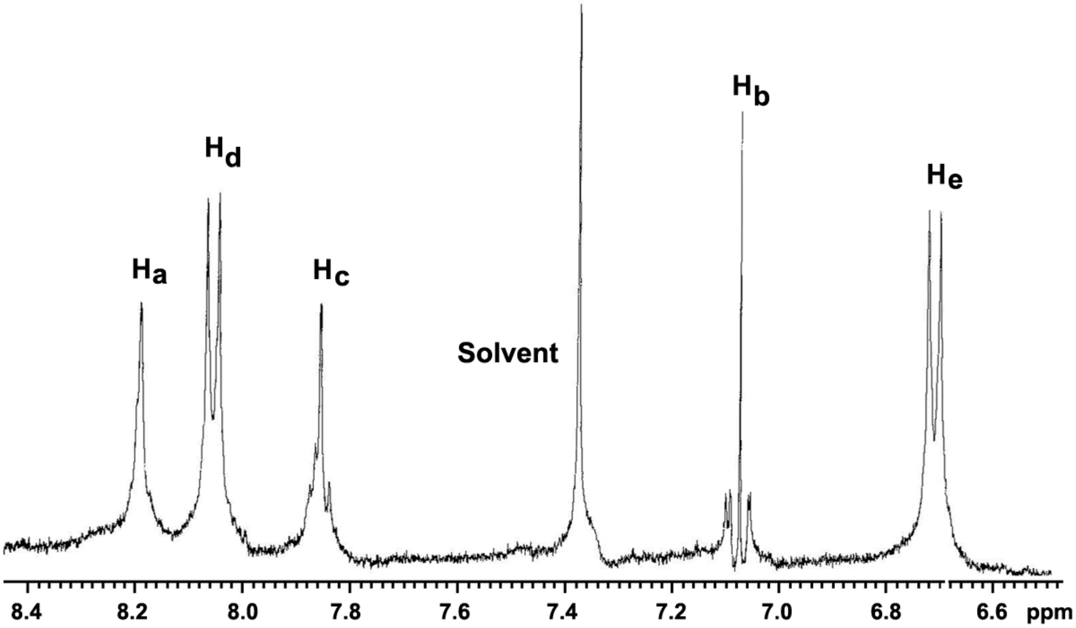

Figure S3: H_b proton decoupled aromatic region of ^1H NMR spectrum of DMAPIP-b in $CDCl_3$.

Appendix II

Crystal Structure of DMAPIP-b

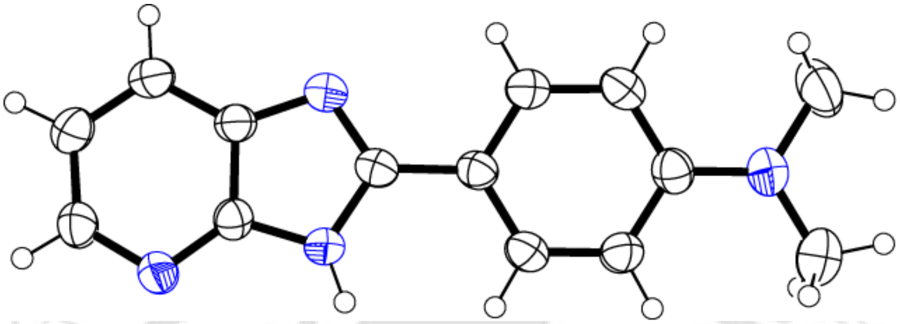

Chemical formula	$C_{14}H_{14}N_4$
formula wt	238.29
temp (K)	293 (2)
crystal system	Monoclinic
space group	*P* 21/c
a (Å)	12.0272 (11)
b (Å)	6.0933 (6)
c (Å)	16.8406 (16)
α (deg)	–
β (deg)	107.301(4)
γ (deg)	–
V ($Å^3$)	1178.33 (19)
Z	4
μ (mm^{-1})	0.084
ρ_{calcd} ($g\ cm^{-3}$)	1.343
no. of rflns collected	9144
no. of unique rflns	2371
no. of rflns ($I \geq 2\sigma(I)$)	1474
R_1^a, wR_2^b ($I \geq 2\sigma(I)$)	0.0494, 0.1145
R_1^a, wR_2^b (all data)	0.0763, 0.1215
goodness of fit (F^2)	1.000

Scope for future work

1. Due to limitation of our time resolved spectrofluorimeter, we could not measure the rate of formation of the TICT and the reverse process. Therefore, we are not able to follow the kinetic of the process. A femto second time resolved studies may be useful to follow the dynamics of the TICT process.

2. Our studies revealed that DMAPIP-b can acts as water sensor for microheterogeneous systems. Our results are qualitative, studies can be extended to quantify the water content in those systems.

3. It is reported in the literature DMAPIP-b act as inhibitor for Aurora-A, Aurora-B and Aurora-C kinases, but not DMAPIP-c. It was speculated that the nitrogen position plays a major role in bind of the molecule with proteins. But a detailed study will be useful to understand the mechanism of binding and also helpful to design similar inhibitors. We have studies the interaction of DMAPIP-b with BSA, the studies should be extended to other proteins to understand the interaction of these molecules with other proteins.

4. We have used TDDFT method for excited state energy calculation, as it fails in some charge transfer systems we have not performed any calculation on TICT state. Theoretical calculation may be performed with CASSCF or other methods to gain knowledge on the TICT processes of these molecules.

Publications

1. **N. Dash**, F. A. S. Chipem, R. Swaminathan and G. Krishnamoorthy, Hydrogen bond induced twisted intramolecular charge transfer in 2-(4'-*N*,*N*-dimethylamino phenyl)imidazo[4,5-*b*]pyridine, *Chem. Phys. Lett.* 2008, 460, 119-124.

2. **N. Dash**, F. A. S. Chipem, and G. Krishnamoorthy, Encapsulation of 2-(4'-*N*,*N*-dimethylamino)phenylimidazo[4,5-*b*] pyridine in β-cyclodextrin: Effect on H-bond induced intramolecular charge transfer emission, *Photochem. Photobiol. Sci.* 2009, 8, 1708 – 1715.

3. **N. Dash** and G. Krishnamoorthy, Photophysics of 2-(4'-*N*,*N*-dimethylamino phenyl)imidazo[4,5-*b*]pyridine in micelles: Selective dual fluorescence in sodium dodecylsulphate and triton X-100, *J. Fluoresc*. 2010, *20*, 135-142.

4. **N. Dash** and G. Krishnamoorthy, Effect of N-long chain alkylations on the photophysical properties of 2-(4'-*N*,*N*-dimethylamino phenyl)imidazo[4,5-*b*] pyridine (Communicated).

5. **N. Dash** and G. Krishnamoorthy, Effect of Temperature on the photophysical properties of 2-(4'-*N*,*N*-dimethyl aminophenyl)imidazo[4,5-*b*]pyridine (Under preparation).

6. **N. Dash** and G. Krishnamoorthy, Effect of Metal Cations on photophysical properties of 2-(4'-*N*,*N*-dimethylamino phenyl)imidazo[4,5-*b*]pyridine: Selectivity Towards Zinc(II) (Under preparation).

7. **N. Dash** and G. Krishnamoorthy, Intramolecular charge transfer of 2-(4'-*N*,*N*-dimethylaminophenyl)imidazo[4,5-*b*] pyridine in neutral and cationic reverse micelles (Under preparation).

8. **N. Dash** and G. Krishnamoorthy Interaction of 2-(4'-*N*,*N*-dimethylamino phenyl)imidazo[4,5-*b*]pyridine and its alkyalted products with Bovine Serum Albumin (Under preparation).